Structural and functional characterization of *Yersinia enterocolitica* type III secretion effectors and chaperones

Von der Fakultät für Lebenswissenschaften

der Technischen Universität Carolo-Wilhelmina

zu Braunschweig

zur Erlangung des Grades einer

Doktorin der Naturwissenschaften

(Dr. rer. nat.)

genehmigte

D i s s e r t a t i o n

von Renate Carina Büttner
aus Dresden

1. Referent:	Honorarprofessor Dr. Dirk Heinz
2. Referentin:	Professor Dr. Petra Dersch
eingereicht am:	07.01.2008
mündliche Prüfung (Disputation) am:	08.02.2008
Druckjahr	2008

Vorveröffentlichungen der Dissertation

Teilergebnisse aus dieser Arbeit wurden mit Genehmigung der Fakultät für Lebenswissenschaften, vertreten durch den Mentor der Arbeit, in folgenden Beiträgen vorab veröffentlicht:

Publikationen

Büttner, C.R., Cornelis, G.R., Heinz, D.W. & Niemann, H.H. (2005). Crystal structure of *Yersinia enterocolitica* type III secretion chaperone SycT. *Protein Sci*. **14**: 1993-2002

Büttner, C.R., Sorg, I., Cornelis, G.R., Heinz, D.W. & Niemann, H.H. (2008). Structure of the *Yersinia enterocolitica* type III secretion translocator chaperone SycD. *J. Mol. Biol.* **375**: 997-1012

Tagungsbeiträge

Büttner, C.R., Niemann, H.H., Heinz, D.W. Crystal structure of the type III secretion chaperone SycT from *Yersinia enterocolitica*. (Poster) 22nd European Crystallographic Meeting, Eötvös Loránd University, Budapest, Hungary (2004).

Büttner, C.R., Heinz, D.W., Niemann, H.H. Crystal structure of the type III secretion chaperone SycT from *Yersinia enterocolitica*. (Poster) Recent Advances in Macromolecular Crystallization, Le Bischenberg, France (2005).

Büttner, C.R., Heinz, D. W., Niemann, H.H. The crystal structure of the *Yersinia enterocolitica* type III secretion chaperone SycT. (Vortrag) 8th Heart of European Crystallography. Karlovy Vary, Czech Republic (2005).

Büttner, C.R., Heinz, D.W., Niemann, H.H. Crystal structure of the type III secretion chaperone SycT from *Yersinia enterocolitica*. (Poster) Murnau Conference on Structural Biology of Macromolecular Recognition, Murnau (2005). Posterpreis

Büttner, C.R., Heinz, D.W., Niemann, H.H. Crystal structure of the type III secretion chaperone SycT from *Yersinia enterocolitica*. (Poster) Annual Meeting of the German Society for Crystallography, University of Freiburg (2006). Posterpreis

Büttner, C.R., Heinz, D.W., Niemann, H.H. Crystal structure of the *Yersinia enterocolitica* type III secretion chaperone SycT. (Poster) Crystallography School, Como, Italy (2006).

Büttner, C.R., Heinz, D.W., Niemann, H.H. Structure of the *Yersinia enterocolitica* type III secretion translocator chaperone SycD. (Poster) Murnau Conference on Structural Biology of Disease Mechanisms, Murnau (2007).

Contents

Abbreviations

Å	Ångstrøm (0.1 nm)
aa	Amino acids
AEC	Anion exchange chromatography
Amp^R	Ampicillin resistance
APS	Ammonium persulfate
AraC	Transcriptional activator
BESSY	Berliner Elektronenspeicherring-Gesellschaft für Synchrotronstrahlung
BLAST	Basic Local Alignment Search Tool
c	Concentration
C-	Carboxy terminus
CAPS	N-cyclohexyl-3-aminopropane sulfonic acid
CBD	Chaperone-binding domain
CCD	Charge-coupled device
Cdc42	Small GTPase of the Rho family
C/H/D	Catalytic triad in YopT-like cysteine proteases, cysteine/histidine/aspartate
Cm^R	Chloramphenicol resistance
Da	Dalton (equals the mass of 1/12 of the carbon ^{12}C isotope)
DC	Dendritic cell
DESY	Deutsches Elektronensynchrotron
DLS	Dynamic /quasi-elastic light scattering
E. coli	*Escherichia coli*
ECL	Enhanced chemiluminescence
ECM	Extracellular matrix
EDTA	Ethylenediaminetetraacetic acid
EHEC	Enterohemorrhagic *E. coli*
EPEC	Enteropathogenic *E. coli*
ESI	Electro-spray ionization
ESRF	European Synchrotron Radiation Facility
FPLC	Fast protein liquid chromatography
GAP	GTPase activating protein
GDI	Guanine nucleotide dissociation inhibitor
GEF	Guanine nucleotide exchange factors
GenBank	Genetic sequence database maintained by the US National Center for Biology Information
GFP	Green fluorescent protein
GL	Glycine linker
GSH Seph	Glutathione sepharose

GST	Glutathione S-transferase, used as affinity tag
His_6	Six successive histidine residues, affinity tag
HPLC	High performance lipid chromatography
IB	Inclusion body
IPTG	Isopropyl-β-D-thiogalactopyranoside
K	Kelvin
Kan^R	Kanamycin resistance
K_D	Affinity in terms of equilibrium dissociation constant
kDa	Kilodalton
LcrH	SycD homolog in *Y. pestis* and *Y. pseudotuberculosis*
LDAO	N,N-Dimethyldodecylamine-N-oxide
MALDI-TOF-MS	Matrix-assisted laser desorption ionization-Time of Flight-Mass spectrometry
MAPK	Mitogen activated protein kinase
meth	Reductively methylated
MLD	Membrane localization domain
MME	Monomethylether
MR	Molecular replacement
M_r	Molecular mass
$M_{r\ theo}$	Theoretical molecular mass derived from amino acid sequence
$M_{r\ SEC}$	Experimental molecular mass derived from SEC
MWCO	Molecular weight cut-off
N-	Amino terminus
NCS	Non-crystallographic symmetry
NiNTA	Nickel nitrilotriacetic acid
OD_λ	Optical density at wavelength λ
oN	Over night
PAGE	Polyacrylamide gel electrophoresis
PBS	Phosphate buffered saline
PCR	Polymerase chain reaction
PcrH	*Pseudomonas aeruginosa* translocator chaperone
PDB	Protein data bank
PEG	Polyethylene glycol
Rac1	Small GTPase of the Rho family
RFZ	Rotation function Z-score
rH	Relative humidity
r_H	Hydrodynamic radius
RhoA	Small GTPase of the Rho family
r.m.s.d.	Root mean square deviation
σ	Standard deviation
SA	Surface area

SAD	Single-wavelength anomalous dispersion
SDS	Sodium dodecyl sulfate
SEC	Size exclusion chromatography
SeMet	Selenomethionine
SPR	Surface plasmon resonance
Str^R	Streptomycin resistance
Syc	Specific Yop chaperone
*syc*D	Gene sequence coding for *Yersinia* chaperone SycD
SycD	Specific *Yersinia* chaperone for translocators YopB and YopD
*syc*T	Gene sequence coding for *Yersinia* chaperone SycT
SycT	Specific *Yersinia* chaperone for YopT
s*yop*T	Synthetic *yop*T gene
sYopT	Gene product of the synthetic s*yop*T gene, identical with YopT
T3SS	Type III secretion system
TEMED	N,N,N',N'-Tetramethylethylenediamine
TEV	Tobacco etch virus
TFZ	Translation function Z-score
TPR	Tetratricopeptide repeat
Tris	Tris(hydroxymethyl)aminomethane
U	Units
UniProt	Universal protein resource
V_M	Matthews coefficient
wt	Wild-type
Y. enterocolitica	*Yersinia enterocolitica*
Y. pestis	*Yersinia pestis*
Y. pseudotuberculosis	*Yersinia pseudotuberculosis*
Yop	*Yersinia* outer protein
YopB/D	Pore-forming translocator proteins from *Yersinia*
YopE	*Yersinia* outer protein E, an effector
*yop*T	Gene sequence coding for *Yersinia* effector YopT
YopT	*Yersinia* outer protein T, an effector

Summary

Many Gram-negative bacteria, among them human enteropathogenic *Yersinia enterocolitica*, use a type III secretion system (T3SS) to directly inject effector molecules into eukaryotic cells in order to establish a symbiotic or pathogenic relationship with their host. The export of several T3SS proteins requires the assistance of specialized chaperones from the bacterial cytosol. The transient interplay of the chaperones with their cognate effector molecules is an important aspect in the regulation of the T3SS.

The translocation of the cytotoxic *Y. enterocolitica* effector molecule YopT, a cysteine protease that removes prenylated Rho GTPases from the host cell membrane, depends on the Class I/effector chaperone SycT. In investigating biochemically the complex between YopT and SycT, the chaperone-binding domain in the N-terminal part of YopT was specified more precisely. The persistent instability of YopT impairing successful crystallization was addressed using new expression constructs and procedures. Alternatively, the crystal structure of the YopT chaperone SycT was solved to high resolution in three independent crystal forms. SycT shares the homodimeric, canonical fold as well as the conserved hydrophobic surface patches with other T3SS Class I chaperones. In contrast, SycT lacks the dimerization helix and possesses an additional β-strand that is capable of undergoing a conformational rearrangement.

Y. enterocolitica Class II chaperone SycD specifically assists the pore-forming translocator proteins YopB and YopD. Moreover, SycD is involved in the regulation of virulence factor biosynthesis and secretion. The crystal structure of SycD could be determined to 1.95 Å and presents the first experimental structure of a T3SS Class II chaperone. SycD exhibits an entirely α-helical fold composed of three tetratricopeptide repeats (TPR) as previously predicted. Biochemical analysis using site-directed mutagenesis and size exclusion chromatography disclosed the formation of SycD head-to-head homodimers. Structural analysis revealed two alternative head-to-head dimer assemblies that share the same interface but differ in monomer orientation and overall shape. In the SycD dimer, the two faces of the TPR domain are freely accessible for interactions with the cognate translocators YopB and YopD. The *syc*D knockout-like phenotype of a stable but dimerization-defective SycD variant corroborated the physiological role of this newly identified SycD interface *in vivo.*

The structural and functional investigations of SycT and SycD disclosed intriguing features possibly conferring binding specificity and regulatory effect, respectively. The two structures thus contribute to the understanding how the T3SS is orchestrated.

1 Introduction

1.1 The pathogenic bacterium *Yersinia*

The bacterium *Yersinia* is a Gram-negative coccobacillus belonging to the family of Enterobacteriaceae and comprises three human pathogenic species: *Y. pestis* is the causative agent of plague, *Y. pseudotuberculosis* and *Y. enterocolitica* are gastrointestinal pathogens. Plague is a devastating acute infectious disease and caused severe pandemics in medieval times. But still today, smaller outbreaks of plague are reported throughout the world, recently in the Congo (2005/06) (WHO, 2007). Plague is a systemic zoonosis (i.e. transmission from animals to humans), which is maintained in a rodent reservoir host through a transmission cycle involving rat fleas as vector that occasionally bite humans. The bacteria then localize to regional lymph nodes. Bubonic plague (bubo=swollen lymph node) is the most common, beside the septicemic and pneumonic appearance. Pneumonic plague establishes only in rare cases from bubonic plague, or by inhaling respiratory droplets. Compared to 50-60 % mortality of bubonic plague, the pulmonary disease is highly contagious and rapidly fatal if left untreated. It spreads in an epidemic manner *via* the respiratory route (Prentice and Rahalison, 2007).
Unlike *Y. pestis*, the enteric pathogens *Y. enterocolitica* and *Y. pseudotuberculosis* find their habitats in the environment (e.g. soil), where they infect animals and are taken up by humans with contaminated food or water. The bacteria pass to the small intestine, where the *Yersinia* adhesion molecules invasin and multifunctional YadA promote tight adhesion and invasion into epithelial cells. This occurs through either direct (invasin) or indirect, extracellular matrix (ECM)-mediated binding (YadA) to β1-integrin, a eukaryotic surface receptor (Leong *et al.*, 1990; El Tahir and Skurnik, 2001; Isberg and Barnes, 2001). The bacteria cross the intestinal barrier inducing the “zipper mechanism” (Pizarro-Cerda and Cossart, 2006) and transcytosis of antigen-sampling M-cells embedded in the follicle-associated epithelium of the Peyer’s patches (Clark *et al.*, 1998) (Figure 1-1). At the basolateral side, they encounter the cellular immune response of the host. After transport into the Peyer’s patches and mesenteric lymph nodes, the bacteria proliferate extracellularly, colonize spleen and liver and cause localized infections. The clinical symptoms of yersiniosis range from gastroenteritis with mild, self-limiting diarrhea to acute mesenteric lymphadenitis. In very rare cases the bacteria cause a systemic infection with severe sequelae, such as reactive arthritis. As Yersiniae are psychrophilic, these food-borne germs continue growing at 4 °C and thereby pose a significant hygiene challenge especially for pork (~ products). *Y. enterocolitica* is also of significance in

blood transfusion-associated septicemia. The transmission pathways of *Yersinia* are depicted in Figure 1-1.

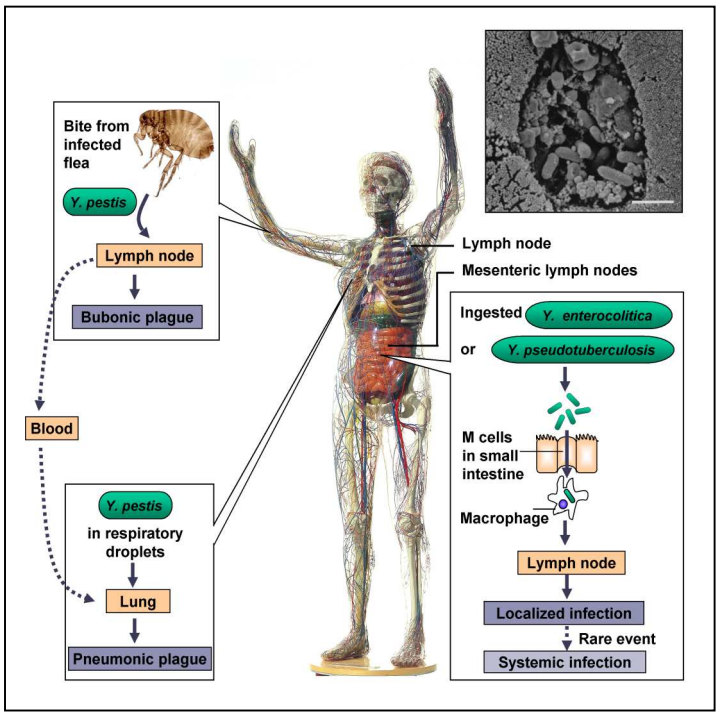

Figure 1-1. Transmission and dissemination of pathogenic Yersiniae in humans. *Y. pestis* from rodent reservoirs is resident in fleas and transmitted to other rodents or occasionally to humans – causing the bubonic plague. Inefficient human-to-human transmission occurs *via* human fleas. Pneumonic plague is transmitted through respiratory droplets. *Y. enterocolitica* and *Y. pseudotuberculosis* are ingested, entering the lymphatic system through M-cells of the small intestine. The inset shows a scanning electron-micrograph of *Y. enterocolitica* proliferating extracellularly within the lymphatic follicle tissue of a Peyer's Patch (Clark *et al.*, 1998). Adapted from Wren, 2003; Glass woman, German Hygiene Museum, Dresden.

The lymphatic tissue swarms with professional phagocytes such as macrophages and neutrophilic leucocytes, which are specialized in destroying invading microbes. *Yersinia* prevents its own phagocytosis by the secretion of phagocyte-affecting cytotoxins (see below), and is thereby able to survive within the lymphatic tissue.

1.2 Type III secretion - *Yersinia*'s stratagem

The three Yersiniae species most likely originate from a common non-pathogenic predecessor, which acquired a virulence plasmid and further elements by lateral gene transfer resulting in enteropathogenic *Y. enterocolitica* and *Y. pseudotuberculosis*. Population genetics revealed that *Y. pestis* recently (within the last 20'000 years) evolved from the enteropathogen *Y. pseudotuberculosis* by further uptake of genetic determinants and chromosomal degeneration (Achtman *et al.*, 1999). Without the virulence plasmid, the bacterium is avirulent as seen for *Y. enterocolitica* biogroup 1A having lost its plasmid.

Y. pestis is non-motile, whereas other species change their appearance and pathogenicity depending on temperature or the concentration of calcium ions. At lower temperatures (< 26.7 °C) or in the presence of calcium, *Yersinia* is non-flagellated and shows a strong

tendency to adhere to phagocytic cells with an increased production of invasin at the cell surface. During infection, the pathogenic Yersiniae depend on a T3SS that is encoded by the ~70 kb *Yersinia* virulence plasmid (pCD/pYV) (Figure 1-2) in order to evade the host immune response and to survive extracellularly. After contacting an eukaryotic cell, *Yersinia* boosts the expression and secretion of the plasmid encoded virulence factors comprising T3SS effector molecules, chaperones and regulatory proteins (Figure 1-2).

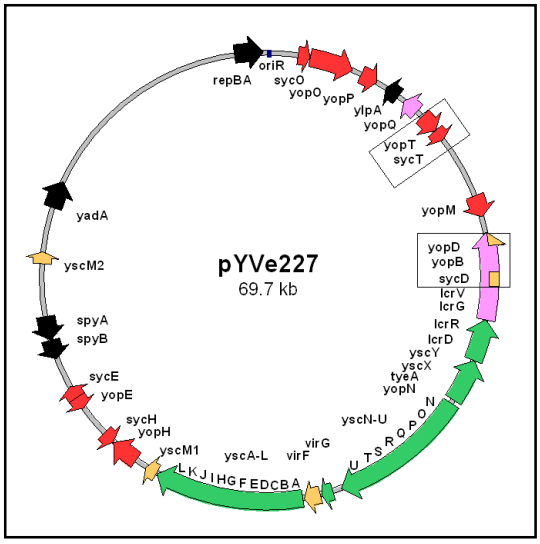

Figure 1-2. Genetic map of the virulence plasmid pYVe227 from *Yersinia enterocolitica* strain W22703 (serotype 0:9). The genes encoding the chaperones (*syc*) are located close to the cognate binding partner (*yop*). Effector and their cognate chaperone loci are colored in red, genes involved in intracellular delivery are colored magenta, loci required in secretion are colored in green, gene loci influencing transcription regulation are designated in bright orange (adapted from Cornelis *et al.*, 1998). (Loci of virulence factors studied in this work are boxed).

The term “type III secretion” was first used to describe one of the mechanisms that Gram-negative bacteria employ in order to export proteins from the cell (Salmond and Reeves, 1993). Further secretion systems exist ranging from T1S to T6S, including one and two step systems (Gerlach and Hensel, 2007). The type III secretion system (T3SS) is widespread among Gram-negative animal- and plant-pathogenic bacteria as well as bacterial symbionts. Although many components from the molecular machinery, the T3SS apparatus, are structurally and functionally conserved among different species, distinct differences exist regarding the genetic basis and the purposes the T3SS is used for by the bacteria. Phylogenetic analysis allows the organization of T3SSs into seven groups, among them the Ysc group including the plasmid encoded *Yersinia* T3SS, or the group comprising the chromosomal *Salmonella* pathogenicity islands. It is not uncommon that the same T3SS is employed by different bacteria species or that a single species is equipped with T3SSs from different groups (Cornelis, 2006).

The T3SS apparatus spans the inner membrane, the peptidoglycan layer and the outer membrane of the bacterium and protrudes in a needle-shaped structure of several nanometers in length (Figure 1-3) (reviewed by Galan and Wolf-Watz, 2006). The hollow assembly

consists of ~30 proteins and resembles a molecular syringe, therefore also called needle-complex or injectisome. The actual mechanism of type III secretion is poorly understood. Upon sensing host cell contact, the machinery is switched on and effector molecules are suggested to be translocated in one step through this hollow conduit directly into the eukaryotic cell where they interfere with host cell signaling cascades. However, the inner channel diameter of ~2-3 nm does not allow the export of completely folded proteins suggesting the proteins to be transported in an at least partially unfolded state (Feldman *et al.*, 2002).

Among the different bacteria, a great diversity of the translocated T3SS effectors exists. However, certain effector groups show the same biological function and/or biochemical activity among different species (for reviews on T3SS see Mota and Cornelis, 2005; Cornelis, 2006).

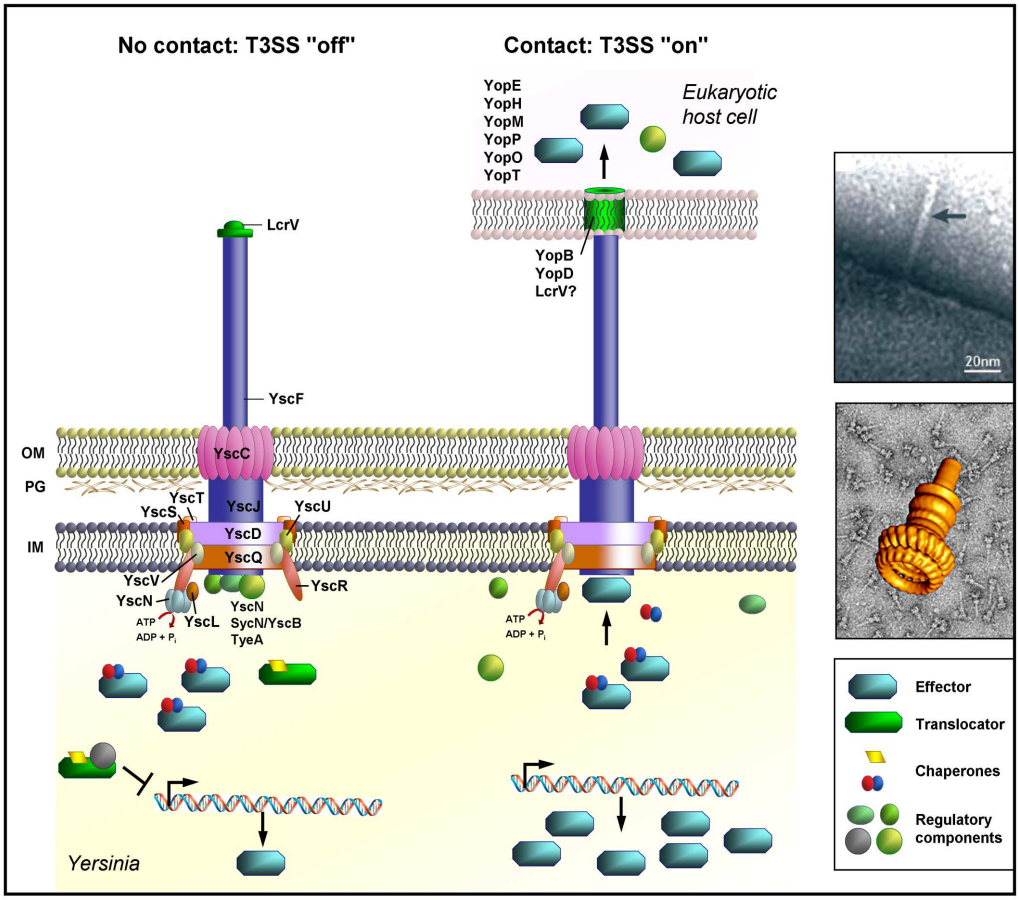

Figure 1-3. The *Yersinia* Ysc-Yop type III secretion machinery. The T3SS apparatus consists of the basal body anchored in the bacterial membranes and a protruding needle-shaped structure. In the absence of host cells, the T3SS is down-regulated and cytotoxin secretion is blocked by a multicomponent plug at the gate. After sensing contact to the host cell, cytotoxin translation and translocation is induced. OM, outer membrane; IM, inner membrane; PG, peptidoglycan. The upper inset shows the needle protruding from the microbial cell (Cornelis, 2006), the lower inset depicts the surface rendering of the structure of the T3SS needle complex from *Salmonella* as well as the electron micrograph of isolated needle complexes (Marlovits *et al.*, 2004). Modified from Mota and Cornelis, 2005; Desvaux *et al.*, 2006.

Interestingly, the virulence- and symbiosis-associated T3SS is closely related to the flagellar T3SS and they most likely share a common evolutionary origin and assembly process (Saier, 2004). This is suggested *inter alia* by the fact that they both export their own distal components. Moreover, both assemblies are ATPase-dependent and include several components, especially from the basal body, that are functionally significantly similar (Auvray *et al.*, 2001; Young and Young, 2002).

1.3 T3SS translocators and effectors in *Yersinia*

Successful translocation of the effector molecules or *Yersinia* outer proteins (Yops) across bacterial and host membranes directly into the host cytosol requires a specialized family of proteins, the translocators. Translocator proteins are also transported by the needle-complex and form a pore in the eukaryotic cell membrane allowing the effectors to enter the host cell (reviewed by Büttner and Bonas, 2002).

In *Yersinia,* translocator proteins comprise the hydrophobic pore-forming proteins YopB and YopD (Tardy *et al.*, 1999) as well as the hydrophilic channel-size determinant LcrV, the most effective immunomodulating yersinial antigen (Holmstrom *et al.*, 2001; Mueller *et al.*, 2005) (Figure 1-3). After secreting the components building the T3SS apparatus that were exported through the nascent machine, the bacterium switches the secretion specificity toward effector secretion. This is triggered by YscP, the proposed "molecular ruler" determining the length of the needle (Agrain *et al.*, 2005), communicating with the basal body component YscU (Edqvist *et al.*, 2003). In order to ensure its survival and spreading, *Yersinia* translocates at least six Yops into the eukaryotic cell. Here, the effectors modulate host cell processes that range from signal transduction to programmed cell death and actin cytoskeletal dynamics (Aepfelbacher *et al.*, 2007). The roles of Yops in *Yersinia* virulence have been investigated in detail in cell culture as well as in the mouse infection model. *Yersinia* accomplishes its primary concern, the inhibition of phagocytosis, with four out of six of its Yop effectors acting synergistically (YopE/H/O/T). These effectors directly modulate the Rho GTPase cycle and focal adhesion complexes normally stimulating actin polymerization required in the formation of the phagocytic cup in macrophages, dendritic cells (DC) and neutrophils (Figure 1-4). Interference with the adaptive immune responses, the second vitally important point in Yop attack, is secured by two further Yops (YopJ/P and YopH).

Rho GTPases play a central role in regulation of cytoskeletal functions. They are activated by guanine nucleotide exchange factors (GEFs) and inactivated by GTPase-activating proteins

(GAPs) therefore representing a molecular switch. Activated Rho GTPases recruit further proteins that stimulate actin nucleation and polymerization. The *Yersinia* effector YopE is a GTPase-activating protein (GAP) acting on small Rho GTPases promoting actin depolymerization (Black and Bliska, 2000) and prevents maturation of proinflammatory cytokine IL-1β (Schotte *et al.*, 2004).

The second antiphagocytic effector, the protein tyrosine phosphatase YopH, dephosphorylates a number of proteins associated with focal adhesions thus blocking their assembly (Black and Bliska, 1997), suppresses the production of reactive oxygen species (Bliska and Black, 1995) and the activation of lymphocytes (Yao *et al.*, 1999).

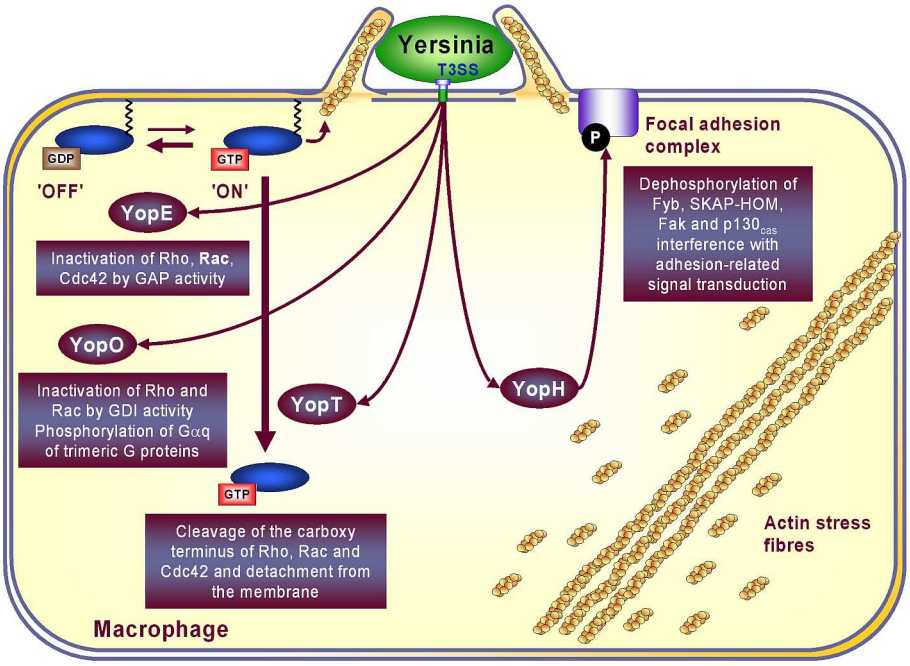

Figure 1-4. Translocated Yop effectors YopE/H/O/T with an anti-phagocytic effect. Four of the six *Yersinia* effector molecules, YopE, H, O and T, interfere with the actin cytoskeletal dynamics thereby preventing the formation of the phagocytic cup. The two other *Yersinia* effectors, YopP and YopM, which target inflammatory MAPK and NF-κB signaling pathways, are not depicted. Adapted from Cornelis, 2002.

YopO (*Yersinia* protein kinase A, YpkA, in *Y. pestis* and *Y. pseudotuberculosis*), the third phagocytosis-antagonist, is a serine/threonine kinase that becomes autophosphorylated upon contact to actin (Trasak *et al.*, 2006), inhibits Rho GTPases by its guanine nucleotide dissociation inhibitor (GDI) activity and blocks signaling of trimeric G-proteins by Gαq subunit phosphorylation (Navarro *et al.*, 2007).

YopP (YopJ in *Y. pseudotuberculosis* and *Y. pestis*) induces apoptosis in macrophages and DCs and was recently discovered to be an acetyltransferase (Mukherjee *et al.*, 2006) forestalling mitogen-activated protein kinase (MAPK) phosphorylation, thereby inhibiting MAPK

signaling pathways (Orth *et al.*, 1999) and nuclear-factor (NF)-κB signaling (Ruckdeschel *et al.*, 2001).

YopM is believed to suppress natural killer (NK) cells (Kerschen *et al.*, 2004), however, the physiological role of the interaction with two host kinases (McDonald *et al.*, 2003) and the YopM localization to the nucleus still remains elusive.

The sixth *Yersinia* effector, YopT, has been discovered quite recently (Iriarte and Cornelis, 1998). YopT is cysteine proteases cleaving small Rho-GTPases and thereby contributes to the antiphagocytic effect. YopT is described in more detail below.

Exported T3SS proteins do not show a secretion signal that is cleaved during transport. The nature of the signal is heavily debated. On the one hand, the N-terminal first 17 amino acids of the protein are believed to contain the secretion signal (Sory *et al.*, 1995). On the other hand, there exists evidence for a 5' mRNA encoded signal (Anderson and Schneewind, 1997). No consensus sequence has yet been found in either the amino terminal part or the 5' region of the mRNA. In addition, the secretion signal was also proposed to reside in the chaperone (T3SS chaperones, see below) bound to the effector (Wattiau and Cornelis, 1993).

The T3SS effectors show an immense structural diversity (reviewed by Johnson *et al.*, 2005). Interestingly, several of these bacterial effectors display structural homology to eukaryotic proteins (Alto *et al.*, 2006; Xiao *et al.*, 2007) and it is likely that this structural mimicry is required for the interference of these effectors with host cell functions.

1.4 The *Yersinia* effector YopT

The *Yersinia* effector molecule YopT is one of the four Yops affecting the dynamics of the actin cytoskeleton (Figure 1-4). YopT comprises 322 residues (36.4 kDa, pI 8.9). Additionally, YopT possesses a specific chaperone SycT (Iriarte and Cornelis, 1998). The chaperone-binding domain in YopT was postulated to comprise at least residues 52-104 (Büttner, 2003).

Both genes are encoded in the *syc*T-*yop*T operon on the *Yersinia* virulence plasmid (Figure 1-2). The *syc*T-*yop*T operon is not present in *Y. pseudotuberculosis* serotype O:3 strains (Aepfelbacher, 2004).

Initially, YopT was shown to cause an isoelectric shift of the small Rho GTPase RhoA (Zumbihl *et al.*, 1999). In general, YopT targets small, membrane-attached GTPases, preferentially RhoA besides Rac1 and Cdc42 (Iriarte and Cornelis, 1998) that are known to be essentially involved in the regulation of the cytoskeleton and phagocytosis (Burridge and Wennerberg, 2004). Several small Rho GTPases were shown to be post-translationally

modified by a lipid moiety (prenylation) at their C-terminal CaaX box (C, cysteine; a, aliphatic residue; X, any residue) (Roskoski, 2003), which allows the GTPase to be anchored in the cell membrane. YopT cleaves the GTPase just before the C-terminal cysteine bearing the thioether-linked geranylgeranyl isoprenoid moiety and recognizes additionally a polybasic sequence N-terminally of the modified cysteine (Shao *et al.*, 2003). Releasing the GTPase into the cytosol reduces its effective concentration at the membrane and results in the disruption of RhoA-controlled actin stress fibers. The visible effect is the rounding-up of the eukaryotic cells (Iriarte and Cornelis, 1998). YopT was identified to be the prototypical member of a new family of papain-like cysteine proteases (clan CA) with an invariant catalytic Cys/His/Asp triad (Shao *et al.*, 2002). The minimal catalytically active YopT fragment was suggested to comprise residues 75 to 318 (Sorg *et al.*, 2003). Moreover, binding to the substrate RhoA was proposed to require YopT residues 75-100, though the RhoA-binding was considerably reduced in an N-terminal 74-amino acid deletion mutant implying the involvement of the very YopT N-terminus (Sorg *et al.*, 2003). In general, YopT possesses a less distinct anti-phagocytic effect compared to YopE (Viboud *et al.*, 2006), although contradicting observations had been made (Grosdent *et al.*, 2002; Adkins *et al.*, 2007). Interestingly, YopT co-operates with YopE in attacking the small Rho GTPase Rac1 (Wong and Isberg, 2005a), thus contributing to the antiphagocytic activity as activated Rac1 is required in invasin-β_1 integrin mediated uptake of bacteria (Wong and Isberg, 2005b). Interestingly, YopT thereby causes the localization of Rac1 to the nucleus, with a so far unknown outcome. Several homologous YopT-like cysteine proteases were found in plant pathogenic bacteria such as AvrPphB from *Pseudomonas syringae* pv. *phaseolicola* or HopPtoC$_{EA}$ in *Erwinia amylovora* (Shao *et al.*, 2002; Zhao *et al.*, 2005).

1.5 T3SS chaperones

In general, a chaperone is defined as a protein that is required for the proper folding or assembly of proteins or protein complexes without being a component of the final structure (Ellis, 2005).

Effective export of several T3SS proteins depends on specialized proteins from within the bacterial cytosol that are not exported themselves. They share a small size (M_r ~12-19 kDa) and a predominantly acidic pI (Table 1-1). The gene loci of these so-called T3SS chaperones are located adjacently to those of their cognate interaction partners (Figure 1-2) and the chaperone and effector genes are co-expressed. The T3SS chaperones specifically bind and

assist the secretion of their cognate effector molecules. The absence of ATP hydrolysis and protein folding properties distinguishes T3SS chaperones from the "universal" molecular chaperones such as many heat shock (Hsp) proteins, DnaK or the chaperonins GroEL/S (Houry, 2001; Ellis, 2005).

Table 1-1. Selected representatives of the different classes of T3SS chaperones.

Species	Chaperone	Size (aa)	pI[†]	Cognate binding partner(s)
Class IA				
Pseudomonas ssp.	**Orf1**	134	5.9	AvrPphF
Salmonella ssp.	**SicP**	116	4.2	SptP
Salmonella ssp.	**SigE**	113	4.2	SigD
Shigella ssp.	IpgA	129	4.8	IcsB
Yersinia ssp.	**SycE** (YerA)	130	4.8	YopE
Yersinia ssp.	**SycN**	123	5.3	YscB (heterodimer moiety), YopN
Yersinia ssp.	SycO	155	4.7	YopO/YpkA
Yersinia ssp.	**SycT**[*]	130	4.6	YopT
Yersinia ssp.	**YscB**	137	9.3	SycN (heterodimer moiety), YopN
Class IB				
EPEC/EHEC	**CesT**	156	4.5	Tir, Map, NleA
Salmonella ssp.	**InvB**	135	4.7	SipA, SopA, SopE, SopE2
Shigella ssp.	**Spa15**	133	4.5	IpgB1, IpaA, OspC3, OspD1
Yersinia ssp.	**SycH**	141	5.1	YopH, LcrQ/YscM1, YscM2
Xantomonas ssp.	HpaB	162	4.3	AvrBs1, AvrBs3
Class II				
Edwardsiella ssp.	EscC	115	7.8	EseB, EseD
EPEC/EHEC	CesD	151	7.4	EspB, EspD
Pseudomonas ssp.	PcrH	167	4.8	PopB, PopD
Salmonella ssp.	SscA	157	8.0	SscC, SscD
Shigella ssp.	IpgC	155	4.7	IpaB, IpaC
Yersinia ssp.	**SycD**[*] /LcrH	168	4.9	YopB, YopD (Ysc-Yop T3SS)
Yersinia ssp.	SycB	169	4.8	YspB, YspC (Ysa T3SS)
Class III				
Aquifex (flagellum)	**FliS**	124	5.0	FliC (flagellin)
EPEC	**CesA**	107	9.5	EspA
Pseudomonas ssp.	**PscE**	67	6.5	PscF
Yersinia ssp.	**YscE**	66	7.4	YscF

The list includes chaperones from animal and plant pathogens as well as one flagellar chaperone. Chaperones in bold are characterized by crystals structures ([*] this study). [†]Calculated with Vector NTI (Invitrogen).

1.5.1 Classes of T3SS chaperones

Although the primary sequence of T3SS chaperones is not conserved, they can be divided in at least three major classes according to the function and number of their cognate binding

partners (Parsot *et al.*, 2003). This classification corresponds also to the structural differences of T3SS chaperones.

Class I or effector chaperones

Class I or effector chaperones specifically bind either one (monovalent, Class IA) or more (multivalent, Class IB) effector molecules. Class I chaperones represent by far the best characterized group. The chaperone-binding domain in their cognate effector is located within the first 100-125 residues in the N-terminal region (Sory *et al.*, 1995; Iriarte and Cornelis, 1998). Although the sequence identity among the effector chaperones is 21 % at most, a common C-terminal amphipathic α-helix has been identified in their amino acid sequences (Wattiau *et al.*, 1994). Moreover, effector chaperones were found to be organized in dimers, an observation that was also supported by several crystal structures, such as that of *Yersinia* SycE (Figure 1-5), the cognate chaperone of the GTPase-activating effector YopE (Wattiau and Cornelis, 1993; Birtalan and Ghosh, 2001; Evdokimov *et al.*, 2002; Trame and McKay, 2003).

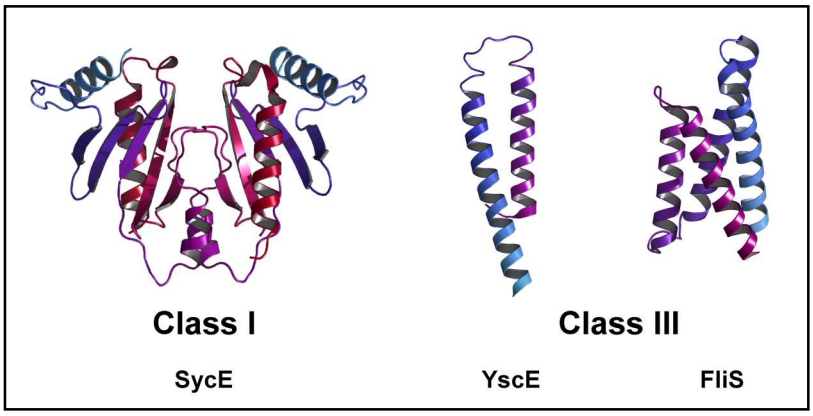

Figure 1-5. Crystal structures of selected T3SS chaperones. Homodimeric Class I chaperone SycE (Protein databank (PDB) accession code 1JYA), the cognate chaperone of Rho GTPase-activating protein YopE from *Yersinia*, and Class III members *Yersinia* YscE (1ZW0) and flagellar chaperone FliS (1ORJ) from *Aquifex*. No crystal structure of a T3SS Class II chaperone has been solved so far.

Class II or translocator chaperones

Class II chaperones are specific for pore-forming translocators, therefore called translocator chaperones. These chaperones are multivalent as they bind both transmembrane translocator proteins, and sometimes even further T3SS components. No crystal structure has been solved so far for Class II chaperones, though recently, α-helical tetratricopeptide repeat (TPR)-like motifs have been predicted from their sequences (Pallen *et al.*, 2003). These degenerated 34-

residues motifs are often arrayed in tandem (Sikorski *et al.*, 1990). These TPR domains usually mediate protein-protein interactions and are found in all biological kingdoms (Gregory L. Blatch, 1999).

Class III chaperones

A third class of T3SS chaperones assists in secretion of distal components of the needle complex that are themselves exported through the nascent secretion apparatus (Creasey *et al.*, 2003; Quinaud *et al.*, 2005). The chaperones from the related flagellar system are also assigned to Class III. In contrast to Class I chaperones, the biological oligomerization state of Class III chaperones seems to be the monomer, corroborated by crystal structures such as that of the *Yersinia* needle protein chaperone YscE (Phan *et al.*, 2005) or the flagellar chaperone FliS (Evdokimov *et al.*, 2003) (Figure 1-5). As the limited number of crystal structures of Class III chaperones reveals a significant structural heterogeneity, a further sub-classification might be required. Table 1-1 gives an overview of T3SS chaperones.

1.5.2 Postulated functions of T3SS chaperones

The role of the T3SS chaperones is still under debate (Feldman and Cornelis, 2003; Letzelter *et al.*, 2006; Wilharm *et al.*, 2007). This might be due to the facts that 1) not all secreted proteins require a chaperone, 2) some secretion cargoes are stable even in the absence of their chaperone and 3) there are possibly different functions according to the classes and some chaperones may fulfill more than one function with the different roles not being necessarily mutually exclusive (Feldman and Cornelis, 2003; Parsot *et al.*, 2003; Wilharm *et al.*, 2007). Selected proposed functions of T3SS chaperone are depicted in Figure 1-6.

1) Stabilization and secretion competency of the effector molecules

It has been suggested that T3SS chaperones ensure effector stabilization. They presumably prevent unproductive interactions prior to secretion as well as aggregation of hydrophobic regions such as the aggregation-prone chaperone-binding domain (CBD) in the effectors or the transmembrane regions in the translocators (Figure 1-6, 1). Recently, the CBD was found to present a membrane-localization domain (MLD) (Letzelter *et al.*, 2006). Coverage of the aggregation prone MLD, thus keeping the protein competent for export, was therefore suggested by the authors to be the primary function of T3SS chaperones.

Additionally, the chaperones are proposed to maintain their binding partners in a secretion-competent, partially unfolded state in which the secretion signal is accessible to the T3SS

apparatus. Remarkably, binding to the chaperone does not necessarily affect the enzymatic activity or binding capacity of the bound proteins (Luo *et al.*, 2001; Birtalan *et al.*, 2002; Neumayer *et al.*, 2004). This finding indicates that prior to secretion the largest part of the polypeptide chain is folded.

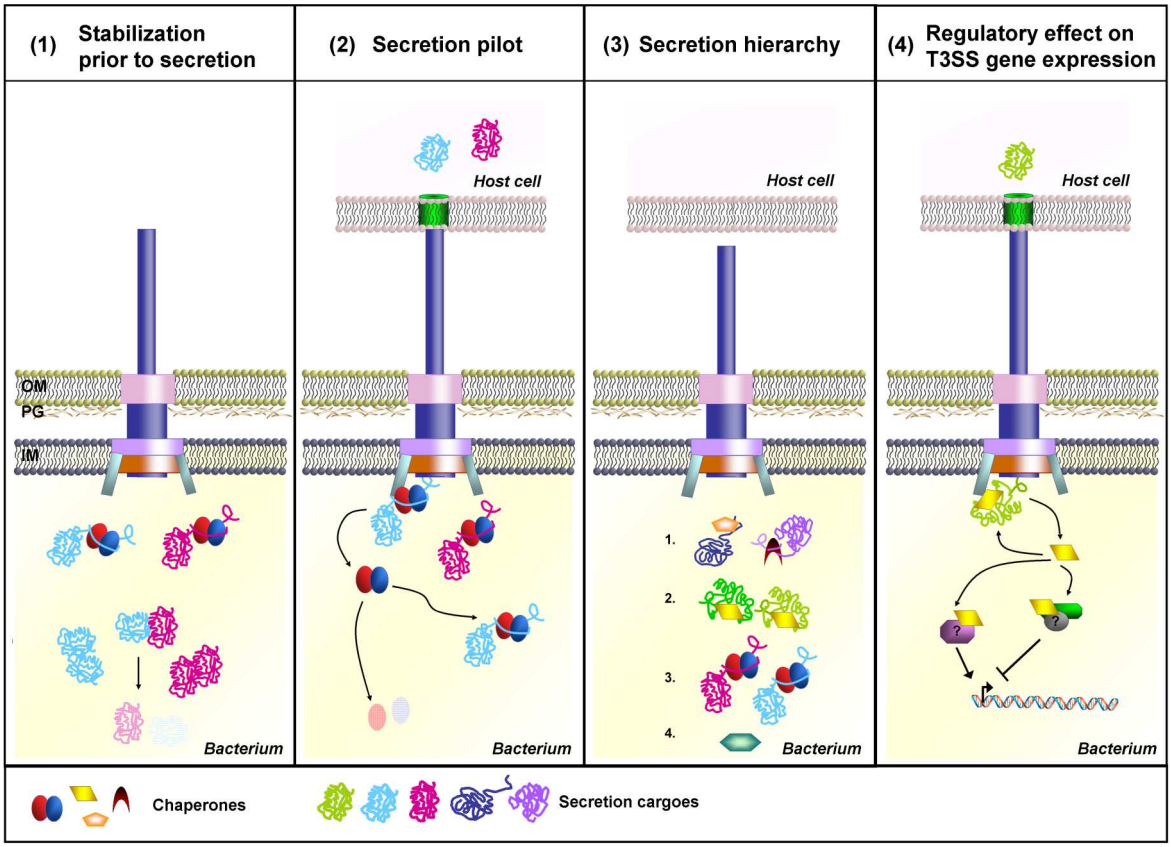

Figure 1-6. Proposed functions of T3SS chaperones. (1) Chaperones are suggested to stabilize their binding partner prior to secretion by masking hydrophobic regions and preventing aggregation and premature interactions, which would otherwise lead to degradation. **(2)** Chaperones might act as secretion pilot toward the needle complex. It is unclear whether T3SS chaperones are recycled or degraded after delivering their cognate binding partners. **(3)** The chaperones could establish a hierarchy among the T3SS secretion cargoes. Highest priority would possess the chaperone-bound components building the nascent secretion apparatus (1.), followed by the chaperone-stabilized pore-forming translocators (2.) and the chaperone-bound effector molecules (3.), before proteins without a chaperone (4.) are exported. **(4)** Some chaperones are involved in the regulatory control of gene expression by either an activating or repressing effect. Not all of the proteins involved in the regulation are known. OM, outer membrane; PG, peptidoglycan; IM, inner membrane. Figures prepared in analogy to Feldman and Cornelis, 2003; Mota *et al.*, 2005.

2) Secretion pilots

Another suggested role is that of secretion pilots toward the membrane-anchored needle-complex (Figure 1-6, 2). The effector chaperone CesT from enteropathogenic *Escherichia coli* (*E. coli*) (EPEC) or the flagellar export chaperone from *Salmonella* were observed to interact with the AAA+ type ATPase of the T3SS (Gauthier and Finlay, 2003; Thomas *et al.*, 2004). This is in line with the finding that chaperone release and unfolding of the secretion cargo is

an ATP-dependent process, induced by the T3SS ATPase (Akeda and Galan, 2005) and possibly facilitated by the T3SS chaperones. In addition, the translocator chaperones CesD from EPEC and *Edwardsiella* EscC were shown to localize to the membrane (Wainwright and Kaper, 1998; Zheng *et al.*, 2007).

Relatedly, the effector-chaperone complex may also present a three-dimensional secretion signal. Chaperone-deficient mutants usually fail to export their cognate binding partner efficiently (Cheng *et al.*, 1997; Lloyd *et al.*, 2001). Interestingly, in *Salmonella,* chaperone binding defines whether the secretion cargo is transported *via* the pathogenicity-related T3SS or the flagellar T3SS (Lee and Galan, 2004).

3) Secretion hierarchy

Furthermore, the T3SS chaperones may uphold a secretion hierarchy among the secretion substrates as indicated by Wulff-Strobel *et al.*, 2002 and Thomas *et al.*, 2007. In this model (Figure 1-6, 3), components of the nascent machine possess highest secretion priority. After the specificity switch, the pore-forming translocators are secreted, followed by the effector molecules and further secretion cargoes.

4) Regulatory control of T3SS gene expression

Noteworthy, several Class II chaperones and probably also some of the Class I chaperones play crucial roles in the regulation of T3SS-associated gene expression (Figure 1-6, 4). SicA, the cognate chaperone of the *Salmonella* translocators SipB and SipC, forms a regulatory complex with the AraC-like transcription factor InvF, thereby activating expression of *Salmonella* T3SS pathogenicity island-1 (SPI-1) genes (Darwin and Miller, 2001). T3SS gene expression is generally stimulated by transcriptional regulators belonging to the AraC-like family (Cornelis *et al.*, 1989). A similar scenario may apply to *Shigella flexneri* translocator chaperone IpgC activating T3SS gene expression by binding to AraC-like MxiE (Mavris *et al.*, 2002). In both cases, secretion of the cognate translocator protein is believed to precede complex formation between the chaperone and the transcription activator (Figure 1-6). In contrast, *Yersinia* Class II chaperone SycD acts as a negative regulator on *yop* expression together with one of its cognate translocators, YopD, and the negative regulator LcrQ/YscM1 (Francis *et al.*, 2001; Anderson *et al.*, 2002). The effector chaperone SycH from *Yersinia* ssp. might be the counterpart of SycD inducing *yop* expression by promoting secretion of LcrQ/YscM1 (Cambronne *et al.*, 2004). Possibly, a regulatory function might be also assigned to the *Yersinia* effector chaperone SycO (Dittmann *et al.*, 2007).

1.6 The *Yersinia* T3SS chaperones SycT and SycD

SycT - the Class I/ effector chaperone for YopT

Four out of six *Yersinia* effector molecules are chaperone-assisted, namely YopE, YopH, YopO/YpkA and YopT (Wattiau and Cornelis, 1993; Wattiau *et al.*, 1994; Iriarte and Cornelis, 1998; Letzelter *et al.*, 2006). In *Yersinia*, these non-flagellar T3SS-associated chaperones are termed specific Yop chaperones (Sycs). The effector protein YopM does not possess a specific chaperone, and so far no chaperone has been identified for YopP/J.

SycT is the specific chaperone for the effector protein YopT. The ~15 kDa chaperone SycT exhibits 130 amino acids and an acidic isoelectric point (pI 4.6) that is typical for Class I chaperones. SycT presumably shares the mixed α/β-fold of previously determined crystals structures of Class I chaperones, such as that of SycE (YerA in *Y. pestis* and *Y. pseudotuberculosis*) (Figure 1-5) (Birtalan and Ghosh, 2001; Evdokimov *et al.*, 2002; Trame and McKay, 2003).

SycD - the Class II/translocator chaperone in *Yersinia*

The corresponding representative of Class II chaperones for the Ysc-Yop T3SS in *Yersinia enterocolitica* is SycD (LcrH in *Y. pestis* and *Y. pseudotuberculosis)*. Like SycT, SycD is a small, acidic protein (168 aa, 19 kDa, pI 4.9). SycD specifically chaperones the translocator proteins YopB and YopD (Wattiau *et al.*, 1994; Neyt and Cornelis, 1999) and prevents their premature, unproductive associations, especially as YopB is cytotoxic in the absence of the chaperone (Neyt and Cornelis, 1999). SycD was shown in a yeast two-hybrid system to bind to the YopD fragments 53-149 as well as to 278-292 near the C-terminus (Francis *et al.*, 2000). For YopB, no defined chaperone-binding domain could be detected (Neyt and Cornelis, 1999). SycD is furthermore involved in the modulation of the T3SS both *via* a negative regulation of *yop* gene expression (see above) and Yop secretion control (Day and Plano, 2000; Francis *et al.*, 2001; Anderson *et al.*, 2002). *Yersinia enterocolitica* biovar 1B possesses an additional, chromosomally encoded T3SS called Ysa, therefore exhibiting a second Class II chaperone, SycB (Foultier *et al.*, 2003). The phylogenetic relationship of *Y. enterocolitica* SycD and other T3SS Class II translocator chaperones indicates *Pseudomonas aeruginosa* PcrH to be the closest relative of SycD, sharing 58 % identical and 76 % similar amino acids. The sequence identity to other T3SS translocator chaperones is less than 23 % on average.

1.7 Aims of the thesis

At the beginning of this work, only few crystal structures of T3SS Class I chaperones, *Salmonella* SicP and SigE, *E. coli* CesT, and a single *Yersinia* effector chaperone, SycE, had been determined (Birtalan and Ghosh, 2001; Luo *et al.*, 2001; Stebbins and Galan, 2001; Evdokimov *et al.*, 2002; Trame and McKay, 2003). Regarding the effector/chaperone complexes, only chaperone-binding domains of the effector molecules but no full-length effector protein had been crystallized in complex with the cognate chaperone, such as *Salmonella* $SptP_{CBD}$/SicP (Stebbins and Galan, 2001) and *Yersinia* $YopE_{CBD}$/SycE (Birtalan *et al.*, 2002). In order to verify the hypothesis of a partial unfolding of the effector upon chaperone-binding, the crystal structure of a full-length effector/chaperone complex was of enormous interest.

One aim of this study was therefore to gain further insight into the T3SS effector/chaperone interactions by applying X-ray crystallographic and biochemical approaches to the *Y. enterocolitica* YopT/SycT complex. Prior to this work, Prof. Guy Cornelis (University of Basel, Switzerland) made the gift of the virulence plasmid pYVe227 of *Y. enterocolitica*, and Dr. Hartmut Niemann (Helmholtz-Zentrum für Infektionsforschung (HZI), Braunschweig) had generated a bicistronic *syc*T/*yop*T co-expression vector. The YopT/SycT complex produced using this construct and an existing protein production and purification protocol was reported to be instable and tended to aggregate (Büttner, 2003). The expression construct and the purification protocol was therefore to be optimized in order to obtain stable and homogeneous proteins suitable for crystallization trials.

T3SS Class II chaperones are involved in multiple functions and protein-protein interactions and represent therefore a highly interesting protein family. As no representative of Class II chaperones had been structurally characterized at that time, another aim of this thesis was the determination of the crystal structure of SycD, the representative of Class II chaperones in *Y. enterocolitica*. In order to analyze SycD by X-ray crystallography, procedures for the recombinant production, purification and crystallization were to be established.

2 Results

2I Characterization of the effector YopT and its cognate chaperone SycT

The full-length effector protein YopT (1-322) was reported to be intrinsically instable and significant soluble amounts could only be heterologously produced in *E. coli* by co-expression with its cognate chaperone SycT, thereby forming a double band together with a truncated YopT species (residues 14-322) (Büttner, 2003). This truncation might be due to autocatalytic activity or proteolytic cleavage by a bacterial host endopeptidase. In order to overcome degradation as well as the poor stability and expression level of YopT, several new approaches were therefore to be tested in this study. This included the generation of new expression constructs, expression analysis of a synthetic *yop*T gene, *in vitro* translation, protein refolding as well as the precise identification of the chaperone-binding domain in order to allow co-expression with the chaperone.

2I.1 Strategies to improve the stability of YopT

2I.1.1 Expression test analysis of new *yop*T and *yop*T/*syc*T constructs

The generation of new *yopT* (*yop*T/*syc*T) expression constructs is elaborated in Table 2I-1.

Table 2I-1. Rationale for the generation of new *yopT* (and *yop*T/*syc*T) expression constructs

	Approach	Rationale
1	*yop*T S13A	Cleavage site mutant, forestalling the double band formation
2	*yop*TΔ13/Δ22/Δ40/Δ49	Systematic N-terminal YopT deletion mutants, compare also section 2I.1.2, still able to bind to the chaperone SycT; forestalling the double band formation
3	Auto-inducing medium	Retarded protein production, promotes correct protein folding
4	*yop*T75-318	N-terminal His_6- and GST-fusions of the postulated minimal enzymatically active core fragment (YopT residues 75-318) (Sorg *et al.*, 2003)
5	s*yop*T	Synthetic *yop*T effector gene with optimized codon usage for expression in *E. coli*, gene product sYopT has the identical amino acid sequence as YopT
6	*yop*T C139S	Inactive YopT mutants with the catalytic cysteine replaced with serine (C139S) in order to verify whether YopT possesses an autocatalytic protease activity and in respect of intended effector/substrate binding studies (see section 2I.2)
7	GL-s*yop*T /TG1	According to a report describing a promising expression system for YopT using *E. coli* TG1 cells in combination with an N-terminal glycine-rich 12 amino acid linker (GL, amino acid sequence SPGISGGGGGSMAGGGRT) (Sorg *et al.*, 2003)
8	+ *cpn*10/*cpn*60	Gene expression at low temperatures (10 °C) using archeal chaperonins Cpn10 and Cpn60 from *Oleispira antarctica* (Ferrer *et al.*, 2003) in order to enhance accurate folding and solubility of YopT

A summary of the expression experiments is provided in the Appendix (Table B1). Without simultaneous chaperone expression, no soluble YopT could be obtained. Interestingly, low temperatures rather provoked overexpression of one of the cold-adapted chaperonins (Cpn60) (not shown). Considerable amounts of soluble protein were only observed for complexes YopTΔ49 (C139S)/SycT and YopTΔ50 (C139S)/SycT. YopTΔ49 (C139S)/SycT was therefore chosen for large scale protein preparation. In contrast to the study of Locher *et al.* (2005), the inactive YopT mutant did not show a diminished binding to SycT (Figure 2I-1A). As expected, N-terminally truncated YopT lacking the internal putative truncation site S13/N14 showed only a single effector band in SDS-PAGE analysis (Figure 2I-1A). However, YopT from the inactive YopTΔ49 C139S / SycT complex gradually degraded as seen for the effector from the wild-type YopT/SycT complex (Figure 2I-1B). This observation excluded an autocatalytic effect. The persistent inhomogeneity still impeded successful protein crystallization.

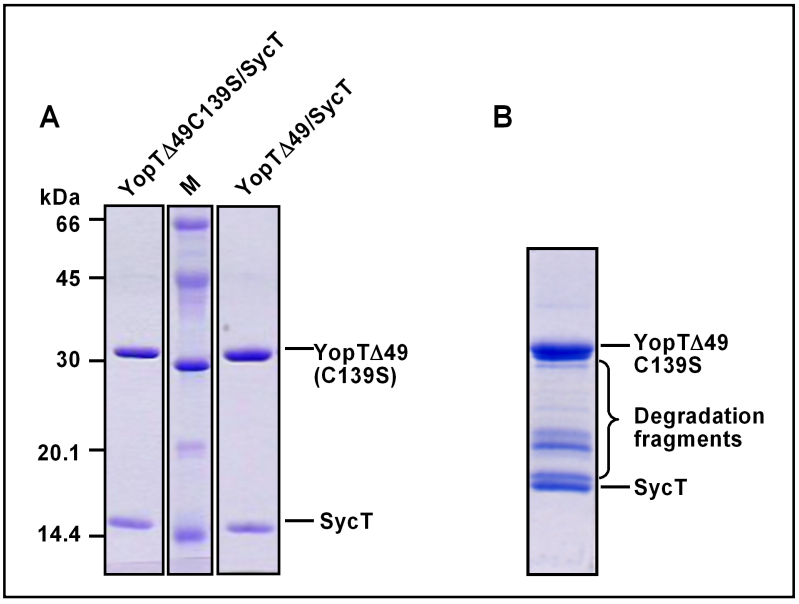

Figure 2I-1. Stability of YopTΔ49 C139S / SycT and YopTΔ49 / SycT complexes. **(A)** YopTΔ49 C139S/ SycT and YopTΔ49/ SycT after NiNTA agarose affinity chromatography. Both complexes were produced and purified in comparable amounts with a similar apparent effector/chaperone ratio. **(B)** Degradation of inactive YopT Δ49C139S / SycT still occured and was not caused by autocatalysis. Sample stored over two weeks at 4 °C. (15 % SDS-PAGEs, Coomassie staining).

2I.1.2 *In vitro* translation of YopT deletion mutants

As an alternative approach, the folding reporter molecule GFP (Waldo *et al.*, 1999) was employed as a protein tag for monitoring the production of soluble (i.e. correctly folded) YopT. However, full-length wild-type sYopT C-terminally fused to GFP proved insoluble in expression tests. Despite the faint fluorescence in the soluble fractions, SDS-PAGE, N-terminal sequencing and Western blot analysis using an α-GFP antibody detected only insoluble fusion protein (Figure 2I-2A,B).

Systematic N-terminal deletion mutants of sYopT (Δ16/Δ24/Δ40/Δ49/Δ65/Δ74) C-terminally fused to GFP were tested for *in vitro* translation using the Rapid Translation System. Only insoluble fusion proteins were detected, whereas soluble GFP was readily produced (Figure 2I-2 C,D).

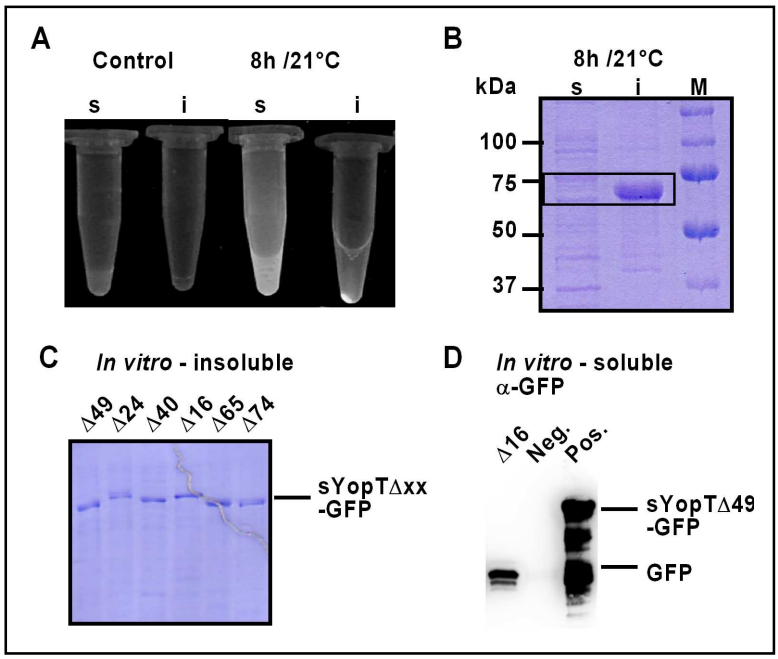

Figure 2I-2. Expression test of pETM-11GFPfus_s*yop*T N-terminal deletion mutants. (A) GFP fluorescence, at 395 nm UV-excitation, of the uninduced cells and of an aliquot taken 8 h after induction of the s*yop*T-GFP expression at 21 °C. Both samples were separated into soluble (s) and insoluble (i) fraction. **(B)** Only insoluble sYopT-GFP-fusion protein could be detected by SDS-PAGE (Coomassie staining). **(C)** 12 % SDS-PAGE of the insoluble *in vitro* translation samples of sYopTΔxx-GFP deletion mutants (Coomassie staining). **(D)** Western blot of soluble *in vitro* fraction of sYopTΔ16-GFP. Neg., negative control (YopT/SycT); Pos., positive control (solubilized insoluble sYopTΔ49-GFP).

2I.1.3 Refolding of YopT

Using heterologous gene expression in *E. coli*, only marginal amounts of soluble YopT fusion protein were detected. In contrast, insoluble YopT fusion proteins as well as the untagged effector could be readily produced in large quantities forming inclusion bodies (Büttner, 2003 and above). This vast resource of YopT was therefore exploited by refolding experiments in order to obtain soluble protein (data not shown). Renaturation of the effector from solubilized inclusion bodies did not yield significant amounts of soluble YopT that was stable over time. Several methods have been applied including rapid dilution, dialysis and on-column refolding. Addition of stabilizing agents such as L-arginine, polyethylene glycol, detergents or the presence of the cognate chaperone SycT did not help either. Most protein precipitated during renaturation. In comparison to the amounts of protein solubilized/denatured from inclusion bodies used in the refolding experiments, only very little soluble effector was detected after refolding with SycT or detergent-assisted renaturation on-column. However, immediate degradation of the reconstituted YopT suggested an non-native conformation.

2I.1.4 Follow-up investigations of the chaperone-binding site in YopT

Production of the YopT/SycT complex and preliminary characterization of the chaperone-binding domain (CBD) in YopT by limited proteolysis of the YopT/SycT complex has been described previously (Büttner, 2003). The CBD has been limited at least to a region of 72 residues (YopT 52-104) extending to residue 140 as determined by fingerprinting of cleavage sites. In case of a stable, protease resistant CBD in YopT, this region is supposed to result in a distinct fragment of at least 6.2 kDa and of significant amount that should be large enough to be visualized by polyacrylamide gel electrophoresis. To characterize the CBD in more detail, the YopT/SycT complex was subjected to a second limited proteolysis, this time using endopeptidase Lys-C and thermolysin. The fragments were analyzed by 16 % Tris/Tricine gels (Figure 2I-3) better suited for separation of oligopeptides than the Tris/Glycine system used previously. The most promising fragment accumulating in considerable amounts was running at the same level as SycT (Figure 2I-3, box 3, ~10 kDa). Bands of interest were analyzed by N-terminal sequencing.

SycT resisted proteolytic degradation with the exception of eight C-terminal residues as previously determined (Büttner, 2003). YopT positions 50 and 51, respectively, as well as residue 122 were found to be recurring N-termini of YopT fragments. This gave rise to new co-expression constructs coding for the putative $YopT_{CBD}$ and SycT. For this, *yop*T codons encompassing residues 52-104 as previously determined, as well as the codons for residues 50-121 and 50-139 were cloned into the expression vector pETM-30-IRES_*syc*T.

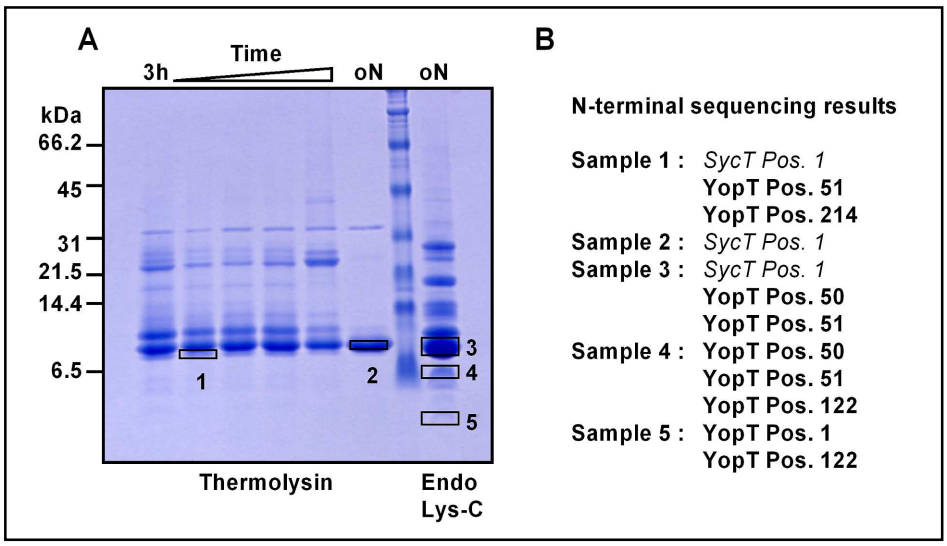

Figure 2I-3. Limited proteolysis of YopT/SycT with endopeptidase Lys-C and thermolysin. (A) Aliquots were taken during the course of the digest and separated by 16 % Tris/Tricine gels (Coomassie staining). Boxed fragments 1-5 were analyzed by N-terminal sequencing. oN, over night. **(B)** N-terminal sequencing detected mixtures of fragments originating from the chaperone and from YopT.

However, carrying out co-expression analyses of these three $YopT_{CBD}$ constructs together with SycT, the $YopT_{CBD}$ oligopeptide could not be detected using Tris/Tricine gel electrophoresis (Figure 2I-4). The different constructs for $YopT_{CBD}$ could not be produced as soluble oligopeptides even in the presence of SycT. The YopT/SycT complex was therefore digested by endopeptidase Lys-C in a preparative scale and the fragments were separated by size exclusion chromatography. However, no distinct peak comprising the complex of SycT bound to a 6-11 kDa fragment corresponding to the chaperone-binding domain of YopT was observed (not shown).

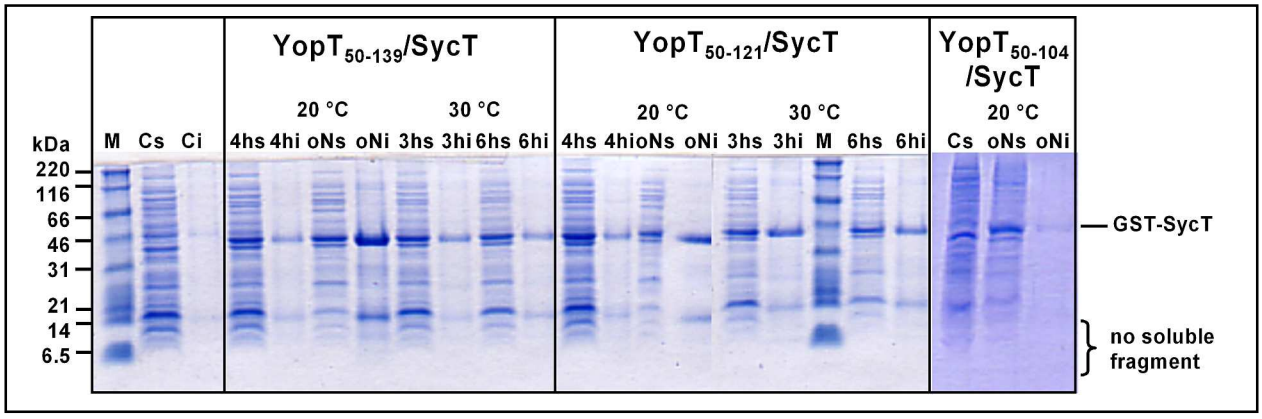

Figure 2I-4. 16 % Tris/Tricine gel of the co-expression test for $YopT_{CBD}$/SycT complexes $YopT_{52-104}$/SycT, $YopT_{50-121}$/SycT and $YopT_{50-139}$/SycT. (Coomassie staining). Samples were taken after 3 h, 6 h and over night (oN) induction at 20 °C, after 4 h when incubated at 30 °C. M, Marker proteins; C, control of uninduced cells; s, soluble; i, insoluble fraction.

2I.1.5 Summary of the attempts to improve the YopT stability

Overall, the different approaches used in order to increase the long-term stability of YopT and the YopT/SycT complex had failed. Furthermore, no isolated stable effector YopT could be obtained. As to the YopT/SycT complex, the expression system for the production of sufficient amounts of several complex variants such as YopTΔ49/SycT and YopTΔ50/SycT and their inactive variants could be established. Still, the effector in these purified complex variants was not stable over time. Attempts aiming at the isolation of a fragment of YopT or the YopT/SycT complex for crystallization were finally abandoned. However, this instability did not exclude rapid analyses techniques if performed subsequently to the YopT/SycT complex purification. Thus, binding studies of freshly prepared YopT/SycT complexes with the YopT substrate RhoA using rapid surface plasmon resonance spectrometry were conducted (see below). Additionally, as the crystal structure of YopT, either alone or in complex with SycT, was not feasible, three-dimensional modeling was applied in order to obtain an estimated structural impression of YopT (section 2I.3).

2I.2 Binding studies between the YopT/SycT complex and RhoA

YopT substrates are small Rho GTPases, preferentially RhoA, that are post-translationally modified at their C-terminal CaaX box cysteine by a lipid (prenyl) moiety. *In vivo*, the lipid modification requires three steps: Geranylgeranylation, proteolysis and methylation (Figure 2I-5A). The last 10 residues in posttranslationally processed RhoA (residues 181-190), with geranylgeranylated {C_{20} unit} or farnesylated {C_{15} unit} Cys190, are sufficient for YopT binding and proteolytic activity (Shao *et al.*, 2003). To investigate whether YopT binds to a RhoA peptide lacking the carboxy methylester and the lipid modification, different RhoA peptides were synthesized (W. Tegge; HZI Braunschweig), which exhibit a biotin tag for use in surface plasmon resonance (SPR) spectroscopy. Peptide synthesis proved difficult, especially the purification step by HPLC, probably due to the polybasic sequence upstream of Cys190 (Figure 2I-5B, blue). Two additional β-alanine residues were therefore inserted between the biotin tag and the RhoA sequence (peptide 1, Figure 2I-5B) without much success.

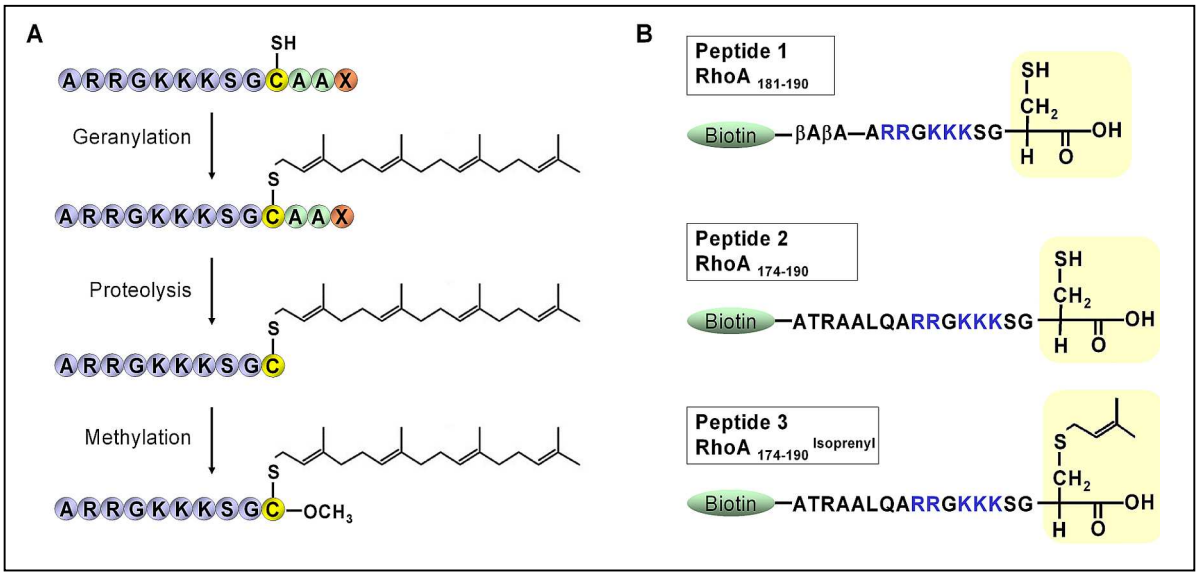

Figure 2I-5. YopT substrate RhoA-GTPase. **(A)** C-terminal RhoA residues 181-193 with the CaaX box (C, cysteine; A, aliphatic residue; X any residue). RhoA CaaX box residues: CLVL. Geranylgeranylation of RhoA *in vivo* encompasses the lipid modification at the thiol group of the CaaX box cysteine, proteolytic removal of the three C-terminal residues and methylation resulting in a C-terminal carboxy methylester. **(B)** Synthesized RhoA-Peptides with an N-terminal biotin-tag. The C-terminal Cys190 is shaded in yellow. The polybasic sequence upstream of the cysteine is highlighted in blue. Two additional β-alanines (βA) served as spacer in peptide 1. Facilitated peptide synthesis was achieved by sequence extension (RhoA 174-190 in peptides 2 and 3). Peptide 3 exhibits low-prenylation (isoprenyl group).

As a geranylgeranylated or farnesylated peptide is insoluble in aqueous solutions and since the synthesis of the fully modified peptide was not feasible, the RhoA peptide was provided

with one isoprenyl moiety only (low-prenylation, C_5 unit) (peptide 3). The extension of the RhoA sequence ($RhoA_{174-190}$) successfully facilitated peptide synthesis and purification. Since no soluble YopT was available, (freshly produced and purified) YopT/SycT complex was used for SPR binding studies as several effector/chaperone complexes have been reported to exhibit full enzymatic activity of the chaperone-bound effector such as YopE/SycE (Birtalan *et al.*, 2002) and YopH/SycH (Neumayer *et al.*, 2004). In order to rule out difficulties in signal detection due to the cleavage of the RhoA peptide by YopT, the inactive complex YopTΔ49 C139S /SycT was also tested for binding. Neither YopT/SycT flushed over peptide 1 nor YopTΔ49 C139S /SycT over peptides 2 and 3 caused a detectable response signal even after increasing the protein concentration (8-16 μM). The missing response signal indicates that the effector/chaperone complexes did not bind to the synthesized RhoA peptides.

2I.3 Modeling of the YopT structure

Several approaches to produce stable, soluble YopT had failed and co-crystallization of YopT variants with its chaperone SycT did not yield crystals. Meanwhile, the crystal structure of the YopT homolog AvrPphB of the plant pathogen *Pseudomonas syringae* pv. *phaseolicola* had been solved (Uniprot Q9FE20, PDB entry 1UKF) (Zhu *et al.*, 2004). Although AvrPphB shares only low sequence homology with YopT (26 % identity, 56 % similar), both possess the invariant catalytic triad C/H/D and are expected to fold in a manner similar to the cysteine protease papain as derived from sequence analysis. Therefore, the YopT sequence (residues 118-316) was modeled onto the crystal structure of AvrPphB (residues 81–267) using the program BRAGI (Reichelt *et al.*, 2005). The papain-like fold of the modeled cysteine protease YopT in comparison with the crystal structure of papain is visualized in Figure 2I-6. Similar to papain, YopT_AvrPphB shares the central antiparallel β-sheet and α-helices.

Pairwise structure alignment of the YopT model and papain using DALI stated 15 % sequence identity with a Z-score of 4.8 for 111 aligned residues. The YopT_AvrPphB model exhibits secondary structure elements for a larger part of the protein, and additionally displays shorter loops and turns, therefore appearing more compact than loop-rich papain. The catalytic triads of the YopT model and papain superpose well for a central α-helix and catalytic Cys139 of YopT and Cys25 of papain, as well as for the catalytic histidine (His258/His159). Superposition of the third catalytic residue, Asp274 in YopT and the

corresponding Asn175 in papain, reveals a larger deviation (Figure 2I-6). The loop involved in formation of the S2 substrate-binding site of papain-like proteases comprises 23 residues in papain but constitutes only a three-residue turn in the YopT model, thus possibly contributing to substrate specificity.

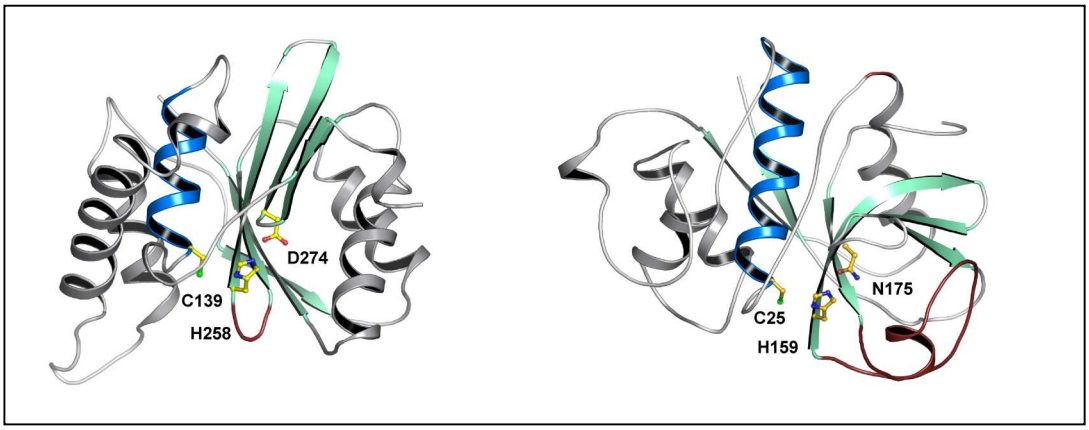

Figure 2I-6. Structural model of YopT(118-316) (left) and crystal structure of papain* (1PPP) (right). The YopT amino acid sequence was modeled based on the crystal structure of AvrPphB from *Pseudomonas syringae* (1UKF). The catalytic triads (YopT Cys139/His258/Asp274, papain Cys25/His159/Asn175) are depicted as yellow ball-and-stick models. Structurally conserved helices and β-strands are colored in blue and green, respectively. The loop involved in substrate binding *via* the S2 site is colored red and differs considerably in length. Molecules were aligned based on the superposition of Cα atoms of the catalytic residues and the central blue α-helix. *Note: Compared to YopT_AvrPphB, papain exhibits few secondary structure elements. This is an intrinsic feature of papain, as all, even high-resolution structures solved in the recent past exhibit the same loop-rich fold (e.g. 1KHQ, 1.6 Å, Janowski *et al.*, 2004).

2I.4 Biochemical characterization of SycT

As the X-ray crystallographic analysis of the effector YopT was not feasible, the focus of the project was therefore shifted to the structure elucidation of the YopT chaperone SycT. One aim was to verify the validity of the Class I chaperone fold with regard to different effector chaperones from the same species (i.e. in comparison to *Yersinia* SycE).

2I.4.1 Generation of *syc*T expression constructs

Full-length SycT (residues 1-130) was heterologously produced in *E. coli* BL21(DE3) CodonPlus cells as N-terminal GST-fusion protein. Wild-type SycT degraded into a C-terminally truncated fragment (SycT residues 1-122) during long-term storage at 4 °C as noted earlier (Büttner, 2003). A second expression construct encompassing SycT residues 1-122 was therefore created by cloning the corresponding *syc*T sequence into the same expression vector (pETM-30).

2I.4.2 Gene expression and protein purification of SycT

Fusion proteins GST-SycT and selenomethionine (SeMet)-labeled GST-$SycT_{1-122}$ were produced as soluble proteins in high amounts according to an existing purification protocol (Büttner, 2003). Substitution of selenomethionine for the amino acid methionine introduces heavy atoms/anomalously scattering atoms that are located at special sites throughout the protein and later in the protein crystal. The resulting anomalous portion in the diffraction pattern allows the direct determination of the phases of the X-ray reflections (see Materials and Methods section 5.14.4), thereby facilitating structure solution.

Proteins were purified by glutathione sepharose affinity chromatography. The GST tag was cleaved on-column with His_6-tagged TEV-protease and the protease was removed by NiNTA agarose re-chromatography of the cleavage supernatant (Figure 2I-7A, isolation of SeMet $SycT_{1-122}$).

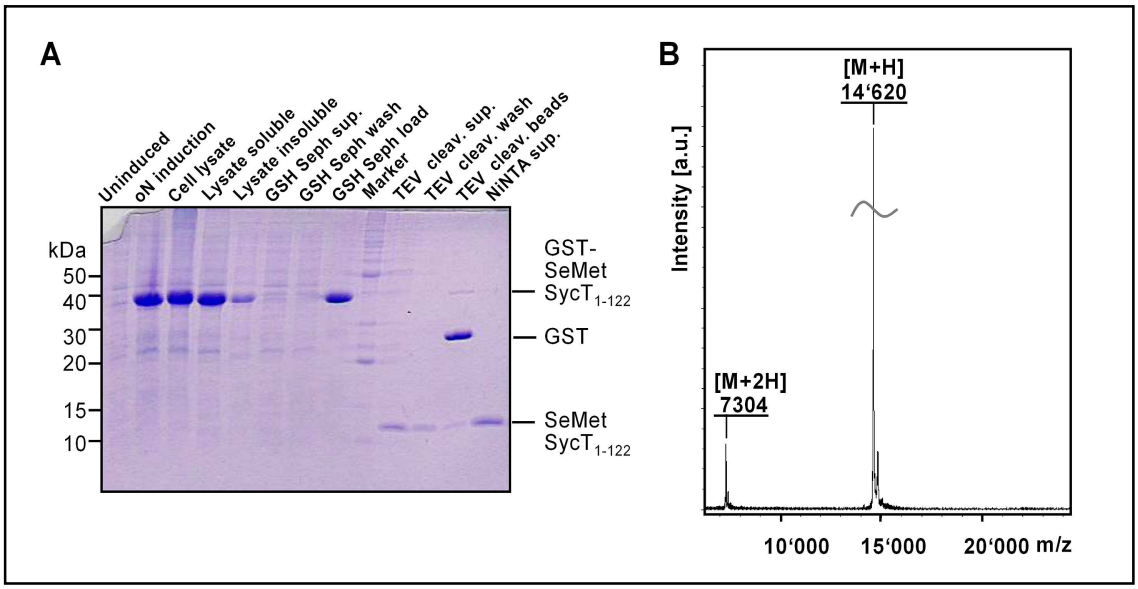

Figure 2I-7. Purification of SeMet $SycT_{1-122}$. (A) 15 % SDS-PAGE (Coomassie staining) of SeMet GST-$SycT_{1-122}$ production and target isolation *via* glutathione sepharose affinity chromatography and TEV protease cleavage (TEV cleav.), followed by NiNTA agarose affinity chromatography. Sup., supernatant. **(B)** MALDI-TOF-MS spectrum of purified SeMet $SycT_{1-122}$. [M+H] indicates the singly-charged species, [M+2H] the doubly-charged ion. Minor mass peaks at larger masses are due to matrix adducts. The calculated molecular mass of completely selenomethionine-labeled $SycT_{1-122}$ is 14’625 kDa.

Due to restriction sites used in cloning and the protease cleavage site, TEV cleaved proteins exhibit a glycine residue inserted after the start methionine as well as two additional residues at the N-terminus (glycine-alanine). The target proteins were further purified by anion exchange chromatography. Peak fractions containing pure SycT or SeMet $SycT_{1-122}$ were pooled and applied to size exclusion chromatography (SEC) as a final purification step. Prior to crystallization trials, purified protein (yield ~14 mg per liter cell culture) was dialyzed to

decrease the salt concentration. MALDI-TOF-MS analysis verified the complete selenomethionine incorporation in SeMet $SycT_{1-122}$ (Figure 2I-7B). Purified SycT as well as SeMet $SycT_{1-122}$ showed a very high grade of purity since no further protein bands could be detected in Coomassie-stained SDS polyacrylamide gels.

2I.4.3 SycT forms homodimers in solution

The formation of full-length SycT homodimers was shown previously by analytical size exclusion chromatography (Büttner, 2003). Investigation by dynamic light scattering (DLS) confirms the results from chromatography (Table 2I-2). The obtained values for the molecular mass correspond to the dimeric species ($M_{r\,DLS}$ ~34 kDa, $M_{r\,SEC}$ ~30 kDa, $M_{r\,theo}$ monomer= 15.3 kDa). As expected, selenomethionine-labeled $SycT_{1-122}$ ($M_{r\,theo}$ = 14.6 kDa), behaves as a dimer during size exclusion chromatography ($M_{r\,SEC}$ = 28 kDa) (Figure 2I-8).

Table 2I-2. Dynamic light scattering of wild-type SycT.

Protein	r_H [nm]	$M_{r\,DLS}$ [kDa]	Polydispersity [%]	Base line	SOS error
SycT	2.77	34	19.1	1.002	2.38

The theoretical molecular mass for full-length SycT is 15.3 kDa. The data represent the best correlation using a monomodal analysis model. Protein concentration was ~10 mg/mL.

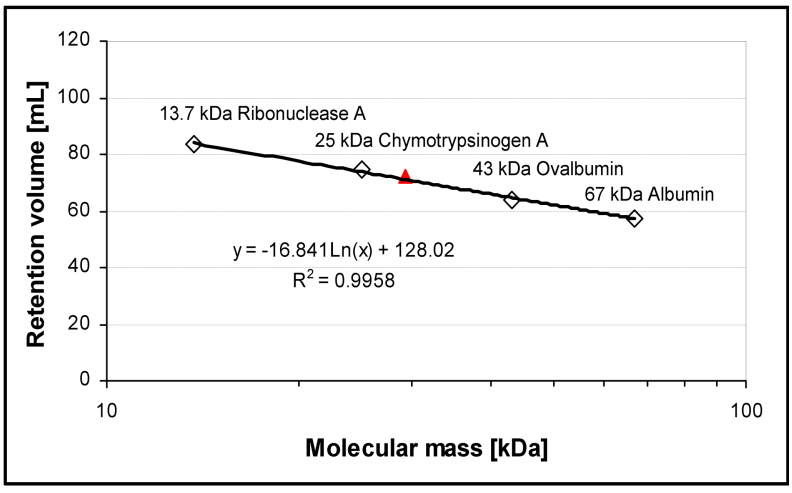

Figure 2I-8. Analytical size exclusion chromatography of SeMet $SycT_{1-122}$. Superdex 75 XK 16/60 column, running buffer 10 mM Tris pH 8.0, 200 mM NaCl, 1 mM DTT. RT, retention volume. Proteins used as calibration standards are specified as well as calibration function and reliability factor. SeMet $SycT_{1-122}$ (RT= 72.16 mL, $M_{r\,SEC}$ = 28 kDa, $M_{r\,theo}$= 14.6 kDa) is indicated as red triangle. As observed for wt SycT, the truncated variant forms dimers in solution.

2I.5 Crystallization of SycT

2I.5.1 Wild-type SycT

Purified full-length SycT could easily be concentrated to final concentrations of more than 10 mg/mL still being monodisperse. Initial screening in 96-well format using sitting drop

vapor diffusion at 4 and 20 °C failed to yield crystals. Several initial conditions presumably showing microcrystalline/birefringent precipitate or phase separation were chosen for optimization (hanging drop vapor diffusion, 24-well format) *via* altering the precipitant concentrations. Finally, one of these optimization attempts resulted in the formation of plate-like, monoclinic crystals (Figure 2I-9) with a powerful diffraction potential.

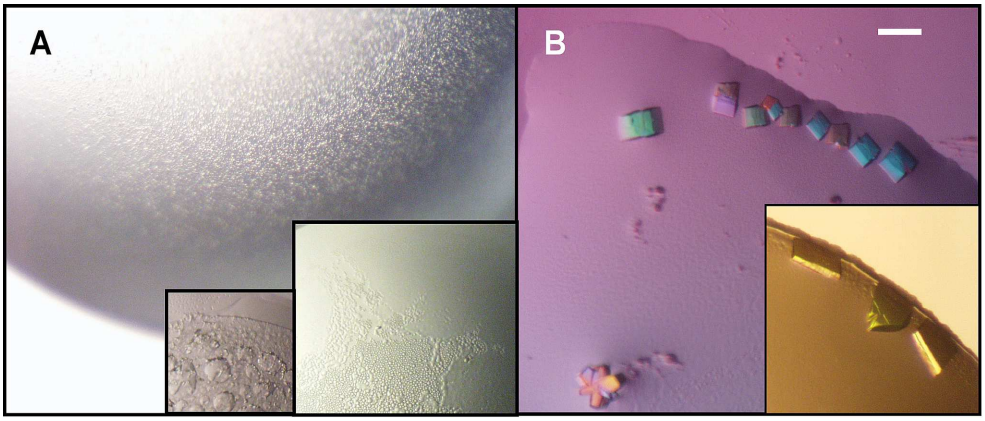

Figure 2I-9. Crystallization of full-length SycT. **(A)** Initial screening for crystallization conditions of native SycT resulted only in micro-crystalline/birefringent precipitate or phase separation (insets). Optimization of these conditions finally yielded monoclinic crystals **(B)** that could be further increased in size (inset). Scale bar = 100 µm.

2I.5.2 Selenomethionine-labeled SycT$_{1\text{-}122}$

Initial screening for SeMet SycT$_{1\text{-}122}$ crystals at 4 °C produced orthorhombic crystal in a single condition that was based on ammonium sulfate (Figure 2I-10A). Since these crystals were clustered and resisted optimization, a second crystal form was aimed at. The alteration of the crystallization cocktail by changing the buffer system and a salt component resulted in single crystals (Figure 2I-10B). Both crystal forms were analyzed by X-ray diffraction.

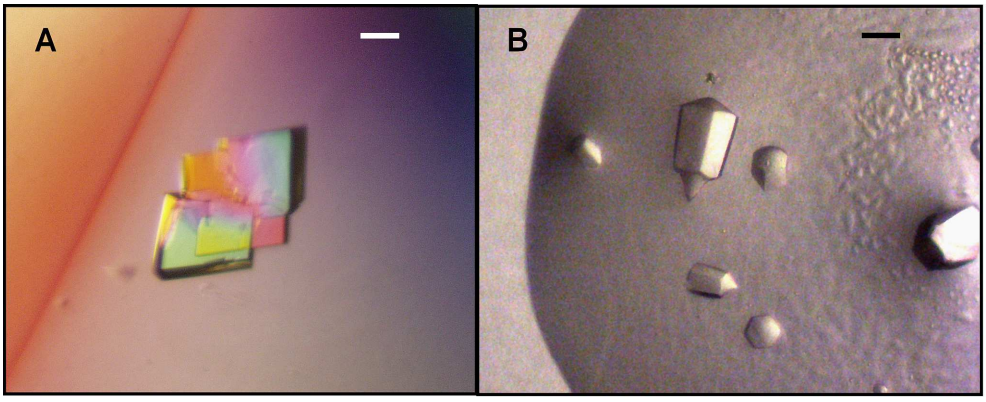

Figure 2I-10. Crystallization of selenomethionine-labeled SycT$_{1\text{-}122}$. (A) Initial screening yielded orthorhombic crystals that where clustered (crystal form 1). **(B)** Changing only the buffer system of the crystallization condition from A yielded single crystals of a second, "sunflower grain"-shaped hexagonal crystal form (crystal form 2). Scale bar = 100 µm.

2I.6 Structure determination of SycT

X-ray diffraction analysis disclosed that native SycT crystallized in monoclinic space group $P2_1$. Selenomethionine-labeled, truncated $SycT_{1-122}$ crystallized in two unrelated crystal forms: Crystal form 1 possessed an orthorhombic space group ($P2_12_12_1$), whereas crystal form 2 exhibited a hexagonal crystal lattice. For crystal form 2, the systematic absence of reflections with indices $\ell \neq 3n$ (n=integer) along the crystallographic ℓ axis indicated a screw axis along this axis and limited the possible space groups to the two enantiomorphs $P6_2$ or $P6_4$. Matthews probability analysis (Matthews, 1968; Kantardjieff and Rupp, 2003) suggested for the native and the two SeMet crystal forms two molecules per asymmetric unit (V_M = 2.1-2.3 $Å^3$ Da^{-1}). The low solvent content of 41 % for $SycT_{1-122}$ crystal form 1 indicated further a dense packing of the molecules in the crystal.

Phasing of the native SycT data set by molecular replacement (MR) using the crystal structures of other T3SS Class I chaperones (compare Introduction Figure 1-5 and Discussion Figure 3I-1) as search models and maximum-likelihood as well as Patterson function-based algorithms surprisingly failed. In order to phase the SycT data experimentally, heavy atom derivatization by crystal soaking was employed. Soaking native SycT crystals with mercury, platinum, osmium or bromide caused crystal cracking, loss of diffraction or the crystals did not incorporate the heavy atom. In contrast, the anomalous signal of the SeMet-labeled $SycT_{1-122}$ crystals could eventually be exploited in a multiple-wavelength dispersion (MAD) experiment. The presence of the anomalously scattering atoms was verified by a selenium fluorescence energy scan. In order to maximize the absorption and dispersive effects, three data sets were collected at the peak, inflection point and high energy remote wavelengths of the absorption curve. As the data sets were collected from the same crystal, the non-isomorphism was nearly zero. However, the anomalous signal of SeMet $SycT_{1-122}$ crystal form 2 deteriorated upon inclusion of one or two additional wavelengths (inflection or high energy remote) of the MAD experiment. Eventually, single-wavelength anomalous dispersion (SAD) allowed phasing of the peak data set for SeMet $SycT_{1-122}$ crystal form 2 using the five selenium sites identified by SHELXD (Schneider and Sheldrick, 2002), with six selenium sites being possible per asymmetric unit. Density modification finally revealed space group $P6_2$ to be correct for crystal form 2 and provided excellent initial electron density (Figure 2I-11) suitable for automated and manual model building. The anomalous signal-to-noise ratio of 1.08 for crystal form 1 was considerably lower than the ratio for crystal form 2 (1.33) and did not suffice for phasing.

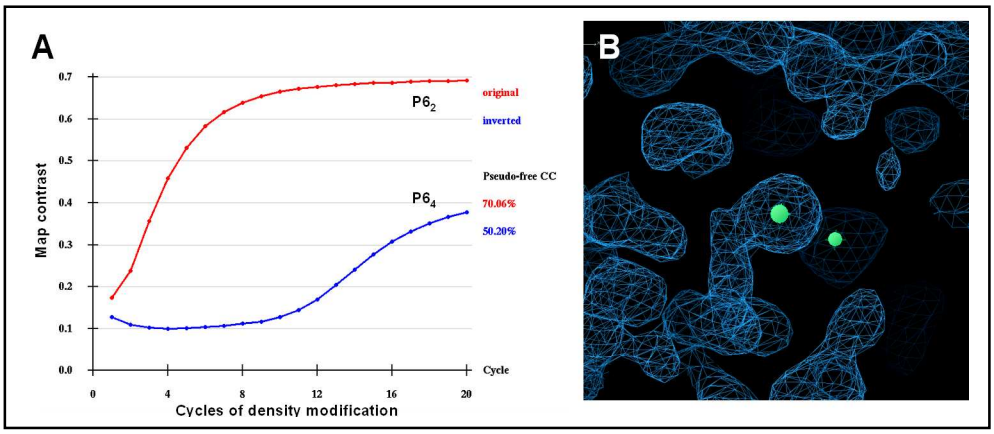

Figure 2I-11. Selenium-SAD phasing of SycT$_{1-122}$ crystal form 2. (A) After phasing using the selenium substructure found in SHELXD, density modification in SHELXE (Sheldrick, 2002) was carried out for both enantiomorph space groups P6$_2$ and P6$_4$. With increasing cycles of density modification, the large difference in the map contrast between the two substructure enantiomorphs together with the high correlation (observed heavy atom structure factors compared to the ones calculated for the selenium substructure model) showing a Pseudo-free correlation coefficient of 69.2 % indicated a correct solution and the original enantiomorph with space group P6$_2$ to be correct. **(B)** The initial electron density map after density modification showed well-defined density, here for a selenomethionine. Selenium atoms are depicted as green spheres.

The complete structural model of SycT$_{1-122}$ crystal form 2, refined to 1.9 Å, was later used to solve the structure of crystal form 1 to 2.0 Å resolution by molecular replacement. Both superposed models (from crystal form 1 and 2) were used as MR search ensemble to finally solve the structure of native SycT to high resolution (1.8 Å).

In all three crystal forms, the asymmetric unit harbors two molecules forming a homodimer due to non-crystallographic two-fold rotational symmetry. The three crystal structures are very similar showing deviations only at the flexible N- and C-terminus and the exceptional region 16-28 in one of the monomers of the native SycT structure. The structure of SycT$_{1-122}$ crystal form 2 compared to native SycT shows an r.m.s.d. of 0.75 Å for 206 common Cα-atoms, and SycT$_{1-122}$ crystal form 1 *vs.* native SycT differs by 0.85 Å for 195 common Cα-atoms. SycT$_{1-122}$ crystal form 1 and 2 are very similar (r.m.s.d. 0.5 Å, 199 Cα-atoms) and the two monomers superpose well with an r.m.s.d. of 0.6 Å (crystal form 1) and 0.7 Å (crystal form 2), respectively.

Electron density was visible for SycT$_{1-122}$ residues 1-113 in monomer A, and 3-122 in monomer B of the refined model of crystal form 2. In the model of crystal form 1, the C-terminal residues 115-122 for both monomers could not be observed in the electron density. The model of native SycT comprises residues 3-130 (A), 2-117 and 125-130 (B). The data processing and refinement statistics are given in Table 2I-3.

Table 2I-3. Data processing and refinement statistics for SycT.

	Native SycT	$SycT_{1-122}$		
		Crystal form 1	Crystal form 2	
Data collection				
Space group	$P2_1$	$P2_12_12_1$	$P6_2$	
Unit cell dimensions [Å], [°]	a= 34.1, b= 79.6, c= 52.1 $\alpha=\gamma=90$, $\beta=101.21$	a= 51.5, b= 63.1, c= 74.4 $\alpha=\beta=\gamma=90$	a=b= 92.0, c= 55.4 $\alpha=\beta=90$, $\gamma=120$	
Dataset		Peak	Peak	Inflection point	High energy remote
Wavelength [Å]	1.05	0.9795	0.97957	0.979760	0.911650
Resolution [Å]	79.5 - 1.83 (1.86 - 1.83)	48.1 - 2.0 (2.1 - 2.0)	79.0 - 1.9 (2.0 - 1.9)	20 - 3.5 (3.6 - 3.5)	20 - 2.3 (2.4 - 2.3)
Mosaicity [°]	0.5	0.25	0.14	0.14	0.14
Completeness [%]	97.6 (83.5)	98.4 (96.4)	99.5 (96.4)	99.4 (100)	99.7 (100)
(Anomalous) redundancy	2.8	3.9	5.8	5.8	5.8
Observations	65'888	118'050	237'251	38'286	135'842
Unique reflections	23’529	16’331	21’134	6587	23’360
I/σ [I]	14.8 (2.1)	12.3 (4.6)	16.6 (5.4)	33.2 (30.2)	34.7 (23.0)
$R_{sym,}$ R_{meas}	5.6 (31.6) [a]	8.0 (37.3) [b]	7.2 (39.8) [b]	4.8 (5.2) [b]	4.1 (7.3) [b]
Phasing	Molecular replacement	Molecular replacement	SAD (selenium)	-	-
Anomalous signal-to-noise ratio	-	-	1.33 (1.1)	1.08 (1.10)	1.14 (1.17)
Number of sites			5		
Molecules per asymmetric unit	2	2	2		
Solvent content [%]	46	41	45		
Refinement					
R / R_{free} [c] [%]	18.4 / 23.3	21.9 / 28.4	19.6 / 23.6		
Number of atoms Protein/Solvent	2131 / 168	1950 / 123	1908 / 139		
R.m.s. deviation					
Bonds [Å] /Angles [°]	0.015 / 1.5	0.018 / 1.85	0.019 / 1.98		
Ramachandran Plot					
Residues in allowed / additionally allowed / generously allowed regions [%]	94.1 / 5.9 / 0.0	86.1 / 13.5 / 0.5	88.2 / 10.4 / 1.4		
Residues in disallowed regions	0	0	0		
B factor [$Å^2$] average / Wilson B	28.2 / 28.5	20.6 / 31.6	32.2 / 32.1		
Protein / Solvent	27.8 / 33.8	21.0 / 26.2	31.0 / 40.5		
Protein data bank accession code	2BSJ	2BSI	2BSH		

Values in parentheses are for the highest resolution shell. [a] $R_{sym} = 100\ \Sigma_n\ (\Sigma_i\ |I_i - \hat{I}|)/\ \Sigma_n\ (\Sigma I_i)$; [b] $R_{meas} = 100\ n\ \Sigma_I\ |\hat{I} - I_i|\ /\Sigma_{hkl}\ (n-1)\ \Sigma_i I_i$, where $\hat{I}$ is the mean intensity of symmetry-related reflections (Diederichs and Karplus, 1997); [c] $R = 100\ \Sigma_{hkl}\ |F_{obs} - F_{calc}|\ /\ \Sigma_{hkl}\ F_{obs}$. Test set size 5 %.

2I.7 Structural analysis of SycT

2I.7.1 Structural overview of SycT

The SycT monomer exhibits a twisted anti-parallel, six-stranded β-sheet flanked on one side by two α-helices (Figure 2I-12, $SycT_{1-122}$ crystal form 2) sharing most features of the globular fold common to other T3SS effector-chaperones (see chapter Discussion Figure 3I-1).

SycT shows only low sequence identity (9-22 %) to other T3SS effector chaperones, but a low r.m.s.d. of < 2.7 Å for common Cα-atoms (79 to 109 aligned residues) compared to structures of SicP and SigE from *Salmonella* ssp. (Luo *et al.*, 2001; Stebbins and Galan, 2001), SycE and SycH from *Yersinia* ssp. (Birtalan and Ghosh, 2001; Evdokimov *et al.*, 2002; Trame and McKay, 2003; Phan *et al.*, 2004), CesT from enterohemorrhagic *E. coli* EHEC (Luo *et al.*, 2001) and AvrPphF Orf1 from plant-pathogenic *Pseudomonas syringae* pv. *phaseolicola* (Singer *et al.*, 2004). SycT shares the highest sequence identity with the structurally uncharacterized Orf1 from *Pseudomonas aeruginosa* (abbreviated as SpcS) believed to be the T3SS chaperone of ExoS (Frithz-Lindsten *et al.*, 1997)(Figure 2I-13).

Despite the overall similarity of the fold to other T3SS effector chaperones, SycT exhibits several unique and distinct characteristics. The depression between the N-terminal α-helices α1 and the adjoining loops L4 and L6, typical for other effector chaperones, is less distinct in the SycT dimer (Figure 2I-12). In contrast, the groove between both loops L5 on the opposite dimer face is more pronounced. Additionally, helices α3 point with their C-terminal ends further outwards compared to other effector chaperones where these helices taper resulting in a rejuvenating dimer shape (compare Discussion section Figure 3I-1).

The dimerization interface in SycT encompasses several residues of the region between residues 43 and 90, in particular residues from strands β4 and β5, loops L4, L6 as well as the extended loop L5 (Figure 2I-12, Figure 2I-13).

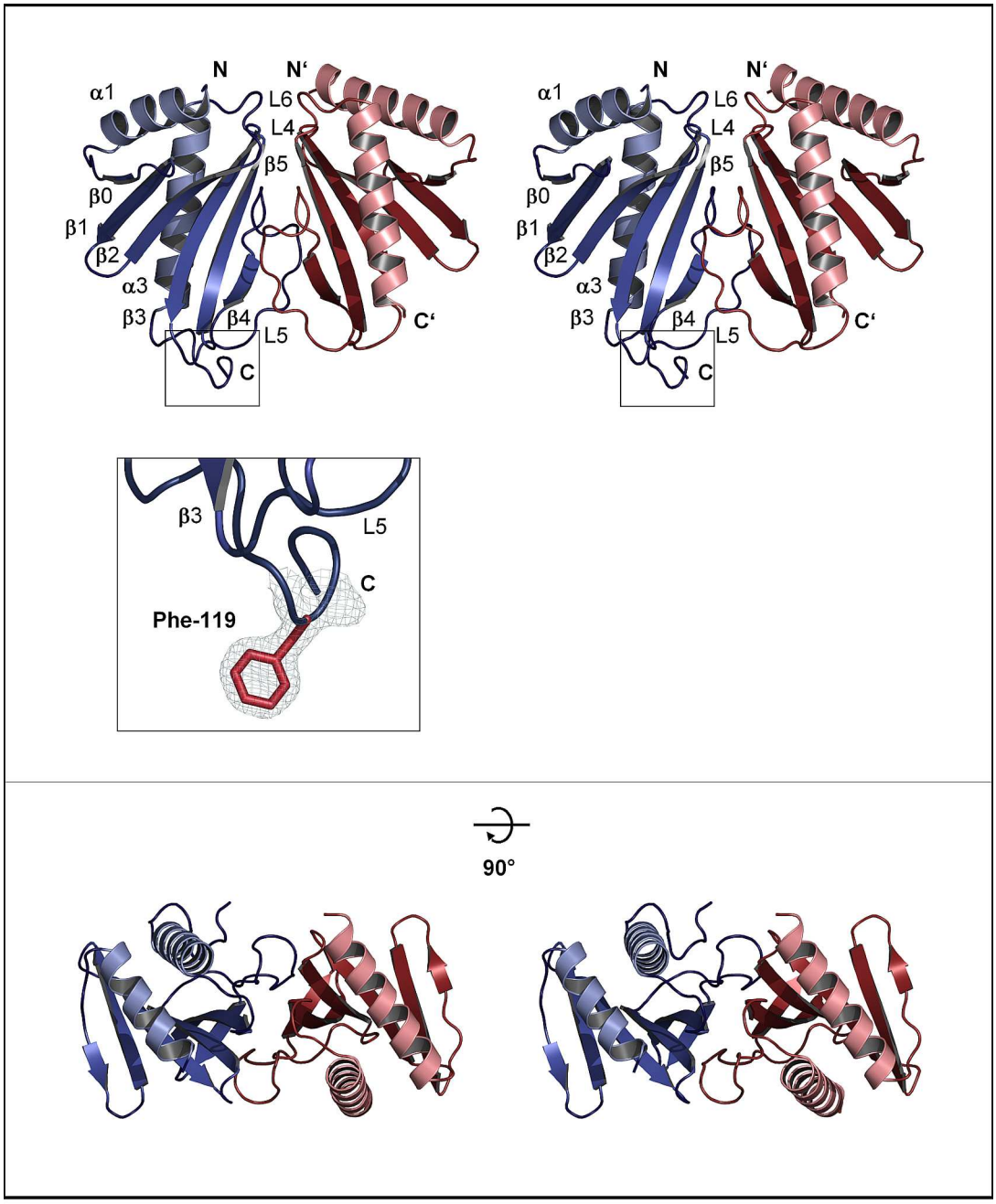

Figure 2I-12. Crystal structure of the *Yersinia enterocolitica* SycT homodimer. Stereo view of $SycT_{1-122}$ crystal form 2 (monomer A colored in blue, monomer B in red). Front view and top view after turning by 90°. The α-helix and β-strand numbering was adapted from earlier T3SS chaperone structures. The SycT monomer exhibits a mixed α/β fold comprising an anti-parallel six-stranded β-sheet packing against two α-helices. The inset shows the well-defined electron density of the protruding Phe119 side chain (red sticks) of monomer A that is involved in a crystal contact (see also Figure 2I-17).

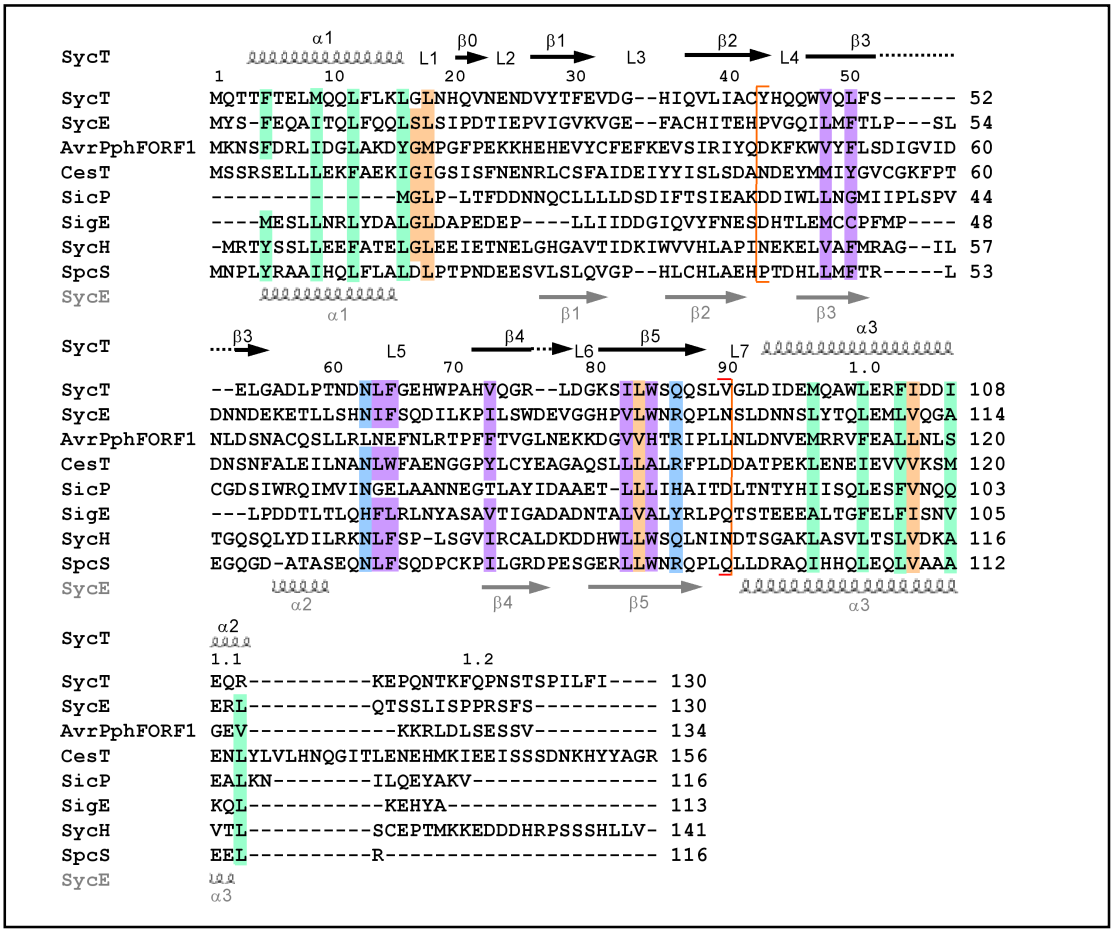

Figure 2I-13. Structure-based sequence alignment of SycT with related T3SS effector chaperones. Conserved hydrophobic residues in SycT helices α1 (Phe5, Met9, Leu12, Leu16) and α3 (Met97, Leu101, Phe104, Ile108) are shaded green. The SycT dimerization interface (red brackets) involves residues Tyr43, His44, Trp47, Gln49, Phe51, Asp62, Asn63, Leu64, Phe65, Trp69, Pro70, Ala71, Val73, Gly75, Arg76, Leu77, Trp84, Gln87, Val90). The sequence section containing the dimerization mediating residues includes also conserved polar residues (blue, Asn63, Gln86) and hydrophobic residues (purple, Val48, Leu50, Leu64, Phe65, Val73, Ile82, Trp84). Other conserved residues (Gly17, Leu18, Leu83, Ile105) are highlighted in orange. The dimerization mediating residues are located in the loops L4, L5 and L6 and the β-strands β4 and β5. Aligned sequences were adjusted by analyzing the SycT structure. Secondary structure elements for SycT are indicated above, those for the *Yersinia* chaperone SycE below the sequences. Aligned sequences comprised *Yersinia enterocolitica* SycT (GenBank entry AAD16809), *Y. pseudotuberculosis* SycE (NC_006153), *Pseudomonas syringae* pv. *phaseolicola* AvrPphF ORF1 (AAF67148), *E. coli* CesT (P58233), *Salmonella typhimurium* SicP (AAC38655), *S. enterica* SigE (NP455587), *Y. pestis* SycH (NP052425), putative chaperone Orf1 from *P. aeruginosa*, abbreviated to SpcS (AAA66490).

2I.7.2 A closed cavity in the SycT dimerization interface

The dimerization interface of SycT harbors a cavity of 150 $Å^3$ (Figure 2I-14). Five to six (native SycT and $SycT_{1-122}$ crystal form 2; crystal form 1) water molecules trapped within the cavity form hydrogen bonds to polar residues. No charged residue is found in the cavity. Symmetrically positioned Ser88 residues from both monomers restrict entry to the cavity and are mutually hydrogen-bonded in the native structure and crystal form 1. The cavity in SycT is closed and both hydrophobic Val90 residues in loop L6 shield the cavity from the outside (Figure 2I-14).

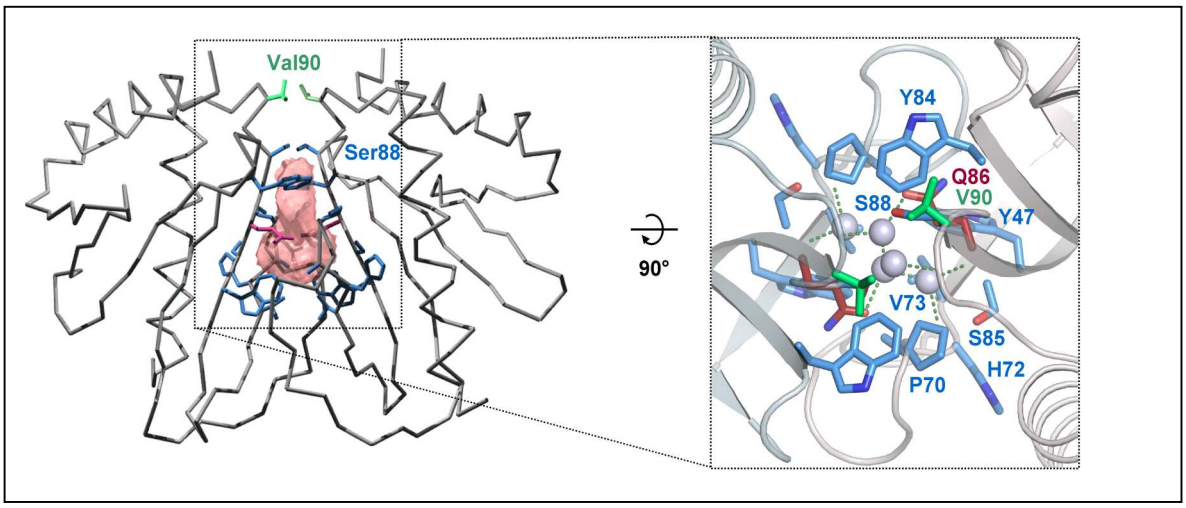

Figure 2I-14. SycT dimerization interface encloses a polar cavity. (Left) SycT harbors a polar, closed cavity ($SycT_{1-122}$ crystal form 1, cavity as pink surface model and side chains of Trp47, Pro70, Ala71, His72, Val73, Leu83, Trp84, Ser85, Ser88 as blue stick model, Gln86 in red). (Right) The inset shows the top view along the two-fold rotational symmetry axis onto the hydrogen bond network (green dashed lines) of the five water molecules within the cavity. Both Val90 residues (green) shield the cavity from the outside.

2I.7.3 Hydrophobic surface patches in SycT

Dimeric SycT exhibits hydrophobic residues that cluster in three hydrophobic patches on the surface. Patch 1 and 2, located remote from the two-fold symmetry axis, are symmetrically duplicated on the dimer surface (Figure 2I-15). Patch 1, near the dimer interface, comprises residues Leu64, Phe65, Gly66, Trp69 of one monomer as well as Val27, Leu39, Ile40, Ala41, Tyr43, Trp47, Gln49, Phe51, Gly75, Ile82 of the second. Patch 2 is formed by the amphipathic α-helix involving residues Leu16, Gly17, Leu18, Phe30, Val32 and Ile105. The third

hydrophobic patch (patch 3) stretches between both N-terminal helices α1 (residues Met0, Leu8, Leu89, Val90, Gly91, Leu92, Ile94) (Figure 2I-15).

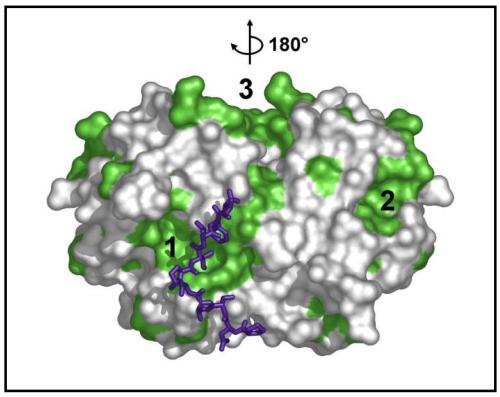

Figure 2I-15. Hydrophobic patches on the SycT dimer surface. Two-fold symmetry of hydrophobic patches 1 and 2 (1, 2) on the surface of SycT ($SycT_{1-122}$ crystal form 1) generates four patches per dimer. In the crystal of native SycT, patch 1 mediates hydrophobic interaction to residues 125-130 of the C-terminal peptide (violet stick model). Surfaces corresponding to hydrophobic side chains are highlighted in green.

In five of the six crystallographically independent monomers obtained for SycT, the residues connecting α1 and β1 form an additional β–strand β0 anti-parallel to β1. In one monomer of the native SycT dimer these connecting residues do not form β0. Instead they form a loop that is flipped toward helix α1 thereby opening a shallow groove (Figure 2I-16). The high temperature factors of these either loop- or β0–forming residues (not shown) indicate an increased flexibility of this protein region.

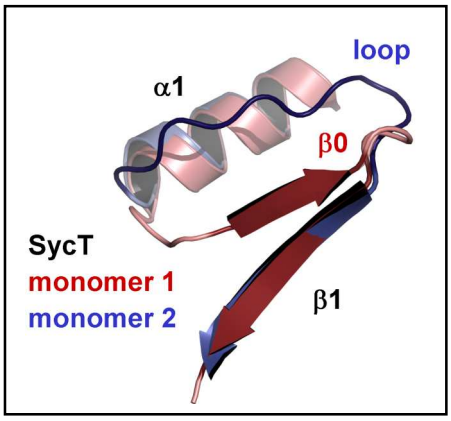

Figure 2I-16. Rearrangement of secondary structure elements in SycT. In native SycT monomer 1 (red), the region connecting α1 and β1 exhibits the additional β-strand β0, while in monomer 2 (blue) β0 has transformed into a loop and moved toward α1 opening a shallow groove.

2I.7.4 Interaction of the C-terminal peptide with hydrophobic surface patches

In full-length SycT, the C-terminal peptide (SPILFI, residues 125-130) of both monomers interacts with the hydrophobic patch 1 of the primary dimer as well as of a symmetry-related molecule simultaneously, thereby mediating extensive crystal contacts (Figure 2I-15).

The C-terminal peptide of truncated $SycT_{1-122}$ crystal form 2, which is only visible in the electron density of one monomer, interacts hydrophobically *via* the well-defined protruding Phe119 (compare Figure 2I-12) with the hydrophobic patch 1 of a symmetry-related molecule. The hydrophobic patch 1 harbors a groove (Phe65 in loop L5 from one monomer, Val27 from β2, Leu39, Ala41, Tyr43 from β3, Gln49, Phe51 from β4 in the other monomer). In crystal form 2 of truncated $SycT_{1-122}$, this hydrophobic groove of one monomer is occupied by Phe119 from the C-terminal peptide of a neighboring monomer in the crystal sustaining an important crystal contact (Figure 2II-17A,B).

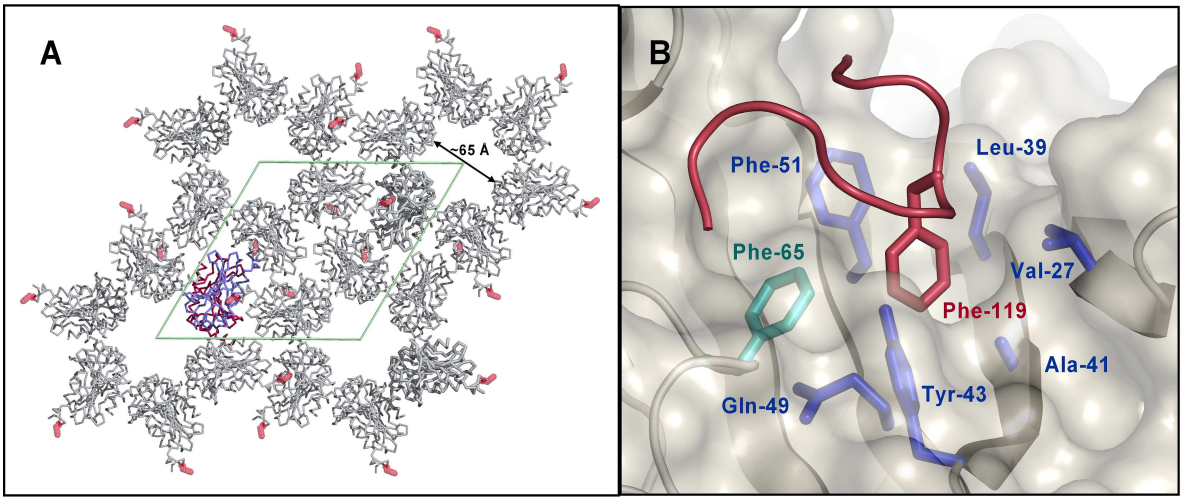

Figure 2I-17. Crystal packing of $SycT_{1-122}$ (crystal form 2) in the hexagonal space group $P6_2$. (A) Crystal packing of $SycT_{1-122}$ crystal form 2. Chain A is colored in blue, chain B in red. Symmetry related dimers are colored in grey. Phe119 (red spheres) that is visible in the electron density of only one monomer in $SycT_{1-122}$ crystal form 2 mediates an important crystal contact by protruding into the hydrophobic patch 1 of symmetry-related molecules. Unit cell depicted as green rhomboid. View along unit cell axis **c**. **(B)** Close-up view of Phe119 interacting with hydrophobic patch 1.

These C-terminal residues (115-122) are disordered in monomer B (crystal form 2) and in both monomers of crystal form 1. Residues 115-122 thus seem to be intrinsically flexible. Depending on the crystal packing environment, these C-terminal stretches in SycT are ordered by fortuitously binding to patch 1 of a neighboring molecule.

2II Type III secretion Class II chaperone SycD

2II.1 Biochemical characterization of SycD

2II.1.1 Gene expression, isolation and purification of full-length SycD

Full-length translocator chaperone SycD (residues 1-168) was recombinantly produced as soluble N-terminal GST-fusion protein in high amounts. Fusion protein was purified by affinity chromatography using glutathione sepharose and the tag was cleaved on column. Full-length SycD was initially purified by ceramic hydroxyapatite (CHT) chromatography. CHT chromatography separated several high and low molecular weight impurities from SycD, though SycD itself did not bind to the column (Figure 2II-1) resulting in negative purification. Non-binding behavior of SycD was also observed with a low phosphate concentration and calcium chloride in the running buffer implying an unfolded polypeptide chain without clustered carboxyl groups. However, circular dichroism measurements of SycD (see Figure 2II-23) verified secondary structure elements and thus the native folding of SycD. SycD was further purified using size exclusion chromatography. During concentrating of purified SycD for crystallization trials, the protein solution exhibited the formation of higher oligomers under certain conditions (see section 2II.1.5).

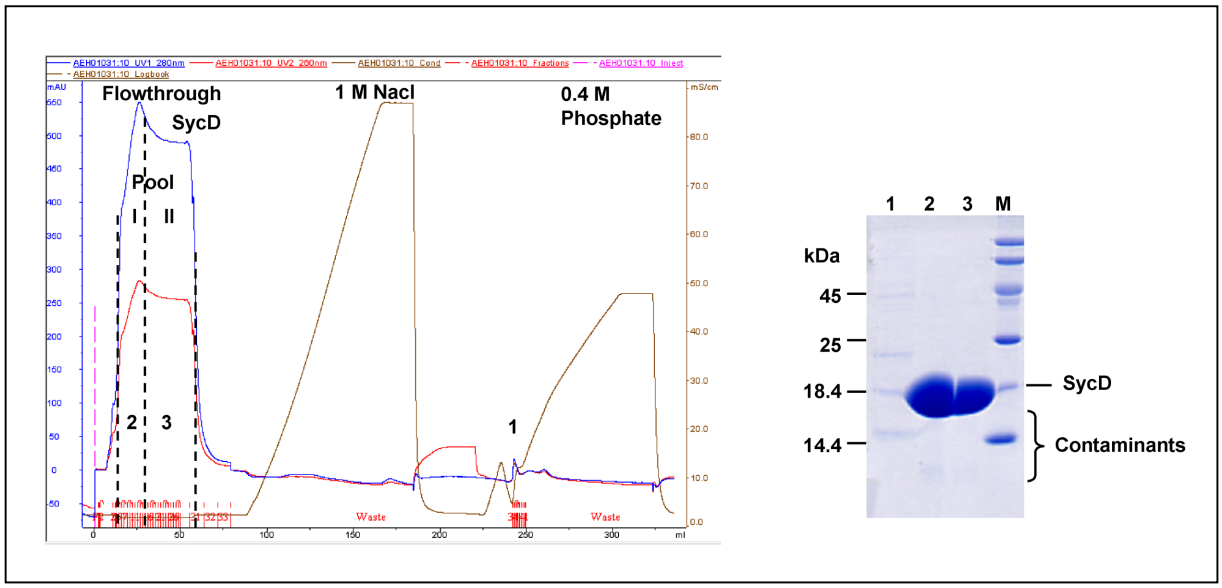

Figure 2II-1. Negative purification of SycD by ceramic hydroxyapatite (CHT) chromatography. (Left) CHT chromatogram. SycD did not bind to the column and eluted with the flowthrough (right, lanes 2 and 3 in SDS-PAGE). Instead, several high and low molecular weight impurities were retained and eluted with the phosphate gradient (right, lane 1). (Right) 15 % SDS-PAGE (Coomassie staining) of the CHT chromatography fractions for SycD. Lane 1: phosphate gradient eluate; Lane 2 and 3: concentrated flow through pools I and II containing SycD; M, marker proteins.

2II.1.2 Limited proteolysis of SycD identifies a stable fragment

Although purification of full-length SycD yielded very pure protein, extensive crystallization trials at room temperature and at 4 °C did not yield crystals. Additionally, SycD stored at 4 °C over a long period of time was degraded N-terminally by 20 amino acids as detected by MALDI-TOF mass spectrometry (Figure 2II-2A). In order to identify a stable fragment within the SycD sequence that was more suitable for crystallization, limited proteolytic digest using trypsin was carried out (Figure 2II-2B). The resulting SycD fragment was identical to the one obtained by degradation comprising residues 21-168.

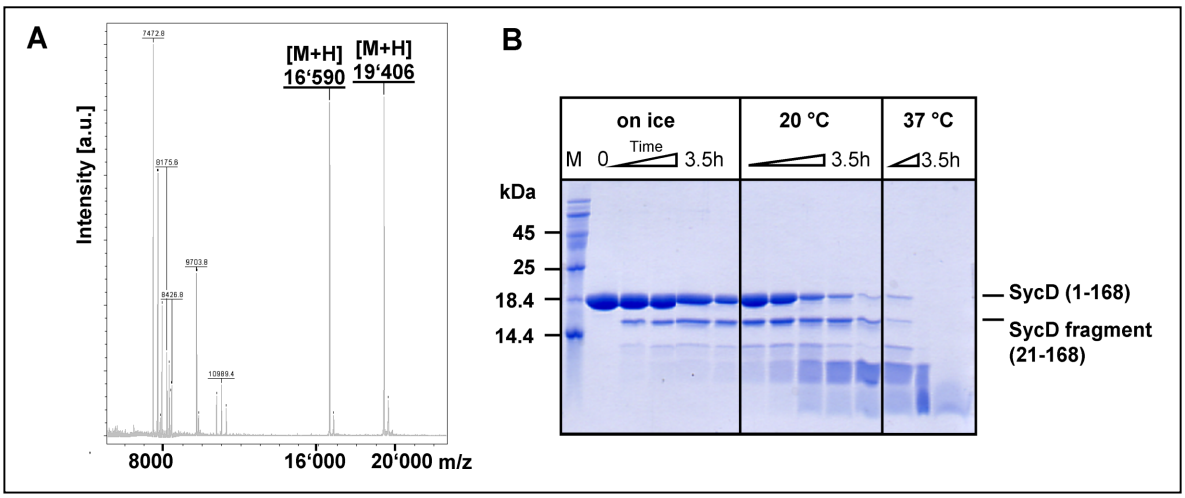

Figure 2II-2. Stable fragment of SycD. (A) MALDI-TOF-MS analysis of SycD stored at 4 °C over six weeks reveals two protein species. Full-length SycD with residual PreScission protease cleavage oligopeptide GPLGS (calculated M_r = 19’406 Da) corresponds to the mass peak on the right. A truncated degradation fragment of SycD with 16’590 Da is present in equal amounts. **(B)** 15 % SDS-PAGE (Coomassie staining) of limited proteolysis of full-length SycD. The tryptic digest (at 0 °C on ice, 20 °C and 37 °C) resulted in a stable fragment of SycD that is N-terminally truncated by 20 amino acids ($M_{r\ theo}$ $SycD_{21-168}$ = 16’591 Da) corresponding to the degradation fragment in panel A. M, marker proteins.

In contrast to this indicated susceptibility that might possibly be due to disorder, secondary structure prediction by the network PROF algorithm (Rost and Sander, 1993) supposed a long α-helix in this N-terminal region (Figure 2II-3). With the P1 cleavage site residue lysine proceeding three glycines, this region is apparently not entirely helical but accessible to proteolytic cleavage.

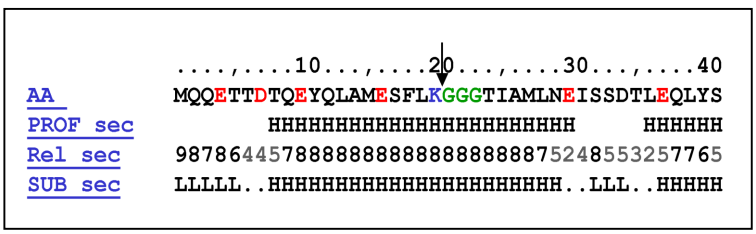

Figure 2II-3. Secondary structure prediction of the N-terminal region in SycD. PROF output of full-length SycD. The cleavage site after Lys20 observed during limited tryptic digest is indicated by an arrow and precedes three successive glycine residues (green).

2II.1.3 New expression construct $SycD_{21-163}$

Unsuccessful crystallization trials, the identification of the fragment $SycD_{21-168}$ by limited proteolysis (section 2II.1.2), higher oligomerization of full-length SycD (see section 2II.1.5, Figure 2II-7) potentially due to disulfide bond formation of Cys164 close to the C-terminus (below) gave rise to the generation of a second expression construct comprising SycD residues 21-163. The truncated chaperone was produced in the same way as full-length SycD and yielded large amounts of soluble protein (Figure 2II-4A).

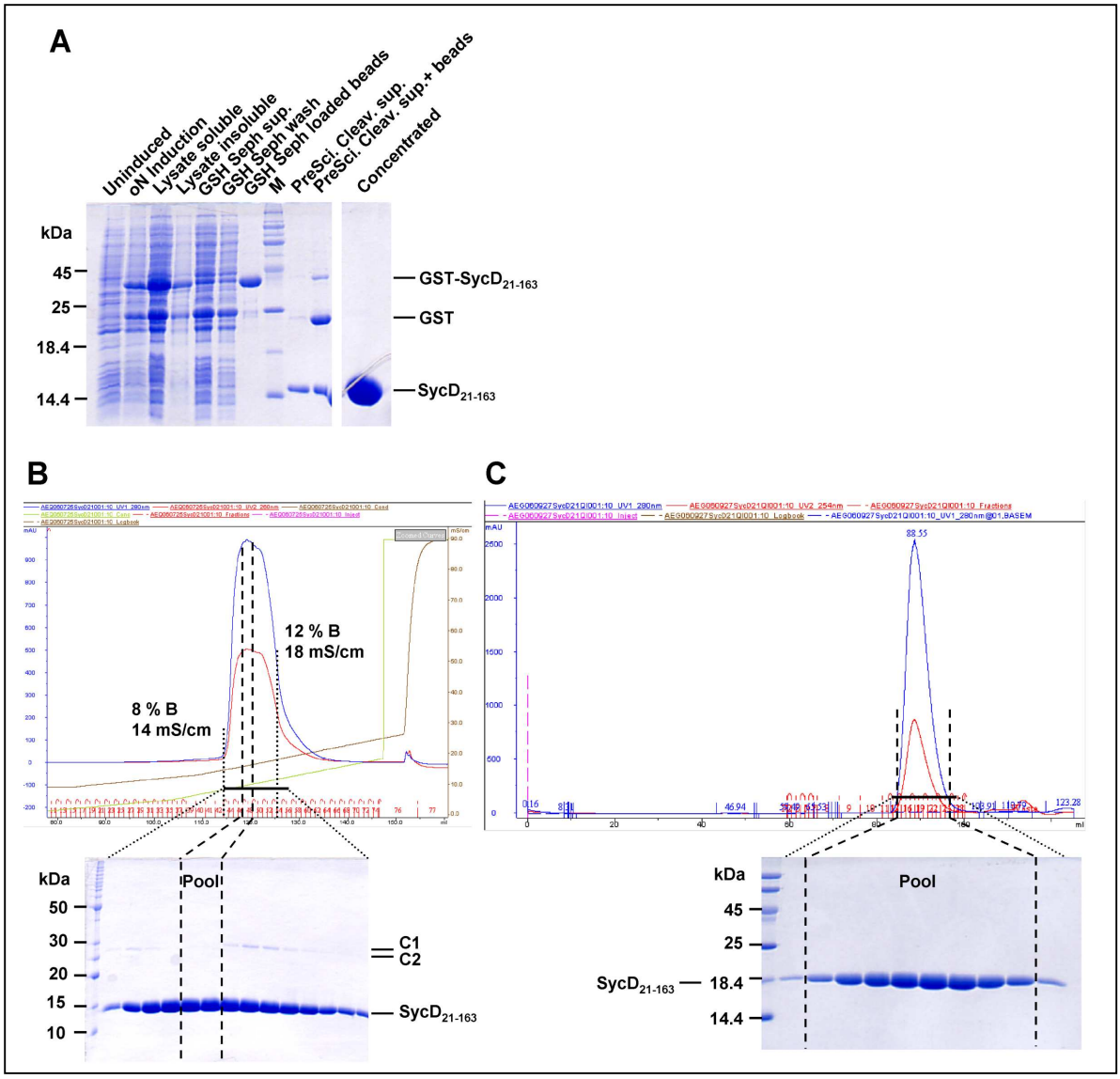

Figure 2II-4. Purification of $SycD_{21-163}$. (A) 15 % SDS-PAGE (Coomassie staining) of the $SycD_{21-163}$ protein preparation *via* glutathione sepharose (GSH Seph) affinity chromatography and PreScission protease cleavage (PreSci. Cleav.) on column. Purified $SycD_{21-163}$ shows a purity level of 99 % (last lane concentrated protein). oN, over night; sup, supernatant; M, marker proteins. **(B)** Anion exchange chromatography AEC (MonoQ HR 10/10 column, GE Healthcare-Amersham Biosciences). Contaminations C1 and C2 were almost completely separated by a flat salt gradient (NaCl) leaving a small window of pure $SycD_{21-163}$ (Pool) that were combined for the next purification step. **(C)** Size exclusion chromatography (Superdex 200 XK 16/60 column) with AEC pool fractions. The elution peak showed slight tailing. Peak fractions were pooled and concentrated for crystallization trials.

Impurities of higher molecular weight (~30 kDa) were observed during the course of purification. Glutathione sepharose re-chromatography did not remove the impurities and reducing and non-reducing gels displayed the same band pattern implying that no disulfide bridges were involved. Negative purification using ceramic hydroxyapatite chromatography neither removed the contaminants. N-terminal sequencing identified one of the impurities as the affinity tag GST that has been N-terminally truncated by 99 amino acids. This GST fragment (residues 100-226) is defective in binding to glutathione-coupled sepharose. However, the size of the GST-fragment observed in SDS-PAGE runs with ~30 kDa, which is double the size of the calculated molecular mass for the $GST_{100-226}$ fragment (Figure 2II-4B). Negative purification *via* ceramic hydroxyapatite chromatography did not remove the contaminants. Anion exchange chromatography using a very flat salt gradient (0-15 % of 1 M NaCl-containing buffer B over 20 column volumes) separated both impurities imperfectly from each other, though leaving a small window of almost contaminant-free $SycD_{21-163}$ in the absorption peak of the chromatogram that could be further used for size exclusion chromatography (Figure 2II-4B,C). By a second anion exchange chromatography of the remaining fractions that resulted in the same chromatogram and band distribution, more pure target protein was obtained. $SycD_{21-163}$ exhibits slight tailing during size exclusion chromatography (Figure 2II-4C and Figure 2II-6), a phenomenon also observed for full-length SycD (Figure 2II-6). Despite the small fraction of target protein suitable for the final purification step and crystallization trials, the yield of $SycD_{21-163}$ was ~16 mg per liter of bacterial culture and purified $SycD_{21-163}$ showed > 99 % purity (Figure 2II-4A, last lane).

2II.1.4 Surface engineering in SycD

In order to optimize the surface properties of the chaperone supposed to favor crystallization and to overcome oligomerization, the SycD amino acid sequence was scrutinized for critical residues (cysteines) and clustered residues of high surface entropy according to the approach of surface engineering (Derewenda and Vekilov, 2006). Inspection of the SycD sequence and analysis by the surface entropy reduction server (Figure 2II-5, left) assisted by secondary structure prediction revealed several regions of clustered lysine and glutamate residues that are supposed to lie at the surface and might prevent crystallization due to flexible side chains. A further site selected for mutation was the C-terminal cysteine Cys164 that might form intermolecular disulfide bonds leading to higher oligomerization observed during purification. Selected K/E clusters and Cys164 were eliminated in the corresponding surface mutants of

full-length or truncated SycD (Figure 2II-5, right). The physicochemical properties of the SycD constructs are listed in Table 2II-1.

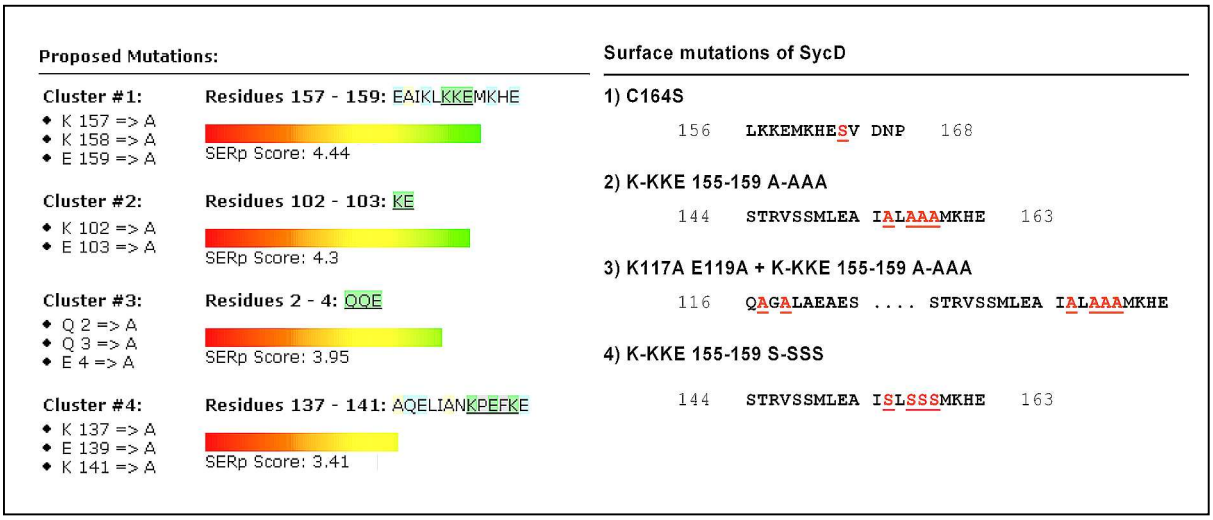

Figure 2II-5. Surface engineering of SycD. (Left) Analysis of SycD amino acid sequence by the Surface Entropy Reduction Server (http://nihserver.mbi.ucla.edu/SER/) reveals several clusters of lysine and glutamate residues supposed to be surface-exposed and possibly interfere with protein crystallization due to side chain flexibility (score ranking). (Right) Resulting SycD surface mutants used in protein production.

Table 2II-1. Physicochemical properties of SycD and SycD variants.

	SycD	SycD C164S	$SycD_{21-163}$	$SycD_{21-163}$ K117A/K155A	$SycD_{21-163}$ K155S
Number of residues	173	173	148	148	148
M_r [Da]	19’404	19’388	16’472	16’128	16’307
Molecular extinction coefficient ε [$M^{-1}\cdot cm^{-1}$]	10’720	10’600	9320	9320	9320
Isoelectric point (pI)	4.9	4.9	5.3	5.0	5.0

Values generated with Vector NTI (Invitrogen), corresponding to PreScission protease cleaved proteins with an extra N-terminal GPLGS peptide.

2II.1.5 Oligomerization state of SycD in solution

During purification, SycD exhibited excellent solubility. The oligomerization state of wild-type SycD and derived constructs was investigated by dynamic light scattering and analytical size exclusion chromatography as well as native PAGEs. Analytical SEC of wild-type SycD and $SycD_{21-163}$ constructs reveals the formation of SycD homodimers in solution (Figure 2II-6) that is confirmed by DLS analysis (Table 2II-2, different constructs).

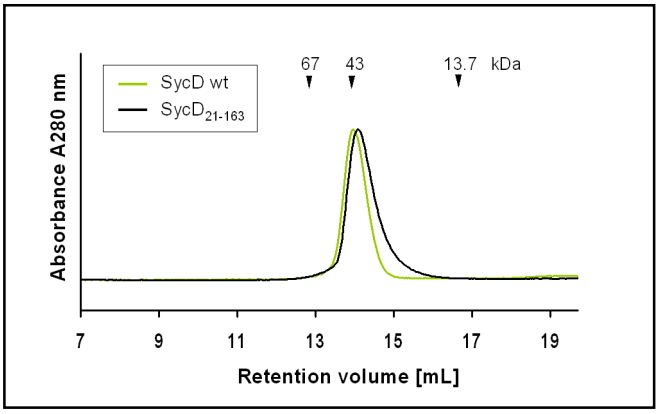

Figure 2II-6. Size exclusion chromatography of SycD and $SycD_{21-163}$. Superdex 200 HR 10/30 (GE Healthcare-Amersham Biosciences), running buffer 20 mM Tris pH 8.0, 200 mM NaCl, 1 mM DTT. Elution of standard molecular weight proteins was used for calibration (arrow heads). The observed SycD retention times correspond approximately to the doubled masses expected of a SycD monomer ($M_{r\ SEC}$ ~40 kDa, $M_{r\ theo}$= 19'404 Da) and a $SycD_{21-163}$ monomer (M_{obs} ~38 kDa, $M_{r\ theo}$ = 16'486 Da) suggesting the formation of homodimers.

Table 2II-2. Dynamic light scattering results for full-length SycD and truncated constructs.

Protein	c [mg/mL]	r_H	$M_{r\ DLS}$ [kDa]	Polydispersity [%]	Base line	SOS error
SycD wt	~6	3.03	42.6	16.2	1.000	2.01
$SycD_{21-163}$	22	2.85	37.2	10.4	0.999	0.87
$SycD_{21-163}$ K155S	20	2.89	37.9	8.6	0.999	1.04

The data present the best fit as obtained by regularized radii distribution.

However, aged or concentrated protein batches of full-length SycD tend to aggregate and SycD apparently formed higher oligomers in native PAGEs (Figure 2II-7A). Under certain conditions, these oligomer bands were even visible in a reducing, denaturing SDS-PAGE. The formation of oligomeric inhomogeneities might hamper crystallization, and its elimination is therefore essential.

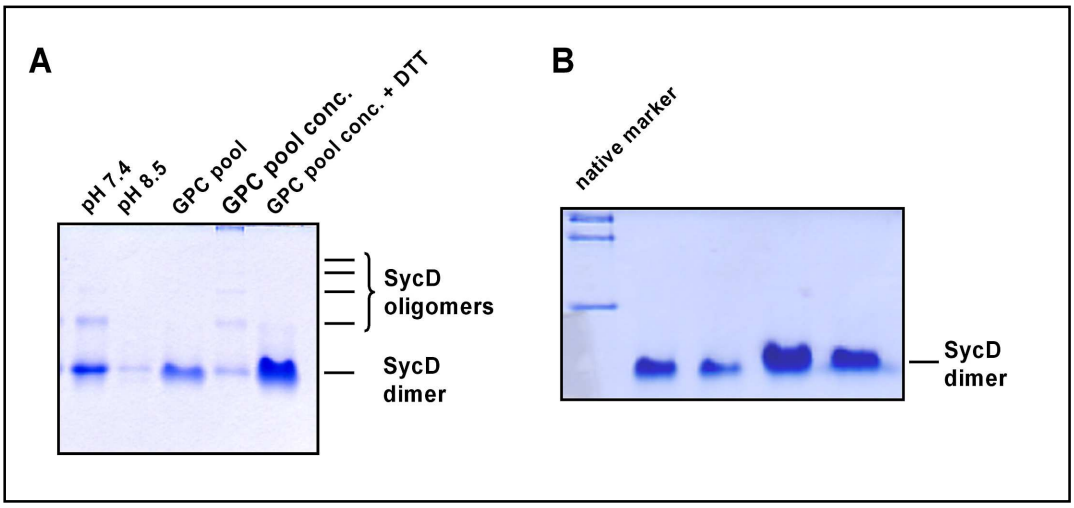

Figure 2II-7. Formation of higher SycD oligomers. (A) 12 % Native PAGE. Concentrated and aged protein solutions of full-length SycD with exhausted DTT were prone to form multimers most likely linked by disulfide bridges as DTT addition reduces the amount of oligomers (last lane). **(B)** 12 % Native PAGE of truncated $SycD_{21-163}$ exhibited a homogeneous population, even after concentrating (22 mg/mL). (Coomassie staining).

This oligomerization might be due to the formation of intermolecular disulfide bonds. Analysis of the SycD amino acid sequence (see section Appendix) suggested that one of four cysteines in total, Cys164 near the C-terminus, is exposed and could be prone to form disulfide bridges. However, investigations of SycD by accurate mass spectrometry (ESI-TOF) only detected a species exhibiting exactly the calculated mass of 19'404 Da (not shown) and did not indicate the presence of oxidized thiol groups or disulfide bonds.

The truncated chaperone variant, $SycD_{21\text{-}163}$, lacking the flexible 20 amino acids at the N-terminus plus the five C-terminal residues including Cys164, as well as its surface-engineered derivative K155S, formed homogenous, monodisperse solutions of homodimers even at higher concentrations (up to 22 mg/mL) (Figure 2II-7B), conferring suitable properties for crystallization.

2II.2 Complex formation studies of SycD with translocator YopD

2II.2.1 $YopD_{278\text{-}300}$ peptides

Prior studies on the cognate translocators had identified a C-terminal fragment of YopD capable of SycD binding (Francis *et al.*, 2000; Tengel *et al.*, 2002). As a first approach, this C-terminal YopD peptide comprising residues 278-300 was recombinantly produced as an N-terminal GST-fusion protein with a TEV protease cleavage site. Sufficient amounts of the soluble GST-fusion could be isolated and purified. TEV protease cleavage was monitored by mass-spectrometry and the observed mass difference corresponded to the calculated mass of the TEV protease-cleaved $YopD_{278\text{-}300\_TEV}$ peptide ($M_{r\ theo}$= 3022 Da) (Figure 2II-8).

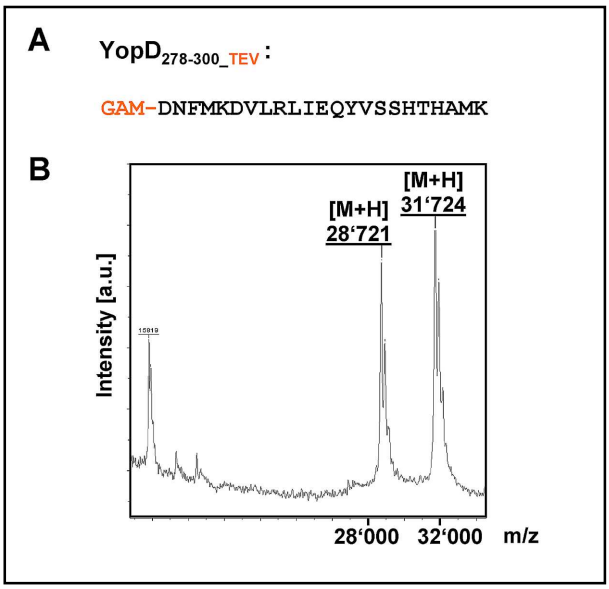

Figure 2II-8. Mass spectrometry of GST-$YopD_{278\text{-}300}$ TEV-cleavage. (A) Amino acid sequence of the $YopD_{278\text{-}300\_TEV}$ peptide. **(B)** TEV protease cleavage of the GST-fusion (31'724 Da) is revealed by the emerging mass peak for GST (28'721 Da) during MALDI-TOF-MS. The mass difference of 3003 Da corresponds to the YopD peptide ($M_{r\ theo}$= 3'022 Da).

However, the attempt to separate the peptide from GST *via* ultracentrifugation using a MWCO of 30'000, which was supposed to retain GST but let pass the peptide, disclosed the aggregation of the peptide. As an alternative approach, the chemical synthesis of the $YopD_{278-300}$ peptide was chosen (by Dr. Peter Henklein; Charité Berlin).

2II.2.2 Binding studies and co-crystallization of SycD with $YopD_{278-300}$

The complex formation between SycD and the YopD peptide variants was analyzed using analytical size exclusion chromatography, native gel shift or an affinity matrix immobilization pull-down assay. Analytical SEC of SycD with GST-$YopD_{278-300}$ and $YopD_{278-300\_TEV}$, respectively, did not reveal peak shifting, nor did SycD bind to GST-$YopD_{278-300,}$ which had been coupled to glutathione sepharose beads. For the synthetic peptide and the truncated chaperone $SycD_{21-163}$, ambiguous results were obtained during SEC as the common retention time error has the magnitude of the peptide mass. Neither was binding observed in the pull-down assay (Figure 2II-9A). Co-crystallization attempts of wild-type SycD with the synthetic peptide $YopD_{278-300}$ were carried out by adding the solubilized peptide to the concentrated protein solution of SycD (c ~20 mg/mL) intending a 1.1 : 1 excess of peptide, followed by nanoliter crystallization setups. Strikingly, immediate precipitation during addition of the peptide to the SycD solution was observed that occurred independently of the pH value of the solubilized peptide, i.e. peptide suspended in water or in 1 M Tris pH 8.0. The supernatant of the protein:peptide mixture analyzed with native PAGE disclosed a distinct shift for a small fraction of $SycD_{21-163}$ (Figure 2II-9B), indicating that the chaperone is at least able to bind partially to the chaperone. However, the considerable shift in the gel exceeded the expected difference that would be induced by the $YopD_{278-300}$ peptide (23 aa, ~2.8 kDa). Presumably, the SycD:$YopD_{278-300}$ interaction detected in the gel differed from a 1:1 binding ratio and might be due to the observed aggregation of the peptide resulting in a SycD:$(YopD_{278-300})_n$ complex where *n* is an unknown integer >1.

Nonetheless, the SycD:$YopD_{278-300}$ mixture was used in screening for crystallization conditions – without success. Co-crystallization was repeated with the peptide solubilized in the presence of a detergent to prevent the aggregation of the peptide. As detergent, n-dodecyl-β-D-maltoside (critical micelle concentration 0.1 - 0.6 mM) was used, with a final detergent concentration of approximately 0.12 - 0.15 mM in the crystallization drop; still no crystals appeared. In previous studies, the peptide was stabilized by trifluorethanol and an acidic milieu not applicable for protein crystallization (Tengel *et al.*, 2002).

However, under the near-physiological conditions used in this work, apparently no significant and useful interaction between SycD and the C-terminal YopD peptide $YopD_{278-300}$ occurred in solution.

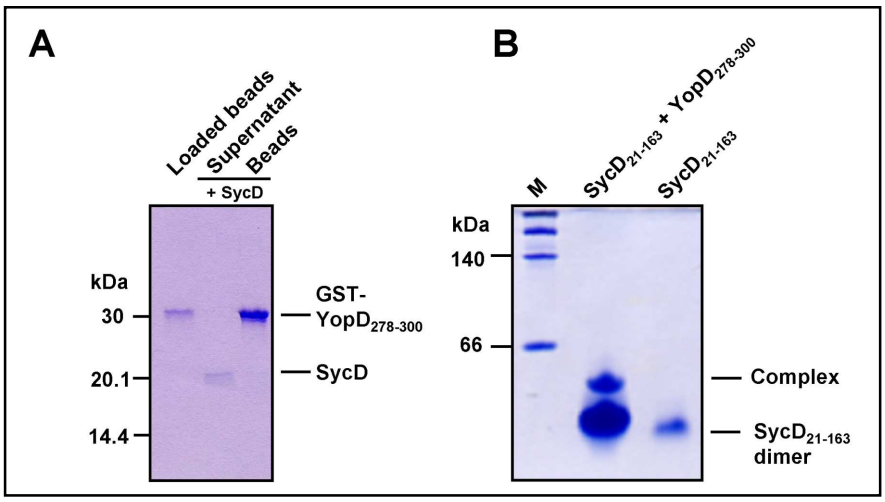

Figure 2II-9. Analysis of the complex formation between SycD and the $YopD_{278-300}$ peptides. (A) Pull-down-like assay of GST-$YopD_{278-300}$ coupled to glutathione sepharose beads and SycD did not disclose binding (15 % denaturing SDS-PAGE, Coomassie staining). **(B)** 12 % native PAGE (Coomassie staining) of the supernatant from the SycD:$YopD_{278-300}$ peptide mixture used for co-crystallization. A distinct shift of a small part of SycD is visible indicating the partial binding of the chaperone to the synthetic $YopD_{278-300}$ peptide, though the interaction is different from a 1:1 ratio possibly due to the observed peptide aggregation. M, native high molecular weight marker.

2II.3 Crystallization of SycD

2II.3.1 Large, beautiful looking $SycD_{21-163}$ crystals diffract only poorly

Extensive nanoliter-scale screening for crystallization conditions of wild-type or reductively methylated full-length SycD as well as of the cysteine mutant SycD C164S, with protein concentrations between 3 and 20 mg/mL and incubation temperatures varying from 4 to 20 °C, did not result in crystalline objects. Crystallization setups for the truncated variant $SycD_{21-163}$ using high concentration (20 mg/mL) and low temperature (4 °C) eventually yielded tiny needles under a high salt condition (potassium acetate) that could be optimized into large, beautiful looking crystals that diffracted very poorly to 3.8 Å (synchrotrons DESY, ESRF) at best (Figure 2II-10C; Figure 2II-11A). However, large $SycD_{21-163}$ crystals grew irreproducibly and usually showers of thin rod-shaped crystals appeared in the crystallization droplet. Therefore, nucleation had to be slowed down. As setups were already incubated at 4 °C and $SycD_{21-163}$ did not respond to (micro-/streak-)seeding, the approach of inserting inorganic nucleants with varying pore sizes (Nanonucleant, London, UK) (Chayen *et al.*,

2006) was applied that was supposed to provide suitable nucleation surfaces and enforce the growth of a few single crystals. Both sitting-drop and hanging drop vapor diffusion techniques were employed (Figure 2II-10). However, $SycD_{21-163}$ crystals grew independently of the nucleant showing the familiar shower.

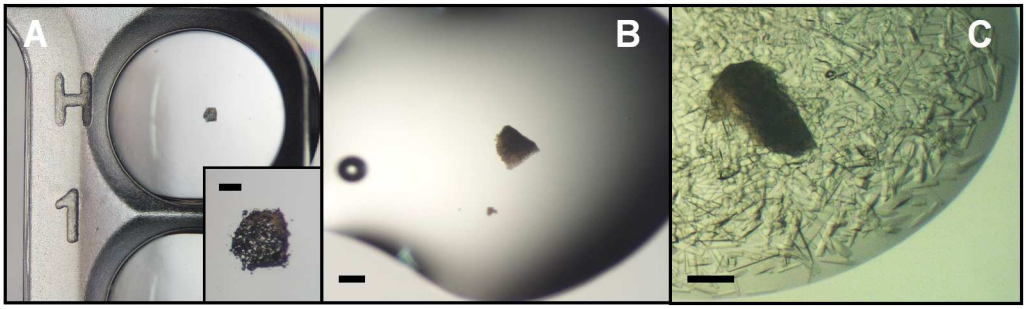

Figure 2II-10. Crystallization trials with porous gel glass (Nanonucleant, UK). (A) Innovadyne Innoplate SD-2 plate with spotted gel glass in droplet chamber (inset). **(B)** Hanging drop crystallization trial with applied Nano-grain, directly after setting-up. **(C)** Crystallization setup after seven days. The nucleant had no impact onto SycD crystallization. Scale bar = 100 µm.

2II.3.2 Engineering of the tetragonal $SycD_{21-163}$ crystals using dehydration

At that time when only the tetragonal crystals of $SycD_{21-163}$ and $SycD_{21-163}$K155S (Figure 2II-11A,B) were available, which diffracted only poorly at room temperature as well as at 100 K (7.5 Å, home source rotating anode), attempts were made to enhance diffraction. In order to improve the apparently imperfect crystal packing, the crystals were subjected to different techniques of dehydration that were supposed to reduce the water content of the crystal and provoke a rearrangement of the molecules resulting in a more regular packing and optimized diffraction pattern. Simple cover slip transfer to higher concentrated crystallization reservoirs as well as stepwise addition of nanoliter-size droplets and finally the use of an humidity control device were tested. Crystals, treated accordingly to the first two methods and tested during the course of dehydration, did not reveal an improved diffraction pattern. To detect a potentially missed optimum, the crystals were hydrated and dehydrated in an automated manner using the free-mounting system for humidity control (FMS, Proteros). For both crystal forms the crystallization reservoir solution containing either potassium or lithium acetate possesses a very low relative humidity rH (91.2 %) already bearing a dehydrating effect. During controlled dehydration (rH_{end} = 75.0 %) the diffraction deteriorated and could not be rescued by a successive re-hydration gradient, nor did the initial increase of rH up to 97.0 % have a positive effect on the diffraction potential. In summary, the diffraction potential of the tetragonal $SycD_{21-163}$ crystals could not be improved by dehydration experiments.

2II.3.3 Reductive methylation of $SycD_{21-163}$ yields well-diffracting crystals

In order to overcome this futile crystal form and to induce an alternative crystal packing, a surface-engineered variant $SycD_{21-163}$ K155S (see section 2II.1.4) was screened for crystallization conditions. As lysine side chains hamper crystal contacts, this mutant was supposed to crystallize more easily, possibly providing different crystal contacts. Indeed, crystals appeared in a different condition (Figure 2II-11B, see Materials and Methods section 5.14.1), however, they exhibited the same bad diffraction potential and tetragonal crystal lattice parameters as the wild-type $SycD_{21-163}$ crystals, indicating a defective packing of the molecules in the lattice. As a second approach, crystallization trials for $SycD_{21-163}$ were set up utilizing commercial and hand-made PEG-based screening solutions to enforce crystallization and possibly a more favorable packing from a PEG-based instead of a salt-based cocktail. In a PEG 350 MME as well as in a PEG 400-based condition, long, thin needles (< 10 µm width) grew, which could not be increased in size and that diffracted even worse (resolution 9 Å, synchrotron DESY) (Figure 2II-11C).

As a last resort, the manipulation of the protein itself by reductive methylation of lysine side chains was employed, a method that had already been applied to the full-length chaperone in vain. In fact, the modified protein $SycD_{21-163}{}^{meth}$ produced a different crystal form, this time exhibiting a monoclinic packing and diffraction to 1.95 Å (Figure 2II-11D), suitable for structure determination.

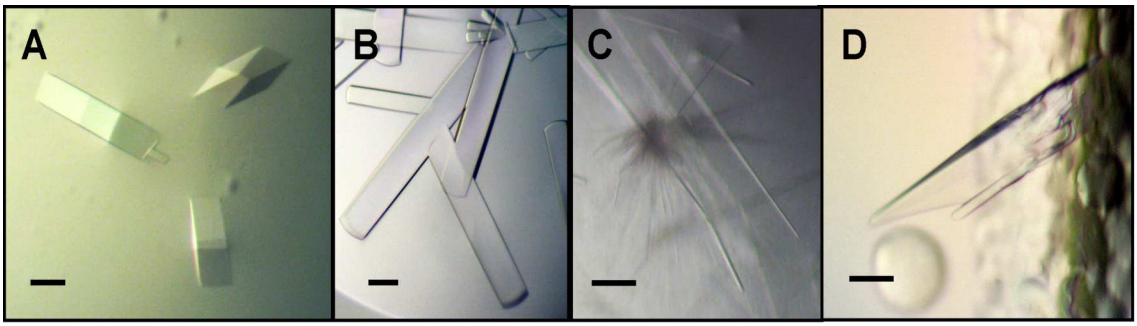

Figure 2II-11. Crystals of SycD variants. (A) Optimized tetragonal $SycD_{21-163}$ crystals, large and beautiful looking but poorly diffracting due to imperfect packing of the huge unit cells with ~34 molecules per asymmetric unit. **(B)** Optimized crystals of a quadruple lysine/glutamate surface mutant, $SycD_{21-163}$ K1555S, grow under a different condition, however, they possess the same diffraction properties, crystal lattice and unit cell parameters as the wild-type. **(C)** Crystals of $SycD_{21-163}$ obtained in a self-made PEG screen. They could not be improved in size and diffraction. **(D)** After reductive methylation of $SycD_{21-163}$, an alternative (=monoclinic) well-diffracting (<2 Å) crystal form was obtained that was used for structure determination. Scale bar = 100 µm.

2II.3.4 Engineering of the $SycD_{21\text{-}163}^{meth}$ crystals *via* heavy atom derivatization

To accelerate and facilitate structure solution of the monoclinic $SycD_{21\text{-}163}^{meth}$ crystal form, heavy atom derivatization was applied that would overcome the phasing problem in case of a failure of molecular replacement (further details in Materials and Methods section 5.14.2). The Heavy Atom Databank (Islam *et al.*, 1998) listed heavy atom binding sites for mercury, platinum and osmium in SycD. Therefore, thimerosal, ethylmercurylphosphate, potassium tetracyanoplatinate, potassium tetrachloroplatinate(II) and osmium(III)chloride hydrate were selected. Additionally, crystals of $SycD_{21\text{-}163}^{meth}$ were quick-soaked in halogenide solutions (potassium and sodium bromide, potassium iodide) following the described method (Dauter *et al.*, 2000). Soaking provoked usually crystal cracking and loss of diffraction. Potential derivative candidates did not prove as genuine derivatives as examined by fluorescence energy scan or diffraction data analysis. Xenon pressurizing as an alternative derivatization method was later used successfully to derivatize $SycD_{21\text{-}163}^{meth}$ crystals (section 2II.4.2), although the $SycD_{21\text{-}163}^{meth}$ structure eventually could only be solved by molecular replacement (below).

2II.4 Structure determination of $SycD_{21\text{-}163}$

2II.4.1 How to pack 34 $SycD_{21\text{-}163}$ molecules ?

Preliminary X-ray analysis of the tetragonal $SycD_{21\text{-}163}$ crystals revealed a huge unit cell with Matthews' probability analysis (Matthews, 1968; Kantardjieff and Rupp, 2003) (V_M = 2.42 $Å^3\,Da^{-1}$, solvent content 49.2 %) suggesting approximately 34 molecules per asymmetric unit. Molecular replacement of wild-type $SycD_{21\text{-}163}$ failed. Neither the use of different search algorithms (Patterson function superposition, maximum likelihood) by applying several programs such as EPMR (Kissinger *et al.*, 1999), AMORE (Navaza, 1994), MOLREP (Vagin and Teplyakov, 1997) or PHASER provided a correct solution, nor did different search strategies with tetratricopeptide repeat (TPR)-containing proteins and parts of them such as O-linked N-acetylglucosamine transferase (OGT), protein phosphatase 5 (PP5) or the homology model LcrH/SycD introduced by Pallen *et al.* (2003). Structure solution of this crystal form was finally abandoned and the search for an alternative crystal form enforced that was finally obtained by reductive methylation (section 2II.3.3).

2II.4.2 Attempts to solve the $SycD_{21\text{-}163}{}^{meth}$ structure by anomalous phasing

X-ray analysis of $SycD_{21\text{-}163}$ crystals obtained after reductive methylation assigned them to the monoclinic space group C2. The Matthews coefficient V_M (V_M = 2.16 $Å^3\,Da^{-1}$, solvent content 43 %) indicated two molecules per asymmetric. With the smaller unit cell parameters, these crystal appeared more promising than the tetragonal crystals with respect to successful structure determination. The self-rotation function indicated non-crystallographic two-fold rotational symmetry (Figure 2II-12) suggesting dimerization of the two molecules per asymmetric unit, although actually two two-fold non-crystallographic symmetry (NCS) peaks were visible corresponding to two distinct dimeric assemblies.

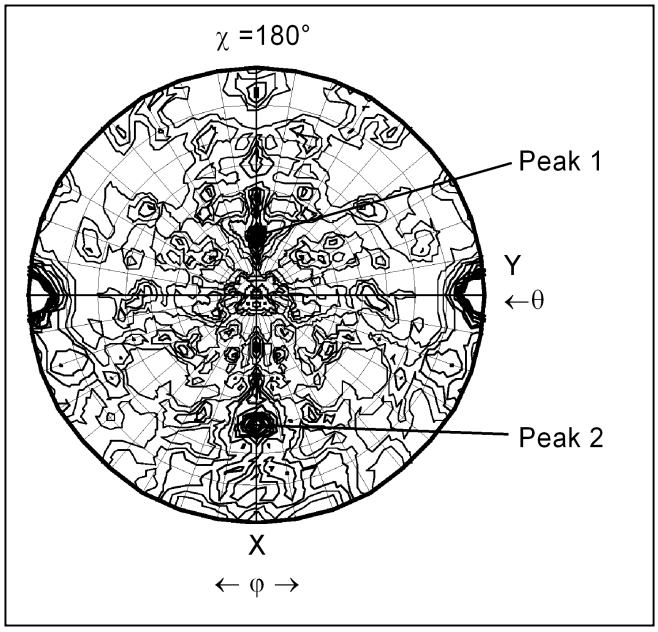

Figure 2II-12. Self-rotation function for $SycD_{21\text{-}163}{}^{meth}$. In this self-rotation function map, the crystallographic two-fold rotational symmetry of the space group C2 is present (maxima at the edges of the Y-axis). Moreover, the rotational component of a non-crystallographic symmetry (NCS) operator is visible, which represents the local symmetry, i.e. rotational symmetry relating the $SycD_{21\text{-}163}$ molecules in the asymmetric unit. The maximum peak 1 at polar angles θ=120°, φ=180°, χ=180° indicates a two-fold rotational NCS (implied by χ=180°), though a minor peak 2 is also present (θ~30°). The self-rotation function was calculated using the program MOLREP.

However, molecular replacement as described above failed again. Therefore, heavy atom derivatization was carried out in parallel of which only xenon treatment resulted in a genuine derivative. Single-wavelength anomalous dispersion (SAD) data of the xenon-derivatized $SycD_{21\text{-}163}{}^{meth}$ crystals were directly input into the beamline version of the automated structure determination platform Auto-Rickshaw (Panjikar *et al.*, 2005), although the quality of the obtained phases did not suffice to solve the structure. Further attempts to locate the xenon atoms by different methods revealed one common, fully-occupied xenon site and several, inconsistent sites of minor occupancy. Localization of the xenon positions was also attempted in an anomalous difference Patterson map. The relevant Harker section of the Patterson map in space group C2 at v= 0 disclosed only one significant peak corresponding to the symmetry self-vector of the single xenon site already determined (Figure 2II-13).

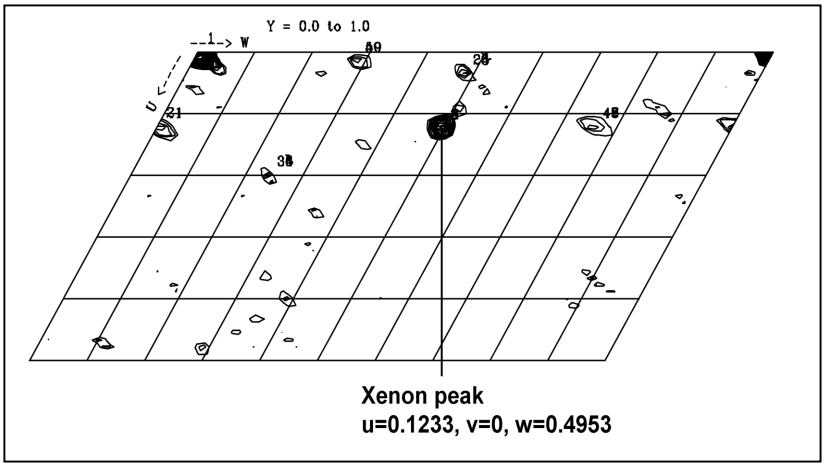

Figure 2II-13. Harker section of the anomalous difference Patterson map for the $SycD_{21-163}^{meth}$ xenon derivative. The anomalous Patterson map was calculated at 3.5 Å and the relevant Harker section u= 0 - 0.5, y= 0 w= 0 - 1 is depicted. Only one self-vector peak (u= 0.1233, w= 0.4953) is visible, corresponding to a single xenon site. Due to the weak anomalous signal, this single site did not suffice to phase the dataset.

As no further xenon sites were localized and due to the weak anomalous signal, anomalous phasing of the $SycD_{21-163}^{meth}$ data was not feasible. The structure of the xenon derivative was later solved by molecular replacement using the refined structural model of $SycD_{21-163}^{meth}$ as search model (see below). In the difference Fourier map (F_o-F_c), four distinct spheres corresponding to xenon sites could be localized (**Fehler! Ungültiger Eigenverweis auf Textmarke.**) of which only one was fully occupied, corresponding to the single solution derived from the anomalous Patterson map.

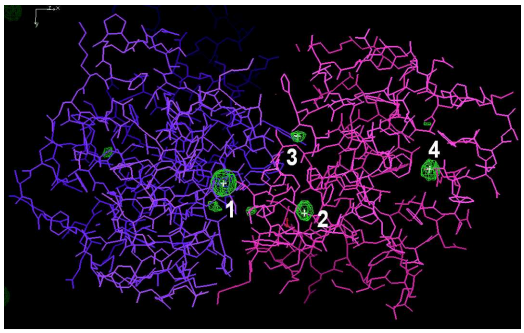

Figure 2II-14. Xenon atoms incorporated in the crystal packing of $SycD_{21-163}^{meth}$. Anomalous phasing using the single xenon site failed. Later, molecular replacement with the $SycD_{21-163}^{meth}$ structure (see below) was possible and revealed the positions of four xenon atoms (1-4) incorporated in hydrophobic cavities within the molecule and in crystal contact voids. Only xenon 1 is fully occupied and corresponds to the solution identified in the anomalous Patterson and in SHELXD. Difference Fourier (F_o-F_c) map (green mesh) contoured at 5 σ. View along unit cell axis **c**.

2II.4.3 Molecular replacement of $SycD_{21-163}^{meth}$ and PHASER sensitivity

As experimental phasing of the $SycD_{21-163}^{meth}$ Xe data had failed, enforced attempts were made to solve the $SycD_{21-163}^{meth}$ structure by molecular replacement. These included also the modification of the search model. Attempts using one to three TPR motifs of the SycD/LcrH homology model were not successful, nor was the trial with a search model that had been transformed into a polyalanine chain. Alternatively, searches with TPR domains of structurally related TPR-containing proteins such as Heat shock protein organizing protein (Hop),

OGT, PP5 or cyclophilin 40 were carried out. However, independent of searching with a single molecule or aligned ensembles, these efforts did not succeed either. Unfortunately, the NCS operator of the dimer (i.e. the rotation and translation vectors required to superpose both monomers) was not known, which could have been used otherwise for searching the dimer directly. Therefore, the program PHASER was extensively used in order to locate one monomer after another. The MR search round attempting to find the first monomer comprised a rotation function search followed by a translation function search. In the second MR round that was supposed to locate the second monomer by running also a rotational and translational search, the found solution(s) from the first round were manually re-entered and kept fix. However, the two search steps from the first MR round gave only low rotation function Z-scores (RTZ) and translation function Z-scores (TFZ) that did not indicate a correct solution. The scoring did neither improve in the successive round searching for the second molecule. However, correct solutions with only low scoring have been reported (Keegan and Winn, 2007). Therefore, the packing of the potential solutions found by PHASER was visually analyzed in order to detect an appropriate dimeric assembly. Still, none of the packing was convincing due to severely penetrating, clashing main chains.

Literature search for help in challenging MR cases came across the importance of an accurately prepared search model and the superior success rate of using so-called mixed models that were identified and modified by the Fold and Function Assignment System (FFAS03) (Rychlewski *et al.*, 2000; Jaroszewski *et al.*, 2005). With regard to the SycD amino acid sequence, FFAS03 returned PDB entry 2FO7, a synthetic 8-repeat consensus TPR protein (Kajander *et al.*, 2007), as most suitable MR search model. The FFAS03-aligned sequences for SycD (residues 2-137) and 2FO7 (1-136) shared 20 % identical residues. The generated model was truncated to three TPR motifs (98 residues) and transformed into a mixed model consisting of identical (25.5 %) and otherwise serine residues (Figure 2II-15). This 3-TPR mixed model was used with PHASER for a stepwise MR search of $SycD_{21\text{-}163}{}^{meth}$.

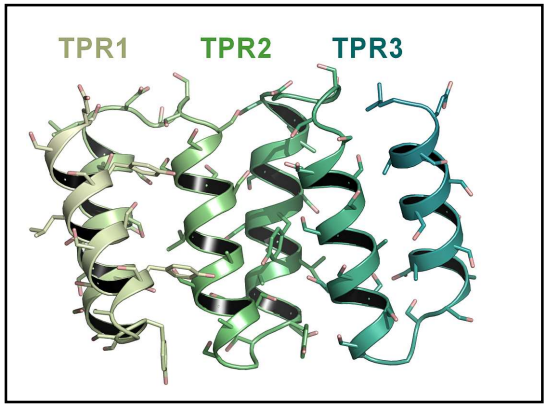

Figure 2II-15. Ribbon presentation of the mixed model successfully applied in the structure solution of $SycD_{21\text{-}163}{}^{meth}$ by molecular replacement. The FFAS03 method used in determination of a MR search model proposed an artificial TPR repeat protein (PDB entry 2FO7) as most suitable model. The final search model comprised 98 residues forming three TPR motifs (TPR1-3, colored in light green, green, dark green) and was additionally prepared as a so-called mixed model exhibiting only identical side chains (25.5 %) otherwise serine residues (stick model).

The first MR round locating monomer 1 resulted in a single solution with low RFZ and TFZ. As before, this solution was fixed in the following search round locating the second molecule in the asymmetric unit. The RFZ of the second search gave low, dissatisfying Z-score values again (PHASER manual guide line for a correct solution: Z>5). However, the translation function finally increased significantly (Table 2II-3) indicating the success of the MR search. Thus, the correct solution became evident only after placing the second (last) molecule.

Table 2II-3. Summary of the stepwise MR search for $SycD_{21-163}^{meth}$ in the program PHASER.

Round	Search step	Search details	Z-score	Correct solution ?
1	Rotation function	-	**3.9**	No
1	Translation function	-	**4.2**	No
2	Rotation function	Solution from 1st round kept fix, searching the 2nd molecule	**3.7**	No
2	Translation function	Placing the 2nd molecule	**10.0**	Yes

Both solutions for $SycD_{21-163}^{meth}$ were improved and completed in several rounds of manual model building and refinement. The final, refined model of $SycD_{21-163}^{meth}$ was used in turn to perform a stepwise MR search in PHASER for the tetragonal $SycD_{21-163}$ crystal form with roughly 34 molecules per asymmetric unit. However, attempts to locate one $SycD_{21-163}$ monomer after another, similar to the procedure described above in combination with manual and subjective (since carried out by eye) selection of the correct solutions only by judging the crystal packing, did not exceed six located monomers and was eventually abandoned.

Table 2II-4. Data collection and refinement statistics for $SycD_{21-163}$.

	$SycD_{21-163}$	$SycD_{21-163}^{meth}$	$SycD_{21-163}^{meth}$ Xe	$SycD_{21-163}^{meth}$ S94E/Y95E	$SycD_{21-163}$ A61E/L65E(V64M)[d]
Data collection					
Space group	$P4_122$ / $P4_322$	C2	C2	$P3_221$	I222
Unit cell dimensions [Å], [°]	a=b= 211.6, c= 242.5 α=β=γ= 90	a= 107.3 b= 33.0, c= 96.7 α=γ= 90, β= 122.3	a= 106.6 b= 32.6, c= 94.1 α=γ= 90, β= 121.0	a=b= 90.6, c= 54.2 α=β= 90, γ= 120	a= 40.9, b= 80.3, c= 109.1 α=β=γ= 90
Wavelength [Å]	1.2781	0.979250	1.5	0.934	0.91841
Resolution [Å]	50-3.85 (3.99-3.85)	45-1.95 (2.05-1.95)	27-2.5 (2.56-2.5)	39-2.6 (2.7-2.6)	38-2.98 (3.18-2.98)
Mosaicity [°]	0.3	0.32	1.5	0.315	0.33
Completeness [%]	99.9 (99.9)	99.6 (99.8)	99.1 (95.2)	99.6 (100)	99.9 (100)
(Anomalous) redundancy	7.8	4	6.2	7.2	6.6
Observations	412'632	84'992	60'619	58'856	25'644
Unique reflections	53'183	21'282	9827	8163	3914
I/σ [I]	12.0 (3.0)	13.1 (3.8)	15.4 (7.3)	20 (3.7)	19.6 (3.2)
R_{sym} , R_{meas}	17.2 (75.2) [a]	9.5 (40.6) [b]	11.1 (26.8) [a]	10.5 (56.2) [b]	8.8 (66.5) [b]
Phasing	-	Molecular replacement	Molecular replacement	Molecular replacement	Molecular replacement
Anomalous χ^2 values (SCALEPACK)	-	-	1.243	-	-
Number of sites	-	-	1(4) (xenon)	-	-
Molecules per asymmetric unit	~34	2	2	1	1
Solvent content [%]	49	43	43	68	54
Refinement					
R / R_{free} [c] [%]		17.5 / 22.6		21.3 / 23.4	25.7 / 34.4
Number of atoms Protein/Solvent		2343 / 138		1069 / 28	1086 / 0
R.m.s. deviation					
Bonds [Å] /Angles [°]		0.017 / 1.455		0.003 / 0.529	
Ramachandran Plot					
Residues in allowed / additionally allowed / generously allowed regions [%]		93.5 / 6.5 / 0.0		90.0 / 10.0 / 0.0	
Residues in disallowed regions [%]		0		0	
B factor [$Å^2$] average / Wilson B	- / 81.4	19.9 / 22.1	- / 48.4	55.5 / 49.6	135 / 61.6
Protein / Solvent		18.4 / 30.0		54.4 / 52.8	
Protein databank accession code		2VGX	Not deposited	2VGY	Not deposited

Values in parentheses are for the highest resolution shell. [a] $R_{sym} = 100\ \Sigma_n\ (\Sigma_i \left| I_i - \hat{I} \right|) / \Sigma_n\ (\Sigma I_i)$; [b] $Rmeas = 100\ n\ \Sigma I \left| \hat{I} - I_i \right| / \Sigma_{hkl}\ (n-1)\ \Sigma_i I_i$, where $\hat{I}$ is the mean intensity of symmetry-related reflections (Diederichs and Karplus, 1997), [c] $R = 100\ \Sigma_{hkl} \left| F_{obs} - F_{calc} \right| / \Sigma_{hkl}\ F_{obs}$. Test set size 5 %; [d] V64M mutation due to nucleotide sequencing ambiguity caused by imperfect population of site-directed mutagenesis primers.

2II.5 Structural overview of $SycD_{21-163}$

The monoclinic crystal form contains two $SycD_{21-163}^{meth}$ molecules per asymmetric unit. The dimethylated amino head groups of lysine side chains were crucial for crystallization as they were actually involved in crystal contacts (Figure 2II-16) maintaining the crystal lattice. The electron density is well defined for residues 21-154 in monomer A, and for residues 21-160 in monomer B. Both monomers differ only in the position of 10 N-terminal residues indicating this region to be flexible. The rest of the molecule superposes well with an r.m.s. deviation of 1.3 Å for 125 common Cα atoms.

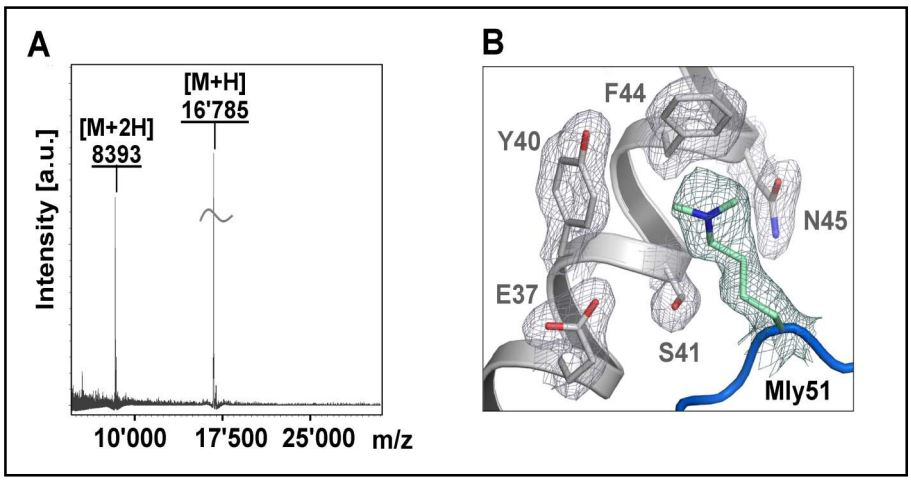

Figure 2II-16. Reductive methylation of $SycD_{21-163}$ was crucial for crystallization (A) MALDI-TOF mass spectrum of reductively methylated $SycD_{21-163}$. [M+H] indicates the singly-charged species, [M+2H] the doubly-charged ion. Molecular mass for $SycD_{21-163}^{meth}$ calculated from amino acid sequence with complete dimethylation of 10 lysines and the N-terminus is 16'794 Da. **(B)** Composite omit map of electron density contoured at 1.0 σ for dimethylated residue Lys51 (Mly51, green) involved in a crystal contact, 2Fo - Fc Fourier difference map at 1.0 σ for remaining residues. Five out of 10 lysine side chains per monomer, Lys51, Lys57, Lys102, Lys117 and Lys137, were well defined in electron density.

The SycD monomer consists of eight α-helices (h0, 1A, 1B, 2A, 2B, 3A, 3B, h8) (Figure 2II-17). The structure reveals the tetratricopeptide repeat (TPR)-like motifs that had been predicted for T3SS Class II chaperones (Pallen *et al.*, 2003). The repeat domain in $SycD_{21-163}$ spans residues 36 to 137 and is composed of six α-helices with the helices arranged in an anti-parallel manner. The six helices 1A, 1B, 2A, 2B, 3A and 3B are organized in TPR1-3, followed by the C-terminal helix (h8) that is joined also in an antiparallel orientation resulting in 3.5 repeats overall. In a single TPR motif of SycD, helices A and B pack against each other with dihedral packing angles Ω ranging from -152° to -164°, whereas packing between helices B and A' from adjoining TPR motifs show slightly lower angles

(-149° to -158°) as calculated by PROMOTIF (Hutchinson and Thornton, 1996). The twist per repeat in the overall right-handed superhelical TPR domain of SycD is 43-49° between TPR1 and TPR2, 46-47° between TPR2 and TPR3 and 91-95° for the whole domain TPR1-TPR3 (rotation angles chi as obtained by superposition in LSQKAB, Kabsch, 1976). These values are comparable with data from the literature (Main *et al.*, 2003). The twisted arrangement of the TPR motifs results in a concave and convex face of SycD (Figure 2II-17).

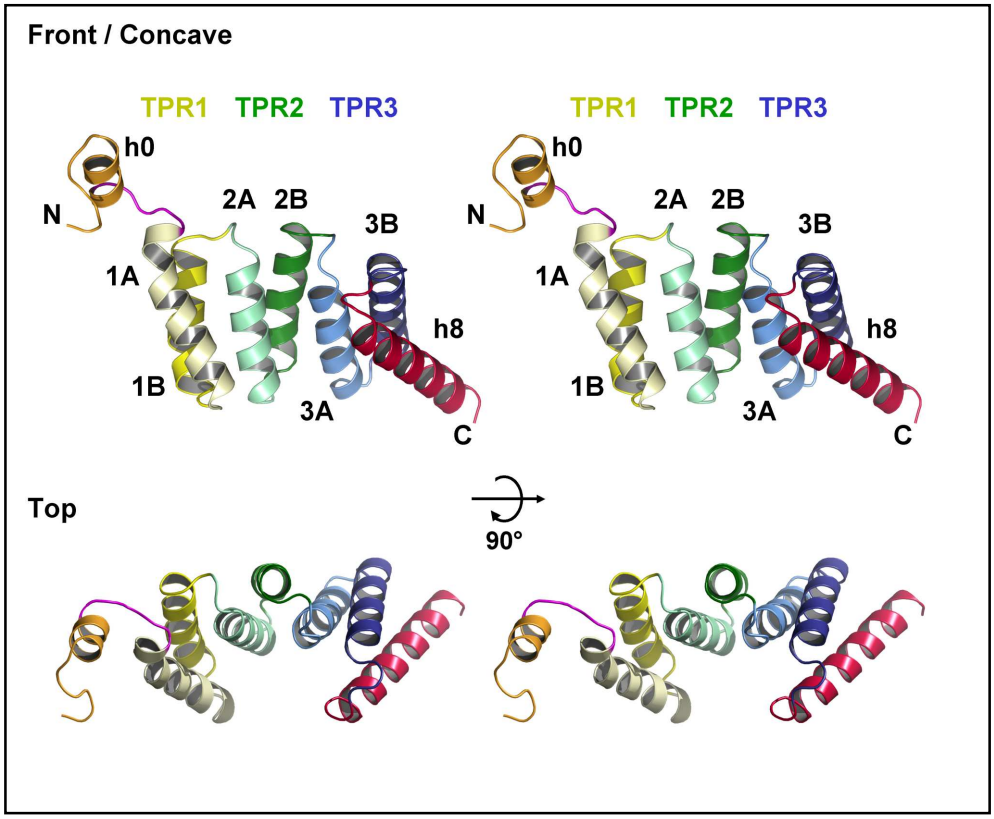

Figure 2II-17. Ribbon presentation of the crystal structure of $SycD_{21-163}$. Stereo image of monomeric $SycD_{21-163}$. Front view of the concave side and top view after turning by 90 °, with TPR1 colored in yellow, TPR2 in green and TPR3 in blue. 'A' helices are pastel-colored. The C-terminal stabilization helix h8 is colored in red.

The integrity of the SycD TPR fold is maintained by a pattern of small and large residues consistent with the canonical TPR sequence motif (Trp4-Leu7-Gly8-Tyr11-Ala20-Phe24-Ala27-Pro32) (Sikorski *et al.*, 1990). The majority of these connecting residues are hydrophobic and accumulate at the inner faces between the repeat helices, depicted in a helix wheel chart (Figure 2II-18). The long C-terminal α–helix h8 following the TPR motifs exhibits numerous charged, hydrophilic amino acids. For that reason, this helix is also termed capping, stabilization or solvating helix and is found in almost all currently known structures of TPR-containing proteins such as PP5 (Das *et al.*, 1998) and Hop (Scheufler *et al.*, 2000).

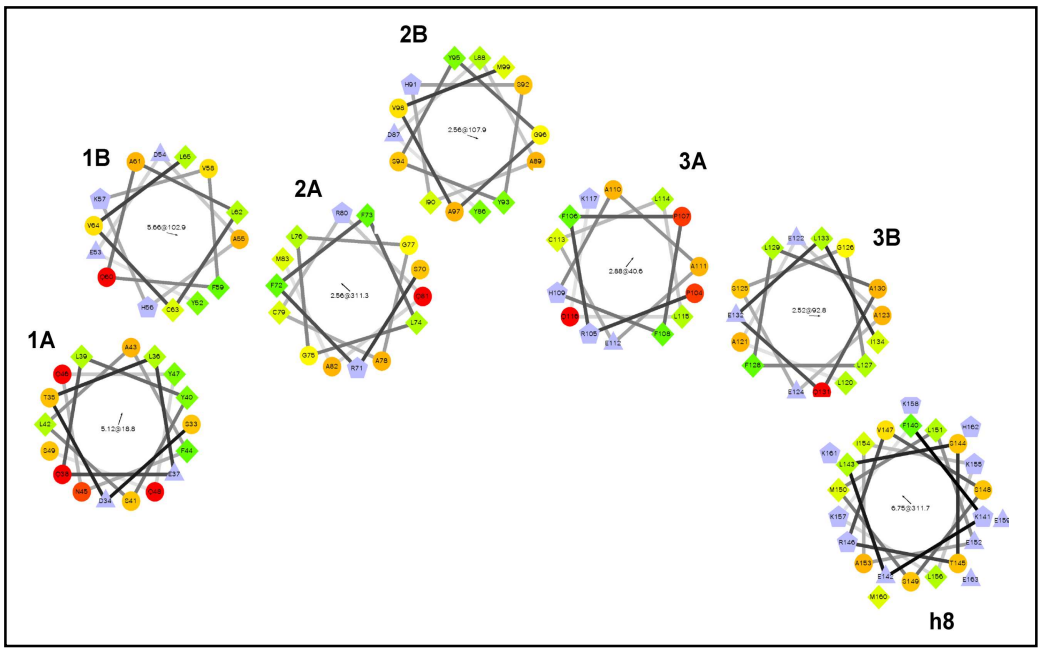

Figure 2II-18. Helix wheel representation of the SycD monomer (top view). Hydrophobic residues are depicted as diamonds, according to descending hydrophobicity colored in green to yellow. Hydrophilic residues are presented as red to orange circles, accordingly. Negatively charged residues correspond to blue triangles, positively charged amino acids to blue pentagons. The wheels were generated by http://rzlab.ucr.edu/scripts/wheel/wheel.cgi.

Table 2II-5. The first 20 results of the structural alignment search with DALI (Holm, 1993) **for SycD residues 21-160 (monomer B).**

Rank	Protein	PDB ID	Z-score	Seq.ID [%]	Align.res.	R.m.s.d. [Å]
1	Ser/Thr-Protein phosphatase PP5	1A17	16.6	13	128	2.3
2	CHIP U box E3 ubiquitin ligase	1C2L	16.0	17	106	2.1
3	*Model of a Ca2+ binding protein*	2AK6	15.3	8	128	2.9
4	Peroxisomal targeting signal 1 receptor PEX5p	1FCH	15.3	18	130	3.4
5	O-linked GlcNAc transferase OGT	1W3B	15.2	17	126	2.4
6	*Model of LcrH (residues 32-165)*	1OOL	15.2	87	124	2.4
7	FK Binding Protein 51 isomerase	1KT0	14.8	14	124	2.3
8	PilF fimbral pili type 4, lipoprotein	2FI7	14.5	15	126	2.5
9	PilF fimbral pili type 4, lipoprotein	2HO1	14.2	18	125	2.2
10	PFL2275c C-terminal domain	2FBN	14.0	14	134	3.3
11	p67phox Ras-related C3 botulinum toxin	1E96	13.8	16	126	1.9
12	TOM70 mitochondrial importer	2GW1	13.3	18	133	2.7
13	Hydrolase prolyl-4-hydroxylase	1TJC	12.7	13	85	1.8
14	NlpI lipoprotein	1XNF	12.5	17	131	2.4
15	Peroxisomal targeting signal 1 receptor PEX5	1HXI	12.3	15	93	2.3
16	FK Binding Protein 42	2IF4	12.0	17	108	2.5
17	Sec17 vesicular transport protein	1QQE	11.8	15	138	4.5
18	transcription factor MalT domain III	1HZ4	11.6	18	139	1.6
19	14-3-3 protein (signaling)	1IJP	10.9	10	120	2.6
20	TOM20 mitochondrial importer	1ZU2	10.2	10	109	2.3

Seq.ID, Sequence identity; Align.res., Number of aligned residues.

A DALI search (Holm, 1993) for structural homologs of SycD using the refined structural model (monomer B, residues 21-160) returned Ser/Thr protein phosphatase 5, the TPR domain of CHIP U box E3 ubiquitin ligase, the peroxisomal targeting signal receptor Pex5p and the O-linked N-acetylglucosaminyl transferase OGT as best matches (Z-scores 16.6, 16.0, 15.3, 15.2; r.m.s.d. 2.3, 2.1, 3.4, 2.4 Å) (Table 2II-5). Taken together, the α-helical fold of Class II chaperone SycD reveals genuine TPR repeats.

2II.6 Ambiguity of the SycD quaternary structure

2II.6.1 $SycD_{21\text{-}163}^{meth}$ packing analysis reveals two possible dimer assemblies

The apparent molecular mass for $SycD_{21\text{-}163}$ determined experimentally by size exclusion chromatography and dynamic light scattering gives significantly larger values (M_r ~39 - 42 kDa) than expected for the monomeric chaperone (~17 kDa) (compare Figure 2II-6 and Table 2II-2), suggesting that the SycD dimer in the asymmetric unit is also present in solution. However, in the monoclinic crystal packing, different quaternary assemblies of the two SycD monomers are possible resulting in two distinct dimers (Figure 2II-19).

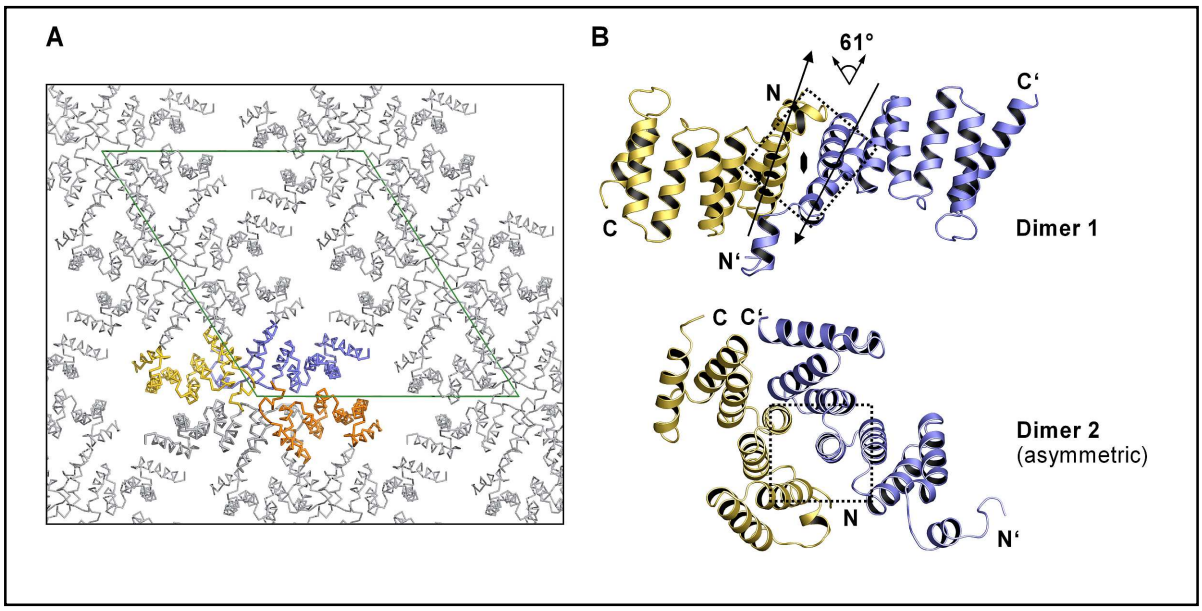

Figure 2II-19. Alternative homodimer assemblies of $SycD_{21\text{-}163}$. (A) Monoclinic crystal packing of $SycD_{21\text{-}163}$ allows two different dimer assemblies. Elongated dimer 1 is composed of the blue and yellow monomer, compact dimer 2 of the blue and orange monomer. A tetrameric assembly, which is a dimer-of-dimers, was also identified by PISA to be stable comprising the blue, orange and yellow monomer as well as the adjoining grey molecule. **(B)** Ribbon diagram of dimer 1 (upper part) and dimer 2 (lower part) with the monomers colored in blue and yellow. View along the two-fold rotation axis in dimer 1 with the monomers tilted by ~61°. View perpendicular to the imperfect two-fold rotation axis in dimer 2. The interface in dimer 2 is asymmetric. Interface sections are indicated by dashed lines.

In the elongated dimer 1, both monomers interact head-to-head *via* TPR1. The second assembly (dimer 2) shows the two monomers dimerizing asymmetrically back-to-back *via* the convex face of the TPR repeats involving TPR2 and the turns between the repeats (Figure 2II-19B and below). The two dimer assemblies explain also the two peaks present in the self-rotation function (Figure 2II-12). The rotational component of the non-crystallographic symmetry in dimer 1 determined by superposition of both monomers is ω= 61°, φ= 0°, χ= 179° in polar angles, whereas dimer 2 is related by an imperfect rotational symmetry (ω= 29°, φ= 178°, χ= 172°) indicated by a χ angle significantly smaller than 180°.

2II.6.2 Characterization of dimer assembly alternatives 1 and 2

To obtain a qualitative characterization of the assemblies, the structure and crystal packing were analyzed by the PISA server (Krissinel and Henrick, 2007) as well as the protein-protein interaction server (Laskowski, 1995). Both analyses suggested the assemblies in dimer 1 and in dimer 2 to be stable. Interestingly, the PISA analysis detected a tetrameric/dimer-of-dimers assembly in the crystal packing that is suggested to be stable as well (Figure 2II-19A).

Table 2II-6. Comparison of dimer interface characteristics for potential $SycD_{21-163}$ dimer 1 and dimer 2.

Interface statistics	Dimer 1 - elongated	Dimer 2 - compact
Monomer buried SA [Å^2]	924	655
% Monomer SA	11.4	7.8
Number of residues	25	18
% Non-polar atoms [a]	72.6	78.7
% Polar atoms [a]	27.6	22.8
Planarity [a]	2.3	1.9
Hydrogen bonds [c]	2 symmetric Q60_O⋯E30_NE2	3 ^{A}Y68_OH⋯^{B}S94_OG ^{B}H91_O ⋯ ^{A}H67_NE2 ^{B}S94_O ⋯ ^{A}Y95-OH
Salt-bridges	0	0
Gap volume index [a]	2.03	4.07
Shape correlation statistics [b]	0.617	0.699
Interfacing residues	symmetric I31, T35, Q38, L39, L42, D54, Mly57, V58, Q60, A61, V64, L65	asymmetric V64, H67, Y68, F73, H91,Y95, I101 A : V64, H67, Y68, F73, H91, Y95, M99, I101 B : V64, H67, Y68, F73, H91, S94, Y95, V98, I101

Data were obtained with PISA. SA, surface area; [a] Calculated using the Protein-Protein Interaction server; [b] calculated by SC (Lawrence and Colman, 1993); [c] hydrogen bond donor and acceptor atoms/groups are listed.

However, as SycD behaved as a dimer in solution, the crystallographic dimer-of-dimers was excluded from further examination. The dimerization interfaces in the potential dimer assemblies 1 and 2 are both centered at the corresponding local rotation axis and mediated by hydrophobic interactions supported by hydrogen bonds (Figure 2II-21). Dimethylated lysine Mly57 at the edge of the dimerization interface of dimer 1 supports the dimerization only *via* its aliphatic side chain whereas the dimethylamino head group is not involved. The structural and statistical analyses (summarized in Table 2II-6) favor dimer 1, however, alternative dimer 2 could not be excluded with certainty.

2II.6.3 SycD forms head-to-head dimers in solution

To verify which dimer assembly SycD adopts in solution, key residues involved in the potential interfaces were chosen for site-directed mutagenesis in order to disrupt the interaction, followed by an analysis of the mutants in solution. A structure-based multiple sequence alignment of SycD with other T3SS translocator chaperones (Figure 2II-20) highlights the canonical and conserved residues characteristic for tetratricopeptide repeats that were excluded from mutagenesis. Several further residues are conserved, however, not predominantly in the dimerization interface.

Concerning elongated dimer 1, Ala61 and Leu65 were selected for the mutation into large, charged glutamates (single substitutions A61E, L65E and double mutant A61E/L65E). Both residues are centrally buried in the interface and occur twice due to the two-fold symmetry thereby facing each other (Figure 2II-21A). The introduction of two or four negatively charged residues was expected to cause steric hindrance as well as electrostatic repulsion and, therefore, the disruption of the dimer interface. In the interface of compact dimer 2, Ser94 as well as Tyr95 were selected. Tyr95 is a key residue located at the convex surface mediating hydrophobic and hydrogen-bonded interactions between both monomers (Figure 2II-21B). Replacement of large Tyr95 with small, polar serine instead of alanine was chosen to prevent aggregation. Equivalently to the glutamate double mutant A61E/L65E for the interface in dimer 1, the double mutant S94E/Y95E for potential interface 2 was generated.

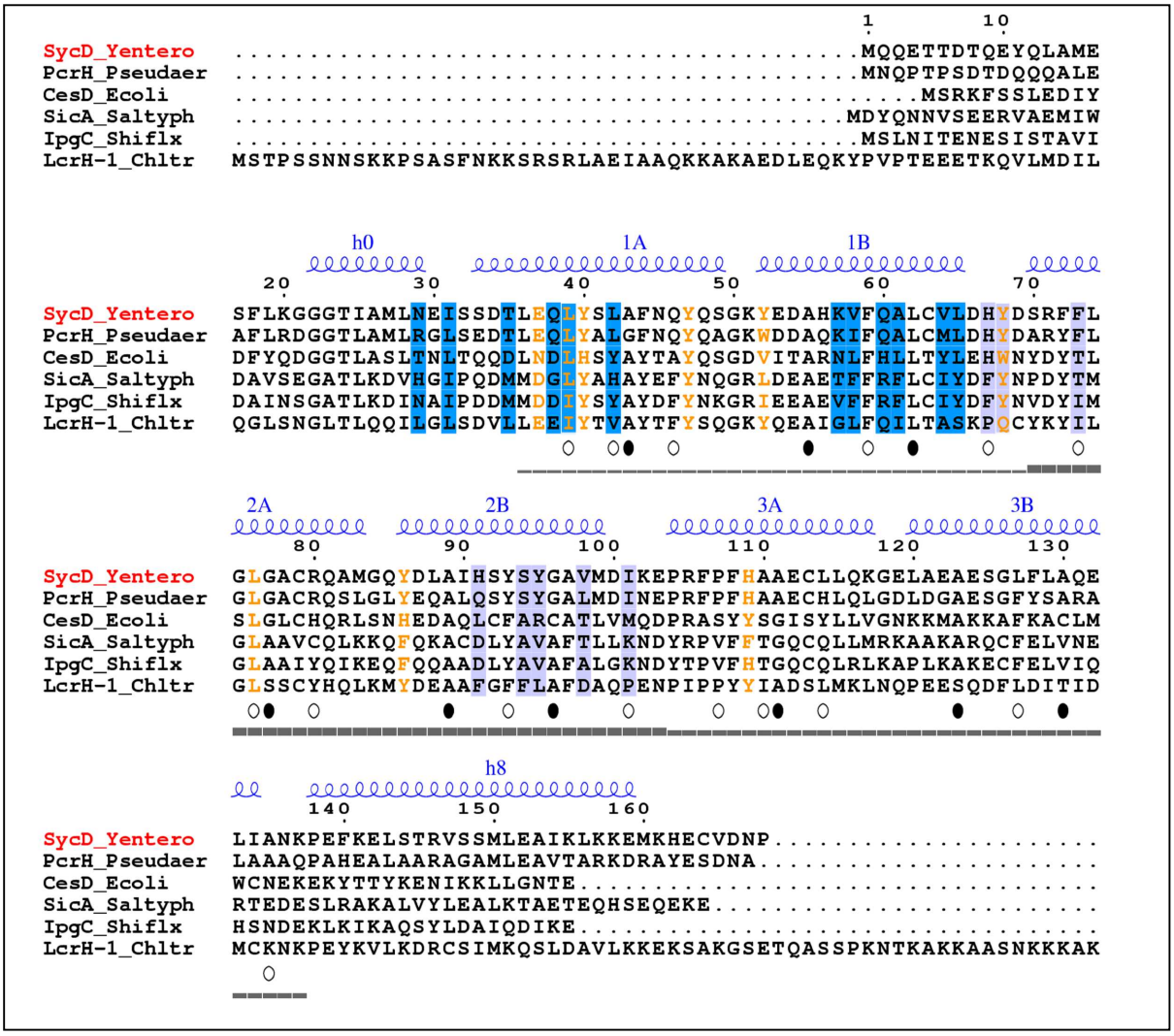

Figure 2II-20. Structure-based sequence alignment of SycD and homologous T3SS chaperones, adjusted with ESPript. *Y. enterocolitica* SycD (GenBank accession number AAD16814), *P. aeruginosa* PcrH (NP250398), *E. coli* CesD (AAC38376), *Salmonella typhimurium* SicA (AAB06794), *Shigella flexneri* IpgC (P0A2U4), *Chlamydia trachomatis* LcrH-1 (NP220091), *Burkholderia pseudomallei* BicA (YP335732), *Y. enterocolitica* SycB (AAM47500), *S. typhimurium* SscB (NP460368) and SscA (NP460364). – TPR1; ≡ TPR2; = TPR3. (●) Canonical residues at TPR positions 8, 20, 27; (○) conserved residues at positions 4, 7, 11, 24, 32. Interfacing residues in dimer 1 are shaded blue, those common in both monomers in dimer 2 are shaded light blue. For purposes of clarity only the first five sequences are depicted. Conserved surface residues, as derived from ProtSkin by analysis of the complete alignment, are highlighted in orange.

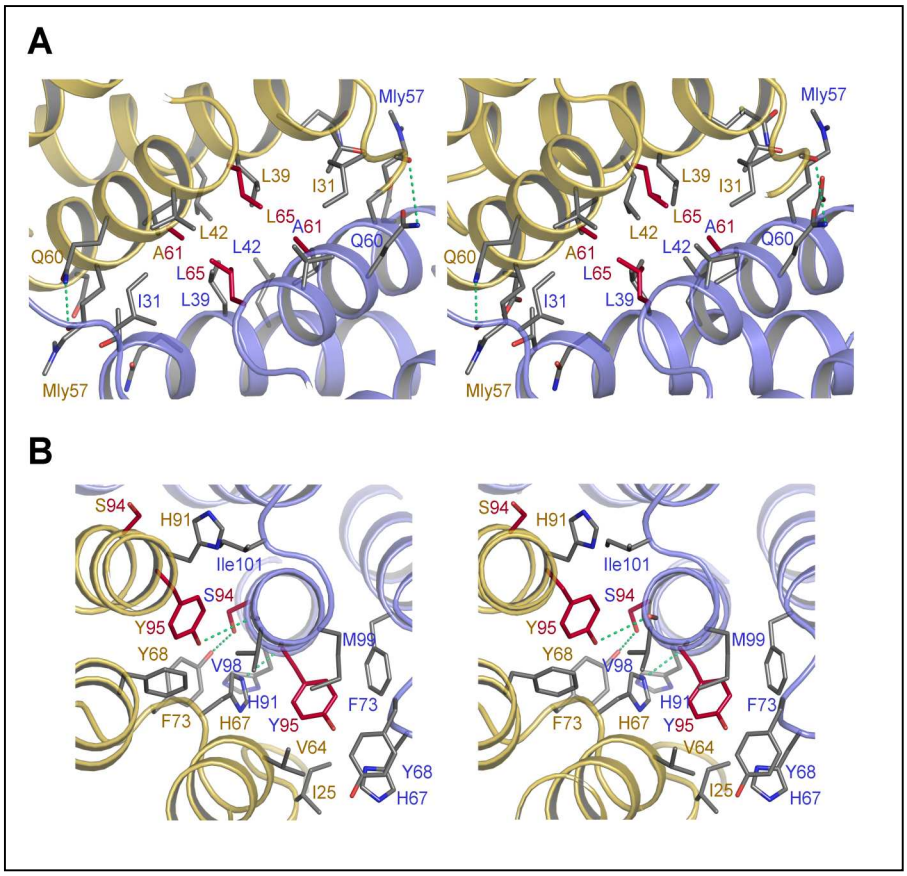

Figure 2II-21. Stereo views of the potential dimerization interfaces in dimer 1 (A) and dimer 2 (B). Residues chosen for mutational analysis are highlighted in red. Hydrogen bonds are depicted as green dashed lines. The residues mediating dimerization are mainly hydrophobic. The potential dimer 1 possesses a more planar interface with a smaller gap volume compared to the potential interface in dimer 2 (see Table 2II-6).

All five $SycD_{21\text{-}163}$ mutant proteins, single site mutants A61E, L65E and Y95S as well as the double mutants A61E/L65E and S94E/Y95E, were highly soluble and could be purified in wild-type-like quantities using the same protocol as for $SycD_{21\text{-}163}$. Their physicochemical properties are listed in Table 2II-7.

Table 2II-7. Physicochemical properties of $SycD_{21\text{-}163}$ and the dimer interface mutants.

	$SycD_{21\text{-}163}$ wt	Interface 1 A61E	L65E	A61E/L65E	Interface 2 Y95S	S94E/Y95E
Number of residues	148					
M_r [Da]	16'472	16'531	16'488	16'546	16'396	16'481
Mol ext. coeff. ε	9320	9320	9320	9320	8040	8040
Isoelectric point (pI)	5.3	5.2	5.2	5.1	5.3	5.1

Values generated with Vector NTI (Invitrogen). M_r , molecular mass; Mol. ext. coeff., molecular extinction coefficient, dimensions $[M^{-1} \cdot cm^{-1}]$. Due to PreScission protease cleavage, the proteins contain an extra N-terminal GPLGS peptide.

Analytical size exclusion chromatography and dynamic light scattering measurements were applied to investigate the oligomerization state of wild-type and mutant $SycD_{21-163}$. In size exclusion chromatography, wild-type $SycD_{21-163}$ as well as both dimer interface 2 mutants Y95S and S94E/Y95E eluted with an apparent molecular mass of 40 - 43 kDa, whereas the single and double interface 1 mutants, A61E, L65E and A61E/L65E, eluted with an apparent molecular mass of ~25 kDa suggesting a monomeric species (Figure 2II-22).

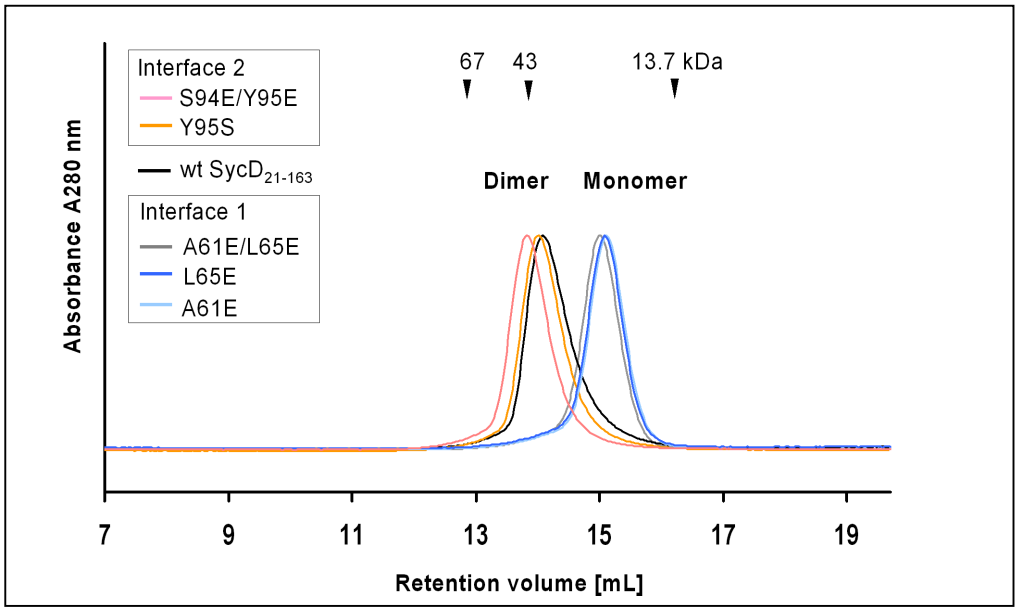

Figure 2II-22. Analytical size exclusion chromatography for $SycD_{21-163}$ and interface mutants. Superdex 200 HR 10/30 column (GE Healthcare-Amersham Biosciences). Running buffer 10 mM Tris pH 8.0, 150 mM NaCl, 1 mM DTT. Elution of calibration standard proteins are indicated by arrows. Interface mutants of putative elongated dimer 1 (interface 1) and compact dimer 2 (interface 2) are termed by mutations. Mutations introduced in the potential interface 1 resulted in a significant shift of retention time, thus indicating the monomeric species. Mutations applied to the potential interface 2 had no effect and the proteins behaved like a wild-type dimer. In conclusion, $SycD_{21-163}$ forms head-to-head dimers (dimer 1) in solution.

Dynamic light scattering measurements of the peak fractions gave ~38 kDa for wild-type $SycD_{21-163}$, ~40 kDa for the potential interface 2 mutant Y95S and ~41 kDa for S95E/Y95E, but only ~21 kDa for interface 1 mutants A61E, L65E and A61E/L65E (Table 2II-8). This is in line with the results derived from chromatography.

To ensure that the monomeric behavior of $SycD_{21-163}$ A61E, L65E and A61E/L65E was not caused by destroying the integrity of the TPR fold, wild-type $SycD_{21-163}$ and the mutants were analyzed by native PAGE (Figure 2II-23A). Wild-type $SycD_{21-163}$ and the monomeric A61E/L65E mutant were additionally examined by circular dichroism (CD) (Figure 2II-23B).

Table 2II-8. Dynamic light scattering results for the SycD interface mutants.

Protein	c [mg/mL]	r_H [nm]	$M_{r\ DLS}$ [kDa]	Polydispersity [%]	Base line	SOS error
$SycD_{21-163}$ wt	22	2.85	37.2	10.4	0.999	0.87
$SycD_{21-163}$ A61E	1.75	2.26	21.0	13	1.000	3.62
$SycD_{21-163}$ L65E	1.4	2.26	20.7	11	0.999	4.95
$SycD_{21-163}$ A61E/L65E	3.95	2.24	20.5	8.3	1.000	2.93
$SycD_{21-163}$ Y95S	3.7	2.88	37.5	11.0	0.999	0.71
$SycD_{21-163}$ S94E/Y95E	3.5	2.95	39.8	8	1.000	0.79

rH, hydrodynamic radius. Best fits for regularized radii distribution are listed. The calculated molecular mass of monomeric wild-type and mutant $SycD_{21-163}$ is ~16.5 kDa.

In the native gel, $SycD_{21-163}$ wild-type and the interface mutants migrated as focused single bands consistent with folded proteins. Wild-type $SycD_{21-163}$ and the mutant Y95S (pI 5.3) migrated on the same level, whereas the single glutamate mutants A65E, L65E (pI 5.2), and more significantly the double mutants A61E/L65E and S94E/Y95E (pI 5.1) migrated faster due to the additional surface-exposed negative charges accelerating migration in the electric field (Figure 2II-23A).

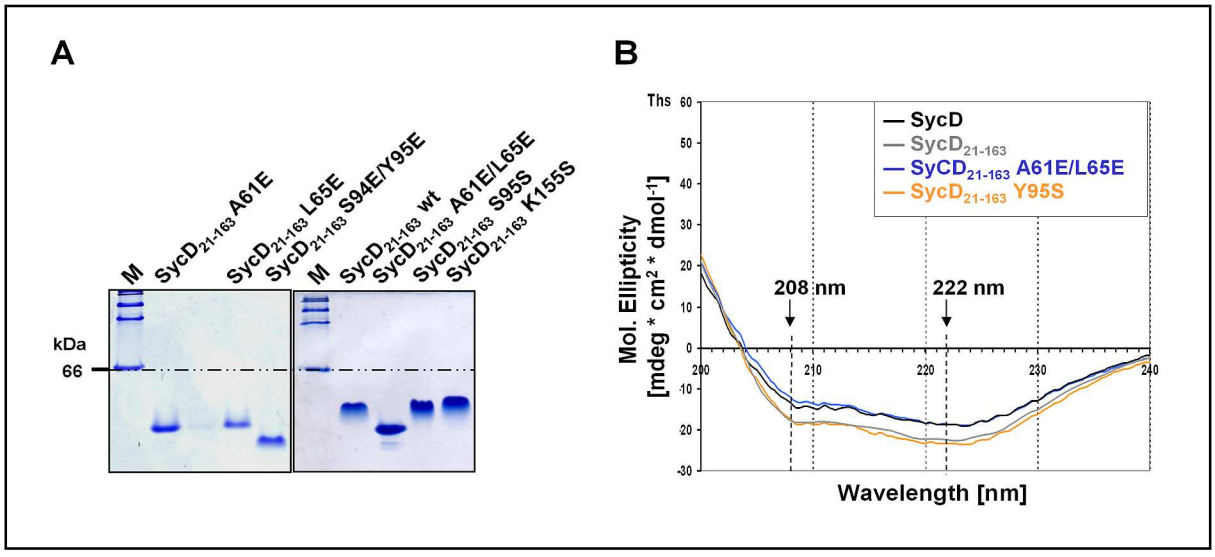

Figure 2II-23. Native PAGE and circular dichroism analysis of SycD and derivatives verify the native fold. (A) All mutants ran as focused bands corresponding to correctly folded proteins. The extra-charge mutants A61E, L65E and more obvious the double-mutants A61E/L65E and S94E/Y95E ran faster. M, native high molecular weight marker. **(B)** Circular dichroism spectra. $SycD_{21-163}$ wt and interface mutants exhibit virtually identical CD spectra corresponding to α-helical secondary structure elements. Measurements were carried out in 10-20 mM potassium sodium phosphate pH 7.5. Protein concentration was ~6-9 mM.

The CD spectra of the wild-type and the mutant proteins were virtually identical displaying two minima at 208 and 222 nm (Figure 2II-23B). This results are characteristic for α-helical secondary structure elements indicating that the mutants were correctly folded. Further, CD spectra analysis *via* least square fitting (Bolotina *et al.*, 1980) calculated an α-helical content of 68 % for wild-type SycD and 67 % for $SycD_{21\text{-}163}$. In comparison, the content of α-helical secondary structure elements derived from the crystal structure of $SycD_{21\text{-}163}$ is 78 % with 111 residues out of 143 being located in α-helices (see section 2II.5). The CD spectra of both interface mutants A61E/L65E and Y95S were apparently identical with the CD spectra of $SycD_{21\text{-}163}$ and full-length, wild-type SycD suggesting that all SycD species possessed the intact secondary structure elements and the native fold.

2II.6.4 A third dimer assembly indicates flexible SycD dimerization

In addition to wild-type $SycD_{21\text{-}163}{}^{meth}$, crystals were obtained for dimethylated mutants $SycD_{21\text{-}163}$ S94E/Y95E ^{meth} (dimeric) and $SycD_{21\text{-}163}$ L65E ^{meth} (monomeric) as well as for non-methylated $SycD_{21\text{-}163}$ A61E/L65E (monomeric) (section 2II.6.3).

Intriguingly, the monomeric interface 1 mutant A61E/L65E crystallized by chance in the same condition as wild-type $SycD_{21\text{-}163}{}^{meth}$, however, exhibiting inferior diffraction and an orthorhombic space group (I222) with only one molecule per asymmetric unit (Table 2II-4). The structure was solved by MR using one monomer of the refined $SycD_{21\text{-}163}$ structural model from the monoclinic crystal form as search model. No stable oligomeric assembly within the crystal packing was detected, which is consistent with the mutant's monomeric behavior observed in solution. The refined structural model of $SycD_{21\text{-}163}$ A61E/L65E comprises SycD residues 29 - 163.

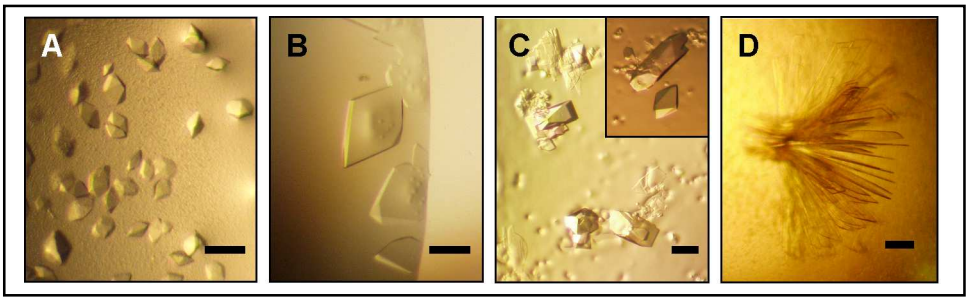

Figure 2II-24. Crystals of $SycD_{21\text{-}163}$ interface mutants. (A) and **(B)** Trigonal crystals of $SycD_{21\text{-}163}$ S94E/Y95E ^{meth} (space group $P3_221$). The varying morphology is due to different ratios of two PEG precipitants. **(C)** By chance, the unmethylated monomeric interface mutant $SycD_{21\text{-}163}$ A61E/L65E crystallized under the same condition as $SycD_{21\text{-}163}{}^{meth}$, although in an orthorhombic space group (I222). **(D)** Monomeric $SycD_{21\text{-}163}$ L65E ^{meth} yielded bizarre book-like clusters with very thin plate-leaves, which could not be improved in thickness. Scale bar = 100 µm.

As to the well-diffracting crystals of $SycD_{21\text{-}163}{}^{meth}$ S94E/Y95E, the PHENIX program XTRIAGE used for a twinning analysis of the diffraction data, initially indexed as P3, suggested a higher point group symmetry, P321. Systematic absences along the reciprocal ℓ axis indicated the presence of either a 3_1 or 3_2 screw axis along the three-fold rotation axis. Matthews coefficient calculation did not clearly indicate a probability maximum at an integer number of molecules per asymmetric unit, rather ranged between one or two molecules and a solvent content of 68 % and 37 %, respectively (Figure 2II-25B). However, as $SycD_{21\text{-}163}{}^{meth}$ S94E/Y95E behaved as a dimer in solution, two molecules in the asymmetric unit related by non-crystallographic symmetry were also conceivable. Molecular replacement for $SycD_{21\text{-}163}{}^{meth}$ S94E/Y95E provided the correct solution for the first molecule without difficulties. Attempts to place the second monomer of the assumed $SycD_{21\text{-}163}{}^{meth}$ S94E/Y95E homodimer in the asymmetric unit during a further MR search run was not successful. Inspection of the packing revealed sufficient crystal contacts between the symmetry related monomers, principally *via* the long C-terminal helix h8 (Figure 2II-25C). The asymmetric unit thus harbors only one molecule.

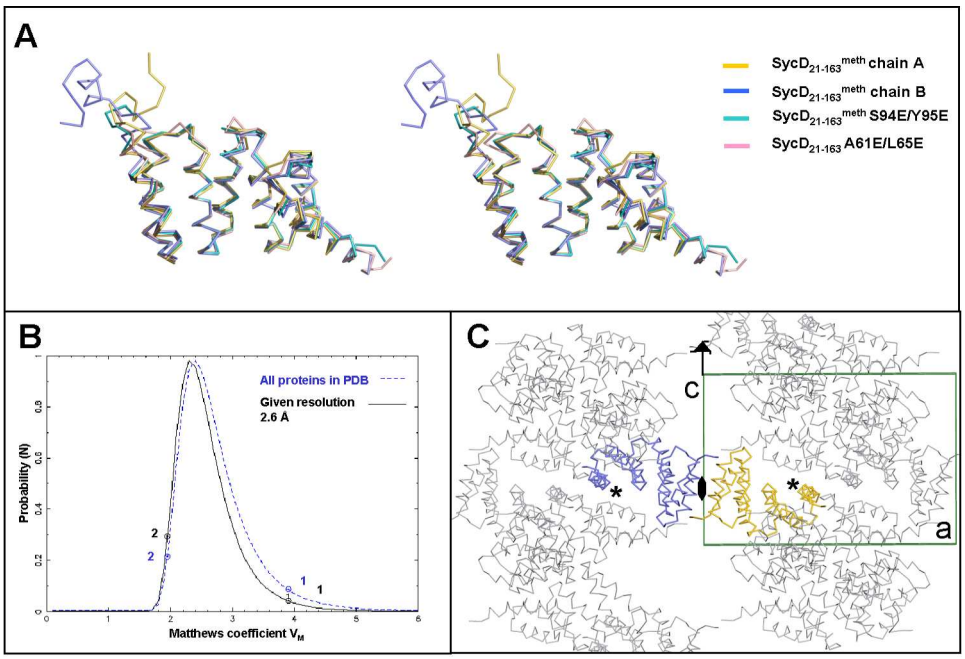

Figure 2II-25. SycD monomer overlay and crystal packing for $SycD_{21\text{-}163}{}^{meth}$ S94E/Y95E. (A) Stereo image of the superposed monomer structures of wild-type $SycD_{21\text{-}163}$ and the interface mutants. All monomers show the intact TPR domain fold and a higher flexibility of the terminal regions. **(B)** Corresponding to Matthews' probability calculation two molecules per asymmetric unit seemed more probable, though only one molecule is actually present in the asymmetric unit with a high solvent content of 68 %. **(C)** Crystal packing. View perpendicular to the three-fold rotational screw axis and along the crystallographic two-fold rotational symmetry axis parallel to unit cell axis **b**. The blue monomer is symmetry-related to the yellow monomer by the crystallographic symmetry operation (-x, -x+y, -z + 2/3) forming dimer 3. Main crystal contacts are mediated by the C-terminal helix h8 (designated by asterisks).

Well-defined electron density was observed for SycD residues 29-160. Furthermore, the packing disclosed the assembly of homodimers as well, with the two $SycD_{21-163}$ S94E/Y95E monomers sitting at the two-fold crystallographic rotational symmetry axis (Figure 2II-25C). The $SycD_{21-163}$ S94E/Y95E dimer is again a head-to-head dimer. Strikingly, the monomers in this new dimer are orientated differently, with both monomers rotated more heavily with respect to each other (crossing angle 90° *vs.* 61° in dimer 1), resulting in a kinked assembly (Figure 2II-26, compare dimer 1 in Figure 2II-19).

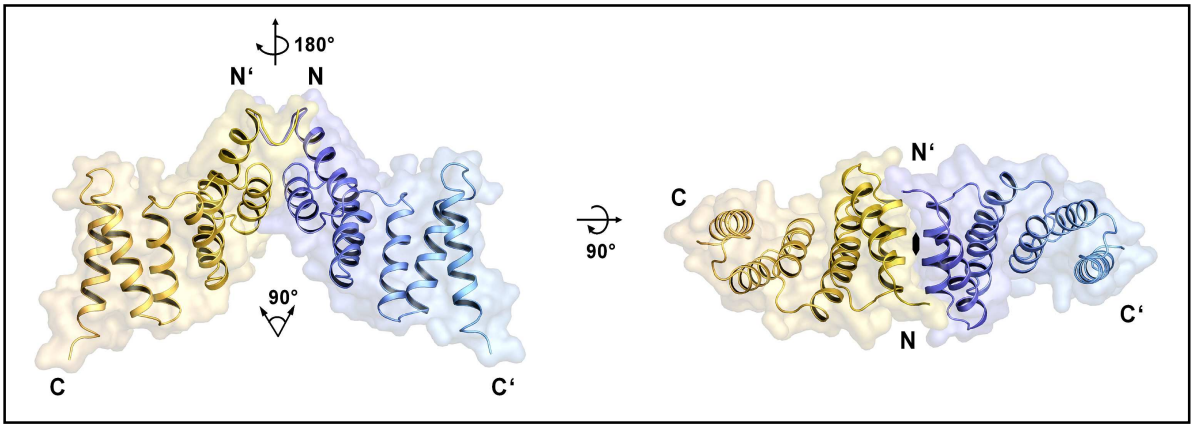

Figure 2II-26. Front and top view of a third dimer assembly of $SycD_{21-163}$. Ribbon and surface presentations of the crystal structure of homodimeric $SycD_{21-163}$ S94E/Y95E, one of the mutants used to determine the real dimerization interface of SycD. One monomer colored in yellow, the other in blue. Basically, the same residues as in dimer 1 are involved in dimerization. However, the monomers in the third dimer are skewed more heavily with respect to each other (90° instead of 61°as in dimer 1), thus forming a kinked dimer (dimer 3).

Interfacing residues in this new dimer (dimer 3) are basically the same as for dimer 1, forming a predominantly hydrophobic surface (Figure 2II-27). The interface is stabilized exclusively by non-polar contacts, lacking hydrogen bonds or salt-bridges between the monomers. However the buried interface area per monomer is considerably smaller in the kinked $SycD_{21-163}$ S94E/Y95E dimer (607 $Å^2$) than in dimer 1 (924 $Å^2$) (Table 2II-9).

Taken together, the results from the mutational analysis and the additional mutant structure strongly suggest that the SycD dimer in solution corresponds to a head-to-head dimer and that dimerization is disrupted in the A61E, L65E and A61E/L65E mutants.

Table 2II-9. Comparison of the dimer interface characteristics for $SycD_{21-163}$ dimer 1 and dimer 3

Interface statistics	Dimer 1 - elongated	Dimer 3 - kinked
Monomer buried SA [Å^2]	924	607
% Monomer SA	11.4	7.5
Number of residues	25	21
% Non-polar atoms [a]	72.6	68.7
% Polar atoms [a]	27.6	31.3
Planarity [a]	2.3	2.9
Hydrogen bonds	2	0
Salt-bridges	0	0
Gap volume index [a]	2.03	3.84
Shape correlation statistics [b]	0.617	0.548
Interfacing residues (buried SA>40 %, both protomers)	I31, T35, Q38, L39, L42, D54, Mly57, V58, Q60, A61, V64, L65	E30, T35, L39, L42, Q46, D54, Mly57, V58, Q60, A61, V64, L65

Data were obtained with PISA; [a] calculated by Protein-Protein Interaction server; [b] calculated by SC (Lawrence and Colman, 1993).

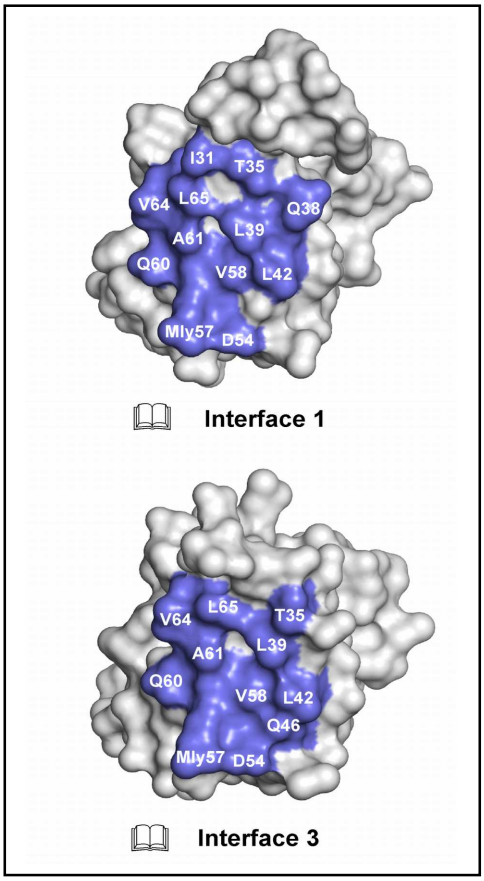

Figure 2II-27. The dimerization interfaces of the head-to-head $SycD_{21-163}$ dimers 1 and 3. Dimerization in both cases utilized roughly the same residues of TPR1. View onto the interfaces opened up.

2II.7 Relevance of the SycD dimerization interface *in vivo*

In order to investigate the physiological role of SycD dimerization, *in vivo* experiments with *Yersinia* were carried out comparing a wild-type strain, a *syc*D null mutant and the *syc*D null mutant reexpressing either wild-type *syc*D or the *syc*D double mutant A61E/L65E. Culture supernatants were analyzed by SDS-PAGE to assay for Yop secretion. Total cell fractions and supernatants were analyzed by Western blot for production and secretion of YopE and of the SycD binding partners YopB and YopD. Experiments were performed in the absence and presence of calcium ions in order to monitor the calcium dependence of Yop production, as *in vitro*, the activation of the T3SS machinery can be achieved by a temperature shift to 37 °C and the depletion of calcium ions by chelating agents (calcium dependent (CD) growth phenotype (Forsberg *et al.*, 1987)), also termed Low calcium response (LCR).

The SycD A61E/L65E mutant shows typical characteristics of a *syc*D null mutant (Figure 2II-28, Table 2II-10). These include the lack of YopB and YopD secretion in the absence of calcium, deregulated Yop production in the presence of calcium (calcium inde-

pendent phenotype) and an increased LcrV secretion independent of the calcium concentration. Mutations in the SycD dimerization interface obviously abrogate the functionality of SycD.

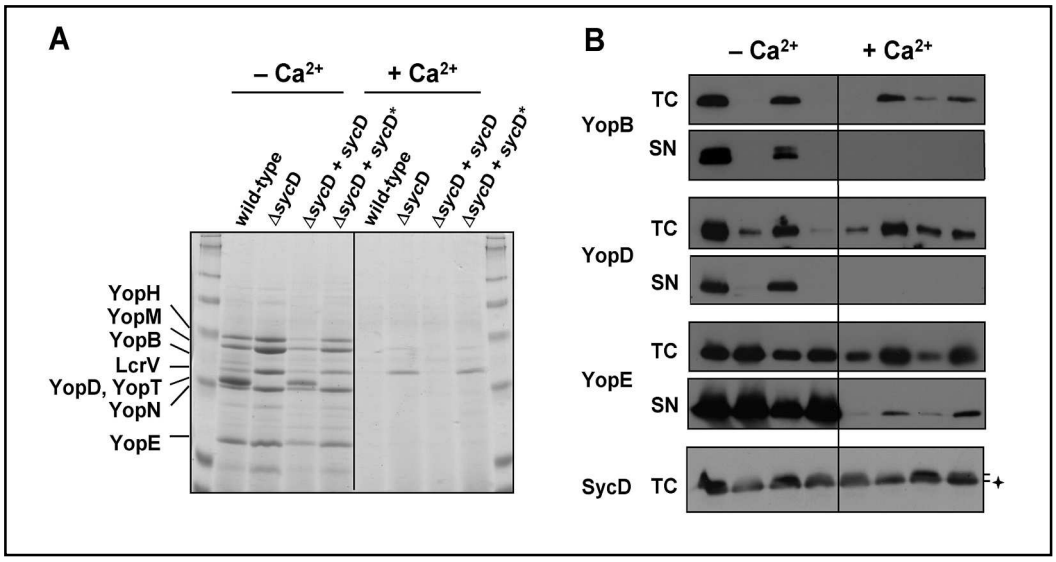

Figure 2II-28. ***In vivo*** **relevance of the SycD dimerization interface.** Expression and secretion of *Yersinia* Yops in the absence and presence of calcium, detected by **(A)** Coomassie-stained SDS-PAGE of the culture supernatant and **(B)** Western blot of total cell and supernatant fractions (sample application pattern as in (A). *Yersinia* wild-type, a *syc*D knockout Δ*syc*D, and Δ*syc*D reexpressing either wild-type *syc*D or the monomeric A61E/L65E mutant (*syc*D*) were examined. The A61E/L65E mutant showed a null mutant-like phenotype. Note: The polyclonal antibody against SycD cross-reacts with a band (marked with a cross, +) running directly below SycD. (Experiments carried out by I. Sorg; Biozentrum of the University of Basel, Switzerland).

Table 2II-10. Quantification of the Western blot results assaying Yop secretion and expression.

No calcium						
Sample	TC (YopB)	SN (YopB)	TC (YopD)	SN (YopD)	TC (YopE)	SN (YopE)
Wild-type	+++	+++	+++	+++	++++	++++
Δ*syc*D	–	–	+	+	++++	++++
Δ*syc*D + *syc*D	++	+	++	+++	+++	++++
Δ*syc*D + *syc*D*	–	–	+	+	++++	++++
+ 5 mM calcium						
Sample	TC (YopB)	SN (YopB)	TC (YopD)	SN (YopD)	TC (YopE)	SN (YopE)
Wild-type	–	–	+	–	+++	–
Δ*syc*D	++	–	+++	–	++++	+
Δ*syc*D + *syc*D	+	–	+	–	+++	–
Δ*syc*D + *syc*D*	++	–	+	–	++++	+

*syc*D*, monomeric A61E/L65E mutant; (TC), total cell fraction; (SN), supernatant fraction; (++++/ +++/ ++/ +), intensity of the signal; (–), no signal.

2II.8 Determination of further interaction surfaces in SycD

To identify potential interfaces in SycD involved in protein-protein interactions, the electrostatic surface potential, conserved sequence features and predicted binding sites in SycD were examined.

The electrostatic surface potential of the elongated dimer 1 of $SycD_{21-163}$ is shown in Figure 2II-29. The flat top/bottom face of the dimer displays an extended negative charge that additionally encompasses the upper part of the concave groove, whereas the lower part of the concave face on the dimer front exposes a predominantly hydrophobic area interspersed with positively charged patches. The side chain of Arg71 in the crystal structure is bent toward Glu37 forming a salt-bridge (compare Figure 3II-1) and does not create a positively charged patch on the concave face together with Arg105 contrary to the predictions derived from the homology model (Pallen *et al.*, 2003).

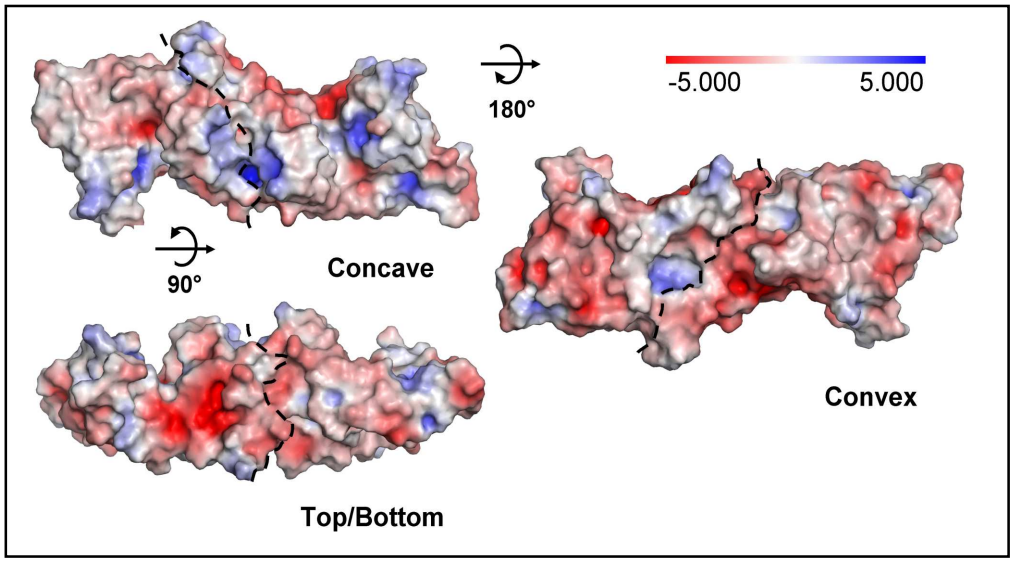

Figure 2II-29. Electrostatic surface potential of the elongated $SycD_{21-163}$ dimer 1. The electrostatic surface potential was calculated using the APBS (Baker *et al.*, 2001) plug-in of PyMOL. The dimer surface exposing both concave TPR faces harbors positively charged patches (blue). A negatively charged patch (red) is located on the flat dimer top/bottom face (after a 90° turn upwards). Neutrally charged regions are colored white.

In addition to the region within the concave face that has been previously identified as binding groove (Edqvist *et al.*, 2006), the prediction program ProMate (Neuvirth *et al.*, 2004) suggested a large continuous patch for protein-protein-interactions comprising additionally residues from the top of the monomer, reaching further to the upper part of the opposite,

convex face, comprising residues Tyr40, Phe44, Gln48, Tyr59, His67, Tyr68, Asp69, Ser70, Arg71, Phe73, Leu74, Gly75, Ser92, Ser94, Tyr95 (not shown). In order to visualize the conservation of surface residues in SycD and other T3SS Class II chaperones and thus putative conserved interaction sites, the structure-based multiple alignment of Figure 2II-20 was converted into a property file *via* ProtSkin (http://www.mcgnmr.ca/ProtSkin/). The concave surface of SycD exhibits numerous conserved amino acids, whereas the convex side of the chaperone shows little sequence conservation (Figure 2II-30).

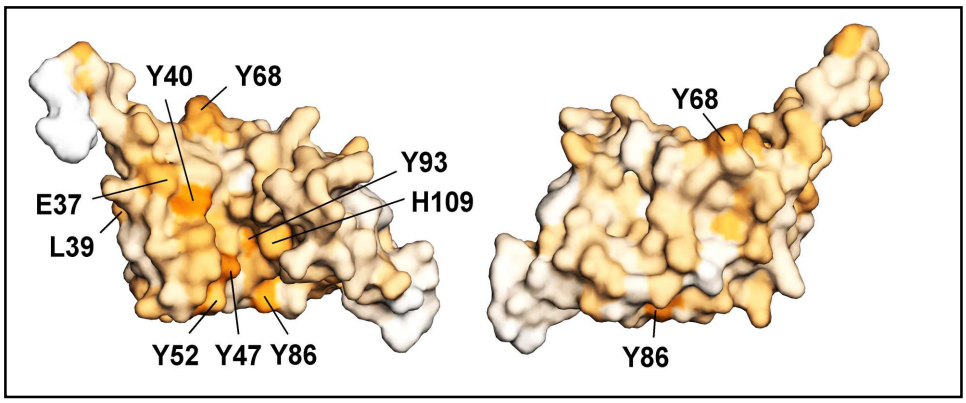

Figure 2II-30. Sequence conservation of T3SS Class II chaperones. Sequence conservation drawing for the $SycD_{21-163}$ monomer as obtained by ProtSkin (http://www.mcgnmr.ca/ProtSkin/). Orange denotes conserved regions. Tyrosines are highly conserved and line the inner groove. In comparison to the concave face (left), the convex side (right) shows only minimal conservation.

Most of the protein's tyrosine residues on the concave face are conserved throughout the majority of the T3SS Class II chaperones. Additionally conserved, surface exposed residues comprise an acidic and a heterocyclic/aromatic side chain (Glu37, His109), as well as two leucine residues at TPR consensus positions (Leu39, Leu76) (Figure 2II-30). All of these residues line the concave face/binding groove of the chaperone with exception of Leu39 in the dimer interface, Leu76 pointing toward the convex outside and the protruding Tyr68.

In summary, SycD exhibits several distinct surface areas possessing favorable properties for protein-protein interactions.

3 Discussion

3I SycT – a typical and special T3SS effector chaperone ?

3I.1 SycT lacks the dimerization helix

SycT shares the global mixed α/β-fold fold with other homodimeric effector chaperones (Figure 3I-1). All crystal structures of T3SS effector chaperones determined before and after SycT display three α-helices arranged around the anti-parallel β-sheet, with helix α2 being considerably involved in dimerization (Parsot *et al.*, 2003) (Figure 3I-1). Strikingly, α-helix α2 is consistently absent in all three crystals forms of SycT.

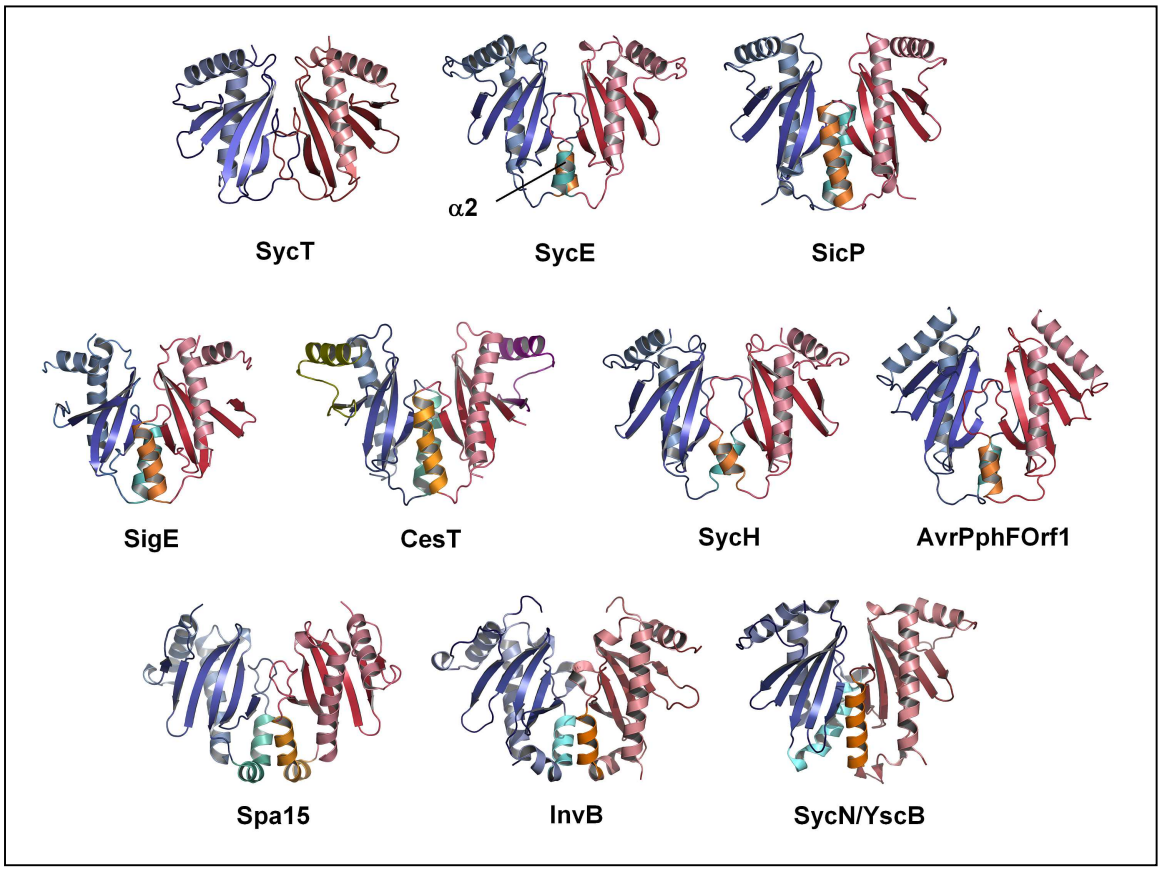

Figure 3I-1. Ribbon representations of homodimeric SycT$_{1-122}$ and of all T3SS effector chaperones structurally characterized so far. SycT shares the global mixed α/β-fold of other effector chaperones. However, SycT lacks α-helix α2, designated as dimerization helix in other effector chaperones. *Y. enterocolitica* SycT, *Y. pseudotuberculosis* SycE (PDB identifier 1L2W) (Birtalan and Ghosh, 2001), *Salmonella typhimurium* SicP (1JYO) (Stebbins and Galan, 2001), *Salmonella enterica* SigE (1K3S) and *E. coli* CesT (1K3E) (Luo *et al.*, 2001), *Y. pestis* SycH (1TTW) (Phan *et al.*, 2004), *Pseudomonas syringae* pv. *phaseolicola* AvrPphF ORF1 (1S28) Singer *et al.*, 2004, and multivalent *Shigella flexneri* Spa15 (1R9Y) (Van Eerde *et al.*, 2004) and *S. typhimurium* InvB (2FM8) (Lilic *et al.*, 2006) as well as *Y. pestis* heterodimeric SycN/YscB (1XKP) (Schubot *et al.*, 2005). The monomers in a homodimer are colored in blue and red, respectively. The helices α2 are highlighted in orange and turquoise.

Instead, dimerization involves hydrophobic and polar residues exclusively located in loops and β-strands (Figure 2I-13). The accessible surface area buried per monomer comprises 1100 $Å^2$, corresponding to ~15 % of the total surface area value that lies within the range of buried surfaces found for other T3SS effector chaperones (900 to 1200 $Å^2$).

The missing α-helix α2 in SycT, confirmed by the SycT structure solved by a second group at the same time (Locher *et al.*, 2005), might well be the cause of the failure of molecular replacement attempts for SycT. SycT lacking α-helix α2 can be regarded as a dimerization helix-free variant of effector chaperones with helices α2 varying from absent (SycT) to short (e.g. SycH) and long (e.g. SicP) (Figure 3I-1).

In conclusion, dimerization in effector chaperones depends predominantly on the hydrophobic nature of the involved residues and is independent of an α-helical conformation.

3I.2 The hydrophobic surface patches in SycT are spatially conserved

In the crystal structures of other effector chaperone structures, the hydrophobic patches 1 and 2 seen in SycT are present at approximately the same position (Figure 3I-2), whereas patch 3 is not observed. The interaction of the C-terminal peptide of SycT with one of the hydrophobic patches resembles the situation in one of the SycE structures where the flexible C-terminus similarly binds to the hydrophobic patch 1 of an adjacent dimer (Trame and McKay, 2003).

The conserved position of patches 1 and 2 in SycT suggests a similar mode of effector binding. In the recent past, several T3SS effector chaperones have been structurally characterized in complex with their cognate effector such as *Salmonella* SicA/SicP (Stebbins and Galan, 2001) and InvB/SipA (Lilic *et al.*, 2006) as well as *Yersinia* YopE/SycE (Birtalan *et al.*, 2002) (Figure 3I-2) and YscM2/SycH (Phan *et al.*, 2004). In theses complex structures, the N-terminal region of the effector wraps around the chaperones displaying only secondary but no tertiary structure. In the YopE/SycE complex, both patches 1 bind α-helices while both patches 2 bind β-strands of the YopE chaperone-binding domain (Figure 3I-2). Strikingly, only one monomer in the *Salmonella* InvB dimer contacts the effector SipA, which might confer the binding specificity of this multivalent chaperone.

Despite the spatially conserved hydrophobic patches 1 and 2 representing the postulated effector-binding sites, the details of the YopT/SycT interaction could differ from those of

other effector/chaperone pairs. The third hydrophobic patch of SycT may indicate an enlarged contact area and the effector YopT may follow a different path wrapping around SycT.

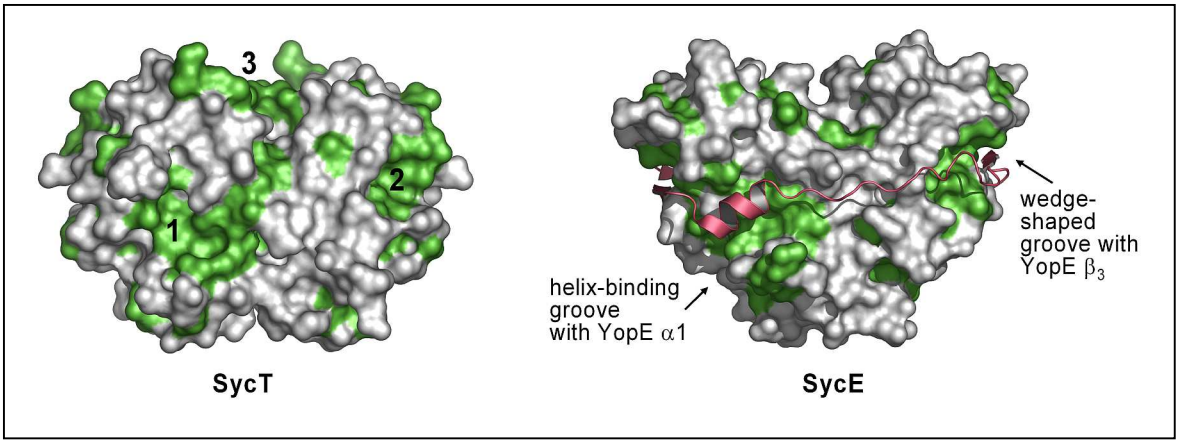

Figure 3I-2. Hydrophobic patches on the SycT dimer surface. Patches 1 and 2 in SycT correspond to those of a SycE dimer where these patches are involved in effector binding (right, SycE in complex with the CBD of YopE, $YopE_{23-78}$, red). SycT possesses an additional hydrophobic patch (3) not present in SycE. Surfaces corresponding to hydrophobic side chains are highlighted in green.

3I.3 Does effector binding require conformational rearrangements of SycT?

The vicinity of hydrophobic patch 2 in SycT exhibits significant differences compared to other T3SS effector chaperones (except probably Spa15). In most chaperones structurally characterized to date, patch 2 comprises also a pocket, formed by conserved hydrophobic residues from α-helices α1 and α3, as well as a shallow groove between β–strand β1 and the loop connecting the N-terminal α-helix α1 with β1. In SycT, the residues connecting α1 and β1 form an additional β–strand β0 anti-parallel to β1 that occupies this shallow groove (Figure 3I-3, left) and results in a more compact shape compared to the heart-shaped outline of other effector chaperones such as SycE (Figure 3I-2).

In one SycT monomer, the additional β-strand is transformed into a loop and flipped toward helix α1, thereby opening up the abovementioned groove (Figure 3I-3, left). This strongly resembles the situation in Spa15 (Van Eerde *et al.*, 2004) (Figure 3I-3, left). Effector proteins that had been co-crystallized with their cognate chaperone such as the complexes YopE/SycE, SptP/SicP, SipA/InvB and YopN/SycN-YscB (Schubot *et al.*, 2005) bind to the chaperone's patch 2 filling this shallow groove and extending the chaperone β-sheet by an additional strand along side strand β1 (Figure 3I-3, right). This effector β-strand is a common feature of effector CBDs, therefore called β-motif, and is strictly required for effective binding to the wedge-shaped groove of the cognate chaperone (Lilic *et al.*, 2006).

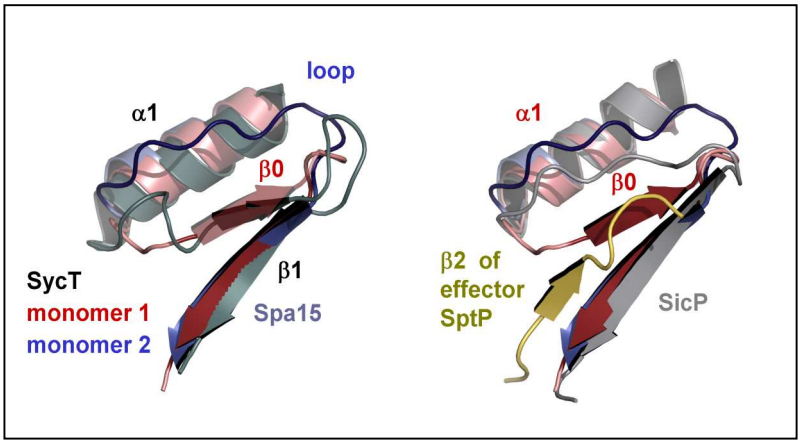

Figure 3I-3. Effector binding and rearrangement of secondary structure elements in SycT. The shallow groove near hydrophobic patch 2 is involved in effector binding such as in the SptP/SicA complex. In SycT and Spa15, this groove is filled by the additional β-strand that is formed by the region connecting α-helix α1 and β-strand β1. Superposed native SycT monomers 1 (red) and 2 (blue) are depicted in both overlays. (Left) Superposition of both SycT monomers onto *Shigella flexneri* Spa15 (grey). Despite the longer loop (+4 residues) connecting α1 and β1 in Spa15, the structural organization is similar to the red SycT monomer. (Right) In the SicP/SptP complex (SicP in grey, SptP in yellow) superposed on SycT monomer 1 (red), the effector strand β2 occupies the groove and extends the chaperone β-sheet. If YopT binds in the same manner to SycT as SptP to SicA, it would partially overlap with β0 in the red monomer, but not with the conformationally rearranged blue monomer.

The chaperone residues involved in forming the corresponding β-motif-binding pocket comprise conserved hydrophobic residues that are located in α-helices α1 and α3 and β-strand β1 (compare Figure 3I-4A). Structural overlay revealed also their spatial conservation (Lilic *et al.*, 2006). The work of Lilic *et al.* based on the SipA/InvB complex did not address the YopT/SycT complex. Therefore the SycT structure and the YopT sequence were analyzed in order to identify the corresponding pocket and β-motif. A structure-based alignment and the structural overlay of InvB with rearranged native SycT monomer 1 (lacking β0) disclosed hydrophobic residues in SycT (Leu16, Tyr28, Phe30, Val32, Leu101, Ile105) that match with the β-motif-binding pocket in InvB (Figure 3I-4A,B).

The structure-based sequence alignment of the YopT sequence with effectors that had been co-crystallized with their cognate chaperone allowed the assignment of two similar β-motif triplets to the YopT sequence, comprising residues Leu65, Leu69, Asp72 as well as Leu95, Val99, Val102 (Figure 3I-4C). Secondary structure prediction does not consistently assign any secondary structure to these YopT regions. Apart from insufficient prediction, the proposed β-motifs in YopT, which are very likely required in binding to SycT, might be formed during the binding process. Although no conformational changes have been observed

upon effector binding in the chaperone SycE (Birtalan *et al.*, 2002), the conformational rearrangement of SycT β0 is thus likely to be additionally required for binding to YopT.

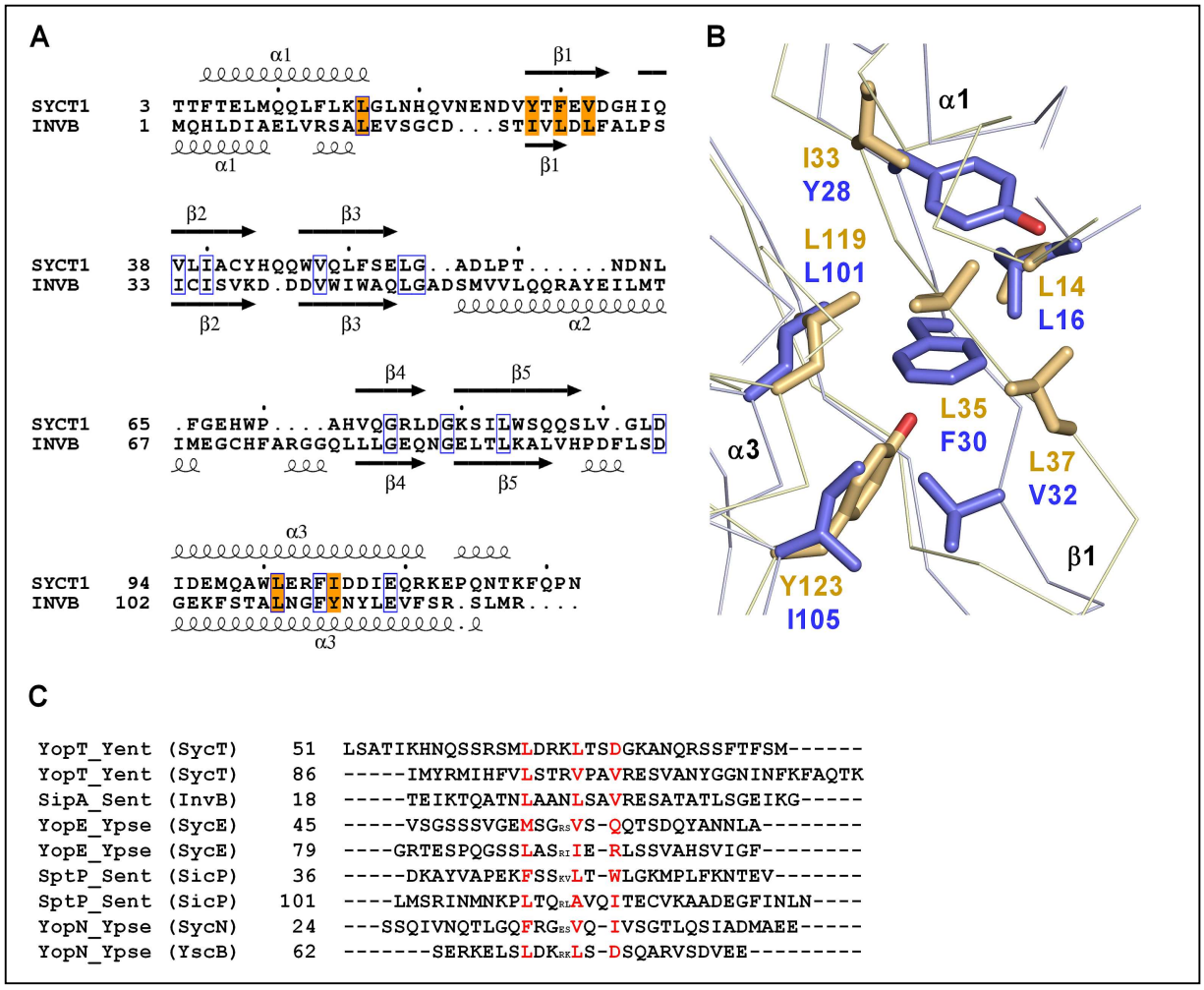

Figure 3I-4. β-motif binding pocket in SycT. (A) Structure-based sequence alignment of native SycT (monomer 1 = chain A) and InvB. InvB residues located in the shallow groove near hydrophobic patch 2 that are involved in binding to the β-motif of effector SptP are shaded orange and superpose well with hydrophobic residues in SycT. Identical and homologous residues are boxed in blue. **(B)** In the structural overlay (ribbon and stick model), these hydrophobic residues of *Salmonella enterica* InvB (GenBank, PDB-ID 2FM8) (yellow, Leu14, Ile33, Leu35, Leu37, Leu119, Tyr123) (Lilic *et al.*, 2006) superpose well with the corresponding residues in rearranged monomer 1 of native SycT (blue, Leu14, Tyr28, Phe30, Val32, Leu101, Ile105), thus these SycT residues are most likely involved in binding to YopT. **(C)** Structure-based sequence comparison of YopT with T3SS effectors co-crystallized with their cognate chaperones (in parentheses). The β-motif identified in the SipA sequence in the first place by Lilic *et al.* (2006) is also found twice in the YopT chaperone-binding domain (YopT 51-121, see section 2I.1.4). *Y. enterocolitica* YopT (GeneBank entry AAD16808), *Salmonella enterica* SipA (AAA86618), *Y. pseudotuberculosis* YopE (P08008), *S. typhimurium* (P74873), *Y. pseudotuberculosis* YopN (YP068474).

3I.4 The cavity in the SycT dimerization interface is closed and uncharged

A polar cavity located at the dimerization interface of T3SS effector chaperones was first described for SycE (Evdokimov *et al.*, 2002). Fully enclosed cavities as in SycT are also present in Spa15 and AvrPphF Orf1 dimers (Singer *et al.*, 2004; Van Eerde *et al.*, 2004). The dimerization interfaces of other T3SS effector chaperones, e.g. SycE, SycN/YscB (Schubot *et al.*, 2005) or SycH (Phan *et al.*, 2004), reveal similar yet open, solvent accessible cavities (Figure 3I-5). Compared to other solvated intersubunit cavities (Hubbard and Argos, 1994) that of SycT is quite large with ~100 $Å^2$ or 9 % of the dimerization interface per monomer not being involved in direct protein-protein interactions.

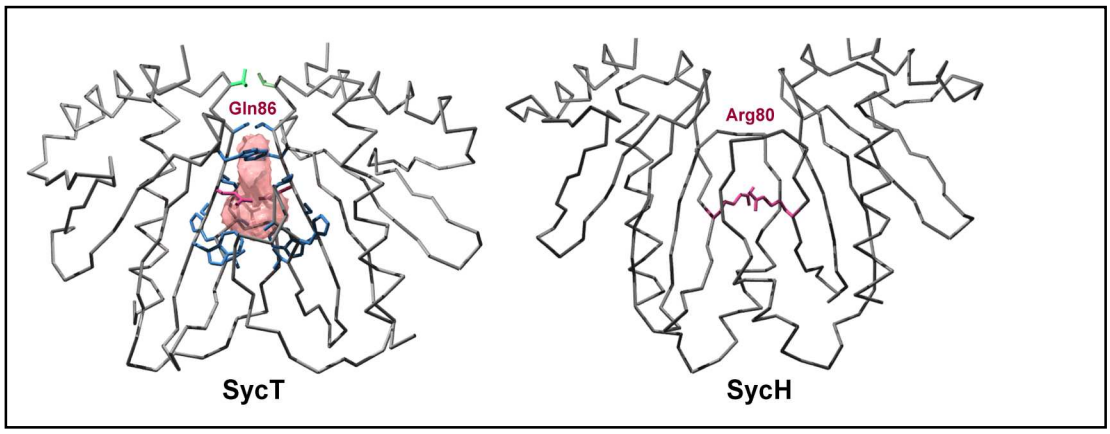

Figure 3I-5. SycT dimerization interface encloses a polar cavity. In contrast to the closed cavity in SycT (left), the cavity in the dimerization interface of SycH (right) is accessible and dotted by the positive charges of Arg80 (red stick model) at the position where in SycT an uncharged residues is found (Gln86, red stick model).

Conservation of the cavity, open or closed, among T3SS effector-binding chaperones is strongly suggestive of a biological role. In SycE, SycH and SycN/YscB, the three chaperones from *Y. pestis* for which structural information is available, two arginines create a positively charged patch inside the cavity (Evdokimov *et al.*, 2002; Phan *et al.*, 2004; Schubot *et al.*, 2005). These arginines are conserved among many of the effector chaperones and were therefore proposed to be functionally relevant, possibly for interaction with the type III secretion machinery (Phan *et al.*, 2004; Schubot *et al.*, 2005). The lack of charged residues in the cavity of SycT means that they are unlikely to be a general point of interaction between T3SS effector chaperones and the secretion machinery.

Overall, SycT shares the common characteristics of other Class I chaperones, at the same time exhibiting unique features that may be required for the special interaction with the cognate effector YopT.

3I.5 YopT structural model and chaperone-binding domain

Apart from the close sequence relationship among YopT from the three pathogenic *Yersinia* species showing 94-96 % identical residues, the BLAST homology search for further YopT family members returned the T3SS effector LopT from animal pathogenic *Photorhabdus luminescence* (51 % identity, 67 % similarity). The following proteins also share considerable sequence identity with YopT: *Pasteurella multocida* filamentous hemagglutinin PfhB1 and the putative immunoglobulin binding protein (37 %/56 %), *Haemophilus influenza* large supernatant protein (31 %/52 %) as well as the putative YopT-like cysteine protease from marine microbe *Hahella chejuensis* (28 %/47 %). Other family members are found in plant pathogens such as *Pseudomonas syringae* pv. *phaseolicola* AvrP3 (=AvrPphB, 26 %/56 %) and *Erwinia amylovora* HopPtoC (19 % identical), but also in symbionts such as *Bradyrhizobium japonicum* ID797 (17 %). Secondary structure prediction for YopT provides only a very rough estimation concerning the location of structural elements. The prediction was partially corroborated by the crystal structure of the C-terminal, catalytic part of the cysteine protease AvrPphB (Zhu *et al.*, 2004), which was therefore used in this study to model the YopT structure for residues 118 to 316 (see Results section 2I.3). The YopT model presented here lacks the N-terminal part comprising the complete CBD that is postulated to be located between residues 51 and 121 and to contain the β-motifs (see above). In view of the compact fold of the C-terminal part of AvrPphB, binding of SycT to an N-terminal, flexible CBD of YopT missing tertiary structure seems possible. However, the N-terminal region of YopT, in particular residues 75-100, were suggested to be involved in binding to substrate RhoA (Sorg *et al.*, 2003). Thus, a YopT/SycT complex might be incapable of interacting with the substrate or accomplishing the enzymatic reaction. This eventuality might account for the negative findings during SPR analysis, apart from the possibility that the RhoA peptides used in the experiments may not be suitable for YopT binding.

Recently, a chaperone was also identified for the fourth *Yersinia* effector YopO/YpkA (Letzelter *et al.*, 2006), for which additionally a GDI activity for membrane–anchored Rho-GTPases was found. Intriguingly, all four chaperone-assisted effectors YopT, YopE, YopH and YopO target the host cell membrane, and the CBD was therefore suggested to present the hydrophobic membrane localization domain (Letzelter *et al.*, 2006). In contrast to YopT, the membrane–localizing homolog AvrPphB does not possess a cognate chaperone, rather the autocatalytic cleavage at the N-terminus reveals a myristoylation site that promotes the membrane targeting of AvrPphB (Nimchuk *et al.*, 2000).

3II SycD – a multi-faceted Class II chaperone with multiple faces

3II.1 Comparison with the LcrH/SycD homology model

The crystal structure of SycD presents the first experimental structure of a T3SS Class II chaperone specific for translocators. Moreover, it shows that a structural model of the SycD monomer based on the structure of serine/threonine phosphatase 5 (Pallen *et al.*, 2003, 1OOL) is in good overall agreement with the crystal structure of the SycD monomer. It confirms the prediction that T3SS Class II chaperones contain TPR-like repeats despite their low sequence similarity. The monomers A and B of $SycD_{21-163}$ superpose with the LcrH/$SycD_{32-165}$ model showing an r.m.s. deviation of ~1.0 Å for the repeats TPR1-3 (103 equivalent Cα atoms). However, superposition of all common residues between SycD and the model (32-160, 129 Cα atoms) increases the r.m.s. deviation to 3.6 Å, due to a completely different orientation of the C-terminal helix h8 (Figure 3II-1A). Additional striking differences between the model and the crystal structure were observed for the side chains of Tyr93, Phe106 and Arg71 (Figure 3II-1B).

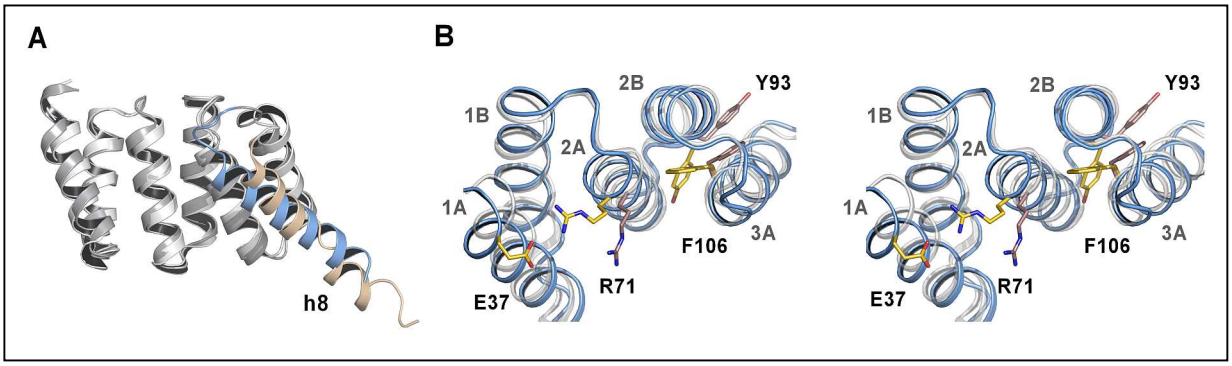

Figure 3II-1. Superposition of the $SycD_{21-163}$ structure and the LcrH homology model. (A) SycD residues 32-160 (dark grey, blue) superposed onto the LcrH/SycD homology model (light grey, orange) (Pallen *et al.*, 2003) exhibit different orientations of helix h8. **(B)** Stereo close-up view of SycD (blue, side chains as yellow sticks) and the LcrH model (light grey, brown), revealing side chain deviations for Tyr93, Phe106 and Arg71. Tyr93 in the crystal structure points toward the concave face, maintaining the TPR fold. Its hydroxyl group might represent a hydrogen donor/acceptor in translocator binding, explaining a Y93A non-functional mutant.

In the model the side chains of Tyr93 and Phe106 point outwards to the convex surface, whereas in the crystal structure both side chains are flipped by 180° and deeply buried in the interstice between TPR2 and TPR3, stabilizing the TPR fold by hydrophobic interactions. Moreover, in the crystal structure the hydroxyl group of Tyr93 points into the concave groove (Figure 3II-1) where it may serve as hydrogen bond donor/acceptor in translocator binding. The dual function of Tyr93 might explain the unexpected null mutant phenotype observed for

LcrH Y93A (Edqvist *et al.*, 2006). Interestingly, in the crystal structure, the side chain of Arg71 in helix A of TPR2 does not freely project into the concave groove, rather it is bent toward Glu37 from TPR1 forming an intramolecular salt-bridge that neutralizes its positive charge. To summarize, the crystal structure of SycD is similar to the LcrH homology model but discloses several differences that might help to explain observations of previous mutagenesis studies (see section 3II.4).

3II.2 Alternative dimerization of SycD

Under physiological conditions, SycD forms dimers in solution (this study and Schmid *et al.*, 2006) similar to the homodimeric Class I chaperones. Oligomerization of other T3SS Class II chaperones has not been examined so far by standard biophysical methods except for SycD (this work and Schmid *et al.*, 2006). The closest SycD homolog is *Pseudomonas aeruginosa* PcrH that shares 76 % sequence similarity and 58 % identity. SycD and PcrH are functionally partially interchangeable since they reciprocally bind to YopD and the homolog PopD, respectively (Broms *et al.*, 2006), although not to YopB/PopB (Allmond *et al.*, 2003). Therefore, PcrH might very likely form head-to-head dimers in the absence of the translocators as well. Interestingly, PopD/PcrH complexes were reported to exhibit a 1:1 ratio only (Schoehn *et al.*, 2003; Faudry *et al.*, 2007).

TPR-containing proteins usually dimerize *via* the convex outer side formed by TPR motifs in the middle of the repeat domain as observed in the crystal structures of human OGT (Jinek *et al.*, 2004), *P. aeruginosa* type 4 pilus protein PilF (Kim *et al.*, 2006) or for the mitochondrial outer membrane transporter Tom70p (Wu and Sha, 2006) (Figure 3II-2). The monomers in these dimers are tilted (in the PilF dimer by approximately 20°).

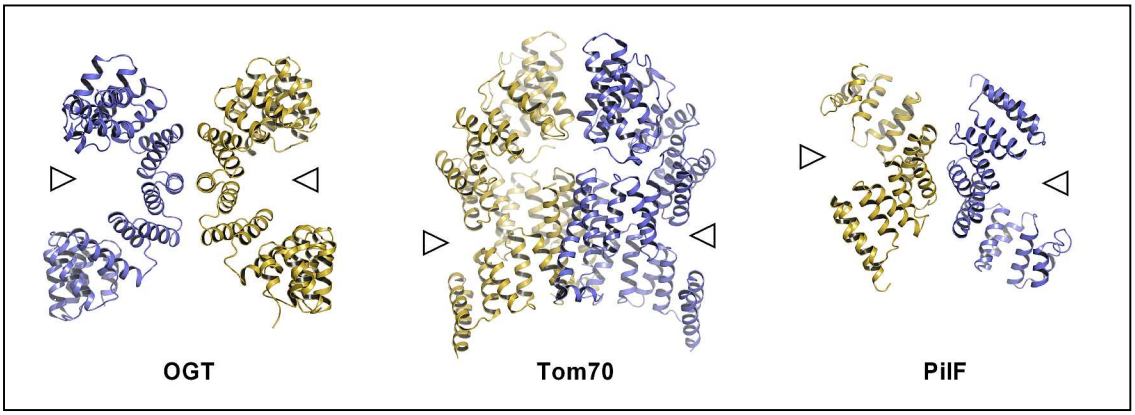

Figure 3II-2. Homodimerization of TPR proteins. The predominant dimerization mode is *via* the convex back faces of the TPR domain involving the middle TPR repeats. O-linked GlcNac transferase OGT (PDB accession code 1W3B); mitochondrial transporter protein Tom70 (2GW1); type IV pilus assembly protein PilF (2FI7). The arrow head designates the concave face of the TPR domain.

A minimal region for dimerization of the TPR domain of Hsp90 co-chaperone Sti1 has been recently identified to be located in helix A of the second TPR motif (Flom *et al.*, 2007).

Based on the packing in the monoclinic crystals, two different assemblies of the monomers into a dimer seemed possible for SycD. The compact dimer 2 shows a back-to-back dimerization *via* the convex outer side, as described for other TPR-containing proteins above, exhibiting an asymmetric interface – very unusual but not unprecedented for homodimers (Cha *et al.*, 2002; Deo *et al.*, 2002). The back-to-back dimer 2 was finally excluded by mutagenesis studies. In contrast, SycD dimerization involves mainly helices A and B of the first TPR motif generating a head-to-head assembly of either a rather elongated shape with the monomers tilted by a larger angle (dimer 1, ~61°) or a kinked arrangement (dimer 3, 90°). The latter might still also be due to a crystallization artifact.

The comparison of the head-to-head dimers 1 and 3 of $SycD_{21\text{-}163}$ disclosed that both the concave and convex faces of the monomer are freely accessible in the dimer assemblies (Figure 3II-3). In contrast to the elongated dimer 1, where equal faces are located on the same dimer front, in the kinked dimer 3 each front exhibits both a concave and a convex face.

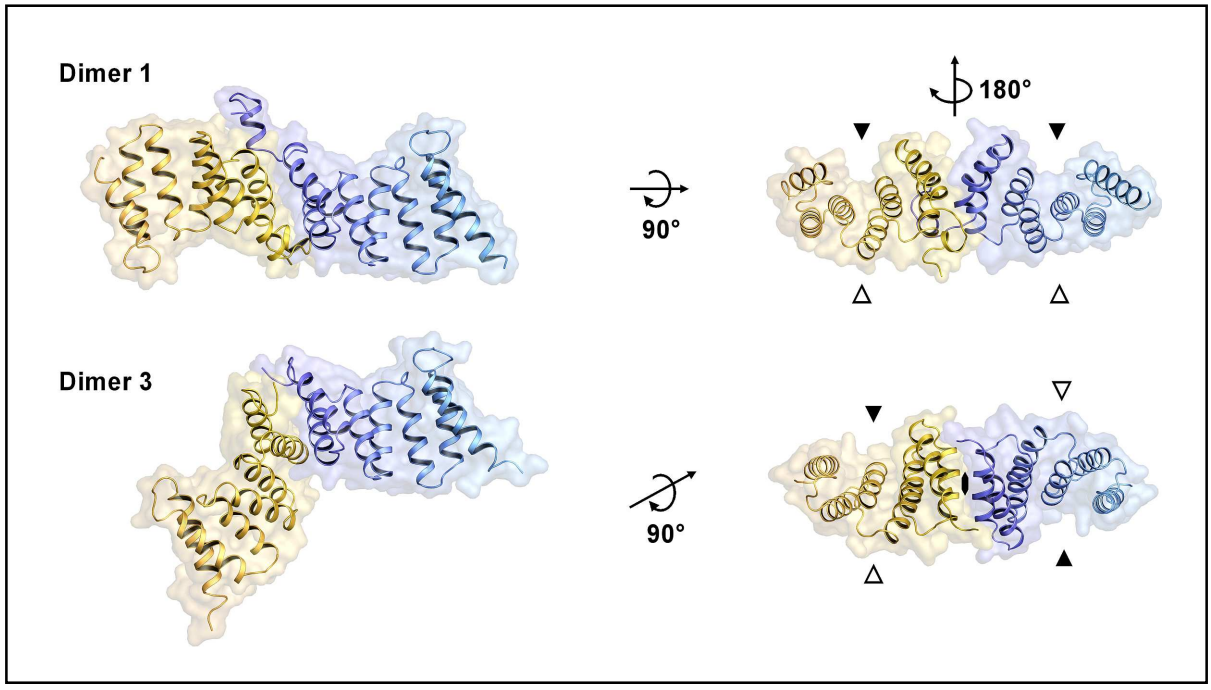

Figure 3II-3. Accessibility of the concave and convex TPR faces in the different SycD dimer assemblies. Front view (left) and top view (right) of $SycD_{21\text{-}163}$ dimer 1 and dimer 3. Aligned front view with respect to the blue monomer. In both assemblies the concave and convex face of each monomer are freely accessible for protein interactions. In dimer 1, both the concave (▲) as well as the convex (△) surfaces are located on opposite dimer faces, whereas in dimer 3, convex and concave surfaces are found together on the same face.

The formation of alternative dimers is extremely unusual. Up to now, this is the first example of a homodimer exhibiting two alternative dimer assemblies sharing the same interface. SycD

dimerization is almost exclusively mediated by hydrophobic contacts. There is only one hydrogen bond in the interface of dimer 1 linking the side chain of Gln60 with the backbone oxygen of Glu30. No polar interaction at all is found in dimer 3 (compare Results section, Table 2II-9). While the hydrophobic contacts confer considerable affinity to the SycD dimer *in vitro,* the specificity may be limited, as also suggested by the two different dimer arrangements. In contrast to Class I chaperones, dimerization of SycD is obviously non-obligate. Moreover, the SEC profile tailing observed for the SycD wt and $SycD_{21\text{-}163}$ elution peaks indicates a monomer-dimer equilibrium with a fast kinetic and the dimer being the predominant species (see also below). However, it still remains unclear if the "specifically hydrogen-bonded", elongated dimer 1 can transform to the “unspecific", non-hydrogen-bonded kinked dimer 3 and *vice versa* without dissociation into monomers by simply pivoting around the interface (Figure 3II-4). Further, the question arises as to what extent both dimer assemblies are present in solution and whether even more conformational states exist.

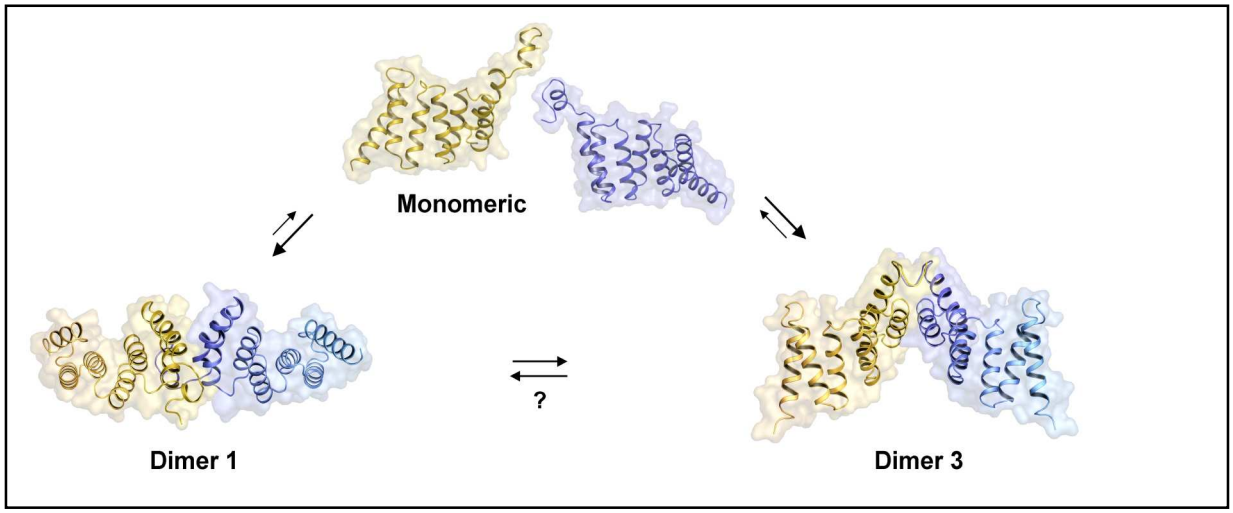

Figure 3II-4. Dimer-monomer equilibrium of SycD in solution. The predominant species of SycD in solution is the dimer. It remains unclear, if the elongated dimer (dimer 1, left) can transform to the kinked dimer (dimer 3, right) or to what extend both dimer species coexist in solution or if there exist even more conformations.

3II.3 Affinity of the SycD homodimer

With respect to the flexible, alternative dimer formation of SycD, it would be interesting to know the affinity of the chaperone homodimer. Handling of wild-type SycD during purification suggests a stable dimer and the explicit stability of monomeric $SycD_{21\text{-}163}$ mutants strongly suggests that SycD dimerization is non-obligate. The SEC elution profiles of wild-type SycD and $SycD_{21\text{-}163}$ display slight tailing, thus indicating a dimer-monomer equilibrium (Stevens, 1989; Yu *et al.*, 2006) (compare Figure 3II-4). This is in line with the finding that

SycD can form two structurally different head-to-head homodimers with distinct arrangements of the monomers utilizing the same interface. In the past, simulated and experimental SEC elution profiles of protein complexes and homodimers have been examined (Stevens, 1989; Yu *et al.*, 2006). According to these, dimerization of wild-type SycD most likely possesses a fast association and dissociation kinetic with a medium to high equilibrium dissociation constant (affinity) of $K_D \sim 10^{-5}$ M or less. The introduction of equally-charged glutamate side chains in the dimer interface mutants $SycD_{21-163}$ A61E, L65E and A61E/L65E leads to electrostatic repulsion. Here, this most likely decreases the association rate constant k_{on}, and consequently K_D *via* the valid relation ship $K_D=k_{on}/k_{off}$, whereas the dissociation rate k_{off} is almost unaffected (also described by Selzer *et al.*, 2000), accompanied by the fronting elution profile that corresponds to slow association and medium/fast dissociation rates (Yu *et al.*, 2006). The experimental determination of K_D of the SycD dimer has not been carried out but should in principle be possible using sedimentation equilibrium analytical ultra centrifugation, isothermal titration calorimetry or fluorescence anisotropy approaches.

3II.4 Mapping of mutagenesis results onto the SycD structure

Extensive random and subsequent site-directed mutational analyses complemented by investigations of mutant stability had been carried out for the binding groove, the canonical sequence motif and additional surface-exposed residues in SycD (Francis *et al.*, 2000; Francis *et al.*, 2001; Edqvist *et al.*, 2006; Edqvist *et al.*, 2007), covering also most of the conserved residues mentioned above (summarized in Table 3II-11). These studies had identified surface-located residues that are indispensable in binding to the translocators. Residues whose alanine mutants are defective in YopB but not in YopD binding (Phe59, Arg71, Phe72, Leu74, Gly75, His109) (Francis *et al.*, 2000) point into the concave groove and are primarily located in TPR2 helix A (surface-located residues Arg71 and His109 depicted in Figure 3II-5). Of these, Arg71 contributes to the TPR stability *via* a salt-bridge to conserved Glu37 (Figure 3II-1, Figure 2II-30). Conserved His109 opposite in the concave groove is probably involved in YopB binding as well, since mutation to alanine weakens the interaction (Edqvist *et al.*, 2006)(Figure 3II-5). Thus, the concave face of SycD is most likely involved in YopB binding. YopD binding and secretion strictly depends on His67 (Francis *et al.*, 2000; Edqvist *et al.*, 2006), located in the turn separating TPR1 from TPR2, and Leu76, both accessible only from the convex TPR face. YopD binding requires further Leu42 at the edge of the dimerization interface (Figure 3II-5 and Figure 2II-27).

Table 3II-11. Correlation of previous mutagenesis results (Francis *et al.*, 2000; Edqvist *et al.*, 2006) **with the SycD crystal structure.**

Residue/Mutation	Binding/Secretion/Stability	Structure
H67*A	– / D↓ / WT	Turn, convex face
L42*A	– / D↓ / WT	Dimerization interface
L76*A	– / D↓ / ↓	Accessible from convex face, fold (?)
E30G, I31V, L42*F, H91Y, D136G	Suppressor mutations D↑	Loops, convex face, dimeriz. interface
I101*M, K102R	D↓ / n.d./ n.d.	Turn, convex face
R71A	D B↓ / B↓ / ↓	Salt-bridge to Glu37
H109A (as double mutant F108A)	D B↓ / B↓ / ↓	Concave face
E37	n.d. / n.d. / n.d.	Concave, salt-bridge to Arg71
Y52A	WT / WT / WT	Concave face
Y86	n.d. / n.d. / n.d.	Concave face
L39A	n.d./ WT/ ↓	Dimerization interface
Y40C/A, Y47A	B↓ D↓ / B↓ D↓ / ↓	Concave face, fold
L74A	B↓ / B↓ / ↓	Buried, fold
Y93A	B↓ D↓ / B↓ D↓ / ↓	Buried, fold, hydroxyl group points into concave face, hydrogen bond donor / acceptor
F72L/S/A, F73L/S, C79Y, F108S, I134T	B↓ D↓ / ~ / ~	Buried, fold

(B): YopB; (D): YopD; (↓) Binding abolished/reduced; (↑) re-established; (-) neither YopB nor YopD; (WT) wild-type; (n.d.) not determined; (~), differing. Asterisks designate residues at TPR consensus positions 4/7/11/24/32. Conserved sequence residues are underlined.

Screening for suppressor mutations in the chaperone that re-established the binding to YopD mutants unable to bind wild-type LcrH disclosed additional, surface located sites involved in YopD binding, e.g. Glu30, Ile31, Leu42, His91, Asn136 (Francis *et al.*, 2000). Together with two additional sites associated with YopD binding that had been identified in multiple mutants (Ile101, Lys102) (Francis *et al.*, 2000), these residues are located on the convex face of the chaperone (Figure 3II-5).

Substitution of the surface exposed, conserved Tyr52 in the lower part of the concave groove has no effect albeit hydrophobic residues are preferred at this position (Edqvist *et al.*, 2006). Tyr86 and the Glu37 represent so far uninvestigated residues near the groove (mentioned above), although the aromatic side chain and the negative charge are well conserved at these positions, suggesting that these two residues may be involved in the interaction with binding partners.

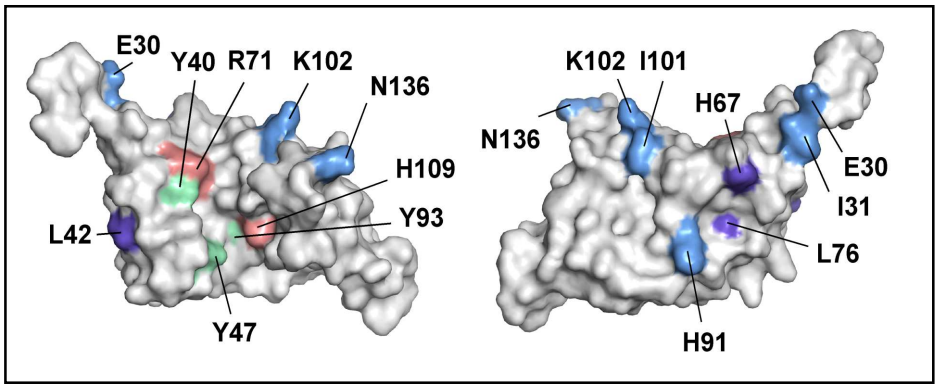

Figure 3II-5. Mutations abrogating YopB or YopD binding mapped onto the SycD surface. Mutational analyses of SycD/LcrH previously carried out by Francis *et al.*, 2000; Edqvist *et al.*, 2006. Key residues located at the surface of $SycD_{21-163}$ that are involved in YopD secretion (dark blue, single mutations; light blue, likely involved, multiple mutations) and YopB binding and secretion (red). Residues accompanied by a non-binding and non-secreting phenotype (Tyr40, Tyr47, Tyr93) are colored green.

Alanine substitutions of conserved Tyr40 and Tyr47, exposed on the concave face, resulted in a less stable chaperone, abrogated the binding and secretion of YopB and YopD and impaired the regulatory function on Yop synthesis and secretion (Edqvist *et al.*, 2006), indicating that these amino acids are also necessary for maintaining the TPR integrity (Figure 3II-5, green). As already mentioned, conserved, buried Tyr93 with its hydroxyl group pointing into the concave groove most likely stabilizes the TPR fold, simultaneously enabling hydrogen bonds potentially required in translocator binding (Figure 3II-1, Figure 3II-5). Residues Phe72, Phe73, Leu74, Cys79, Phe108 and Ile134 are buried and their mutation will most likely affect the TPR fold. Overall, surface-exposed residues affecting YopB binding map to the concave face of the structure, whereas those required for YopD binding are located on the convex surface (Figure 3II-5, red and blue). This strongly supports the idea that YopB binds to the concave face and YopD to the convex face of SycD. This hypothesis is corroborated by a recent crystal structure of the yeast mitochondrial fission assembly protein Fis1 in complex with its binding partners (Zhang and Chan, 2007). The N-terminal arm of Fis1 preceding the TPR domain was recently reported to adopt an α-helical structure (Suzuki *et al.*, 2005), and this helical conformation is also present in SycD. In contrast to SycD, the Fis1 helix binds to a part of the concave groove. It remains there packed even after binding to the adapter proteins Caf4 or Mdv1 where it stabilizes the interaction partners (Figure 3II-6).

The N-terminal helix h0 comprising residues 22-29 in the $SycD_{21-163}$ structure might extend even further into the N-terminus according to secondary structure predictions of full-length wild-type SycD. It is conceivable that this N-terminal helix that is flexibly attached to the TPR domain might stabilize the translocator upon binding either in a manner similar to Fis1

or by embracing the translocator. Recent findings on the *Pseudomonas* YopD homolog PopD indicate a molten globule conformation of the translocator that is independent from binding to the chaperone (Faudry *et al.*, 2007), whereas the *Shigella* translocator IpaC apparently undergoes significant conformational changes upon chaperone binding (Birket *et al.*, 2007). Obviously, the hydrophobic translocators have to be kept in a state between folded and unfolded that is both non-cytotoxic for the bacterium and at the same time secretion-competent. This delicate balance might require the assistance of the chaperone.

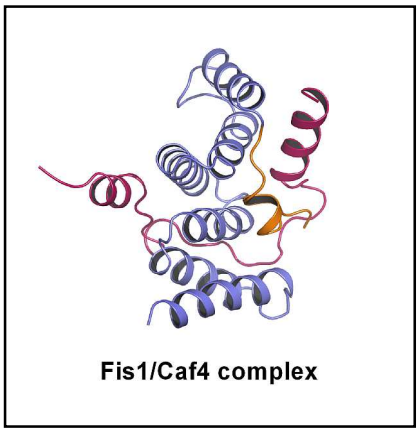

Figure 3II-6. TPR domain interaction involving both faces. Fis1 (blue) binds to Caf4 (red) by using both its concave and convex face of the TPR domain. The N-terminal helical region (orange, residues 9-14) is embedded in the concave groove stabilizing the binding partner (Zhang and Chan, 2007).

Most intriguingly, Fis1 binds different parts of the adapter Caf4 simultaneously *via* its concave and convex TPR face (Figure 3II-6). Fis1 presents therefore the first TPR-containing protein for which the structural evidence exists that both faces of the TPR domain are actually involved in protein-protein interactions. These findings substantiate the conclusions on translocator binding in SycD with YopB binding to the concave and YopD to the convex face of the TPR domain.

3II.5 Implications for further interaction surfaces in SycD

In contrast to T3SS Class I chaperones, where distinct features such as hydrophobic surface patches and a so-called β-motif (Lilic *et al.*, 2006, see Discussion section 3I.3) have been identified that are essential for the interaction with the specific secretion target, Class II chaperones interact with multiple binding partners of different fold and function and consequentially had to develop a panoply of binding sites. TPR-containing proteins predominantly interact with their binding partners *via* both the concave groove (the prevalent binding site) and the convex outer side (compare Figure 3II-6), but basically use all possible faces of the TPR domain for ligand and interdomain contacts (for a review see D'Andrea and Regan,

2003). So far, only limited information on binding sites in Class II chaperones is available, and the prediction of further interaction sites in these multivalent T3SS regulators is therefore challenging.

SycD is also involved in the control of effector biosynthesis by establishing a negative regulatory network on *yop* gene expression together with YopD and LcrQ (YscM1 and YscM2 in *Y. enterocolitica*) (Francis *et al.*, 2001; Anderson *et al.*, 2002). Additionally, SycD was reported to have a regulatory effect on Yop secretion *via* an YscY-YscX loop (Iriarte and Cornelis, 1999). Regions in SycD required for YscY binding and the regulatory effect were mapped to TPR1 and a so-called NEISS region, comprising residues 29-33, that is located between helix h0 and TPR1 with Glu30 as key regulatory residue (Francis *et al.*, 2001; Broms *et al.*, 2005). In the crystal structure of SycD, the NEISS element is freely accessible due to its linear, exposed structure (compare Results section Figure 2II-17, NEISS sequence colored in magenta). Thus, experimental results on its regulatory role appear plausible.

Additionally, SycD exhibits striking conserved sequence features such as tyrosines residues located mainly on the concave chaperone face predicted to be a protein-protein interaction surface (Results section Figure 2II-30). Tyrosine, an amino acid with a polar hydroxyl group, displays a high propensity to occur in protein-protein interfaces, acting as binding energy hotspot (Bogan and Thorn, 1998), and to protrude from the surface to offer suitable interaction sites (Jones and Thornton, 1995). Protruding tyrosines were identified to be the functional residues of a TPR domain required in binding to a proline-rich ligand (Pekkala *et al.*, 2004). YopB possesses five proline residues within a short N-terminal fragment (residues 24-55). However, systematic sequence deletions in YopB did not unravel a clearly defined chaperone-binding domain. Rather several parts of the YopB sequence seem to be required for SycD binding (Neyt and Cornelis, 1999). And although both the convex as well as the concave side of the TPR in the SycD head-to-head dimers are freely accessible (compare Figure 3II-3) and SycD therefore could theoretically bind to two YopB and two YopD molecules simultaneously, the stoichiometry and affinity of the SycD/YopD/YopB interactions remain to be determined.

The tetrameric $SycD_{21\text{-}163}$ assembly (dimer-of-dimers), suggested by PISA due to the crystal contacts in the monoclinic packing, might present an appealing transient solution state of the chaperone. This would explain the occasional formation of higher oligomers of SycD (Results section Figure 2II-7, also observed by Tengel *et al.*, 2002; Schmid *et al.*, 2006), utilizing so far unknown surfaces in SycD. The effector chaperone SycH was also reported to form a dimer-of-dimers (Neumayer *et al.*, 2004). Although the interaction of these polymerized

chaperone structures with their cognate binding partners has still to be confirmed, this presents a compelling possibility of a bandoleer of chaperones preloaded with their cognate Yops and ready to release them at the injectisome. Only a very short period of time has been observed between the bacterial attachment and a visible cytotoxic effect due to effector activity. This short time frame is in the range of < 600 s for injection of all *Salmonella* SipA effector molecules (Schlumberger *et al.*, 2005) and 241 s for the depletion halftime of *Shigella flexneri* translocators (Enninga *et al.*, 2005). This fast phenomenon cannot be explained by biosynthesis on demand, rather the virulence factors must be stored within the bacterial cytosol prior to cell contact and translocation. In summary, there exist at least two potential interaction surfaces that could be employed in the protein-protein interactions of multi-functional SycD.

3II.6 The dimerization interface in SycD – a new interaction surface?

The apparent lack of specificity in the SycD dimerization interface implies that *in vivo* this interface could be involved in interactions other than homodimerization, e.g. localization to the membrane or the T3SS apparatus, potentially *via* binding to so far unknown interaction partners.

Until now, only few SycD mutations had been described that localize to the dimerization interface and show an effect on translocator binding (Leu39, Leu42) (Francis *et al.*, 2000; Edqvist *et al.*, 2006). However, the *in vivo* phenotype of the monomeric SycD mutant A61E/L65E clearly indicates that this dimerization interface is functionally relevant. This SycD mutant is stable and folded under physiological conditions *in vitro* and both the concave and convex binding faces are intact. The null mutant-like behavior, however, suggests that either dimerization is indispensable for appropriate SycD function or that the mutation has eliminated so far undetected interactions of the chaperone with the translocators or other interaction partners.

Apart from the cognate translocators YopB and YopD, SycD has been recently shown to interact with other T3SS proteins. Further known SycD/LcrH binding partners include additional regulatory T3SS components such as TyeA and YscE (Iriarte *et al.*, 1998; Swietnicki *et al.*, 2004). SycD could possibly bind YscE *via* TPR motif 1 in a manner similar to that observed for the *Pseudomonas* YscE homolog PscE in complex with the TPR-like protein PscG (Quinaud *et al.*, 2007).

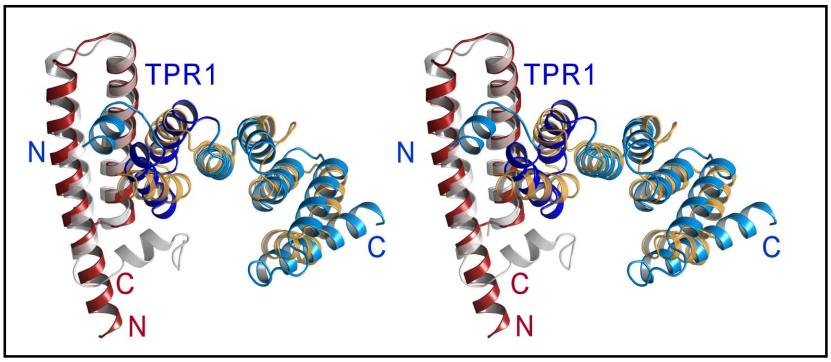

Figure 3II-7. Stereo view of a potential interaction of SycD (blue) **with YscE** (red), **modeled onto heterodimeric PscG/PscE from *P. aeruginosa*** (yellow/grey) (Quinaud *et al.*, 2007, PDB entry 2UWJ). Due to three TPR-reminiscent motifs, chaperone PscG superposes with SycD (r.m.s.d. 3.5 Å, 113 aligned residues). Surface plasmon resonance and native mass spectrometry experiments have recently elucidated the interaction of SycD with YscE (Swietnicki *et al.*, 2004), though its physiological role needs exploration. The model illustrates how SycD - *via* its TPR1 - might bind to YscE in a manner similar to the PscG/PscE interaction.

Interestingly, PscG exhibits a TPR-like fold that was not predicted from its amino acid sequence. PscG binds to PscE *via* its first two (TPR motif-like) helices. Superposition of the SycD monomer onto PscG and the crystal structure of YscE (Phan *et al.*, 2005) onto PscE might therefore demonstrate how the interaction of SycD with YscE could involve TPR1 (Figure 3II-7).

3III Concluding remarks

Despite their low sequence homology, Class I chaperone structures proved to be well conserved and structure prediction for Class II chaperones approaches surprisingly well the experimental, atomic structure. As to Class III chaperones, the identification and characterization of further members will clarify whether this group actually encloses a heterogeneous set of structures or whether the structurally deviant flagellar chaperones should be grouped separately. On first sight, a single, representative structure of Class I or Class II chaperones virtually holds all the characteristics of these small accessory proteins. However, with the growing collection of chaperone structures it became evident that, in contrast to their assumed static nature, several of these chaperones, such as of SycT, InvB or SycD, disclose intriguing, deviant structural and functional details. These variations provide insight into the fine-tuning of type III secretion. Therefore, future chaperone structures will contribute to filling the gaps in understanding the complex process of type III secretion and its regulation that is far from being complete.

4 Outlook

4I SycT and its cognate effector YopT

Several Yops other than YopT have been previously reported to be aggregation-prone (Michiels *et al.*, 1990; Birtalan *et al.*, 2002; Letzelter *et al.*, 2006). Moreover, the two effector/chaperone complexes that have been solved in the recent past could take advantage of stable protease digestion products of the effector ($YopN_{32-277}$/YscB-SycN, $SipA_{48-264}$/InvB) (Schubot *et al.*, 2005; Lilic *et al.*, 2006). This approach is not applicable to the YopT/SycT complex as the effector is intrinsically instable even in the complex with the chaperone (this work). Thus, a crystal structure of (near) full-length YopT represents a challenging target that might be well out of reach. Potentially, the co-expression of an inactive YopT variant (C139S) together with the substrate RhoA in eukaryotic cells ensuring the proper RhoA geranylgeranylation might result in a stable effector/substrate complex suitable for isolation and crystallization.

Many effector/chaperone complexes have been reported to be still enzymatically active or capable of binding to the target protein (Luo *et al.*, 2001; Birtalan *et al.*, 2002; Neumayer *et al.*, 2004) due to the separation of the CBD from the catalytically active protein part and only partial unfolding during binding to the chaperone. However, YopT has been shown to bind to its cognate substrate RhoA using residues within the N-terminal part of the protein that partially overlaps with the CBD. It would be interesting to clarify whether SycT-complexed YopT is actually capable of interacting with RhoA. To achieve this end, the binding studies from this work will have to be continued and extended. Possible approaches are further SPR binding experiments either with full-length geranylgeranylated RhoA or the physiologically adequate C-terminal RhoA-peptide. This would also help to determine the binding affinity of the complex.

In order to verify the suggested conformational change in SycT upon effector binding, the crystal structure of the (possibly synthesized) chaperone-binding domain of YopT with SycT would be the most convincing evidence. However, if a soluble $YopT_{CBD}$ can be obtained or the aggregation of full-length YopT minimized, nuclear magnetic resonance investigations could constitute an alternative approach to unravel rearranging SycT residues.

4II Translocator chaperone SycD

The crystal structure of SycD solved in this thesis presents the first experimental structure of a T3SS Class II chaperone specific for translocators. The crystal structure of SycD and the identification of a new interaction surface in the translocator chaperone contribute to the understanding of its versatile functionality. Certainly, a crystal structure of SycD in complex with one of its cognate binding partners YopB or YopD would answer many remaining questions. However, since the translocators are hydrophobic transmembrane proteins and can apparently bind to the chaperone in a molten globule conformation (Faudry *et al.*, 2007), such a complex structure represents a major challenge or might not be feasible at all. Under near-physiological conditions, as used in this study, a C-terminal YopD peptide, $YopD_{278-300}$, did not show any significant or useful interaction with SycD in solution. A more promising approach would therefore be the co-expression of SycD together with one of the pore formers, either in the form of the full-length protein or of a covalently linked peptide.

The alternative dimerization properties of SycD premise an appropriate, yet unknown affinity of the dimer. The determination of the affinity in self-associating systems is far from routine, and eligible methods such as dilution ITC, fluorescence anisotropy and SE-AUC might not exhibit a suitable sensitivity range for detecting the affinity in SycD. The intrinsic protein fluorescence by tryptophan constitutes an elegant way to follow protein dissociation. However, as SycD does not possess any tryptophan residue, site-directed mutagenesis would have to be used to introduce a single tryptophan residue in a suitable position.

The *in vivo* experiments with *Yersinia* performed in this study investigating the behavior of the monomeric $SycD_{21-163}$ mutant A61E/L65E should be completed by *in vitro* analyses using pull-down or co-immunoprecipitation methods in order to probe the binding of the mutant to the translocators YopB and YopD. In the courses of these experiments, investigations concerning the behavior of a specifically covalently cross-linked SycD dimer would be of particular interest. Moreover, the stoichiometric ratio of the SycD/YopB/YopD interactions still needs to be unraveled. The molecular and structural examination of the interaction with further binding partners such as YscE or YscY etc. would be of further interest and might elucidate the concrete *in vivo* function of the dimerization interface.

5 Materials and Methods

Methods in molecular biology were derived from standard procedures (Sambrook and Russell, 2001; Coligan *et al.*, 2007) and are not described in detail unless essential modifications were made.

5.1 Chemicals and material

If not stated otherwise, chemicals were purchased from Aldrich, J.T. Baker, DIFCO, Emerald Biostructures, Fluka, GE-Healthcare-Amersham Biosciences, GIBCO-BRL, Hampton Research, Invitrogen, Merck, Millipore, New England BioLabs, Qiagen-Nextal, Riedel-de-Haën, Roche, Roth, Sigma, Stratagene. The standard quality was *pro analysis* (p.a.).

5.2 Molecular weight standards

Table 5-1. Molecular weight standards used in protein biochemistry.

Name	Source	Type
BenchMark	Invitrogen	SDS-PAGE protein marker
Low molecular weight	Fermentas	SDS-PAGE protein marker
Precision Plus Protein All Blue Standards	BIO-RAD	SDS-PAGE protein marker
Broad range protein/peptide standard (unstained)	BIO-RAD	SDS-PAGE protein marker
High molecular weight (native)	GE-Healthcare-Amersham Biosciences	Native PAGE Protein marker
HMW und LMW Gel Filtration Calibration	GE-Healthcare-Amersham Biosciences	Protein marker for SEC

5.3 Enzymes

Table 5-2. Enzymes used in protein production and limited proteolysis.

Enzyme	EC	Source	Sepecification
Endoproteinase LysC	EC 3.4.21.50	Promega	Serine endopeptidase
Lysozyme	EC 3.2.1.17	Fluka	Glucoside hydrolase
PreScission protease	EC 3.4.22.28	GE Healthcare	Cysteine endopeptidase
TEV protease	EC 3.4.22.44	Lab prepared	Cysteine endopeptidase
Thermolysin	EC 3.4.24.27	Boeringer M./Roche	Metallo-endopeptidase
Trypsin	EC 3.4.21.4	Promega	Serine endopeptidase, modified, sequencing grade

5.4 Special chemicals

Table 5-3. Additional chemicals used in this study.

Chemical	Source
Complete - protease inhibitor cocktail tablets	Roche
Complete, EDTA free	Roche
BugBuster Protein Extraction Reagent	Novagen
Pefablock - Serine protease inhibitor	Roche

5.5 Oligonucleotides

5.5.1 Primers used in polymerase chain reactions

Table 5-4. Sequences of primers used in PCR and ligation. Forward orientation (FW) and reverse (RV, 5'→3' complement). Restriction sites are included in the primer name and underlined in the sequence.

Oligonucleotide	Sequence 5'→3'	Source
*yop*T_104_Stop3_ RV_*Not*I	AAGCGGCCGCTTAGTTAGTTACTCTCTCACCGCG	this work
*yop*T_*Nco*I_FW	AGGAGCCATGGACAGTATTCACGGACACTACCATATCC	this work
*yop*T_RV_*Sal*I	AAGTCGACAACCTCCTTGGAGTCAAATG	this work
*yop*T_RV_*Xho*I	AACTCGAGAACCTCCTTGGAGTCAAATG	this work
*yop*T1-74_Stop_*Not*I_RV	AAGCGGCCGCTTATTTGCCGTCGCTGGTCAAC	this work
*yop*T318_Stop_*Not*I_RV	AAGCGGCCGCTTAGTCAAATGTTAACACG	this work
*yop*Tdel22_*Nco*I_FW	AGGAGCCATGGGGTCAGCTACACTCACCGAAGGG	this work
*yop*Tdel49_*Nco*I_FW	AAGAGCCATGGGGAAGTTATCAGCTACC	this work
*yop*Tdel49_*Nde*I_FW	AGGAGCATATGAAGTTATCAGCTACCATAAAAC	this work
*yop*Tdel50_*Nco*I_FW	AGGAGCCATGGGGTTATCAGCTACCATAAAAC	this work
*yop*Tdel50_*Nde*I_FW	AGGAGCATATGTTATCAGCTACCATAAAAC	this work
*yop*Tdel52_*Nde*I_FW	AACATATGTCAGCTACCATAAAACATAACCAGTCAAGCCG	this work
*yop*Tdel74_*NcoI*_FW	AACCATGGCTAACCAACGAAGCAGCTTTACCTTC	this work
*yop*Tdel74_*Nde*I_FW	AACATATGGCTAACCAACGAAGCAGCTTTACC	this work
s*yop*T_*BamH*I_FW	AGGAGGGATCCATGATAGCATCCACGGCC	this work
s*yop*T_*EcoR*I_RV	AGGAGGAATTCTTACACTTCTTTGCTATCG	this work
s*yop*T_*Nco*I_FW	AGGAGCCATGGATAGCATCCACGGCCATTATC	this work
s*yop*T_Stop_*Not*I_RV	AGGAGGCGGCCGCTCACACTTCTTTGCTATCGAAGGTCAGCAC	this work
s*yop*T_*Xho*I_RV	AGGAGCTCGAGCACTTCTTTGCTATCGAAGGTCAGCAC	this work
s*yop*Tdel16_*Nco*I_FW	AACCATGGCGGGTGAAAACTTGCAGAGC	this work
s*yop*Tdel24_*Nco*I_FW	AACCATGGGGACCCTGACCGAAGGTGTTATTG	this work
s*yop*Tdel40_*Nco*I_FW	AACCATGGGGACCGCGCTGAGCCATAGC	this work
s*yop*Tdel49_*Nco*I_FW	AACCATGGGGAAACTGAGCGCGACCATC	this work

Oligonucleotide	Sequence 5'→3'	Source
s*yop*Tdel49_*Nde*I_FW	AGGAGCATATGAAACTGAGCGCGACCATC	this work
s*yop*Tdel50_*Nco*I_FW	AGGAGCCATGGGGCTGAGCGCGACCATCAAAC	this work
s*yop*Tdel50_*Nde*I_FW	AGGAGCATATGCTGAGCGCGACCATCAAAC	this work
s*yop*Tdel65_*Nco*I_FW	AACCATGGATCGTAAACTGACCAGCGATGG	this work
s*yop*Tdel74_*BamH*I_FW	AGGAGGGATCCATGGCGAATCAGCGTAGC	this work
s*yop*Tdel74_*Nco*I_FW	AACCATGGCGAATCAGCGTAGCAGCTTTAC	this work
s*yop*Tdel181_*Pst*I_RV	AACTGCAGCTGTTTAATGCTGTACAGGGTATC	this work
*syc*T_*Nco*I_FW	AACCATGGGACAGACAACCTTGACAGAAC	H. Niemann; HZI, Braunschweig
*syc*T_RV_Stop_*Not*I	AAGCGGCCGCTCAGATGAATAATATAGGTG	H. Niemann; HZI, Braunschweig
*syc*T122_Stop_*Not*I_RV	AAGCGGCCGCTCAGTTGGGCTGAAACTTAGTATTTTGCGG	this work
*syc*D_*BamH*I_FW	AGGAGGGATCCATGCAACAAGAGACGACAGACACTCAAG	this work
*syc*D_Pos21_*BamH*I_FW	AGGAGGGATCCGGAGGGGGAACTATCGCCATGCTCAACG	this work
*syc*D_Stop_*EcoR*I_RV	AGGAGGAATTCTCATGGGTTATCAACGCACTCATGTTTCATCTCC	this work
*syc*D163_Stop_*EcoR*I_RV	AGGAGGAATTCCTCACTCATGTTTCATCTCCTTTTTC	this work
*yop*D$_{278-300}$_*Nco*I*Not*I_FW	CATGGATAACTTTATGAAAGATGTCCTGCGCTTGATTGAACAATATGTTAGCAGTCATACTCACGCCATGAAATAAGC	this work
*yop*D$_{278-300}$_*Nco*I*Not*I_RV	GGCCGCTTATTTCATGGCGTGAGTATGACTGCTAACATATTGTTCAATCAAGCGCAGGACATCTTTCATAAAGTTATC	this work
Gly-Linker_*BamH*I*Nco*I*Not*I_*BamH*I*Eco*RI_FW	GATCTCCGGGAATTTCCGGTGGTGGTGGTGGATCCATGGCAGGCGGCGGCCGCACTGG	this work
Gly-Linker_*BamH*I*Nco*I*Not*I_*BamH*I*Eco*RI_RV	AATTCCAGTGCGGCCGCCGCCTGCCATGGATCCACCACCACCACCGGAAATTCCCGGA	this work

5.5.2 Site-directed mutagenesis

The following cycling parameters were applied for site-directed mutagenesis using a thermocycler (Biometra, Whatman) and 18 cycles comprising steps 1 to 3. Oligonucleotides used for site-directed mutagenesis are listed in Table 5-5.

Step 0.) 4 min 95 °C, denaturation
1.) 45 s 95 °C, denaturation
2.) 1 min 55 °C, primer binding
3.) 2 min/1 kb plasmid length 68 °C, extension
4.) 7 min 68 °C
5.) Hold, 4 °C

Table 5-5. Sequences of oligonucleotides used in site-directed mutagenesis. Reverse primer sequences correspond to complement sequences of the listed forward (FW) primers. Mutation sites are highlighted.

Oligonucleotide	Mutation	Sequence
*yop*TS13A_FW	S13A	5' CGGACACTACCATATCCAACTAG**CGA**ATTATTCTG CCGGTG 3'
*yop*T_140stop_FW	E140Stop	5' GACACCGCTAGCGGTGTCTGT**TAA**GCTTTATGTGC ACATTGG 3'
*yop*T_C139S_FW	C139S	5' CCGCTAGCGGTGTC**TCA**GAGGCTTTATGTGCACAT TGG 3'
s*yop*T_C139S_FW	C139S	5' CCGCGAGCGGTGTT**AGC**GAAGCGCTGTGCGCGCA TTGG 3'
*yop*T121stop_FW	K121Stop	5' CAATTTCAAGTTTGCTCAGACC**TAA**GGGGCTTTTC TTCATC 3'
*syc*D_K155-159A_FW	K155A/K157A/ K158A/E159A	5' TCCACCCGAGTTAGCTCAATGTTAGAAGCAATT**GC A**TTG**GCAGCGGCG**ATGAAACATGAG 3'
*syc*D_K117-119A_FW	K117A/E119A	5' GCCGAATGTTTACTGCAA**GCG**GGA**GCG**CTTGCTG AAGCAGAAAGTGGC 3'
*syc*D_K155S_FW	K155S/K157S/ K158S/E159S	5' TCCACCCGAGTTAGCTCAATGTTAGAAGCAATT**AG C**TTG**AGCTCGTCG**ATGAAACATGAG 3'
*syc*D_C164S_FW	C164S	5' GGAGATGAAACATGAG**AGC**GTTGATAACCCATGA GAATTCCCGGGTC 3'
*syc*D_Y95S_FW	Y95S	5' GCGATTCATAGCTACAGC**TCT**GGCGCCGTAATGG ATATAAAAGAACCTCG 3'
*syc*D_S94E/Y95E_FW	S94E/Y95E	5' GCGATTCATAGCTAC**GAGGAA**GGCGCCGTAATGG ATATAAAAGAACCTCG 3'
*syc*D_AL6165EE_FW	A61E/L65E	5' GATGCTCACAAGGTCTTTCAA**GAA**CTCTGTGTG**GA A**GACCACTATGATTCACG 3'
*syc*D_A61E_FW	A61E	5' GATGCTCACAAGGTCTTTCAA**GAA**CTCTGTGTGCT AGACCACTATGATTCACG 3'
*syc*D_L65E_FW	L65E	5' GATGCTCACAAGGTCTTTCAAGCTCTCTGTGTG**GA A**GACCACTATGATTCACG 3'

5.6 Plasmids

Table 5-6. Virulence plasmid used as PCR template.

Plasmid	Organism	GenBank entry	Source
pYVe227	*Yersinia enterocolitica* strain W22703, serotype 0:9	AF102990	G.R. Cornelis; Biozentrum, University of Basel, Switzerland

Table 5-7. Synthesized *yop*T gene, cloned into a transport vector.

Plasmid	Original gene	Optimized gene	Source
pPCRscript_s*yop*T	*yop*T from *Yersinia enterocolitica* strain W22703, serotype 0:9	s*yop*T [†] (No. 04691, *E.coli* codon usage, removal of internal *Eco*RI site)	GENEART; Regensburg

[†] Nucleotide sequence in the Appendix.

Table 5-8. Plasmids used.

Plasmid	Tag	Protease cleavage site	Selection	Source
pETM-11	N-terminal, His_6	TEV protease	Kan^R	G. Stier; EMBL, Heidelberg
pETM-30	N-terminal, His_6 N-terminal, GST	TEV protease	Kan^R	G. Stier; EMBL, Heidelberg
pETM-41	N-terminal, MBP	TEV protease	Kan^R	G. Stier; EMBL, Heidelberg
pETM-60	N-terminal, NusA	TEV protease	Kan^R	G. Stier; EMBL, Heidelberg
pET-28c+	N/C-terminal, His_6	Thrombin	Kan^R	Novagen
pGEX-2T	N-terminal, GST	Thrombin	Amp^R	GE Healthcare-Amersham Biosciences
pGEX-6P-1	N-terminal, GST	PreScission protease	Amp^R	GE Healthcare-Amersham Biosciences
pETM-11GFPfus	N/C-terminal, His_6, C-terminal, GFP	-	Kan^R	Joop van den Heuvel; HZI, Braunschweig

Table 5-9. Recombinant plasmids used.

Plasmid	Features	Size	Source
pETM-30-IRES_*syc*T_*yop*T	976 bp *Nde*I/*Not*I-*yop*T fragment and 398 bp *Nco*I/*Asc*I *syc*T fragment from *Y. enterocolitica* into pETM-30-IRES (1. *Nco*I/*Asc*I, 2. *Nde*I/*Not*I)	6.4 kb	H. Niemann; HZI, Braunschweig
pETM-30-IRES_*syc*T _Δ49*yop*T	828 bp *Nde*I/*Not*I *yop*T fragment in pETM-30-IRES_*syc*T_*yop*T (*Nco*I/*Not*I)	6.2 kb	this work
pETM-30-IRES_*syc*T _Δ49*yop*T C139S	Site-directed mutagenesis of pETM-30-IRES_*syc*T_Δ49*yop*T	6.2 kb	this work
pETM-30-IRES_*syc*T _Δ50*yop*T	825 bp *Nde*I/*Not*I *yop*T fragment in pETM-30-IRES_*syc*T_*yop*T (*Nco*I/*Not*I)	6.2 kb	this work
pETM-30-IRES_*syc*T _Δ49*yop*TC139S	Site-directed mutagenesis of pETM-30-IRES_*syc*T_Δ50*yop*T	6.2 kb	this work
pETM-30-IRES_*syc*T _Δ13*yop*T	938 bp *Nde*I/*Not*I *yop*T fragment in pETM-30-IRES_*syc*T_*yop*T (*Nde*I/*Not*I)	6.3 kb	this work
pETM-30-IRES_*syc*T _*yop*TS13A	Site-directed mutagenesis of pETM-30-IRES_*syc*T_*yop*T	6.4	this work
pETM-30-IRES_*syc*T _*yop*TC139S	Site-directed mutagenesis of pETM-30-IRES_*syc*T_*yop*T	6.4	this work
pETM-30-IRES_*syc*T _*yop*T52-104	168 bp *Nde*I/*Not*I *yop*T fragment in pETM-30-IRES_*syc*T_*yop*T (*Nde*I/*Not*I)	5.6 kb	this work
pETM-30-IRES_*syc*T _*yop*T50-139	Site directed mutagenesis (E139Stop) of pETM-30-IRES_*syc*T_Δ49*yop*T	6.4 kb	this work
pETM-30-IRES_*syc*T _*yop*T50-121	Site directed mutagenesis (K121Stop) of pETM-30-IRES_*syc*T_Δ49*yop*T	6.4 kb	this work
pETM-11GFPfus6His _s*yop*T	974 bp *Nco*I/*BamH*I s*yop*T fragment cut from pCRscript_s*yop*T into pETM11GFPfus (*Nco*I/*BamH*I)	7.1 kb	this work

Plasmid	Features	Size	Source
pETM-11GFPfus6His _Δ16*yop*T	498 bp *Nco*I/*Pst*I s*yop*T fragment into pETM11GFPfus (1. *Nco*I/*BamH*I, 2. *Nco*I/*Pst*I)	7.0 kb	this work
pETM-11GFPfus6His _Δ24*yop*T	477 bp *Nco*I/*Pst*I s*yop*T fragment into pETM11GFPfus (1. *Nco*I/*BamH*I, 2. *Nco*I/*Pst*I)	7.0 kb	this work
pETM-11GFPfus6His _Δ40*yop*T	432 bp *Nco*I/*Pst*I s*yop*T fragment into pETM11GFPfus (1. *Nco*I/*BamH*I, 2. *Nco*I/*Pst*I)	7.0 kb	this work
pETM-11GFPfus6His _Δ49*yop*T	402 bp *Nco*I/*Pst*I s*yop*T fragment into pETM11GFPfus (1. *Nco*I/*BamH*I, 2. *Nco*I/*Pst*I)	7.0 kb	this work
pETM-11GFPfus6His _Δ65*yop*T	351 bp *Nco*I/*Pst*I s*yop*T fragment into pETM11GFPfus (1. *Nco*I/*BamH*I, 2. *Nco*I/*Pst*I)	7.0 kb	this work
pETM-11GFPfus6His _Δ74*yop*T	324 bp *Nco*I/*Pst*I s*yop*T fragment into pETM11GFPfus (1. *Nco*I/*BamH*I, 2. *Nco*I/*Pst*I)	7.0 kb	this work
pETM-11-*yop*T	976 bp *Nco*I/*Not*I *yop*T fragment in pETM-11 (*Nco*I/*Not*I)	6.3 kb	H. Niemann; HZI, Braunschweig
pETM-30-*yop*T	976 bp *Nco*I/*Not*I *yop*T fragment in pETM-30 (*Nco*I/*Not*I)	7.0 kb	H. Niemann; HZI, Braunschweig
pETM-41-*yop*T	976 bp *Nco*I/*Not*I *yop*T fragment in pETM-41 (*Nco*I/*Not*I)	6.3 kb	H. Niemann; HZI, Braunschweig
pETM-60-*yop*T	976 bp *Nco*I/*Not*I *yop*T fragment in pETM-60 (*Nco*I/*Not*I)	7.8 kb	H. Niemann; HZI, Braunschweig
pETM-30-*yop*TC139S	Site directed mutagenesis of pETM-30-*yop*T	7.0 kb	this work
pETM-11_*yop*T75-318	741 bp *Nco*I/*Not*I *yop*T fragment in pETM-11 (*Nco*I/*Not*I)	5.0 kb	this work
pETM-30_*yop*T75-318	741 bp *Nco*I/*Not*I *yop*T fragment in pETM-30 (*Nco*I/*Not*I)	5.7 kb	this work
pETM-11_s*yop*T	976 bp *Nco*I/*Not*I s*yop*T fragment in pETM-11 (*Nco*I/*Not*I)	6.3 kb	this work
pETM-30_s*yop*T	976 bp *Nco*I/*Not*I s*yop*T fragment in pETM-30 (*Nco*I/*Not*I)	7.0 kb	this work
pGEX-2TGL_s*yop*T	58 bp *BamH*I/*EcoR*I Glycine linker fragment and 972 *Nco*I/*Not*I s*yop*T fragment in pGEX-2T (1. *BamH*I/*EcoR*I, 2. *Nco*I/*Not*I)	6.0 kb	this work
pET-28c+_s*yop*T 6His	969 bp *Nco*I/*Xho*I s*yop*T fragment in pET-28c+ (*Nco*I/*Xho*I)	6.2 kb	this work
pET-28c+_s*yop*T	976 bp *Nco*I/*Not*I s*yop*T fragment in pET-28c+ (*Nco*I/*Not*I)	6.2 kb	this work
pETM-30_*syc*T	399 bp *Nco*I/*Not*I *syc*T fragment in pETM-30 (*Nco*I/*Not*I)	6.4 kb	C. Büttner, (dipl. thesis)
pETM-30_*syc*T_{1-122}	375 bp *Nco*I/*Not*I *syc*T fragment in pETM-30 (*Nco*I/*Not*I)	6.4 kb	this work
pGEX-6P-1_*syc*D	513 bp *BamH*I/*EcoR*I fragment of *syc*D in pGEX-6P-1 (*BamH*I/*EcoR*I)	5.5 kb	this work
pGEX-6P-1_ *syc*DC164S	Site directed mutagenesis of pGEX-6P-1_*syc*D	5.5 kb	this work

Plasmid	Features	Size	Source
pGEX-6P-1_ *syc*D21-163	438 bp *BamH*I/*EcoR*I fragment of *syc*D in pGEX-6P-1 (*BamH*I/*EcoR*I)	5.4 kb	this work
pGEX-6P-1_ *syc*D21-163K155A	Site directed mutagenesis of pGEX-6P-1_*syc*D21-163	5.5 kb	this work
pGEX-6P-1_*syc*D21-163 K155A/K117A	Site directed mutagenesis of pGEX-6P-1_*syc*D21-163	5.4 kb	this work
pGEX-6P-1_*syc*D21-163 K155S	Site directed mutagenesis of pGEX-6P-1_*syc*D21-163	5.4 kb	this work
pGEX-6P-1_*syc*D21-163 Y95SS	Site directed mutagenesis of pGEX-6P-1_*syc*D21-163	5.4 kb	this work
pGEX-6P-1_*syc*D21-163 S94E/Y95E	Site directed mutagenesis of pGEX-6P-1_*syc*D21-163	5.4 kb	this work
pGEX-6P-1_*syc*D21-163 A61E/L65E	Site directed mutagenesis of pGEX-6P-1_*syc*D21-163	5.4 kb	this work
pGEX-6P-1_*syc*D21-163 A61E	Site directed mutagenesis of pGEX-6P-1_*syc*D21-163	5.4 kb	this work
pGEX-6P-1_*syc*D21-163 L65E	Site directed mutagenesis of pGEX-6P-1_*syc*D21-163	5.4 kb	this work

5.7 Oligopeptides

Table 5-10. Synthetic peptides used in surface plasmon resonance or co-crystallization.

	Peptide	Length	Sequence	Source
1	$RhoA_{181\text{-}190}$_1C	17 aa	Biotin - ATRAALQARRGKKKSGC	W. Tegge; HZI, Braunschweig
2	$RhoA_{181\text{-}190}$_2	17 aa	Biotin - ATRAALQARRGKKKSG$\underline{C}^{Isoprenyl}$	W. Tegge; HZI, Braunschweig
3	$YopD_{278\text{-}300}$	23 aa	DNFMKDVLRLIEQYVSSHTHAMK	P. Henklein; Charité, Berlin

The isoprenylated cysteine is underlined**.**

5.8 Bacterial strains

Table 5-11. Bacterial strains used for gene expression.

Strain	Genotype	Selection marker	Source
ArcticExpress (DE3)-RIL	*E. coli* B, F^- *ompT hsd*S (r_B^- m_B^-) *dcm*$^+$ Tet^R *gal*λ(DE3) *end*A *Hte* [*arg*U, *ile*Y, *leu*W, Str^R]	Cm^R	Stratagene, Amsterdam
BL21 CodonPlus (DE3)-RIL	F^- *ompT hsd*SB(r_B^- m_B^-) *dcm*$^+$ *dam*$^+$ Tet^R *gal*λ (DE3) *end*A *Hte* [*arg*U, *ile*Y, *leu*W, Cm^R]	Cm^R	Stratagene, Amsterdam
Rosetta(DE3)	F^- *ompT hsd*S(r_B^- m_B^-) *dcm*$^+$ *gal lac*Y1 (DE3) pRARE [*arg*U, *arg*W, *gly*T, *_mmu*, *leu*W, *met*T, *pro*L, *thr*T, *tyr*U, *_mmu*, Cm^R]	Cm^R	Novagen
TG1	*sup*E *thi*-1 Δ(*lac-pro*AB) Δ(mcr_B-*hsd*SM)5 (r_K^- m_K^-) [F´ *tra*D36 *pro*AB, *lacI*^{q}, ΔM15]	-	Stratagene, Amsterdam

5.9 Antibodies

Table 5-12. Primary antibodies used in Western blotting.

Name	Antibody species	Antigen	Source
α-YopT	Rabbit	YopT	G.R. Cornelis, University of Basel, Switzerland
α-GFP	Mouse	Green fluorescent protein (GFP)	Molecular probes
Penta·His HRP Conjugate	Mouse	Penta-His	Qiagen

Table 5-13. Secondary antibodies used in Western blotting.

Name	AB species	A/R species	A/R name	Conjugate	Source
Goat Anti-Rabbit IgG HR conjugate †	Goat	Rabbit	IgG	Horse radish peroxidase	Dianova
Goat Anti-Mouse IgG (H+L) AP Conjugate	Goat	Mouse	IgG (H+L)	Alcaline phosphatase	Promega

† Internal laboratory labeling B4c.

5.10 Protein biochemistry

5.10.1 Solutions and buffers

Table 5-14. Buffers and solutions used in protein biochemistry.

Solution/Buffer	Composition
Anion exchange buffer A1 (SycT)	20 mM Tris pH 8.0, 50 mM NaCl, 1 mM DTT
Anion exchange buffer A2 (SycD)	50 mM Tris pH 8.0, 4 mM DTT
Anion exchange buffer B1 (SycT)	20 mM Tris pH 8.0, 1 M NaCl, 1 mM DTT
Anion exchange buffer B2 (SycD)	50 mM Tris pH 8.0, 1 M NaCl, 4 mM DTT
BIAcore buffer	20 mM Tris pH 8.0, 200 mM NaCl, 2 mM DTT
BugBuster lysis buffer	1 mL BugBuster reagent, 1000 U lysozyme, 25 U benzonase, 5 mM Pefablock
CD buffer 1	20 mM Sodium/potassium phosphate pH 7.5,
CD buffer 2	10 mM Sodium/potassium phosphate pH 8.0, 150 mM NaCl
CHT buffer A	10 mM Sodium/potassium phosphate pH 7.0, 2 mM DTT
CHT buffer B	10 mM Sodium/potassium phosphate pH 7.0, 1 M NaCl, 2 mM DTT
CHT buffer C	400 mM Sodium/potassium phosphate pH 7.0, 2 mM DTT
Dialysis buffer 1 (SycT)	10 mM Tris pH 8.0, 10 mM NaCl, 1 mM DTT
GPC running buffer 1 (SycT, YopT)	20 mM Tris pH 8.0, 150 mM NaCl, 1 mM DTT
GPC running buffer 2 (SycD)	10 mM Tris pH 8.0, 50 mM NaCl, 1 mM DTT
GSH-SepH wash buffer 1 (SycT, YopT)	50 mM Tris pH 7.0, 150 mM NaCl, 5 mM DTT

Solution/Buffer	Composition
GSH-SepH wash buffer 2 (SycD)	50 mM Tris pH 7.5, 150 mM NaCl, 10 mM β-mercaptoethanol
Lysis buffer 1 (SycT, YopT)	50 mM Sodium phosphate pH 8.0, 150 mM NaCl, 10 mM β-mercaptoethanol, 1 tablet protease inhibitor cocktail (Complete, Roche), 125 U DNase (Benzonase, Merck)
Lysis buffer 2 (SycD)	1xPBS, 10 mM β-mercaptoethanol, 1 tablet protease inhibitor cocktail (Complete, Roche), 125 U DNase (Benzonase, Merck)
Master mix for *in vitro* translation RTS	12 µL *E. coli* cell lysate, 10 µL reaction mix, 12 µL amino acids, 1 µL methionine, 35 µL restoration buffer
5x Native sample buffer	0.31 M Tris/HCl, pH 6.8, 50 % glycerol, 0.1 % bromophenol blue
10x Native PAGE running buffer	0.4 M Tris, 1.92 M glycine, adjust pH 8.3
NiNTA binding buffer	10 mM Imidazole, 50 mM Tris pH 8.0, 150 mM NaCl, 1 mM DTT
NiNTA elution buffer	250 mM Imidazole, 50 mM Tris pH 8.0, 150 mM NaCl, 1 mM DTT
NiNTA wash buffer	25 mM Imidazole, 50 mM Tris pH 8.0, 150 mM NaCl, 1 mM DTT
1x PBS	137 mM NaCl, 3 mM KCl, 12 mM Na_2HPO_4, 2 mM K_2HPO_4, pH 7.4
PreScission protease cleavage buffer	50 mM Tris pH 7.4, 200 mM NaCl, 1 mM EDTA, 10 mM β-mercaptoethanol
Protease inhibitor mix	40 µM Pefablock, 0.3 µM aprotinin, 10 µM E-64, 1 mM EDTA
Selenomethionine salt solution	0.3 % w/v $MgSO_4$, 20 % w/v glucose, 100 mg/L $Fe(SO_4)_3$, 100 mg/L thiamine
20x TEV protease cleavage buffer	1 M Tris pH 8.0, 10 mM EDTA, 20 mM DTT
Trace metal mixture (1000x)	50 mM $FeCl_3 \cdot 6\ H_2O$, 20 mM $CaCl_2$, 10 mM $MnCl_2 \cdot 4\ H_2O$, 10 mM $ZnSO_4 \cdot 7\ H_2O$, 2 mM $CoCl_2 \cdot 6\ H_2O$, 2 mM $NiCl_2 \cdot 6H_2O$, 2 mM $Na_2MoO_4 \cdot 2\ H_2O$, 2 mM Na_2SeO_3, 2 mM $H_3BO\cdot$, 60 mM HCl
Transfer buffer for Western blotting	20 mM Tris pH 8.0, 192 mM glycine, 15 % methanol
Tris-Tricine gel electrophoresis cathode buffer	0.1 M Tris, 0.1 M Tricine, and 0.1% SDS
Tris-Tricine gel electrophoresis anode buffer	0.2 M Tris/HCl, pH 8.9
2x Tris/Tricine sample buffer	1 mL 1 M Tris/HCl pH 6.8, 2.4 mM (3 g) glycerol, 0.8 g SDS, 2 mg Coomassie blue G-250, 0.31 g DTT, add H_2O to 10 mL
Tris-Tricine stacking gel	2.43 mL Polyacrylamide solution (Rotiphorese Gel 30, Roth), 6.2 mL Tris/HCl/SDS buffer pH 8.45, 16.38 mL H_2O, 50 µL TEMED, 30 µL APS
Tris-Tricine resolving gel	10.86 mL Polyacrylamide solution, 10 mL Tris/HCl SDS buffer pH 8.45, 5.97 mL H_2O, 2.17 mL glycerol 50 µL TEMED, 15 µL APS
Tris/HCl/SDS buffer	3 M Tris/HCl, 0.3 % SDS, pH 8.45

5.10.2 Media

Media were subjected to autoclave sterilization (121 °C, 2 bar, 20 min, Top7000PST, Sauter, Sulgen, Switzerland). Antibiotics were added after media cooling below 50 °C. Depending on plasmid and bacteria strain following end concentrations of antibiotics were used: Ampicillin (Amp) 100 µg/mL, kanamycin (Kan) 30 µg/mL, chloramphenicol (Cm) 34 µg/mL.

Table 5-15. Media used in bacteria cultivation for protein production.

Medium	Composition
Luria Bertani (LB)	10 g/L Tryptone, 7 g/L, NaCl, 5 g/L yeast extract
MDG (non-inducing)	25 mM Na_2HPO_4, 25 mM KH_2PO_4, 50 mM NH_4Cl, 5 mM Na_2SO_4, 2 mM $MgSO_4 \cdot 7\ H_2O$, 1x trace metal mixture, 0.5% glucose, 0.25 % aspartate
ZYM502 (auto-inducing)	1% Tryptone, 0.5 % yeast extract, 25 mM Na_2HPO_4, 25 mM KH_2PO_4, 50 mM NH_4Cl, 5 mM Na_2SO_4, 2 mM $MgSO_4 \cdot 7\ H_2O$, 1x trace metal mixture, 0.5% glycerol, 0.05% glucose, 0.2 % lactose
2x YT	16 g/L Tryptone, 5 g/L NaCl, 10 g/L yeast extract
Selenomethionine basis	1 g/L NH_4Cl, 3 g/L KH_4PO_4, 4 g/L $NaHPO_4 \cdot 2H_2O$

5.10.3 Absorption coefficients of proteins used for concentration determination

Table 5-16. Calculated absorption coefficients of selected proteins.

Protein	Molar extinction coefficient ε [$M^{-1} \cdot cm^{-1}$]	1 OD_{280} ≡ x mg/ml	1 mg/ml ≡ y OD_{280}
YopT	44’290	0.82	1.22
$YopT_{75-318}$	41’730	0.67	1.49
YopT/SycT	95’170	0.70	1.43
YopTΔ49(C139S)/SycT	92’610	0.67	1.5
SycT	25’440	0.60	1.67
$SycT_{1-122}$	25’440	0.57	1.76
SycD	10’720	0.55	1.81
$SycD_{21-163}$	9320	0.57	1.77
$SycD_{21-163}$ K155S	9320	0.57	1.75
$SycD_{21-163}$ Y95S	8040	0.49	2.04
$SycD_{21-163}$ S94E/Y95E	8040	0.51	2.05
$SycD_{21-163}$ A61E/L65E	9320	0.56	1.77
$SycD_{21-163}$ A61E	9320	0.56	1.77
$SycD_{21-163}$ L65E	9320	0.56	1.77

The OD_{280}-concentration relation for a 1 cm cuvette are listed additionally.

5.11 Protein production

5.11.1 YopT/SycT and SycT

Gene expression and protein production

Expression host bacteria were freshly transformed with the expression vector. Target proteins expressed in large scale were expressed as GST-fusion proteins. Precultures of 50 mL medium with corresponding antibiotics were inoculated with a single colony, incubated for 16 h and served as inoculum for 2 L medium-antibiotic mix in cultivation flasks. Cells were grown at 37 °C till an OD_{600} ~0.45, shifted to the expression temperature and incubated further till an OD_{600} ~0.6. Gene expression was induced with 1 mM IPTG and extended for

15 h at 20 °C, if not mentioned otherwise. Cells were harvested by centrifugation for 15 min at 7100xg (Sorvall Thermo RC6 centrifuge, SLA-3000 rotor). The supernatant was discarded and the pellet suspended in ice-cold lysis buffer. The cell suspension (~40 mL) was lysed using a French Press (SLM Aminco). Soluble and insoluble fractions were separated by centrifugation (37'000xg, 60 min, 4 °C).

Purification of YopT/SycT complex variants

Soluble fusion protein from the centrifugation supernatant was coupled to ~10 mL glutathione sepharose 4B beads (GE-Healthcare) (1 h, 4 °C, shaking) that had been equilibrated with lysis buffer 1. The beads were washed with GSH-Seph wash buffer 1 till the OD_{280} absorption reached a stable, low value. The tag was cleaved on column in 1-3 column volumes of corresponding cleavage buffer with 500 mg TEV protease added and incubated at 16 °C for 16 h. The supernatant containing tag-free target protein as well as the His6-tagged TEV protease was applied to 2 mL NiNTA agarose (QIAGEN) in order to remove the protease. The NiNTA agarose affinity chromatography supernatant containing the YopT/SycT complex was directly subjected to size exclusion chromatography. SEC columns were used with FPLC devices (ÄKTA, GE Healthcare). Prior to this, the affinity chromatography supernatant containing the purified complex was concentrated to 2-3 mL using Vivaspin 20 (Sartorius, MWCO 3500 - 5000) ultrafiltration units. The complex was purified by SEC using a Superdex 75 XK 16/60 column (GE-Healthcare-Amersham Biosciences). Peak fractions were pooled. Purified protein was subjected to dynamic light scattering and MADLI-TOF-MS measurements (Ultraflex Bruker, Dr. Manfred Nimtz and Anja Meier; HZI, Braunschweig) to investigate protein monodispersity and integrity, respectively. Aliquots were frozen at -70 °C until further use.

Purification of SycT

Production as GST-fusion and protein purification ill affinity chromatography was carried out as described above. The supernatant from affinity chromatography was dialyzed against buffer A 1 (2 L, one buffer exchange with 2 L) of the following anion exchange chromatography. Anion exchange material (MonoQ HR 10/10, GE Healthcare) was used with FPLC devices (ÄKTA, GE Healthcare). SycT was purified by anion exchange chromatography (AEC) using a linear NaCl gradient. The AEC peak fractions containing the purified SycT were concentrated to 2-3 mL using Vivaspin 20 (Sartorius, MWCO 3500) ultrafiltration units. SycT was further purified by SEC using a Superdex 75 XK 16/60 column (GE-Healthcare-Amersham Biosciences). Peak fractions were pooled and dialyzed. Purified SycT was concentrated for crystallization trials (see section 5.14.1) and subjected to dynamic light scattering and MADLI-TOF-MS measurements to check protein monodispersity and integrity, respectively. Aliquots were frozen at -70 °C until further use.

5.11.2 SycD

Gene expression of *syc*D and variants

Expression host bacteria were freshly transformed with the expression vector. SycD produced in large scale was expressed as a GST-fusion protein. The preculture of 50 mL medium with corresponding antibiotics was inoculated with a single colony, incubated for 6 h and served as inoculum for 2 L medium-antibiotic mix in cultivation flasks. Cells were grown at 37 °C until

an OD_{600} ~0.6 and shifted to 20 °C. Gene expression was induced at an OD_{600} ~0.9 with 0.25 mM IPTG and extended to 15 h at 20 °C. Cell harvest was carried out by centrifugation for 15 min at 7100xg (Sorvall Thermo RC6 centrifuge, SLA-3000 rotor). The supernatant was discarded and the pellet suspended in ice-cold lysis buffer 2. The cell suspension (~50 mL) was lysed using a homogenizer (Constant Cell Disruption Systems). Soluble and insoluble fractions were separated by centrifugation (37'000xg, 75 min, 4 °C).

Purification of SycD and variants

Soluble fusion protein from the centrifugation supernatant was coupled to ~10 mL glutathione sepharose 4B beads (GE-Healthcare) (1 h, 4 °C, shaking) that had been equilibrated with lysis buffer 2. The beads were washed with GSH-Seph wash buffer 2 till the OD_{280} absorption reached a stable, low value, and further washed with 3 column volumes of PreScission protease cleavage buffer supplied with the protease inhibitor mix. The tag was cleaved on column in 2-3 column volumes of PreScission protease cleavage buffer/inhibitor mix. Proteolytic cleavage required 500 U PreScission protease and 48-60 h at 4 °C. The supernatant containing the tag-free target protein was dialyzed against buffer A 2 (2.5 L, one buffer exchange with 2.5 L) of the following anion exchange or ceramic hydroxyapatite (CHT) chromatography. CHT, a sintered material turned from crystalline to ceramic, possesses different functional groups such as Ca^{2+}, PO_4^{3-} and OH groups. Negatively charged carboxyl groups of the protein can interact with hydroxyapatite calcium ions and are competed out by a phosphate gradient. Here, CHT chromatography was used as a negative purification step with the protein rescued from the flowthrough. Anion exchange material (MonoQ HR 10/10, GE Healthcare), ceramic hydroxyapatite (Bio-Rad) and SEC columns were used with FPLC devices (ÄKTA, GE Healthcare). SycD purification by AEC was carried out using a linear NaCl gradient. The AEC peak fractions or the CHT flowthrough containing the purified target protein were concentrated to 2-3 mL using Vivaspin 20 (Sartorius, MWCO 5000) ultrafiltration units. SycD was further purified by SEC using a Superdex 200 XK 16/60 column (GE-Healthcare-Amersham Biosciences). Peak fractions were pooled. Purified protein was concentrated for crystallization trials (see section 5.14.1) and subjected to dynamic light scattering and MADLI-TOF-MS to check protein monodispersity and integrity, respectively. Aliquots were frozen at -70 °C until further use.

5.11.3 Production of selenomethionine-labeled substituted SycT

The media were prepared as described (Guerrero *et al.*, 2001). An 1 L over night culture of pETM-30_*syc*T1-122/ methionine-auxotroph *E. coli* BL21 CodonPlus(DE3)-RIL in LB-medium was pelleted (15 min, 4000xg), and washed twice *via* suspension in sterilized H2O. After the second wash and centrifugation step, the pellet was suspended in the selenomethionine basis medium/salt (10:1) mixture. The cell suspension was diluted in 2 L of prewarmed selenomethionine basis medium/salt mixture to yield a final OD_{600} of ~0.6 and incubated at 20 °C for 20 min and 140 rpm to use up all residual methionine in the bacterial cells. Gene expression was induced with 1 mM IPTG (14 h, 20 °C, 140 rpm). Cell harvest, lysis and protein purification of selenomethionine (SeMet)-labeled GST-$SycT_{1-122}$ were performed as described above.

5.11.4 Gene expression using auto-inducing medium

Expression host containing the expression vector was grown over night at 30 °C in non-inducing (MDG) medium (Studier, 2005) with corresponding antibiotics. The desired volume

of auto-inducing medium (Studier, 2005) was inoculated with the over-night culture (ratio 1:100) and incubated at 20 °C for 24-36 h.
In case of glucose and lactose being in the culture medium simultaneously, the bacteria first use glucose as carbon source and later activate the catabolit activator protein (CAP)-dependent lactose operon (catabolit repression). Lactose serves as an inducer for expression of the target genes that are controlled by the LacI repressor. The lactose induced gene expression is less strong and slower compared to IPTG induction. As a result, the nascent target protein chain has more time to fold correctly and the bacterium produces in total more biomass and therefore more soluble target protein.

5.11.5 Expression test

Expression constructs were transformed into suitable bacterial expression hosts. Precultures of a single colony picked into 3 mL medium with appropriate antibiotics were grown over night at 30 °C. Expression test cultures of 50 mL medium/antibiotics were inoculated with the pre-culture (ratio 1:100) and incubated at 37 °C to an OD_{600} ~0.45, shifted to the expression temperature and induced at OD_{600} ~0.6 with IPTG (1 mM end concentration). Samples were taken during expression progress (3-5 h, over night induction) and their OD_{600} determined. Samples were centrifuged (21'000xg, 1 min) and BugBuster lysis buffer was used to suspend the cell pellet (100 µL lysis buffer to 1 mL cell culture with an OD_{600} = 1). After 20 min incubation at room temperature the tubes were centrifuged (21'000xg, 10 min), the super-natant containing soluble protein fraction was pipetted off and the pellet suspend in the same volume of 8 M urea (50 mM Tris-buffered, pH 8). Aliquots of soluble and insoluble fractions were analyzed by denaturing polyacrylamide gel electrophoresis.

5.11.6 *In vitro* translation

GFP-fusion proteins were produced *in vitro* using the pETM-11GFPfus expression constructs (requirements: T7 promoter, ribosomal binding site and T7 terminator) with the Rapid Translation System (RTS 100 *E. coli* HY Kit and ProteoMaster, Roche) according to the manufacturer's instructions. One reaction tube was filled with 10 µL containing 0.5 µg DNA, mixed with 40 µL of *in vitro* translation master mix and incubated (6 h, 30 °C, 150 rpm).

5.11.7 Reductive methylation of lysines

The target protein purified by anion exchange chromatography was subjected to ultrafiltration (Vivaspin, Sartorius, MWCO 5000) for buffer exchange with 50 mM sodium potassium phosphate/150 mM NaCl, pH 7.5. The protein was concentrated to ~10 mg/mL in a total volume of 2x 1 mL and methylated as described (Rypniewski *et al.*, 1993). All reagents were freshly prepared. 1 mL protein solution was gently mixed with 20 µL of 1 M dimethylamine-borane complex (ABC) immediately followed by the addition of 40 µL 1 M formaldehyde and incubated on ice and in the dark for 2 h. The reaction step was repeated twice with only half of the volumes added in the third round followed by incubation for 36 h. Quenching of the reaction was achieved by the addition of 100 µL 1 M ammonium sulfate and incubation for 24 h. The methylated protein was mixed with 50 mM DTT to a final concentration of 5 mM and separated from reaction residue by size exclusion chromatography as described above. Peak fractions were concentrated for crystallization trials.

5.12 Protein analytical methods

5.12.1 Gel electrophoresis

Discontinuous polyacrylamide gel electrophoresis (PAGE) was carried out using a gel electrophoresis device (Mini Protean III, Bio-Rad). Gels for native PAGE were prepared in the same way as described for denaturing sodium dodecyl sulfate (SDS) discontinuous gel electrophoresis (Laemmli, 1970) with the exception of using for both gel parts Tris/HCl buffer pH 8.8 and leaving out SDS. Samples were mixed with an equal volume of native sample buffer, and with half the volume of SDS sample buffer, respectively. The native PAGE was run at 30 mA until the tracking dye was 1 cm away from the gel edge. 16 % Tris Tricine gels were prepared as described (Schägger and Jagow, 1987) using the appropriate solutions listed above and run at constant voltage (110 V).

5.12.2 Limited proteolysis

Purified protein was mixed with 1x protease cleavage buffer to yield a final protein concentration of ~1-2 mg/mL in 200 µL reaction volume. Proteases were added resulting in a protein:protease ratio of 70:1 or 100:1, respectively. The reaction tubes were kept on different temperatures (on ice, 20 °C, 37 °C). Aliquots were taken at different time points during the reaction progress and immediately mixed with 2 µL protease inhibitor mix, incubated for 5 min, mixed with 10 µL sample buffer and denaturated (5 min, 95 °C) for further analysis by denaturing gel electrophoresis.

5.12.3 Western blotting

Transfer of proteins separated by molecular size *via* gel electrophoresis to polyvinyl difluoride (PVDF) membranes was carried out according to the described method (Towbin and Staehelin, 1979). The membrane was activated by treatment with methanol for 1 min, followed by washing in transfer buffer. The gel was incubated in transfer buffer as well (15 min). The anode of the semi-dry blot chamber (TransBlot semi-dry transfer cell, Bio-Rad) was covered with two stacked tissue papers (Whatman) of slightly larger size than the gel that had been soaked in transfer buffer, followed by the membrane, the gel and two additional soaked tissue papers on top. The transfer was carried out for 40 min at 15 V. Unspecific binding-sites on the membrane were blocked (5 % non-fat dry milk in PBS, 1 h) and the membrane was washed with PBS (10 min). The primary antibody was diluted (α-YopT 1:100, others 1:2000) in 0.3 - 5 % non-fat dry milk/PBS and incubated with the membrane for 1 h at room temperature and gentle shaking. After washing with PBS (3x 5 min) the membrane was incubated for 2 h with the secondary antibody (1:5000-1:10'000 in PBS) and finally washed with PBS (3x 10 min). The protein on the blot was detected by chloronaphthol staining or Enhanced Chemiluminescence (ECL) (LumiLight, Roche).

5.12.4 N-terminal sequencing

Protein bands separated by SDS-PAGE, blotted onto PVDF membrane (see section 5.12.3) and visualized by Coomassie staining were sequenced by automated Edman degradation

(Edman and Begg, 1967) performed by Rita Getzlaff (HZI, Braunschweig) using an 494A HT Protein Sequenzer (Applied Biosystems).

5.12.5 Dynamic light scattering

In order to determine the particle size distribution of a protein solution, dynamic light scattering (also quasi-elastic light scattering) experiments were carried out on a DynaPro 801TC instrument (ProteinSolutions/Wyatt Technologies). The protein sample, approximately 15 µL of a prior centrifuged (15 min, 21'000xg) protein solution, was introduced in the cell and the scattering intensity fluctuations were recorded at room temperature until the signal stabilized (approx. 30 data points). The data were analyzed assuming a globular shape of the particles using the instrument software. As a rule of thumb, a polydispersity of the sample of < 20 % was used as an indicator for a monodisperse protein solution suitable for crystallization trials.

5.12.6 Surface plasmon resonance spectroscopy

Surface plasmon resonance (SPR) is a biosensing technique that allows the detection of biomolecular interactions. One of the molecules of interest is immobilized onto one side of a metallic film. Light coming from the opposite side of the film excites surface plasmons (oscillation of free electrons on the film surface) and is refracted with a certain refractive index. Binding of a ligand to the immobilized molecule on the opposite side results in an alteration in surface plasmons. The subsequent change of refractive index measured is proportional to the amount of bound ligand. Binding studies between analyte (protein) and ligand (peptide) were carried out using the BIACORE 2000 (BIACORE AB) device and BIAcore buffer (flow rate 10 µL/min, 25 °C). Dilutions of biotinylated RhoA peptides were coupled to a streptavidin coated sensor chip (SA, GE Healthcare) until sufficient response units (RU) were coated. The analyte, protein complexes YopT/SycT and YopTΔ49 C139S/ SycT with a concentration of 8-16 µM, respectively, were directed over the immobilized RhoA peptides for binding studies.

5.12.7 Circular dichroism

Protein solutions were subjected to dialysis or buffer exchange *via* ultrafiltration against CD buffer 1 or 2, respectively, diluted to an end concentration of ~0.1 mg/mL (6-9 mM) and analyzed with a spectropolarimeter (JASCO J-810). Typically, 10 spectra in the 180-250 nm range were collected at room temperature, averaged and converted to molar ellipticity. Data were evaluated in DICROPROT (Deleage and Geourjon, 1993) using a least square fitting algorithm by Bolotina *et al.*, 1980.

5.13 Bioinformatics

Sequences of genes and gene products were analyzed and archived in Vector NTI version 6. Amino acid sequences were analyzed for potential surface entropy reduction of residues suitable for site-directed mutagenesis (Derewenda and Vekilov, 2006) using the surface entropy reduction server http://nihserver.mbi.ucla.edu/SER/.

Pairwise and multiple sequence alignments were performed using CLUSTALW (Thompson, 1994) and EMBOSS (Pearson *et al.*, 1997).
Modeling the YopT amino acid sequence onto the crystal structure of AvrPphB (PDB accession code 1UKF) was carried out using the program BRAGI (Reichelt *et al.*, 2005) and Joachim Reichelt's (HZI, Braunschweig) assistance.
The identification and generation of the SycD mixed model used in molecular replacement was carried out using the Fold & Function Assignment System (http://ffas.ljcrf.edu/ffas-cgi/cgi/ffas.pl, FFAS03) (Jaroszewski *et al.*, 2005).

5.14 X-ray structural analysis

5.14.1 Crystallization experiments

Initial screening for crystallization conditions was carried out in 96-well format using several commercially available screens (Nextal/Qiagen, Emerald Biostructures, Hampton Research) and sitting drop vapor diffusion at 20 °C and 4 °C, partially supported by nano-drop pipetting (Mosquito, Molecular Dimensions). Tests were further carried out with porous gel-glass, a universal nucleant, spotted onto Innovaplate SD-2 drop chambers or in the form of small grains (Nano-Grain) (cooperation with Jason Maroothynaden from Nanonucleant, London, UK), which was supposed to provide suitable nucleation surfaces and enforce crystallization. Optimization of crystallization conditions (buffer system, pH, precipitant concentrations) was carried out using hanging drop (24-well plate) and sitting drop vapor diffusion at 4 °C. An overview of the different crystallization conditions is given in Table 5-17.

Table 5-17. Crystallization conditions of target proteins crystallized in this study. Initial and optimized conditions as well as specifications on the crystallization droplet are given.

Protein	Initial condition	Optimized reservoir condition	Droplet/Incubation
SycT			
SycT	Birefringent spherulites CrystalScreen1 No.40	5 % 2-Propanol, 0.1 M trisodium citrate pH 5.6, 21 % PEG 4000	11.2 mg/mL, 1 µL protein + 1 µL reservoir, hanging drop, over night
SeMet $SycT_{1-122}$ (crystal form 1)	Emerald Biostructures Wizard I No.33	1.6 M Ammonium sulfate, 0.1 M CAPS pH 10.5, 0.15 M lithium sulfate	12.3 mg/mL, 0.5µL + 0.5 µL, hanging drop, over night
SeMet $SycT_{1-122}$ (crystal form 2)	-	1.8 M Ammonium sulfate, 0.1 M sodium bicarbonate pH 10.5, 0.05 M magnesium chloride	12.3 mg/mL, 0.5 µL + 0.2 µL, hanging drop, over night
SycD			
$SycD_{21-163}$	Nextal Cations No.92	1.9-2.2 M Potassium acetate, 0.1 M Tris pH 8.2	23 mg/mL, 2 µL + 0.5 µL hanging drop, 14 d
	Nextal MbClassII, No.28	0.1 M Trisodium citrate pH 5.5, 0.1 M sodium chloride, 0.1 M lithium sulfate, 25 % PEG 350 MME	*not to optimize*

Protein	Initial condition	Optimized reservoir condition	Droplet/Incubation
$SycD_{21-163}$K155S	Nextal Cations No.45	1.85 M Lithium acetate, 0.1 M Tris pH 8.4	25 mg/mL,2 µL + 0.5 µL, hanging drop, 14 d
	Nextal MbClassII, No.28	0.1 M Trisodium citrate pH 5.5, 0.1 M sodium chloride, 0.1 M lithium sulfate, 25 % PEG 400	29-47mg/mL, 1 µL + 0.5 µL, 13 d, *not to optimize*
	(hand-made PEG screen)	45 % PEG 400, 0.1 M Tris pH 8.2	47 mg/mL, sitting drop, 0.2 µL + 0.1 µL, 4 d, *not to optimize*
$SycD_{21-163}^{meth}$	Nextal SM4 No.61	0.1 M Trisodium citrate, 10-20 % 2-propanol, 20-23 % PEG 4000, pH adjusted to ~7.8	14.3 mg/mL, 0.5 µL + 0.25 µL sitting drop, 4 - 21 d
$SycD_{21-163}^{meth}$S94E/Y95E	Emerald Biostructures Synergy Precipitant P1 No. 38 & No. 47	Original bulk screen solutions 40 % PEG 400, 5 % PEG 3350, 0.1 M sodium acetate pH 5.5 25 % PEG 3350, 5 % PEG400 0.1 M sodium acetate pH 5.5	15.3 mg/mL, 0.2 µL +0.1 µL, 6 d
$SycD_{21-163}$A61E/L65E ^{meth} $SycD_{21-163}$L65E^{meth}	Emerald Biostructures Synergy Precipitant P1 No.45	0.1 M Tris pH 8.5, 30 PEG 1500, 8 % 2-methyl-2,4-pentanediol	~12.6-13.8 mg/mL, 1 µL + 0.5 µL, hanging drop, 7 d, *not to optimize*
$SycD_{21-163}$A61E/L65E	Optimization of Nextal SM4 No.61	0.1 M Trisodium citrate 15 % 2-propanol, 23 % PEG 4000	15.4 mg/mL, 0.5 µL + 0.25 µL, sitting drop, 14 d

Crystals were subjected to quick-soaks (10 - 60 sec) in cryo-protection solutions (summarized in Table 5-18) to protect crystals from ice formation and radiation damage, and flash-frozen in liquid nitrogen.

Table 5-18. Cryo-protection used. Cryo-protection solution were freshly prepared based on the crystallization condition supplemented with cryo-protectant, potentially with increased precipitant concentration.

Protein	Cryo-protectant	Adjusted precipitant concentration
SycT	19-26 % Glycerol	22 % PEG 4000
SeMet $SycT_{1-122}$ (crystal form 1)	19 % Glycerol	-
SeMet $SycT_{1-122}$ (crystal form 2)	23 % Glycerol	-
$SycD_{21-163}$	25 % Glycerol	2.1 M Potassium acetate
	26 % Glucose	2.1 M Potassium acetate
$SycD_{21-163}$ K155S	25 % Glycerol	2.0 M Lithium acetate
	26 % Glucose	2.0 M Lithium acetate
	-	2.0 M Lithium acetate
$SycD_{21-163}^{meth}$	20 % Glycerol	-
$SycD_{21-163}^{meth}$ S94E/Y95E	- (directly from well)	-
	10 % Glycerol	27 % PEG 3350
$SycD_{21-163}$ A61E/L65E	23 % Glycerol	23.4 % PEG 4000

Crystals were mounted on the goniometer head using cryo-tongues or nitrogen-filled vials, and maintained at 100 K *via* a nitrogen cryo-stream device. Diffraction images were further collected at room temperature (MicroMounts & Room Temperature Mounting System, MiTeGen) to confirm the diffraction potential of crystals poorly diffracting after flash-freezing.

5.14.2 Crystal engineering

Heavy atom derivatization

Heavy-atom derivatized crystals were prepared by quick and medium soaks (seconds to several minutes) in either near-molar concentrations of halides (potassium/sodium bromide or chloride) (Dauter *et al.*, 2000) or in 10 mM heavy metal solutions (Sun and Radaev, 2002) of thimerosal ($C_6H_9HgO_2SNa$), ethylmercurylphosphate ($C_2H_7HgO_4P$), potassium tetracyano-platinate ($K_2Pt(CN_4)\cdot xH_2O$), potassium tetrachloroplatinate (II) (K_2PtCl_4) or osmium(III)chloride hydrate ($OsCl_3\cdot xH_2O$) containing appropriate cryo-protectants. Crystals treated with heavy metals were back-soaked (1 min) in 1 mM heavy atom solution with cryo-protectant. Crystals were finally flash-frozen in liquid nitrogen. Xenon pressure derivatization (Panjikar and Tucker, 2002) was carried out with the help of S. Panjikar (EMBL Hamburg/DESY). The crystals, prior soaked in cryo-protection solution, were pressurized with xenon gas (room temperature, 4 MPa,1 min), the pressure was gradually released (20 s) and the crystals were flash-frozen in liquid nitrogen.

Dehydration

To improve the diffraction potential by homogenizing the packing and shrinking the unit cell in $SycD_{21\text{-}163}$ and $SycD_{21\text{-}163}$ K155S crystals different approaches were used. First, cover slides were simply transferred to even more concentrated reservoir wells. As second technique, introduced by Björn Klink (HZI, Braunschweig), three ~200 nL droplets of reservoir solutions already containing the cryo-protectant as well as high concentrations of precipitants (see Table 5-19) were pipetted around the rim of a crystals-containing reservoir drop followed by 15-30 min of equilibration. These steps were repeated until the doubled drop volume and the final concentration were achieved. To monitor the progress, crystals were flash-frozen after 3/6/9 addition cycles or over night equilibration and the diffraction pattern was analyzed. Controlled dehydration/hydration (Free mounting system, Proteros/Rigaku (Kiefersauer *et al.*, 2000)) by running gradients of relative humidity in combination with on-line X-ray measurements (Bruker; MAR345 detector) was applied as a third technique.

Table 5-19. Solutions used in the second, droplet dehydration technique.

No.	Dehydration solution	Applied to
1	2.8 M Potassium acetate, 0.1 M Tris pH 8.2, 20 % glycerol	$SycD_{21\text{-}163}$
2	3.6 M Potassium acetate, 0.1 M Tris pH 8.2	$SycD_{21\text{-}163}$
3	2.4 M Potassium acetate, 0.1 M Tris pH 8.2, 30 % polyethylene glycol 400	$SycD_{21\text{-}163}$
4	4.5 M Lithium acetate, 0.1 M Tris pH 8.4	$SycD_{21\text{-}163}$ K155S
5	4.45 M Lithium acetate, 0.1 M Tris pH 8.4 + 1 % trehalose	$SycD_{21\text{-}163}$ K155S
6	4.42 M Lithium acetate, 0.1 M Tris pH 8.4 + 1.6 % trehalose	$SycD_{21\text{-}163}$ K155S
7	3.5 M Lithium acetate, 0.1 M Tris pH 8.2 + 20 % glycerol	$SycD_{21\text{-}163}$ K155S

5.14.3 Data collection and processing

Data were collected using synchrotron radiation and MAR CCD and ADCS CCD detectors (Marresearch, Germany and Area Detector Systems Corporation, USA) (see Table 5-20).
After fluorescence scanning, a multiple-wavelength anomalous dispersion (MAD) experiment was carried out for selenomethionine-labeled $SycT_{1-122}$ at the peak, inflection and high remote energies of the selenium K-edge. Wavelengths used in data collection are listed in Table 5-20. Data of native SycT, $SycD_{21-163}$ and $SycD_{21-163}^{meth}$ Xe were processed and scaled with DENZO/ SCALEPACK (Otwinowski, 1997), data of SeMet $SycT_{1-122}$ crystal form 1 and 2 as well as $SycD_{21-163}^{meth}$ and mutants were processed with XDS and scaled with XSCALE (Kabsch, 1993). The CCP4 program suite (Collaborative Computational Project, 1994) provided further tools to manipulate reflection data and proceed in structure solution.

Table 5-20. Synchrotron beamlines used for data collection.

Protein crystals	Synchrotron light source	Beamline	Wavelength [Å]
SycT	DESY / EMBL-Hamburg	BW6	1.05
$SycT_{1-122}$ crystal form 1 - Peak	BESSY / Berlin	BL14.1	0.9795
$SycT_{1-122}$ crystal form 2 - Peak	BESSY / Berlin	BL14.1	0.97957
- Inflection point	BESSY / Berlin	BL14.1	0.97976
- High energy remote	Cryo-protection	BL14.1	0.91165
$SycD_{21-163}$	DESY / EMBL-Hamburg	X12	1.27815
$SycD_{21-163}^{meth}$	DESY / EMBL-Hamburg	X12	1.27815
	ESRF / Grenoble	ID23-1	0.97925
$SycD_{21-163}^{meth}$ Xe	DESY / EMBL-Hamburg	X12	1.5
$SycD_{21-163}^{meth}$ S94E/Y95E	ESRF / Grenoble	ID14-1	0.934
$SycD_{21-163}$ A61E/L65E(V64M)	BESSY / Berlin	BL14.1	0.91841

5.14.4 Anomalous dispersion in structure solution

The presence of a heavy atom (element with high atomic number) in the crystal lattice allows the *de novo* phase determination of the diffraction data. Anomalous scattering (also dispersion) occurs when the energy of the incident X-ray photon is close to the absorption edge/transition energy required to promote an electron to an unoccupied higher orbital or to eject it completely from an atom. The absorption of incident energy by the crystal results in a reduced intensity of the coherent scattering and a slight change in the phase of the scattered X-ray beams. This is expressed by the atomic scattering factor f of the heavy atom comprising now the normal scattering component ${}^{0}f$ and a non-negligible wavelength-dependent real (dispersive, f') and an imaginary (absorption, f'') correction term for the anomalous scattering. The experimental determination of the actual shape of the absorption curve *via* fluorescence energy scan of the heavy atom-labeled crystal provides the precise values for f'' and of its derivative f'. As the absorption term f'' is always 90° advance in phase, the resonant/anomalous scattering causes a slight deviation from Friedel's Law (Friedel, 1913). Friedel pairs F_{hkl} and F_{-h-k-l} (short F^+ and F^-) are Bragg reflections related by inversion through the origin exhibiting the same magnitude of the structure factor intensity but opposite phase angles at normal scattering using wavelengths far from the absorption edge. In anomalous scattering, Friedel mates no longer have equal structure factor amplitudes (Bijvoet, 1954): $|F_{hkl}| \neq |F_{-h-k-l}|$ and their phase angles are no longer complementary. Near the absorption

edge energy ("peak" wavelength), the imaginary anomalous component f'', which is proportional to the atomic absorption coefficient of the heavy atom, shows its largest value. The dispersive part f' of the anomalous signal shows its minimum at the inflection point of the scan. The structure factors of the derivative at these wavelengths differ significantly in their amplitudes compared to the native data (or the equivalent data of a derivative collected at a remote energy). The advantage of such a multiple-wavelength anomalous dispersion (MAD) experiment is the resolution of the phase ambiguity and the (almost) perfect isomorphism of the collected datasets as they are collected from a single crystal. Non-isomorphism (changes of unit cell parameters or protein orientation in the unit cell) interferes with the phasing success. It has been shown that even a single wavelength is sufficient to obtain good phase estimates and to solve novel structures (single-wavelength anomalous dispersion (SAD) (Dauter *et al.,* 2002). In SAD, the phase ambiguity is broken by density modification protocols. The correct enantiomorph (handedness) of the anomalous scatterer substructure is thereby revealed by comparison of the electron-density maps treated by density modification. The incorrect enantiomorph contains no image of the macromolecule, whereas the correct map features clear solvent boundary and a macromolecular-like density histogram.
The positions of the anomalously scattering heavy atoms in the unit cell can be deduced from an anomalous difference Patterson map (Patterson function introduced by Patterson, 1935), which is calculated using only the coefficients ΔF^2 derived from the anomalous structure factor amplitude differences of the Friedel pairs (and their symmetry mates) $\Delta F = |F^+| - |F^-|$, also called Bijvoet amplitude differences. Significant non-origin peaks in the three-dimensional Patterson map correspond to interatomic vectors between anomalously scattering atoms only that are related by crystallographic symmetry and are found in two-dimensional slices of the map (called Harker sections, Harker, 1936). From the Harker peaks (u,v,w), the coordinates of the heavy atoms (x,y,z) in the unit cell can be calculated. The normal scattering structure factor amplitude and phase, together with f'' and its derivative f', allows the estimation of the phases of the anomalous structure factors F_A for the anomalous scatterer substructure. This allows a first approximation of the phase angles for the native protein structure factors F_T.

5.14.5 Structure determination

Five out of six selenium atoms in the hexagonal packing of $SycT_{1\text{-}122}$ crystal form 2 could be located by heavy-atom search, phasing and solvent flattening programs SHELXD (Uson and Sheldrick, 1999) and SHELXE (Sheldrick, 2002) that were run using the graphical user interface HKL2MAP (Pape and Schneider, 2004). SHELXE phases for crystal form 2 provided interpretable electron density and were used to trace an initial model using the same anomalous dataset (see section 5.14.6). The structure for the orthorhombic (crystal form 1) data set was solved by molecular replacement using the refined structural model of crystal form 2 as search model in the program PHASER (Storoni *et al.*, 2004). The native structure was solved using both refined $SycT_{1\text{-}122}$ structural models of crystal form 2 and 1 as search ensemble for molecular replacement in PHASER.
The structure of $SycD_{21\text{-}163}{}^{meth}$ could be solved by MR in the program PHASER searching with a mixed model of the TPR domain of a synthetic repeat protein (PDB accession code 2FO7), obtained by application of the Fold & Function Assignment System (FFAS) algorithm to the SycD sequence (Rychlewski *et al.*, 2000) (see Bioinformatics section 5.13). The correct MR solution became evident only after placing the second monomer. The completed and refined model for $SycD_{21\text{-}163}{}^{meth}$ (see section 5.14.6) was successfully used as MR search model to solve the structure of the xenon derivative and the mutants A61E/L65E and S94E/Y95E, but still failed to phase the tetragonal $SycD_{21\text{-}163}$ crystal form.

5.14.6 Model building and structure refinement

ARP/wARP (Lamzin and Wilson, 1993) was used to build first models into the initial electron densities of SeMet $SycT_{1-122}$ crystal form 2 (80 % complete) and $SycD_{21-163}{}^{meth}$ (68 % complete). The initial models were refined by rigid body refinement and simulated annealing using the programs CNS (native SycT) (Brunger *et al.*, 1998) and the PHENIX program tools ($SycD_{21-163}$) (Adams *et al.*, 2002). The obtained partial models of SycT were improved and completed by several cycles of manual building in the program O (Jones *et al.*, 1991), models of SycD were improved in COOT (Emsley and Cowtan, 2004), followed by restrained (SycD) or TLS restrained refinement (SycT, SycD mutants), respectively, with REFMAC5 (Murshudov, 1997) or PHENIX (SycD mutants). Structural models were validated using WHATIF (Vriend, 1990) and MOLPROBITY (Davis *et al.*, 2004).

5.14.7 Structural analysis and visualization

Structures were analyzed regarding structural homology using a DALI (Holm, 1993) search and aligned with LSQKAB (Kabsch, 1976). Pairwise and multiple sequence alignments assigned with secondary structure elements were visualized with ESPript (Gouet *et al.*, 1999). Sequence conservation was calculated in ProtSkin (http://www.mcgnmr.ca/ProtSkin/). Protein interfaces and quaternary structures were identified using AREAIMOL (SycT) (Lee and Richards, 1971), PISA (Krissinel and Henrick, 2007), the protein-protein interaction server (http://www.biochem.ucl.ac.uk/bsm/PP/server/) (Jones, 1998) and ProMate (Neuvirth *et al.*, 2004). Cavity volumes were calculated with VOIDOO (Kleywegt, 1994). Ribbon diagrams and surfaces were produced with PyMOL (DeLano, 2002) and Swiss-PDB Viewer (Guex and Peitsch, 1997), secondary structure assignment was calculated using STRIDE (Heinig and Frishman, 2004).

5.15 Experiments *in vivo*

The *in vivo* expression and secretion experiments with *Yersinia enterocolitica* were kindly carried out by Dr. Isabel Sorg (Biozentrum of the University of Basel, Switzerland) as part of a collaboration. The aim of the experiments was to assay the phenotype of the full-length monomeric SycD A61E/L65E (see Results section 2II.1.5) mutant regarding *yop* expression and secretion in comparison to wild-type SycD.

SycD wild-type and mutant A61E/L65E sequences were cloned into the *Nco*I/*Eco*RI sites of pBADmycHisA (silent mutation of the internal *syc*D *Nco*I site) giving plasmids pISO156 and pISO157. Induction of the *yop* regulon was described by Cornelis *et al.*, 1987. The bacteria were cultivated in permissive (Brain-heart infusion, BHI, supplemented with 20 mM sodium oxalate ($-Ca^{2+}$)) or non-permissive conditions (BHI supplemented with 5 mM calcium chloride ($+Ca^{2+}$)) (Cornelis *et al.*, 1987; Marenne *et al.*, 2003). Expression of the different genes cloned downstream from the pBAD promoter was routinely induced by adding 0.2 % L-arabinose to the culture just before the shift to 37 °C, and again 2 h later. The carbon source was glycerol (4 mg/ml). Total cell and supernatant fractions were separated by centrifugation at 20'800xg for 10 min at 4 °C. The cell pellet was taken as total cell fraction. Proteins in the supernatant were precipitated using trichloroacetic acid 10 % (w/v) final for 1 h at 4 °C.
Secreted proteins were analyzed on Coomassie-stained 12 % SDS-PAGE. In each case proteins secreted by $3x10^8$ bacteria were loaded per lane. For detection of proteins by immunoblotting, $1.6x10^8$ bacteria (total cell fraction) and supernatants from $2.5x10^7$ bacteria

(supernatant fraction) were loaded per lane. Immunoblotting was carried out using polyclonal rat-antibodies directed against YopB (MIPA98; 1:300), YopD (MIPA96; 1:300) and YopE (MIPA94; 1:10’000) or polyclonal rabbit-antibodies directed against SycD (MIPA35; 1:1000). Detection was performed with the respective secondary antibodies conjugated to horseradish peroxidase (1:5000; Dako) before development with supersignal chemiluminescent substrate (Pierce).

References

Achtman, M., Zurth, K., Morelli, G., Torrea, G., Guiyoule, A. and Carniel, E. (1999). *Yersinia pestis*, the cause of plague, is a recently emerged clone of *Yersinia pseudotuberculosis*. *Proc. Natl. Acad. Sci. USA* **96**: 14043-14048.

Adams, P. D., Grosse-Kunstleve, R. W., Hung, L.-W., Ioerger, T. R., McCoy, A. J., Moriarty, N. W., Read, R. J., Sacchettini, J. C., Sauter, N. K. and Terwilliger, T. C. (2002). PHENIX: building new software for automated crystallographic structure determination. *Acta Cryst. D* **58**: 1948-1954.

Adkins, I., Koberle, M., Grobner, S., Bohn, E., Autenrieth, I. B. and Borgmann, S. (2007). *Yersinia* outer proteins E, H, P, and T differentially target the cytoskeleton and inhibit phagocytic capacity of dendritic cells. *Int. J. Med. Microbiol.* **297**: 235-244.

Aepfelbacher, M. (2004). Modulation of Rho GTPases by type III secretion system translocated effectors of *Yersinia*. *Rev. Physiol. Biochem. Pharmacol.* **152**: 65-77.

Agrain, C., Callebaut, I., Journet, L., Sorg, I., Paroz, C., Mota, L. J. and Cornelis, G. R. (2005). Characterization of a Type III secretion substrate specificity switch (T3S4) domain in YscP from *Yersinia enterocolitica*. *Mol. Microbiol.* **56**: 54-67.

Akeda, Y. and Galan, J. E. (2005). Chaperone release and unfolding of substrates in type III secretion. *Nature* **437**: 911-915.

Anderson, D. M., Ramamurthi, K. S., Tam, C. and Schneewind, O. (2002). YopD and LcrH regulate expression of *Yersinia enterocolitica* YopQ by a posttranscriptional mechanism and bind to yopQ RNA. *J. Bacteriol.* **184**: 1287-1295.

Anderson, D. M. and Schneewind, O. (1997). A mRNA signal for the type III secretion of Yop proteins by *Yersinia enterocolitica*. *Science* **278**: 1140-1143.

Baker, N. A., Sept, D., Joseph, S., Holst, M. J. and McCammon, J. A. (2001). Electrostatics of nanosystems: application to microtubules and the ribosome. *Proc. Natl. Acad. Sci. USA* **98**: 10037-10041.

Bijvoet, J. M. (1954). Structure of Optically Active Compounds in the Solid State. *Nature* **173**: 888-891.

Birket, S. E., Harrington, A. T., Espina, M., Smith, N. D., Terry, C. M., Darboe, N., Markham, A. P., Middaugh, C. R., Picking, W. L. and Picking, W. D. (2007). Preparation and characterization of translocator/chaperone complexes and their component proteins from *Shigella flexneri*. *Biochemistry* **46**: 8128-8137.

Birtalan, S. and Ghosh, P. (2001). Structure of the *Yersinia* type III secretory system chaperone SycE. *Nat. Struct. Biol.* **8**: 974-978.

Birtalan, S. C., Phillips, R. M. and Ghosh, P. (2002). Three-dimensional secretion signals in chaperone-effector complexes of bacterial pathogens. *Mol. Cell* **9**: 971-980.

Black, D. S. and Bliska, J. B. (2000). The RhoGAP activity of the *Yersinia pseudotuberculosis* cytotoxin YopE is required for antiphagocytic function and virulence. *Mol. Microbiol.* **37**: 515-527.

Bogan, A. A. and Thorn, K. S. (1998). Anatomy of hot spots in protein interfaces. *J. Mol. Biol.* **280**: 1-9.

Bolotina, I. A., Chekhov, V. O., Lugauskas, V., Finkelshtein, A. V. and Ptitsyn, O. B. (1980). Determination of the secondary structure of proteins from their circular dichroism spectra. I. Protein reference spectra for alpha-, beta- and irregular structures. *Mol. Biol. (Mosk)* **14**: 891-902.

Broms, J. E., Edqvist, P. J., Forsberg, A. and Francis, M. S. (2006). Tetratricopeptide repeats are essential for PcrH chaperone function in *Pseudomonas aeruginosa* type III secretion. *FEMS Microbiol. Lett.* **256**: 57-66.

Burridge, K. and Wennerberg, K. (2004). Rho and Rac Take Center Stage. *Cell* **116**: 167-179.

Büttner, C. (2003). Versuche zur Reinigung und Kristallisation der Virulenzfaktoren YopT und SycT aus *Yersinia enterocolitica*. Fachbereich für Biowissenschaften und Psychologie. Technische Universität Braunschweig, Braunschweig.

Büttner, D. and Bonas, U. (2002). Port of entry - the type III secretion translocon. *Trends Microbiol.* **10**: 186-192.

Cambronne, E. D., Sorg, J. A. and Schneewind, O. (2004). Binding of SycH chaperone to YscM1 and YscM2 activates effector yop expression in *Yersinia enterocolitica*. *J. Bacteriol.* **186**: 829-841.

Chayen, N. E., Saridakis, E. and Sear, R. P. (2006). Experiment and theory for heterogeneous nucleation. *Proc. Natl. Acad. Sci. USA* **103**: 597-601.

Clark, M. A., Hirst, B. H. and Jepson, M. A. (1998). M-cell surface beta1 integrin expression and invasin-mediated targeting of *Yersinia pseudotuberculosis* to mouse Peyer's patch M cells. *Infect. Immun.* **66**: 1237-1243.

Coligan, J. E., Dunn, B. M., Speicher, D. W. and Wingfield, P. T., Eds. (2007). Current Protocols in Protein Science. New York, John Wiley and Sons, Inc.

Collaborative Computational Project, N. (1994). The CCP4 suite: programs for protein crystallography. *Acta Cryst. D* **50**: 760-763.

Cornelis, G., Sluiters, C., de Rouvroit, C. L. and Michiels, T. (1989). Homology between virF, the transcriptional activator of the *Yersinia* virulence regulon, and AraC, the *Escherichia coli* arabinose operon regulator. *J. Bacteriol.* **171**: 254-262.

Cornelis, G., Vanootegem, J. C. and Sluiters, C. (1987). Transcription of the yop regulon from *Y. enterocolitica* requires trans acting pYV and chromosomal genes. *Microb. Pathog.* **2**: 367-379.

Cornelis, G. R. (2006). The type III secretion injectisome. *Nat. Rev. Microbiol.* **4**: 811-825.

D'Andrea, L. D. and Regan, L. (2003). TPR proteins: the versatile helix. *Trends Biochem. Sci.* **28**: 655-662.

Darwin, K. H. and Miller, V. L. (2001). Type III secretion chaperone-dependent regulation: activation of virulence genes by SicA and InvF in *Salmonella typhimurium*. *EMBO J.* **20**: 1850-1862.

Das, A. K., Cohen, P. W. and Barford, D. (1998). The structure of the tetratricopeptide repeats of protein phosphatase 5: implications for TPR-mediated protein-protein interactions. *EMBO J.* **17**: 1192-1199.

Dauter, Z., Dauter, M. and Dodson, E. (2002). Jolly SAD. *Acta Cryst. D* **58**: 494-506.

Dauter, Z., Dauter, M. and Rajashankar, K. R. (2000). Novel approach to phasing proteins: derivatization by short cryo-soaking with halides. *Acta Cryst. D* **56**: 232-237.

Davis, I. W., Murray, L. W., Richardson, J. S. and Richardson, D. C. (2004). MOLPROBITY: structure validation and all-atom contact analysis for nucleic acids and their complexes. *Nucl. Acids Res.* **32**: W615-619.

Day, J. B. and Plano, G. V. (2000). The *Yersinia pestis* YscY protein directly binds YscX, a secreted component of the Type III secretion machinery. *J. Bacteriol.* **182**: 1834-1843.

DeLano, W. L. (2002). *The PyMOL Molecular Graphics System*. San Carlos, CA, USA, DeLano Scientific.

Deleage, G. and Geourjon, C. (1993). An interactive graphic program for calculating the secondary structure content of proteins from circular dichroism spectrum. *Comput. Appl. Biosci.* **9**: 197-199.

Derewenda, Z. S. and Vekilov, P. G. (2006). Entropy and surface engineering in protein crystallization. *Acta Cryst. D* **62**: 116-124.

Diederichs, K. and Karplus, P. A. (1997). Improved R-factors for diffraction data analysis in macromolecular crystallography. *Nat. Struct. Biol.* **4**: 269-275.

Dittmann, S., Schmid, A., Richter, S., Trulzsch, K., Heesemann, J. and Wilharm, G. (2007). The *Yersinia enterocolitica* type three secretion chaperone SycO is integrated into the Yop regulatory network and binds to the Yop secretion protein YscM1. *BMC Microbiol.* **7**: 67.

Edman, P. and Begg, G. (1967). A protein sequenator. *Eur. J. Biochem.* **1**: 80-91.

Edqvist, P. J., Broms, J. E., Betts, H. J., Forsberg, A., Pallen, M. J. and Francis, M. S. (2006). Tetratricopeptide repeats in the type III secretion chaperone, LcrH: their role in substrate binding and secretion. *Mol. Microbiol.* **59**: 31-44.

Edqvist, P. J., Olsson, J., Lavander, M., Sundberg, L., Forsberg, A., Wolf-Watz, H. and Lloyd, S. A. (2003). YscP and YscU regulate substrate specificity of the *Yersinia* type III secretion system. *J. Bacteriol.* **185**: 2259-2266.

Ellis, J. R., Ed. (2005). Chaperone function: The orthodox view. Molecular chaperones and cell signalling. Cambridge, Cambridge University Press.

Emsley, P. and Cowtan, K. (2004). COOT: model-building tools for molecular graphics. *Acta Cryst. D* **60**: 2126-2132.

Enninga, J., Mounier, J., Sansonetti, P. and Tran Van Nhieu, G. (2005). Secretion of type III effectors into host cells in real time. *Nat. Meth.* **2**: 959-965.

Evdokimov, A. G., Phan, J., Tropea, J. E., Routzahn, K. M., Peters, H. K., Pokross, M. and Waugh, D. S. (2003). Similar modes of polypeptide recognition by export chaperones in flagellar biosynthesis and type III secretion. *Nat. Struct. Biol.* **10**: 789-793.

Evdokimov, A. G., Tropea, J. E., Routzahn, K. M. and Waugh, D. S. (2002). Three-dimensional structure of the type III secretion chaperone SycE from *Yersinia pestis*. *Acta Cryst. D* **58**: 398-406.

Faudry, E., Job, V., Dessen, A., Attree, I. and Forge, V. (2007). Type III secretion system translocator has a molten globule conformation both in its free and chaperone-bound forms. *FEBS Journal* **274**: 3601-3610.

Feldman, M. F. and Cornelis, G. R. (2003). The multitalented type III chaperones: all you can do with 15 kDa. *FEMS Microbiol. Lett.* **219**: 151-158.

Ferrer, M., Chernikova, T. N., Yakimov, M. M., Golyshin, P. N. and Timmis, K. N. (2003). Chaperonins govern growth of *Escherichia coli* at low temperatures. *Nat. Biotechnol.* **21**: 1266-1267.

Flom, G., Behal, R. H., Rosen, L., Cole, D. G. and Johnson, J. L. (2007). Definition of the minimal fragments of Sti1 required for dimerization, interaction with Hsp70 and Hsp90 and *in vivo* functions. *Biochem. J.* **404**: 159-167.

Foultier, B., Troisfontaines, P., Vertommen, D., Marenne, M.-N., Rider, M., Parsot, C. and Cornelis, G. R. (2003). Identification of substrates and chaperone from the *Yersinia enterocolitica* 1B Ysa type III secretion system. *Infect. Immun.* **71**: 242-253.

Francis, M. S., Aili, M., Wiklund, M.-L. and Wolf-Watz, H. (2000). A study of the YopD-LcrH interaction from *Yersinia pseudotuberculosis* reveals a role for hydrophobic residues within the amphipathic domain of YopD. *Mol. Microbiol.* **38**: 85-102.

Francis, M. S., Lloyd , S. A. and Wolf-Watz, H. (2001). The type III secretion chaperone LcrH co-operates with YopD to establish a negative, regulatory loop for control of Yop synthesis in *Yersinia pseudotuberculosis*. *Mol. Microbiol.* **42**: 1075-1093.

Friedel, G. (1913). Sur les symétries cristallines que peut révéler la diffraction des rayons X. *C.R. Acad. Sci. Paris* **157**: 1533-1536.

Frithz-Lindsten, E., Du, Y., Rosqvist, R. and Forsberg, A. (1997). Intracellular targeting of exoenzyme S of *Pseudomonas aeruginosa via* type III-dependent translocation induces phagocytosis resistance, cytotoxicity and disruption of actin microfilaments. *Mol. Microbiol.* **25**: 1125-1139.

Galan, J. E. and Wolf-Watz, H. (2006). Protein delivery into eukaryotic cells by type III secretion machines. *Nature* **444**: 567-573.

Gerlach, R. G. and Hensel, M. (2007). Protein secretion systems and adhesins: The molecular armory of Gram-negative pathogens. *Int. J. Med. Microbiol.* **297**: 401-415.

Gouet, P., Courcelle, E., Stuart, D. I. and Metoz, F. (1999). ESPript: analysis of multiple sequence alignments in PostScript. *Bioinformatics* **15**: 305-308.

Gregory L. Blatch, M. L. (1999). The tetratricopeptide repeat: a structural motif mediating protein-protein interactions. *BioEssays* **21**: 932-939.

Grosdent, N., Maridonneau-Parini, I., Sory, M.-P. and Cornelis, G. R. (2002). Role of Yops and adhesins in resistance of *Yersinia enterocolitica* to phagocytosis. *Infect. Immun.* **70**: 4165-4176.

Guerrero, S. A., Hecht, H. J., Hofmann, B., Biebl, H. and Singh, M. (2001). Production of selenomethionine-labelled proteins using simplified culture conditions and generally applicable host/vector systems. *Appl. Microbiol. Biotechnol.* **56**: 718-723.

Guex, N. and Peitsch, M. C. (1997). SWISS-MODEL and the Swiss-PdbViewer: an environment for comparative protein modeling. *Electrophoresis* **18**: 2714-2723.

Harker, D. (1936). The application of the three-dimensional patterson method and the crystal structures of proustite, Ag_3AsS_3, and pyrargyrite, Ag_3SbS_3. *J. Chem. Phys.* **4**: 381-390.

Heinig, M. and Frishman, D. (2004). STRIDE: a web server for secondary structure assignment from known atomic coordinates of proteins. *Nucl. Acids. Res.* **32**: W500-502.

Holm, L., Sander, C. (1993). Protein structure comparison by alignment of distance matrices. *J. Mol. Biol.* **233**: 123-138.

Hubbard, S. J. and Argos, P. (1994). Cavities and packing at protein interfaces. *Protein Sci.* **3**: 2194-2206.

Hutchinson, E. G. and Thornton, J. M. (1996). PROMOTIF - a program to identify and analyze structural motifs in proteins. *Protein Sci.* **5**: 212-220.

Iriarte, M. and Cornelis, G. R. (1998). YopT, a new *Yersinia* Yop effector protein, affects the cytoskeleton of host cells. *Mol. Microbiol.* **29**: 915-929.

Iriarte, M. and Cornelis, G. R. (1999). Identification of SycN, YscX, and YscY, three new elements of the *Yersinia* Yop virulon. *J. Bacteriol.* **181**: 675-680.

Islam, S. A., Carvin, D., Sternberg, M. J. and Blundell, T. L. (1998). HAD, a data bank of heavy-atom binding sites in protein crystals: a resource for use in multiple isomorphous replacement and anomalous scattering. *Acta Cryst. D* **54**: 1199-1206.

Janowski, R., Kozak, M., Jankowska, E., Grzonka, Z. and Jaskolski, M. (2004). Two polymorphs of a covalent complex between papain and a diazomethylketone inhibitor. *J. Pept. Res.* **64**: 141-150.

Jaroszewski, L., Rychlewski, L., Li, Z., Li, W. and Godzik, A. (2005). FFAS03: a server for profile-profile sequence alignments. *Nucl. Acids. Res.* **33**: W284-288.

Jinek, M., Rehwinkel, J., Lazarus, B. D., Izaurralde, E., Hanover, J. A. and Conti, E. (2004). The superhelical TPR-repeat domain of O-linked GlcNAc transferase exhibits structural similarities to importin alpha. *Nat. Struct. Mol. Biol.* **11**: 1001-1007.

Johnson, S., Deane, J. E. and Lea, S. M. (2005). The type III needle and the damage done. *Curr. Opin. Struct. Biol.* **15**: 700-707.

Jones, S. (1998). Protein-Protein Interaction Server. http://www. biochem.ucl.ac.uk/ bsm/PP/ server/.

Jones, S. and Thornton, J. M. (1995). Protein-protein interactions: A review of protein dimer structures. *Prog. Biophys. Mol. Biol.* **63**: 31-59.

Jones, T. A., Zou, J. Y., Cowan, S. W. and Kjeldgaard (1991). Improved methods for building protein models in electron density maps and the location of errors in these models. *Acta Cryst. A* **47**: 110-119.

Kabsch, W. (1976). A solution for the best rotation to relate two sets of vectors. *Acta Cryst. A* **32**: 922-923.

Kabsch, W. (1993). Automatic processing of rotation diffraction data from crystals of initially unknown symmetry and cell constants. *J. Appl. Cryst.* **26**: 795-800.

Kajander, T., Cortajarena, A. L., Mochrie, S. and Regan, L. (2007). Structure and stability of designed TPR protein superhelices: unusual crystal packing and implications for natural TPR proteins. *Acta Cryst. D* **63**: 800-811.

Kantardjieff, K. A. and Rupp, B. (2003). Matthews coefficient probabilities: Improved estimates for unit cell contents of proteins, DNA, and protein-nucleic acid complex crystals. *Protein Sci.* **12**: 1865-1871.

Keegan, R. M. and Winn, M. D. (2007). Automated search-model discovery and preparation for structure solution by molecular replacement. *Acta Cryst. D* **63**: 447-457.

Kiefersauer, R., Than, M. E., Dobbek, H., Gremer, L., Melero, M., Strobl, S., Dias, J. M., Soulimane, T. and Huber, R. (2000). A novel free-mounting system for protein crystals: transformation and improvement of diffraction power by accurately controlled humidity changes. *J. Appl. Cryst.* **33**: 1223-1230.

Kim, K., Oh, J., Han, D., Kim, E. E., Lee, B. and Kim, Y. (2006). Crystal structure of PilF: Functional implication in the type 4 pilus biogenesis in *Pseudomonas aeruginosa*. *Biochem. Biophys. Res. Commun.* **340**: 1028-1038.

Kissinger, C. R., Gehlhaar, D. K. and Fogel, D. B. (1999). Rapid automated molecular replacement by evolutionary search. *Acta Cryst. D* **55 (Pt 2)**: 484-491.

Kleywegt, G. J. (1994). Detection, delineation, measurement and display of cavities in macromolecular structures. *Acta Cryst. D* **50**: 178-185.

Krissinel, E. and Henrick, K. (2007). Inference of macromolecular assemblies from crystalline state. *J. Mol. Biol.* **372**: 774-797.

Laemmli, U. K. (1970). Cleavage of structural proteins during the assembly of the head of bacteriophage T4. *Nature* **227**: 680-685.

Lamzin, V. S. and Wilson, K. S. (1993). Automated refinement of protein models. *Acta Cryst. D* **49**: 129-147.

Laskowski, R. A. (1995). SURFNET: a program for visualizing molecular surfaces, cavities, and intermolecular interactions. *J. Mol. Graph. Model.* **13**: 323-330.

Lawrence, M. C. and Colman, P. M. (1993). Shape complementarity at protein/protein interfaces. *J. Mol. Biol.* **234**: 946-950.

Lee, B. and Richards, F. M. (1971). The interpretation of protein structures: estimation of static accessibility. *J. Mol. Biol.* **55**: 379-400.

Lee, S. H. and Galan, J. E. (2004). *Salmonella* type III secretion-associated chaperones confer secretion-pathway specificity. *Mol. Microbiol.* **51**: 483-495.

Letzelter, M., Sorg, I., Mota, L. J., Meyer, S., Stalder, J., Feldman, M., Kuhn, M., Callebaut, I. and Cornelis, G. R. (2006). The discovery of SycO highlights a new function for type III secretion effector chaperones. *EMBO J.* **25**: 3223-3233.

Lilic, M., Vujanac, M. and Stebbins, C. E. (2006). A common structural motif in the binding of virulence factors to bacterial secretion chaperones. *Mol. Cell* **21**: 653-664.

Locher, M., Lehnert, B., Krauss, K., Heesemann, J., Groll, M. and Wilharm, G. (2005). Crystal structure of the *Yersinia enterocolitica* type III secretion chaperone SycT. *J. Biol. Chem.* **280**: 31149-31155.

Luo, Y., Bertero, M. G., Frey, E. A., Pfuetzner, R. A., Wenk, M. R., Creagh, L., Kay, C., Haynes, C., Finley, B. B. and Strydnaka, N. C. J. (2001). Structural and biochemical characterization of the type III secretion chaperones CesT and SigE. *Nat. Struct. Biol.* **8**: 1031-1036.

Main, E. R., Xiong, Y., Cocco, M. J., D'Andrea, L. and Regan, L. (2003). Design of stable alpha-helical arrays from an idealized TPR motif. *Structure* **11**: 497-508.

Marlovits, T. C., Kubori, T., Sukhan, A., Thomas, D. R., Galan, J. E. and Unger, V. M. (2004). Structural insights into the assembly of the type III secretion needle complex. *Science* **306**: 1040-1042.

Matthews, B. W. (1968). Solvent content of protein crystals. *J. Mol. Biol.* **33**: 491-497.

Mavris, M., Page, A.-L., Tournebize, R., Demers, B., Sansonetti, P. and Parsot, C. (2002). Regulation of transcription by the activity of the *Shigella flexneri* type III secretion apparatus. *Mol. Microbiol.* **43**: 1543-1553.

McDonald, C., Vacratsis, P. O., Bliska, J. B. and Dixon, J. E. (2003). The *Yersinia* virulence factor YopM forms a novel protein complex with two cellular kinases. *J. Biol. Chem.* **278**: 18514-18523.

Mota, L. J., Sorg, I. and Cornelis, G. R. (2005). Type III secretion: The bacteria-eukaryotic cell express. *FEMS Microbiol. Lett.* **252**: 1-10.

Mukherjee, S., Keitany, G., Li, Y., Wang, Y., Ball, H. L., Goldsmith, E. J. and Orth, K. (2006). *Yersinia* YopJ acetylates and inhibits kinase activation by blocking phosphorylation. *Science* **312**: 1211-1214.

Murshudov, G. N., Vagin, A. A., Dodson, E. J. (1997). Refinement of macromolecular structures by the maximum-likelihood method. *Acta Cryst. D* **53**: 240-255.

Navarro, L., Koller, A., Nordfelth, R., Wolf-Watz, H., Taylor, S. and Dixon, J. E. (2007). Identification of a molecular target for the *Yersinia* protein kinase A. *Mol. Cell* **26**: 465-477.

Navaza, J. (1994). AMoRe: an automated package for molecular replacement. *Acta Cryst. A* **50**: 157-163.

Neumayer, W., Groll, M., Lehmann, V., Antoneka, U., Kahler, S., Heesemann, J. and Wilharm, G. (2004). *Yersinia enterocolitica* type III secretion chaperone SycH. Recombinant expression, purification, characterisation, and crystallisation. *Protein Expr. Purif.* **35**: 237-247.

Neuvirth, H., Raz, R. and Schreiber, G. (2004). ProMate: A structure based prediction program to identify the location of protein-protein binding sites. *J. Mol. Biol.* **338**: 181-199.

Neyt, C. and Cornelis, G. R. (1999). Role of SycD, the chaperone of the *Yersinia* Yop translocators YopB and YopD. *Mol. Microbiol.* **31**: 143-156.

Nimchuk, Z., Marois, E., Kjemtrup, S., Leister, R. T., Katagiri, F. and Dangl, J. L. (2000). Eukaryotic fatty acylation drives plasma membrane targeting and enhances function of several type III effector proteins from *Pseudomonas syringae*. *Cell* **101**: 353-363.

Otwinowski, Z., Minor, W. (1997). Processing of X-ray difraction data collected in oscillation mode. *Methods Enzymol.* **276**: 307-326.

Pallen, M. J., Francis, M. S. and Fütterer, K. (2003). Tetratricopeptide-like repeats in type-III-secretion chaperones and regulators. *FEMS Microbiol. Lett.* **223**: 53-60.

Panjikar, S., Parthasarathy, V., Lamzin, V. S., Weiss, M. S. and Tucker, P. A. (2005). Auto-Rickshaw: an automated crystal structure determination platform as an efficient tool for the validation of an X-ray diffraction experiment. *Acta Cryst. D* **61**: 449-457.

Panjikar, S. and Tucker, P. A. (2002). Xenon derivatization of halide-soaked protein crystals. *Acta Cryst. D* **58**: 1413-1420.

Pape, T. and Schneider, T. R. (2004). HKL2MAP: a graphical user interface for phasing with SHELX programs. *J. Appl. Cryst.* **37**: 843-844.

Parsot, C., Hamiaux, C. and Page, A.-L. (2003). The various and varying roles of specific chaperones in type III secretion systems. *Curr. Opin. Microbiol.* **6**: 7-14.

Patterson, A. L. (1935). A direct method for the determination of the components of interatomic distances in crystals *Z. Kristallogr.* **90**: 517–542.

Pearson, W. R., Wood, T., Zhang, Z. and Miller, W. (1997). Comparison of DNA sequences with protein sequences. *Genomics* **46**: 24-36.

Pekkala, M., Hieta, R., Bergmann, U., Kivirikko, K. I., Wierenga, R. K. and Myllyharju, J. (2004). The peptide-substrate-binding domain of collagen prolyl 4-hydroxylases is a tetratricopeptide repeat domain with functional aromatic residues. *J. Biol. Chem.* **279**: 52255-52261.

Phan, J., Austin, B. P. and Waugh, D. S. (2005). Crystal structure of the *Yersinia* type III secretion protein YscE. *Protein Sci.* **14**: 2759-2763.

Phan, J., Tropea, J. E. and Waugh, D. S. (2004). Structure of the *Yersinia pestis* type III secretion chaperone SycH in complex with a stable fragment of YscM2. *Acta Cryst. D* **60**: 1591-1599.

Pizarro-Cerda, J. and Cossart, P. (2006). Bacterial adhesion and entry into host cells. *Cell* **124**: 715-727.

Prentice, M. B. and Rahalison, L. (2007). Plague. *Lancet* **369**: 1196-1207.

Quinaud, M., Ple, S., Job, V., Contreras-Martel, C., Simorre, J.-P., Attree, I. and Dessen, A. (2007). Structure of the heterotrimeric complex that regulates type III secretion needle formation. *Proc. Natl. Acad. Sci. USA* **104**: 7803-7808.

Reichelt, J., Dieterich, G., Kvesic, M., Schomburg, D. and Heinz, D. W. (2005). BRAGI: linking and visualization of database information in a 3D viewer and modeling tool. *Bioinformatics* **21**: 1291-1293.

Roskoski, J., Robert (2003). Protein prenylation: a pivotal posttranslational process. *Biochem. Biophys. Res. Commun.* **303**: 1-7.

Rost, B. and Sander, C. (1993). Prediction of protein secondary structure at better than 70% accuracy. *J. Mol. Biol.* **232**: 584-599.

Ruckdeschel, K., Mannel, O., Richter, K., Jacobi, C. A., Trulzsch, K., Rouot, B. and Heesemann, J. (2001). *Yersinia* outer protein P of *Yersinia enterocolitica* simultaneously blocks the nuclear factor-kappa B pathway and exploits lipopolysaccharide signaling to trigger apoptosis in macrophages. *J. Immunol.* **166**: 1823-1831.

Rychlewski, L., Jaroszewski, L., Li, W. and Godzik, A. (2000). Comparison of sequence profiles. Strategies for structural predictions using sequence information. *Protein Sci.* **9**: 232-241.

Rypniewski, W. R., Holden, H. M. and Rayment, I. (1993). Structural consequences of reductive methylation of lysine residues in hen egg white lysozyme: an X-ray analysis at 1.8-A resolution. *Biochemistry* **32**: 9851-9858.

Saier, M. H., Jr. (2004). Evolution of bacterial type III protein secretion systems. *Trends Microbiol.* **12**: 113-115.

Salmond, G. P. and Reeves, P. J. (1993). Membrane traffic wardens and protein secretion in gram-negative bacteria. *Trends Biochem. Sci.* **18**: 7-12.

Sambrook, J. and Russell, D. W., Eds. (2001). Molecular cloning: A laboratory manual. Cold Spring Harbor, Cold Spring Harbor Laboratory Press.

Schägger, H. and Jagow, G. v. (1987). Tricine-sodium dodecyl sulfate-polyacrylamide gel electrophoresis for the separation of proteins in the range from 1 to 100 kDa. *Anal. Biochem.* **166**: 368-379.

Scheufler, C., Brinker, A., Bourenkov, G., Pegoraro, S., Moroder, L., Bartunik, H., Hartl, F. U. and Moarefi, I. (2000). Structure of TPR domain-peptide complexes: Critical elements in the assembly of the Hsp70-Hsp90 multichaperone machine. *Cell* **101**: 199-210.

Schlumberger, M. C., Muller, A. J., Ehrbar, K., Winnen, B., Duss, I., Stecher, B. and Hardt, W.-D. (2005). Real-time imaging of type III secretion: *Salmonella* SipA injection into host cells. *Proc. Natl. Acad. Sci. USA* **102**: 12548-12553.

Schneider, T. R. and Sheldrick, G. M. (2002). Substructure solution with SHELXD. *Acta Cryst. D* **58**: 1772-1779.

Schoehn, G., Di Guilmi, A. M., Lemaire, D., Attree, I., Weissenhorn, W. and Dessen, A. (2003). Oligomerization of type III secretion proteins PopB and PopD precedes pore formation in *Pseudomonas*. *EMBO J.* **22**: 4957-4967.

Schotte, P., Denecker, G., Van Den Broeke, A., Vandenabeele, P., Cornelis, G. R. and Beyaert, R. (2004). Targeting Rac1 by the *Yersinia* effector protein YopE inhibits caspase-1 mediated maturation and release of interleukin-1beta (IL-1beta). *J. Biol. Chem.* **279**: 25134-25142.

Schubot, F. D., Jackson, M. W., Penrose, K. J., Cherry, S., Tropea, J. E., Plano, G. V. and Waugh, D. S. (2005). Three-dimensional structure of a macromolecular assembly that regulates type III secretion in *Yersinia pestis*. *J. Biol. Chem.* **346**: 1147-1161.

Selzer, T., Albeck, S. and Schreiber, G. (2000). Rational design of faster associating and tighter binding protein complexes. *Nat Struct Mol Biol* **7**: 537-541.

Shao, F., Merritt, P. M., Bao, Z. Q., Innes, R. W. and Dixon, J. E. (2002). A *Yersinia* effector and a *Pseudomonas* avirulence protein define a family of cysteine proteases functioning in bacterial pathogenesis. *Cell* **109**: 575-588.

Shao, F., Vacratsis, P. O., Bao, Z., Bowers, K. E., Fierke, C. A. and Dixon, J. E. (2003). Biochemical characterization of the *Yersinia* YopT protease: Cleavage site and recognition elements in Rho GTPases. *Proc. Natl. Acad. Sci. USA* **100**: 904-909.

Sheldrick, G. M. (2002). Macromolecular phasing with SHELXE. *Z. Kristallogr.* **217**: 644-650.

Sikorski, R. S., Boguski, M. S., Goebl, M. and Hieter, P. (1990). A repeating amino acid motif in CDC23 defines a family of proteins and a new relationship among genes required for mitosis and RNA synthesis. *Cell* **60**: 307-317.

Singer, A. U., Desveaux, D., Betts, L., Chang, J. H., Nimchuk, Z., Grant, S. R., Dangl, J. L. and Sondek, J. (2004). Crystal structures of the type III effector protein AvrPphF and its chaperone reveal residues required for plant pathogenesis. *Structure* **12**: 1669-1681.

Sorg, I., Hoffmann, C., Dumbach, J., Aktories, K. and Schmidt, G. (2003). The C terminus of YopT is crucial for activity and the N terminus is crucial for substrate binding. *Infect. Immun.* **71**: 4623-4632.

Sory, M., Boland, A., Lambermont, I. and Cornelis, G. R. (1995). Identification of the YopE and YopH domains required for secretion and internalization into the cytosol of macrophages, using the cyaA gene fusion approach. *Proc. Natl. Acad. Sci. USA* **92**: 11998-12002.

Stebbins, C. E. and Galan, J. E. (2001). Maintenance of an unfolded polypeptide by a cognate chaperone in bacterial type III secretion. *Nature* **414**: 77-81.

Stevens, F. J. (1989). Analysis of protein-protein interaction by simulation of small-zone size exclusion chromatography. Stochastic formulation of kinetic rate contributions to observed high-performance liquid chromatography elution characteristics. *Biophys. J.* **55**: 1155-1167.

Studier, F. W. (2005). Protein production by auto-induction in high density shaking cultures. *Protein Expr. Purif.* **41**: 207-234.

Sun, P. D. and Radaev, S. (2002). Generating isomorphous heavy-atom derivatives by a quick-soak method. Part II: phasing of new structures. *Acta Cryst. D* **58**: 1099-1103.

Suzuki, M., Neutzner, A., Tjandra, N. and Youle, R. J. (2005). Novel structure of the N-terminus in Yeast Fis1 correlates with a specialized function in mitochondrial fission. *J. Biol. Chem.* **280**: 21444-21452.

Tardy, F., Homble, F., Neyt, C., Wattiez, R., Cornelis, G. R., Ruysschaert, J. M. and Cabiaux, V. (1999). *Yersinia enterocolitica* type III secretion-translocation system: channel formation by secreted Yops. *EMBO J.* **18**: 6793-6799.

Tengel, T., Sethson, I. and Francis, M. S. (2002). Conformational analysis by CD and NMR spectroscopy of a peptide encompassing the amphipathic domain of YopD from *Yersinia*. *Eur. J. Biochem.* **269**: 3659-3668.

Thomas, N. A., Deng, W., Baker, N. T., Puente, J. L. and Finlay, B. B. (2007). Hierarchical delivery of an essential host colonization factor in enteropathogenic *Escherichia coli*. *J. Biol. Chem.* **282**: 29634-29645.

Thompson, J. D., Higgins, D. G., Gibson, T. J. (1994). CLUSTAL W: improving the sensitivity of progressive multiple sequence alignment through sequence weighting, position-specific gap penalties and weight matrix choice. *Nucl. Acids. Res.* **22**: 4673-4680.

Towbin, H. and Staehelin, T. G. J. (1979). Electrophoretic transfer of proteins from polyacryl gel to nitrocellulose sheets: Procedure and some applications. *Proc. Natl. Acad. Sci. USA* **76**: 4350-4354.

Trame, C. B. and McKay, D. B. (2003). Structure of the *Yersinia enterocolitica* molecular-chaperone protein SycE. *Acta Cryst. D* **59**: 389-392.

Trasak, C., Zenner, G., Vogel, A., Yuksekdag, G., Rost, R., Haase, I., Fischer, M., Israel, L., Imhof, A., Linder, S., Schleicher, M. and Aepfelbacher, M. (2006). *Yersinia* protein kinase YopO is activated by a novel G-actin binding process. *J. Biol. Chem.* **282**: 2268-2277.

Uson, I. and Sheldrick, G. M. (1999). Advances in direct methods for protein crystallography. *Curr. Opin. Struct. Biol.* **9**: 643-648.

Vagin, A. and Teplyakov, A. (1997). MOLREP: An automated program for molecular replacement. *J. Appl. Cryst.* **30**: 1022-1025.

Van Eerde, A., Hamiaux, C., Perez, J., Parsot, C. and Dijkstra, B. W. (2004). Structure of Spa15, a type III secretion chaperone from *Shigella flexneri* with broad specificity. *EMBO Rep.* **5**: 477-483.

Viboud, G. I., Mejia, E. and Bliska, J. B. (2006). Comparison of YopE and YopT activities in counteracting host signalling responses to *Yersinia pseudotuberculosis* infection. *Cell. Microbiol.* **8**: 1504-1515.

Vriend, G. (1990). WHAT IF: a molecular modeling and drug design program. *J. Mol. Graph. Model.* **8**: 52-56, 29.

Waldo, G. S., Standish, B. M., Berendzen, J. and Terwilliger, T. C. (1999). Rapid protein-folding assay using green fluorescent protein. *Nat. Biotechnol.* **17**: 691-695.

Wattiau, P., Bernier, B., Deslee, P., Michiels, T. and Cornelis, G. R. (1994). Individual chaperones required for Yop secretion by *Yersinia*. *Proc. Natl. Acad. Sci. USA* **91**: 10493-10497.

Wattiau, P. and Cornelis, G. R. (1993). SycE, a chaperone-like protein of *Yersinia enterocolitica* involved in the secretion of YopE. *Mol. Microbiol.* **8**: 123-131.

WHO (2007). World Health Organization. Plague. http://www.who.int/topics/plague/en/.

Wilharm, G., Dittmann, S., Schmid, A. and Heesemann, J. (2007). On the role of specific chaperones, the specific ATPase, and the proton motive force in type III secretion. *Int. J. Med. Microbiol.* **297**: 27-36.

Wong, K.-W. and Isberg, R. R. (2005a). *Yersinia pseudotuberculosis* spatially controls activation and misregulation of host cell Rac1. *PLoS Pathogens* **281**: 40379-40388.

Wong, K. W. and Isberg, R. R. (2005b). Emerging views on integrin signaling *via* Rac1 during invasin-promoted bacterial uptake. *Curr. Opin. Microbiol.* **8**: 4-9.

Wren, B. W. (2003). The Yersiniae - a model genus to study the rapid evolution of bacterial pathogens. *Nat. Rev. Microbiol.* **1**: 55-64.

Wu, Y. and Sha, B. (2006). Crystal structure of yeast mitochondrial outer membrane translocon member Tom70p. *Nat. Struct. Mol. Biol.* **13**: 589-593.

Wulff-Strobel, C. R., Williams, A. W. and Straley, S. C. (2002). LcrQ and SycH function together at the Ysc type III secretion system in *Yersinia pestis* to impose a hierarchy of secretion. *Mol. Microbiol.* **43**: 411-423.

Yao, T., Mecsas, J., Healy, J. I., Falkow, S. and Chien, Y. h. (1999). Suppression of T and B lymphocyte activation by a *Yersinia pseudotuberculosis* virulence factor, YopH. *J. Exp. Med.* **190**: 1343-1350.

Yu, C.-M., Mun, S. and Wang, N.-H. L. (2006). Theoretical analysis of the effects of reversible dimerization in size exclusion chromatography. *J. Chromatogr. A* **1132**: 99-108.

Zhang, Y. and Chan, D. C. (2007). Structural basis for recruitment of mitochondrial fission complexes by Fis1. *Proc. Natl. Acad. Sci. USA* **104**: 18526-18530.

Zhao, Y., Blumer, S. E. and Sundin, G. W. (2005). Identification of *Erwinia amylovora* genes induced during infection of immature pear tissue. *J. Bacteriol.* **187**: 8088-8103.

Zumbihl, R., Aepfelbacher, M., Andor, A., Jacobi, C. A., Ruckdeschel, K., Rouot, B. and Heesemann, J. (1999). The cytotoxin YopT of *Yersinia enterocolitica i*nduces modification and cellular redistribution of the small GTP-binding protein RhoA. *J. Biol. Chem.* **274**: 29289-29293.

Appendix

A) Nucleotide and amino acid sequences

s*yop*T (synthetic *yop*T gene, *E. coli* codon-usage optimized, GENEART No. 042691)

```
   1 ATGGATAGCA TCCACGGCCA TTATCATATT CAGCTGAGCA ACTATAGCGC GGGTGAAAAC
  61 TTGCAGAGCG CGACCCTGAC CGAAGGTGTT ATTGGTGCGC ATCGCGTGAA AGTTGAAACC
 121 GCGCTGAGCC ATAGCAACCG TCAGAAAAAA CTGAGCGCGA CCATCAAACA TAATCAGAGC
 181 AGCCGTAGCA TGCTGGATCG TAAACTGACC AGCGATGGCA AAGCGAATCA GCGTAGCAGC
 241 TTTACCTTCA GCATGATCAT GTACCGCATG ATCCATTTTG TTCTGAGCAC CCGTGTTCCG
 301 GCGGTTCGTG AAAGCGTTGC GAACTATGGC GGCAACATCA ACTTTAAATT CGCGCAGACG
 361 AAAGGTGCGT TTCTGCACCA GATCATCAAA CACAGCGATA CCGCGAGCGG TGTTTGTGAA
 421 GCGCTGTGCG CGCATTGGAT TTGGAGCCAT GCGCAGGGTC AGAGCCTGTT CGATCAGCTG
 481 TATGTGGGCG GTCGTAAAGG CAAATTCCAG ATCGATACCC TGTACAGCAT TAAACAGCTG
 541 CAGATCGATG GTTGTAAAGC GGATGTGGAT CAGGATGAAG TTACCCTGGA TTGGTTTAAA
 601 AAAAAAGGCA TCAGCGAACG CATGATTGAA CGTCATTGTC TGCTGCGTCC GGTTGATGTT
 661 ACCGGCACCA CCGAAAGCGA AGGTCCGGAT CAGCTGCTGA ATGCGATTCT GGATACCCAC
 721 GGCATTGGCT ACGGCTATAA AAAAATCTAC CTGAGCGGTC AGATGAGCGC GCATGCGATT
 781 GCGGCGTATG TGAACGAAAA AAGCGGCGTG ACCTTTTTTG ATCCGAACTT CGGCGAATTT
 841 CACTTCAGCG ATAAAGAAAA ATTTCGCAAA TGGTTTACCA ACAGCTTCTG GGAAAACAGC
 901 ATGTATCATT ATCCGCTGGG TGTGGGTCAG CGTTTTAGCG TGCTGACCTT CGATAGCAAA
 961 GAAGTG
```

SycT - amino acid sequence (GenBank entry AAD16809)

```
   1 MQTTFTELMQ QLFLKLGLNH QVNENDVYTF EVDGHIQVLI ACYHQQWVQL FSELGADLPT
  61 NDNLFGEHWP AHVQGRLDGK SILWSQQSLV GLDIDEMQAW LERFIDDIEQ RKEPQNTKFQ
 121 PNSTSPILFI
```

YopT - amino acid sequence (GenBank entry AAD16808, catalytic triad in bold)

```
   1 MDSIHGHYHI QLSNYSAGEN LQSATLTEGV IGAHRVKVET ALSHSNRQKK LSATIKHNQS
  61 SRSMLDRKLT SDGKANQRSS FTFSMIMYRM IHFVLSTRVP AVRESVANYG GNINFKFAQT
 121 KGAFLHQIIK HSDTASGV**C**E ALCAHWIWSH AQGQSLFDQL YVGGRKGKFQ IDTLYSIKQL
 181 QIDGCKADVD QDEVTLDWFK KKGISERMIE RHCLLRPVDV TGTTESEGPD QLLNAILDTH
 241 GIGYGYKKIY LSGQMSA**H**AI AAYVNEKSGV TFF**D**PNFGEF HFSDKEKFRK WFTNSFWENS
 301 MYHYPLGVGQ RFSVLTFDSK EV
```

SycD - amino acid sequence (GenBank entry AAD16814)

```
   1 MQQETTDTQE YQLAMESFLK GGGTIAMLNE ISSDTLEQLY SLAFNQYQSG KYEDAHKVFQ
  61 ALCVLDHYDS RFFLGLGACR QAMGQYDLAI HSYSYGAVMD IKEPRFPFHA AECLLQKGEL
 121 AEAESGLFLA QELIANKPEF KELSTRVSSM LEAIKLKKEM KHECVDNP
```

B) Gene expression results for different YopT constructs and conditions

Table B1. YopT expression constructs tested.

ANo.	Expression vector	YopT construct	Expression condition	YopT expression	Soluble
1	pETM-30-IRES_*syc*T_*yop*TS13A	YopTS13A	GST-SycT	+	-
2	pETM-30-IRES_*syc*T_Δ13*yop*T	$YopT_{14-322}$	GST-SycT	+	+
2	pETM-30-IRES_*syc*T_Δ22*yop*T	$YopT_{23-322}$	GST-SycT	++	+
2, 6	pETM-30-IRES_*syc*T_Δ22*yop*T C139S	$YopT_{23-322}$C139S	GST-SycT	++	+
2	pETM-30-IRES_*syc*T_Δ49*yop*T	$YopT_{50-322}$	GST-SycT	+++	+
2, 6	pETM-30-IRES_*syc*T_Δ49*yop*T C139S	$YopT_{50-322}$C139S	GST-SycT	+++	+
2	pETM-30-IRES_*syc*T_Δ50*yop*T	$YopT_{51-322}$	GST-SycT	+++	+
2, 6	pETM-30-IRES_*syc*T_Δ49*yop*TC139S	$YopT_{51-322}$C139S	GST-SycT	+++	+
3	pETM-11_*yop*T	His_6-YopT	AI	-	n.d.
3	pETM-30_*yop*T	GST-YopT	AI	+	n.d.
3	pETM-41_*yop*T	MBP-YopT	AI	-	n.d.
3	pETM-60_*yop*T	NusA-YopT	AI	-	n.d.
3, 4	pETM-11_*yop*T75-318	His_6-$YopT_{75-318}$	AI	++	-
3, 4	pETM-30_*yop*T75-318	GST-$YopT_{75-318}$	AI	+	-
5	pETM-11_s*yop*T	His_6-sYopT	-	++	-
5	pETM-30_s*yop*T	GST-sYopT	-	+	-
5	pET-28c+_s*yop*T 6His	sYopT-His_6	-	-	-
5	pET-28c+_s*yop*T	sYopT	-	++	-
6	pETM-30-IRES_*syc*T_*yop*TC139S	YopTS13A	GST-SycT	+++	+
6	pETM-30_*yop*TC139S	GST-YopTC139S	-	+	n.d.
7	pGEX-2TGL_s*yop*T	GST-GL-sYopT	also TG1	+	-
8	pETM-30_*yop*T	GST-YopT	10 °C, AEx.	-	n.d.
8	pETM-30_*yop*T75-318	GST-$YopT_{75-318}$	10 °C, AEx.	-	n.d.
8	pET28c+_s*yop*T	sYopT	10 °C, AEx.	-	n.d.

ANo., Approach, according to the classification in the Results section 2I.1.1, Table 2I-1; AI: Auto-inducing medium; GL: Glycine linker; TG1, *E. coli* expression host; AEx., ArcticExpress, *E. coli* expression host, psychrophilic due to chaperonin genes *cpn*10/*cpn*60 from *Oleispira antarctica*. YopT expression: from (+++) good to (-) not detected; Soluble: (+), yes, (-), no, (n.d.), not determined.

Danksagung

Prof. Dirk Heinz hatte so viel Vertrauen in meine Fähigkeiten, dass er mir nach der Diplomarbeit auch gleich noch die Stelle als Doktorandin anbot. Dafür danke ich ihm ganz herzlich, aber genauso für die hervorragenden Arbeitsbedingungen in Form einer traumhaften Laborausstattung. Vor allem aber danke ich ihm für sein stetes Interesse an meiner Arbeit, seinen Weg-Weisungen und seinen Glauben an den Erfolg des Projektes, wenn ich selbst kurz vor dem Verzweifeln stand. Gleichfalls danke ihm, dass er mir bei den Projektwichtung relativ freie Hand ließ, wo man doch nicht absehen konnte, dass das Projekt SycD oder die reduktive Methylierung jemals von Erfolg gekrönt sein würden.

Jun. Prof. Dr. Hartmut Niemann hatte mit seiner kontinuierlichen, superben Betreuung (auch jenseits von Braunschweig) erheblichen Anteil am Gelingen meiner Doktorarbeit. Hartmut verkörperte den unverzichtbaren, ausgleichenden Ruhepol zur "Superechtzeit-Forschung". Vielen tausend Dank für die gelassene Reaktion auf meine doch manchmal sehr lebhafte Art, und nicht zuletzt fürs Korrekturlesen diverser Fragmente! Und er schafft es doch tatsächlich eine frustrierte Pessimistin aufzumuntern, auch wenn ich äußerst misstrauisch gegenüber jeglichen Formulierungen wie "Back-up Projekt" und "kleines, lösliches bakterielles Protein" geworden bin. Aber Ende gut, alles gut! Merci, merci beaucoup, Hartmut!

Ich bedanke mich herzlich bei Prof. Petra Dersch für die Übernahme des Zweitgutachtens.

Für die Übernahme des Prüfungsvorsitzes danke ich Prof. Ralf Mendel.

Ebenso bedanke ich mich bei Prof. Jürgen Wehland für sein Mitwirken in meinem begleitenden "Thesis-Komitee".

Vielen Dank an Prof. Guy Cornelis für das Geschenk des *Yersinia*-Virulenzplasmids und die gute Kooperation im Hinblick auf die beiden Chaperone. Insbesondere danke ich Dr. Isabel Sorg aus seiner Arbeitsgruppe für die Ausführung der Experimente mit lebenden Yersinien "à la minute".

Herzlich danke ich Dr. Markus Wahl und seinem Doktoranden Gert Weber für die freundliche Aufnahme und Betreuung während der mehrtägigen Dehydrationsversuche und die Gelassenheit bei der Fehlersuche.

Dr. Wolf-Dieter Schubert danke ich für die unzähligen erbaulichen Exkurse in die Tiefen des Graphik- und reziproken Raums.

Des weiteren bedanke ich mich bei Dr. Manfred Nimtz und seinen Teamkollegen Anja Meier und Undine Felgenträger für die zahllosen Massenspektren samt vertiefender Diskussion, sowie bei Rita Getzlaff für die N-terminalen Sequenzierungen.

Ein großes Dankeschön geht auch an meine fleißigen Kurzzeit-Paktikanten und -Auszubildenden Przemek Zabek, Magdalena Gamm und die unermüdlich Lösungen ansetzende Maren Freund.

Ute Widow und Sabine Schmidt möchte ich ganz besonders danken, nicht nur hinsichtlich des herzlichen Willkommenheißens und der bekundeten Anteilnahme an meiner Nahrungsaufnahme, sondern auch für ihren unschätzbaren Beitrag zu einem fantastischen Arbeitsklima, das einen wesentlichen Anteil am Fortgang meiner Arbeit hatte. Und natürlich danke ich den beiden für den Spaß zwischendrin sowie die lustigen Kaffeerunden.

Vielen Dank an alle ehemaligen und noch wuselnden Kollegen aus der Arbeitsgruppe Strukturbiologie, speziell an Dr. Joop van den Heuvel für die gute Beratung in Klonierungsfragen, und an Daniela Gebauer für die Reserve-der-Reserve-Aushilfsröhrchen und ihre Unterstützung bei der Klonierung der *Yersinia*-Vektoren.
Ebenfalls ein großes Dankeschön geht an Dr. Joachim Reichelt, der immer die Lock- und Log-Dateien der Linux-Stationen unter Kontrolle hatte und tatkräftig bei der YopT-Modellierung half.
Ein extra Dankeschön geht an Jörg Schulze für die musikalischen Inspirationen und die Gedankenaustausche über das Neueste von DER Band.

Ein ganz besonderes Dankeschön geht an die anderen drei Absolventen des "Doktoranden-Quartetts": Vielen Dank für die inspirierenden Diskussionen und subtilen Humorspielereien mit Thomas Wollert und Gregor Hagelüken. Gregors legendäre Skripte erleichterten außer-

dem den Linux-Alltag ungemein. Mit Maike Bublitz gemeinsam unter einer Decke zu stecken und zu Konferenzen zu fahren, war immer abwechslungsreich.

Ganz herzlich gedankt sei auch meinen beiden "Zimmergenossen" Katrin Bolte und Davide Ferraris, sowie Maike Rochon. Katrin gewährte mir ausführliche Einblicke in die wunderliche Welt der niedersächsischen Moore. Die längste Unterhaltung mit einem Kollegen überhaupt hatte ich mit unserem eingedeutschten Italiener Davide. Mit Maike zusammen auf "Nussjagd" oder beim "H.N.-Gedächtnislauf" ging am Ende des Tunnels des öfteren doch noch ein Licht auf. Hab vielen Dank! Und Maike: Entweder die Nuss oder Du!

Den nötigen Ausgleich und Biss für die Forschungsarbeit fand ich in der motivierenden Gemeinschaft des Unisports der TU Braunschweig (vielen Dank an Markus, Leon, Katharina und Renato!) sowie durch die (Staffel-) Marathon-Ambitionen einiger Kollegen, insbesondere von Dr. Marina Eiting, welche mich überhaupt ans Laufen herangeführt hat (Tausend Dank, Marina!).

Dass auch außerhalb des Labors eine Welt existierte, hab ich nicht zuletzt meinen Freunden und Ex-Kommilitonen Djamila, Bernd und Tobi zu verdanken. Ein ganz besonderes Dankeschön geht in diesem Zusammenhang an die rituelle Elbhangfest- und Weihnachtskaffeetrinken-Runde der "Dräsdnr": Mela, Maret, Uli, Das Dicke Ei, Robert, Moni, Yvonne und Kattl.

Ohne die ungebrochene Unterstützung durch meine "Wurzeln" gemäß dem Leitmotiv "All you need is love!" hätte ich diese besondere Zeit fernab der Heimat nicht durchgehalten und ein oder tausend Dankeschön an meine Familie reichen dafür nicht aus. Es ist jedenfalls beruhigend zu wissen, dass es zu Hause immer noch genauso schön ist wie an dem Tag, als ich auszog, das ...

Ein sehr spezielles Dankeschön zum Schluss richte ich an meinen Freund Florian. Ohne Dich wäre ich definitiv verhungert... und mit meinem Fahrrad nie heil wieder angekommen. Um all die Dinge abzudecken, für die ich Dir dankbar bin, käme ein weiteres Buch zusammen! Outdoortauglich und krisenerprobt freue ich mich jedenfalls schon auf die nächsten Kreise, die wir ziehen, ob Lagerfeuer oder Politik.

Lebenslauf

Persönliche Angaben

Renate Carina Büttner
geb. am 10.06.1979 in Dresden
ledig
deutsch

Schulische Ausbildung

1986 - 1992	88. Polytechnische Oberschule, Dresden
1992 - 1998	Gymnasium Dresden-Striesen, Dresden Abschluss: Abitur

Akademischer Werdegang

1998 - 2003	Studium der Biotechnologie and der Technischen Universität in Braunschweig Studienabschluss: Diplom (Note: Sehr gut)
2003	Diplomarbeit an der Gesellschaft für Biotechnologische Forschung (seit 2006 Helmholtz-Zentrum für Infektionsforschung) in Braunschweig: Versuche zur Reinigung und Kristallisation der Virulenzfaktoren YopT und SycT aus *Yersinia enterocolitica*
2003 - 2007	Promotion am Helmholtz-Zentrum für Infektionsforschung, Braunschweig, Bereich Strukturbiologie.